EVALUATION OF THE KINETICS OF BIOLOGICALLY CATALYZED TREATMENT AND REGENERATION OF NO$_X$ SCRUBBING PROCESS WATERS

by

Robert Michael Dilmore

B.S. in Civil Engineering, University of Delaware, 1996

M.S. in Environmental Engineering, University of Pittsburgh, 1999

Submitted to the Graduate Faculty of

the School of Engineering in partial fulfillment

of the requirements for the degree of

Doctor of Philosophy

University of Pittsburgh

2004

UNIVERSITY OF PITTSBURGH

SCHOOL OF ENGINEERING

The dissertation was presented

by

Robert Michael Dilmore

It was defended on

September 23, 2004

and approved by

Leonard W. Casson, Ph. D., Associate Professor, Civil and Environmental Engineering

Radisav D. Vidic, Ph. D., Professor, Civil and Environmental Engineering

James T. Cobb, Jr., Ph. D., Associate Professor Emeritus, Chemical and Petroleum Engineering

Dissertation Director: Ronald D. Neufeld, Ph. D., Professor, Civil and Environmental Engineering

EVALUATION OF THE KINETICS OF BIOLOGICALLY CATALYZED TREATMENT AND REGENERATION OF NO$_X$ SCRUBBING PROCESS WATERS

Robert Michael Dilmore, Ph.D.

University of Pittsburgh, 2004

A prototype apparatus was configured and operated to evaluate the efficacy of a process that integrates the absorption of nitric oxide in an aqueous solution of ferrous ethylenediamintetraacetic acid (Fe(II)EDTA) with biological treatment and regeneration of spent scrubber water. In addition to operation of a continuous-flow, closed-loop prototype process, a series of batch reactor tests were conducted to investigate the kinetics of microbially-catalyzed reduction of the nitrosyl adduct of ferrous EDTA and microbially-catalyzed reduction of oxidized ferric EDTA. Denitrifying and strictly anaerobic biomass from a municipal wastewater treatment process was cultivated using ethanol as the primary electron donor and nitrate and ferric EDTA as electron acceptors. Following 42-days of bioreactor start-up, nitric oxide (NO) scrubbed from a counter-current absorption tower replaced nitrate. After 27 days of aclimation, an 80-day period of steady state operation was observed. During steady state operation, mean NO scrubbing efficiency of 97.9% was achieved, process water oxidation/reduction potential (ORP) remained between -75 and -140 mV (vs. Ag/AgCl ref.), and generated biogas was 91% N$_2$, by volume. Biomass in the prototype reactor was flocculent, and traveled throughout the closed-loop process. Because of the constant recirculation of washed-out biomass and low observed biomass yield (0.0393 g VSS/g COD), mass balance showed the prototype process sludge age to be 75.9 days. During steady state operation, biomass was extracted for kinetic batch analyses. Batch reactor kinetic tests revealed that both ferric EDTA and NO reduction proceed as a result of microbially-catalyzed reactions. Microbially-catalyzed reduction of ferric EDTA proceeds according to the Monod kinetic model, while strong inhibition of the microbially-catalyzed reduction of NO·Fe(II)EDTA was observed at ethanol concentrations above 0.33 g COD/l. Based on observed population parameters, including biomass yield, endogenous decay, and substrate utilization rate, the critical mean cell retention time below which wash out of a continuously-stirred bioreactor would occur was found to be 11.7 days and 51.4 days for NO

reducers and ferric EDTA reducers, respectively. Experimental results provide insight into conditions required for the successful operation of a process for the biological treatment and regeneration of spent scrubber solution from a NO_X absorption process.

DESCRIPTORS

Anaerobic Treatment

Bioreactor

Denitrification

Iron EDTA

Nitrogen oxides

Substrate Inhibition

Anoxic Treatment

Cyclic voltammetry

Flue gas treatment

Iron Reduction

Scrubbing

Upflow bioreactor

TABLE OF CONTENTS

LIST OF TABLES

LIST OF FIGURES

xiii

LIST OF ACRONYMS

Name	ACRONYM
Chemical oxygen demand	COD
Completely stirred tank reactor	CSTR
Ethylenediamintetraacetic acid	EDTA
Mixed liquor volatile suspended solids	MLVSS
National Energy Technology Laboratory	NETL
Plug flow reactor	PFR
Total suspended solids	TSS
Selective catalytic reduction	SCR
Selective non-catalytic reduction	SNCR
United States Department of Energy National	US DOE
Upflow anaerobic sludge blanket reactor	UASB

ACKNOWLEDGEMENTS

1.0 INTRODUCTION AND RESEARCH OBJECTIVES

1.1 INTRODUCTION

Fossil fuel combustion for the purpose of electricity generation is a major anthropogenic source of several air pollutants of significant concern, both domestically and abroad. These pollutants include particulate matter (PM), sulfur oxides (SO_X), nitrogen oxides (NO_X), carbon monoxide (CO), lead, and mercury (U.S. EPA, 2003). As reported by the United States Environmental Protection Agency (EPA), 37% of all domestically generated anthropogenic NO_X is released by non-transportation fuel combustion, resulting primarily from the combustion of fossil fuels by major electric utility boilers (U.S. EPA, 2002).

Typically, greater than 90% of all nitrogen oxides formed as a result of fuel combustion are present in the gaseous combustion effluent as nitric oxide (NO) (Sloss, 1992). Upon release to the atmosphere, nitric oxide reacts readily with diatomic oxygen to form nitrogen dioxide (NO_2), which comprises the vast majority of all atmospheric NO_X (Sloss, 1992). Short-term exposure to elevated concentrations of NO_X can lead to coughing and reversible impact on pulmonary function (U.S. EPA, 2002). Long-term exposure has been implicated in increased incidence of respiratory infection and permanent structural alteration of the lungs. In addition to these direct health impacts, NO_X reacts in the atmosphere to form ground-level ozone and fine particle pollution. These secondary pollutants are also associated with adverse health effects (U.S. EPA, 2002).

Atmospheric NO_X can also significantly impact the natural environment. NO_X contributes to the global environmental problems of global warming and depletion of stratospheric ozone (U.S. EPA, 2002). NO_2 is a major component of urban smog (Sloss, 1992). Deposition of NO_X to terrestrial and aquatic ecosystems can lead to fertilization, eutrophication, and acidification, resulting in significant impact to overall ecosystem health (U.S. EPA, 2002). Direct and indirect impacts to human health and natural environment resulting from NO_X release have led to government regulation of anthropogenic release in most of the industrialized world.

In the United States, recent amendments to the Clean Air Act of 1970 have established emissions standards for large-scale domestic point-sources, and require application of "best-available technology" to

meet those regulated emissions requirements (U.S. EPA, April, 2004). In accordance with the federally approved set of regulations, explicit pollution control measures and an implementation schedule for application of those measures are established on the state level for each regulated emission source (U.S. EPA, 2003). These state implementation plans have met with federal approval, and the deadline for application of NO_X control technology measures was set for May of 2004.

Nitrogen oxide control technologies are categorized as being one of two types: primary controls that decrease the formation of NO_X during combustion and secondary controls that treat NO_X that is present in the combustion flue gas stream. Primary NO_X best-available control technologies involve combustion modification, and are referred to collectively as "low-NO_X burners" (Sloss, 1992).

Secondary best-available NO_X control technologies involve chemical reduction of NO_X in flue gas using a chemical reducing agent such as ammonia or urea, reacting on a specially engineered catalytic surface or reacting without catalysis in the gas stream. Such technologies are referred to as selective catalytic reduction (SCR) and selective non-catalytic reduction (SNCR), respectively. These technologies were first developed more than thirty years ago and experience of their full-scale application have resulted in their refinement, maturation, and acceptance as the best-available technology for large utility boilers (Sloss, 1992; Cooper and Alley, 1994; U.S. EPA, 2003). However, there has been substantial and promising research into an additional secondary NO_X control technology that involves absorption or "scrubbing" of nitrogen oxides from flue gas (Saito et.al, 1976; Sada, 1984; Weisweiler et al. 1986; Dravo, 1992; Kleifges et al., 1997, Buisman et al., 1999, van der Maas, 2003).

Addition of a ferrous iron chelate, such as ferrous ethylenediaminetetraacetic acid (ferrous EDTA), to water dramatically increases the solubility of nitric oxide by the formation of a nitrosyl adduct to the ferrous-chelate complex(Saito et.al, 1976; Sada, 1984; Weisweiler, et al. 1986; Dravo, 1992; Kleifges et al., 1997, Buisman et al., 1999, van der Maas, 2003). Application of such a solution to a packed-bed or spray-tower absorption column (such as is commonly used in SO_X absorption) effectively scrubs NO_X species from flue gas. Spent scrubber solution must then be treated to reduce the nitrosyl adduct of the ferrous chelate to nitrogen gas, as well as to reduce oxidized ferric chelate back to the reduced ferrous form that is active for NO_X scrubbing. Treated and regenerated scrubber solution can be recycled to the absorption stage in a closed-loop process (Saito, 1976; Sada, 1984; Dravo, 1992; Buisman, 1999).

Several researchers have investigated chemical and electrochemical reduction mechanisms for the treatment and regeneration of ferrous chelate-based spent NO_X scrubber waters. Such methods have been shown to successfully reduce oxidized species in solution, but several engineering and economic issues have, as of the present time, prevented full-scale application of such treatment mechanisms. These issues include reagent or electricity costs, formation of reaction intermediates with deleterious effects, and

inability to maintain overall scrubber solution capacity through long periods of closed-loop operation (Saito, 1976; Sada, 1984; Dravo, 1992; Kleifges et al., 1997).

More recently, researchers have demonstrated the ability of microorganisms to reduce the oxidized species present in spent iron chelate-based NO_X scrubber water. Based on the observed success of these microbially-catalyzed reduction reactions, researchers in the Netherlands obtained patents generally directed to a process of achieving biological treatment and regeneration of said scrubber water. As yet, microbially-mediated scrubber technology has not been applied to large coal fired boiler unit flue gas treatment, and, as such, its efficacy is not proven. In addition, the rate at which the microbially-catalyzed reactions proceed has not been characterized in the extant literature (Buisman et al., 1999, Buisman et al., 2001; van der Maas et al., 2002; van der Maas et al., 2003).

The objective of the research described herein is, therefore, to demonstrate process efficacy using a simplified prototype process and to use the culture of bacteria cultivated therein to provide a preliminary description of the kinetics of microbially mediated reactions necessary to treat and regenerate spent scrubber solution. It is believed that results of this investigation will contribute to the body of knowledge related to this novel treatment method, provide insight into factors that affect process configuration and operation, and provide preliminary data to support future efforts to allow bioreactor sizing for cost comparison with current best-available technologies.

1.2 RESEARCH OBJECTIVES

The general objective of the presented work is to investigate the kinetics of microbially-mediated reduction of oxidized species in NO_X scrubbing process streams. Specifically, experiments were designed to support the development of mathematical expressions defining the observed rate of reduction of the nitrosyl adduct of ferrous EDTA and the observed rate of reduction of ferric EDTA as a function of initial ethanol (electron donor) concentration. In addition, the oxidation-reduction conditions under which these reactions proceed were also investigated. The experiments also provide preliminary insight into other constraints that impact process effectiveness.

In order to realize the defined research objectives, experimental investigation was focussed on the following primary tasks:

Task I – Prototype process configuration and startup

- Configuration of the prototype apparatus
- Conduct tracer study on prototype bioreactor for determination of bioreactor hydrodynamic properties
- Inoculation of bioreactor and process startup
- Cultivation of active cultures capable of reducing targeted oxidized species
- Integration of established bioreactor with a prototype NO_X scrubbing packed-bed tower

Task II – Demonstration of the efficacy of the prototype-scale NO_X scrubber/bioreactor process:

- Monitor of prototype bioreactor performance using a number of direct and indirect indicators, including: organic loading rate, biogas volume and composition, NO loading rate, iron reduction efficiency, and process water oxidation-reduction potential
- Monitor scrubber influent and effluent NO_X concentration for the determination of NO_X removal efficiency
- Evaluation of a period of pseudo-steady-state operation to evaluate system performance

Task III – Evaluation of the kinetics of microbially-catalyzed reduction of the nitrosyl adduct of ferrous EDTA:

- Determination of reduction rate as a function of initial substrate concentration
- Evaluation of substrate utilization as compared to that defined by reaction stoichiometry
- Evaluation of observed microbial growth as a function of substrate utilization (microbial yield)
- Evaluation of rate of endogenous decay

Task IV – Evaluation of the kinetics of microbially catalyzed reduction of ferric EDTA:

- Determination of reduction rate as a function of initial substrate concentration
- Evaluation of substrate utilization as compared to that defined by reaction stoichiometry
- Evaluation of observed microbial growth as a function of substrate utilization (microbial yield)
- Evaluation of rate of endogenous decay

Task V – Integration of observed kinetic data with the prototype process performance to identify process constraints and factors that affect process operation:

- Consideration of the impact of bioreactor configuration on performance
- Consideration of observed steady-state performance

- Discussion of periods of poor process performance
- Consideration of implications of observed reaction kinetics and hydrodynamic conditions for overall process engineering considerations

It is believed that this information can be applied in future efforts for preliminary bioreactor sizing and process configuration, in support of preliminary cost evaluation of the process to facilitate its comparison with currently accepted best-available technologies.

2.0 BACKGROUND

This chapter provides an overview of several topics, such as the fate and transport of gas pollutants, domestic regulation, and current best-available technology for the treatment of NO_X generating from coal-fired utility boilers will be discussed. Background on basic electrochemistry and a summary of environmentally significant microbially-catalyzed reduction reactions, including denitrification, iron reduction, sulfate reduction and methanogenesis is given. Finally, a summary of the kinetics of microbially-mediated redox reactions, based on the Monod model of substrate-limited growth, is provided.

2.1 COMBUSTION FLUE GAS – REGULATION AND TREATMENT

Combustion of fossil fuels is the single largest anthropogenic source of several air pollutants of concern, including nitrogen oxides (NO_X), sulfur oxides (SO_X), carbon dioxide (CO_2), particulate matter, particulate lead, and mercury (U.S. EPA, 2003). Fossil fuels (coal and peat in particular) have been used as a combustion source for thousands of years. Excessive smoke resulting from the combustion of "sea coal" in London led King Edward I to ban its combustion in lime kilns in the year 1307 (Cooper and Alley, 1994). Following the industrial revolution, the increased use of fossil fuels for industrial production, transportation, and production of electricity resulted in the development of air pollution as a global concern. In the United States, the population increase and industrial boom following the end of the Great Depression resulted in a substantial increase in the release of primary combustion pollutants. Increased awareness of urban smoke and smog, as well as the deadly inversion episodes of Donora, Pennsylvania (1948) and London, England (1952), led to increased regulation of combustion and emissions at the local and regional levels (Cooper and Alley, 1994). In 1955, the United States Congress passed the Air Pollution Control Act, the first time the federal government had acknowledged what had been considered to be a state and local problem. This act provided money for air pollution research and

technical assistance, but deliberately avoided regulation or mandated pollution control. The Clean Air Act of 1963 replaced the 1955 Air Pollution Control Act, reallocating research funds and establishing federal authority to address interstate air pollution problems. The Motor Vehicle Air Pollution Control Act of 1965 established a program to regulate the air emissions from new motor vehicles, creating a uniform minimum standard for all 50 states, and allowing for increasingly regulated control as technology became available. The Air Quality Act of 1967 recognized that the federal government had the right and responsibility to enforce the use of control equipment to decrease air pollution and mandated the formation of air quality control regions to facilitate air emissions planning and control efforts (Cooper and Alley, 1994; U.S. EPA, 2003).

The Clean Air Act of 1970 is widely recognized as the most significant legislative step in the regulation and enforcement of air pollution control measures. That Act established the role of the federal government as regulator of air quality, a role that was extended by the Clean Air Act Amendments (CAAA) of 1977 and 1990 (U.S. EPA, 2003). The 1990 Clean Air Act Amendments (CAAA) is comprehensive and technically explicit legislation authorizing the EPA to establish standards to limit emissions of a number of atmospheric pollutants, including sulfur dioxide SO_X and NO_X. Title I and Title IV of the 1990 CAAA are relevant to NO_X control (U.S. EPA, 2003; U.S. EPA, April 24, 2004). Title I lists the National Ambient Air Quality Standards (NAAQS) for six criteria pollutants, summarized in Table 1 (U.S. EPA, April 24, 2004).

Table 1. National Ambient Air Quality Standards for six criteria pollutants, as described in the 1990 Clean Air Act Amendments (U.S. EPA, 2003).

POLLUTANT	STANDARD		
	Value (ppm)	Value ($\mu g/m^3$)	Criteria air pollutant type
Carbon Monoxide (CO) 8-hour Average 1-hour Average	9 35	10 40	Primary Primary
Nitrogen Dioxide (NO$_2$) Annual Arithmetic Mean	0.053	100	Primary & Secondary
Ozone (O$_3$) 1-hour Average	0.12	235	Primary & Secondary
Lead (Pb) Quarterly Average		1.5	Primary & Secondary
Particulate < 10 micrometers (PM-10) Annual Arithmetic Mean 24-hour Average		50 150	Primary & Secondary
Sulfur Dioxide (SO$_2$) Annual Arithmetic Mean 24-hour Average 3-hour Average	0.03 0.14 0.50	80 365 1300	Primary Primary Secondary

Title IV, commonly referred to as the Acid Rain Program, addresses control technologies for specific boiler types, including stationary coal-fired utility power plants. Title IV espouses a two-phase NO$_X$ control strategy. Effective January 1, 1996, Phase I established regulations for Group 1 boilers; *i.e.* dry-bottom, wall-fired boilers and tangentially-fired boilers. Phase II, which began on January 1, 2000, lower emissions limits are set for certain Group 1 boilers and regulations are established for Group 2 boilers, which include cell-burner, cyclone, wet-bottom wall-fired, and other types of coal fired boilers (U.S. EPA, 2002; U.S. EPA, 2003).

2.1.1 Secondary Pollutants

In addition to the direct impact that nitrogen oxide release to the atmosphere has on environmental quality, reactive NO_X compounds interact with other atmospheric constituents resulting in further negative impact to environmental quality. Because these pollutants are not present initially in combustion flue gas but are rather formed as a result of interaction of primary pollutants with naturally occurring atmospheric constituents, these newly formed pollutants are referred to as secondary pollutants. Following is a brief description of the relationship between NO_X emission and generation of the secondary pollutants ground-level ozone and fine particulate matter with a diameter less than 2.5 microns, or PM 2.5 (Cooper and Alley, 1994; U.S. EPA, 2002).

Ground level ozone is created by the chemical reaction of hydrocarbons and NO_X in the presence of ultraviolet radiation from sunlight. Since 1970, control of hydrocarbon emissions has been used to achieve ozone standards for individual urban areas (U.S. EPA, April, 2004). Efforts to curb anthropogenic hydrocarbon production have been successful, and now a large percentage of total hydrocarbon production originates from natural sources (Brown, et al., 1997). However, anthropogenic NO_X still constitutes moset of the total national NO_X emission. In order to achieve further reduction in ground level ozone, increased NO_X control has been regulated. Specific emission control technologies that are employed to meet the promulgated standards are determined by each state's implementation planning process, on a state-by-state basis (U.S. EPA, 2003).

The other pollutant targeted in the promulgated revised NAAQS is fine particulate matter. The EPA plans to maintain current PM_{10} standards (particulate matter less than 10 microns in diameter) and add new annual and 24-hour average standards for $PM_{2.5}$ (particulate matter less than 2.5 microns in diameter) (U.S. EPA, 2003). Analyses of ambient $PM_{2.5}$ indicate that these particles are composed primarily of ammonium sulfate and ammonium nitrate, created through atmospheric reactions involving sulfur dioxide and NO_X (U.S. EPA, 2002). Because these particles are so fine and because they are often formed after flue gas release from the stack, bag houses and electrostatic precipitators employed in power utility particulate collection do not address $PM_{2.5}$ problems (Cooper and Alley, 1994). It is therefore necessary to limit emission of the precursors (SO_2 and NO_X) that result in fine particulate production. This can be accomplished in coal fired electric utility processes by employing NO_X and SO_X control technologies.

In July of 1997, the U.S. EPA promulgated revised NAAQS for ozone and particulate matter, and proposed a rule for the regulation of regional haze to which these pollutants contribute. In October of 1998, the EPA promulgated a new rule to address long range transport of ozone by limiting the emissions

of NO_X during the summer in 22 northeastern states and the District of Colombia. This region has been identified as a major contributor to ozone non-attainment in downwind areas, and identified states were required to modify their implementation plans (state implementation plans or SIPs) according to Section 110 of the CAAA. State NO_X budgets were established by the EPA, and a NO_X emissions trading program, implemented by the states and enforced by the federal government. This trading program is designed to allow large stationary sources such as electric utility and industrial sources to trade emissions credits, and was designed based on a similar, successful SO_X emissions trading program. State NO_X budgets were based on the application of a population-wide 0.15 lb/mmBTU NO_X emissions for large energy generating units, 60% reduction from uncontrolled emissions from large non-energy generating boilers and turbines, 30% reduction from large cement kilns, and 90% reduction from large internal combustion engines.   Under this plan, states are allowed to decide what control measures can be adopted to meet emissions requirements. In addition, the cap-and-trade program creates incentives for NO_X generating entities to reduce emissions beyond the required level. Early reduction credits have been used to encourage sources to install controls early. At the time of promulgating the NO_X SIP call in 1998, EPA predicted that about 75 GW of selective catalytic reduction (SCR) treatment technology would be installed to meet the NO_X SIP call compliance. The deadline for SIP call compliance was set for May of 2004 (U.S. EPA, 2003).

2.1.2 Nitrogen Oxide Control Technologies

In primary NO_X control technologies, modifications are made to the combustion mechanism in order to reduce the amount of NO_X generated in the utility boiler. In secondary NO_X control technologies, the flue gas leaving the coal-fired utility boiler is treated to chemically reduce NO_X present in the flue gas to nitrogen gas or remove it from the gas stream via absorption (Sloss, 1992; Cooper and Alley, 1994).

2.1.2.1 Primary NO_X Control Technologies - Combustion Modification

2.1.2.1.1 Low NO_X Burners. The most commonly employed form of NO_X reduction technology is the low NO_X burner, which decreases generation of nitrogen oxides through utility boiler combustion modification steps. Low NO_X burners inhibit NO_X formation by controlling mixing of fuel and air using low excess air and staged (or off-stoichiometric) combustion methods.

Low excess air (LEA) firing simply decreases the amount of oxygen used in combustion to near stoichiometric concentrations. Excess air is air fed to the boiler, providing oxygen in excess of the

theoretical amount required to complete combustion. Standard coal fired electric utility boilers operate within the range of 15-30% excess air, but with new monitoring and control equipment, it is possible to maintain excess air concentrations at or slightly below the 15% level (Sloss, 1992). This operational measure can decrease thermal nitrogen monoxide (NO) production significantly. If, however, excess air concentrations are too low, combustion will become unstable, resulting in increased carbon monoxide (CO) emissions and increased unburnt carbon concentrations in the ash.

Staged combustion burns fuel in two or more steps. The primary zone is fuel-rich, while the secondary and subsequent stages are fuel-lean. In the fuel-rich zone, sub-stoichiometric levels of air are present, and therefore the combustion temperature is lowered and CO is formed, but very low levels of NO are formed. In the second and subsequent stages, air concentration is maintained at typical LEA firing levels. The partially uncombusted fuel is then provided with sufficient oxygen to complete combustion. Compared to conventional burners, low NO_X burners result in 40-60% less NO_X in the effluent gas. However, increased carbon content in the ash presents potential problems for the beneficial reuse of the byproduct.

2.1.2.2 Secondary NO_X Control Technologies - Post-Combustion Flue Gas Treatment

2.1.2.2.1 Selective Catalytic Reduction (SCR). The most advanced flue gas treatment method of NO_X reduction is Selective Catalytic Reduction (SCR). SCR uses a catalyst, typically consisting of a mixture of titanium oxide and vanadium oxide, to selectively reduce NO_X species to N_2 gas. The most commonly used reducing agent is NH_3 (Sloss, 1992).

Common reactions occurring on the catalytic surface are:

$$4NO + 4NH_3 + O_2 \Rightarrow 4N_2 + 6H_2O \tag{1}$$

$$2NO_2 + 4NH_3 + O_2 \Rightarrow 3N_2 + 6H_2O \tag{2}$$

and to a lesser extent:

$$NO + NO_2 + 2NH_3 \Rightarrow 2N_2 + 3H_2O \tag{3}$$

$$6NO_2 + 8NH_3 \Rightarrow 7N_2 + 12H_2O \tag{4}$$

There are several factors affecting efficiency of NO_X reduction in SCR processes. High NO_X concentration entering into the catalyst can exceed catalyst activity, requiring additional catalyst to avoid NO_X emission above the regulated limit. Low NO_X burners are often used in conjunction with SCR to decrease NO_X concentration entering into the catalyst (Sloss, 1992).

Flue gas temperature also affects catalyst efficiency. The temperature window for maximum SCR catalyst activity and selectivity occurs between 300 and 400°C, in which NO_X reduction of 80% or

greater is commonly achieved. Slightly outside this temperature window, this reduction efficiency diminishes greatly (Sloss, 1992).

Concentration and method of ammonia injection are also important factors to consider. Typically, concentrated ammonia is used as the reducing agent, but dilute aqueous (*i.e.* caustic) ammonia has been used in a few cases. Free ammonia is injected into the flue gas duct using a grid of nozzles. Air injected into the flue gas duct is only about 5% ammonia by volume. Concentrations of 15 - 27% ammonia are explosive (Sloss, 1992).

Finally, it is necessary to understand the catalytic properties of the catalyst being employed. As long as the activity of the catalyst is sufficient, increased ammonia injection will lead to increased NO_X reduction. But increased ammonia injection also results in emission of unreacted ammonia, which either passes through the flue gas equipment and leaves the plant out of the stack ("slip"), or adsorbs onto the fly ash and catalyst as ammonium salts. Estimates of the amount of unreacted ammonia that slips through the stack range between 20% and 50% of all unreacted ammonia. The relationship between the ammonia slip and the ammonia concentration on the fly ash is affected by such things as fly-ash concentration in the flue gas, ammonia concentration in the flue gas, and fly ash surface area. Sources state that about 20% of the non-slipping ammonia adsorbs to the air pre-heater while the other 80% precipitates onto the fly ash as ammonium salts.

In addition to increasing efficiency of NO_X conversion, increased catalyst activity results in higher oxidation rates for sulfur dioxide to sulfur trioxide, which can react with free ammonia in the presence of water to produce ammonium bisulfate (NH_4HSO_4). Ammonium bisulfate is a sticky compound that can cause corrosion, fouling, and blocking of equipment located downstream of ammonia injection. In a well designed and operated plant, ammonium bisulfate production can be avoided.
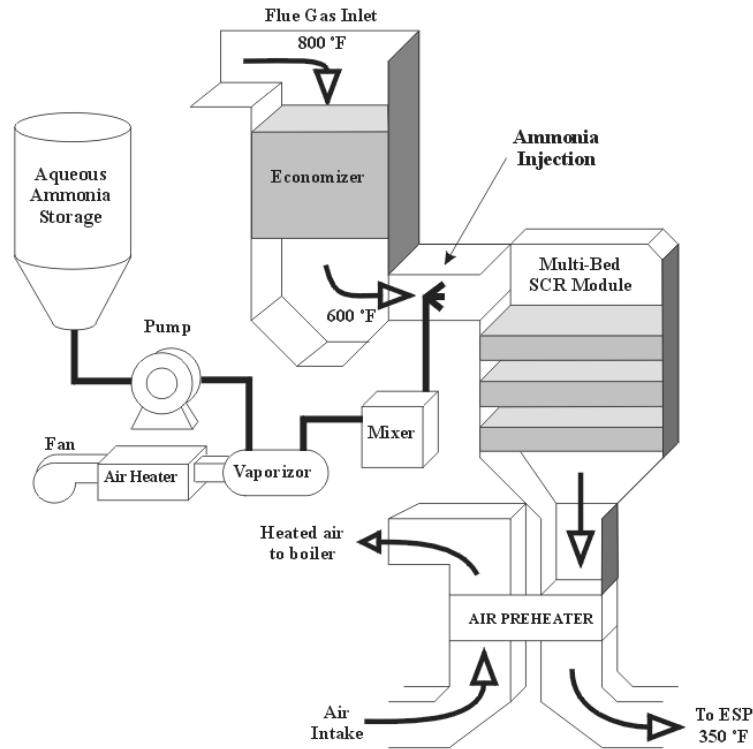
Figure 1. SCR system for NO$_X$ control in a coal fired utility boiler (U.S. DOE, 2004).

2.1.2.2.2 Selective Non-Catalytic Reduction (SNCR). Selective Non-Catalytic Reduction (SNCR) takes advantage of the fact that between 900 and 1000°C, NH$_3$ will reduce NO$_X$ to N$_2$ without the presence of a catalyst. Using SNCR, 40 - 60% reduction of NO$_X$ is possible. If this level of NO$_X$ reduction meets prevailing emissions requirements, then SNCR might be preferable to SCR because it is a simpler process to operate and maintain than SCR, and because initial capital costs and operational costs are less than those of SCR (Sloss, 1992).

      With SNCR treatment, it is important that ammonia addition occur in the previously mentioned temperature window because outside of this range, inadequate reduction of NO$_X$ results in unwanted emissions. Below this temperature window, the ammonia remains un-reacted and exits the system as free ammonia "slip" or precipitated on ash byproducts in the form of ammonium salts. Furthermore, nitrogen oxide reduction is not achieved under these conditions. Above the defined temperature window, NH$_3$ is oxidized to NO, thereby increasing nitrogen oxide concentration in the flue gas (Sloss, 1992).

      By employing low-NO$_X$ burner combustion before SCR flue gas treatment, the amount of NO$_X$ being initially produced is reduced by lowering the amount of NO$_X$ that needs to be chemically reduced in the selective reduction step. Such a combination is less expensive than using selective reduction

exclusively because expensive catalyst capacity is conserved. However, the ash byproduct from such a process is ammonia bearing and has high loss of ignition (6 to 8%).
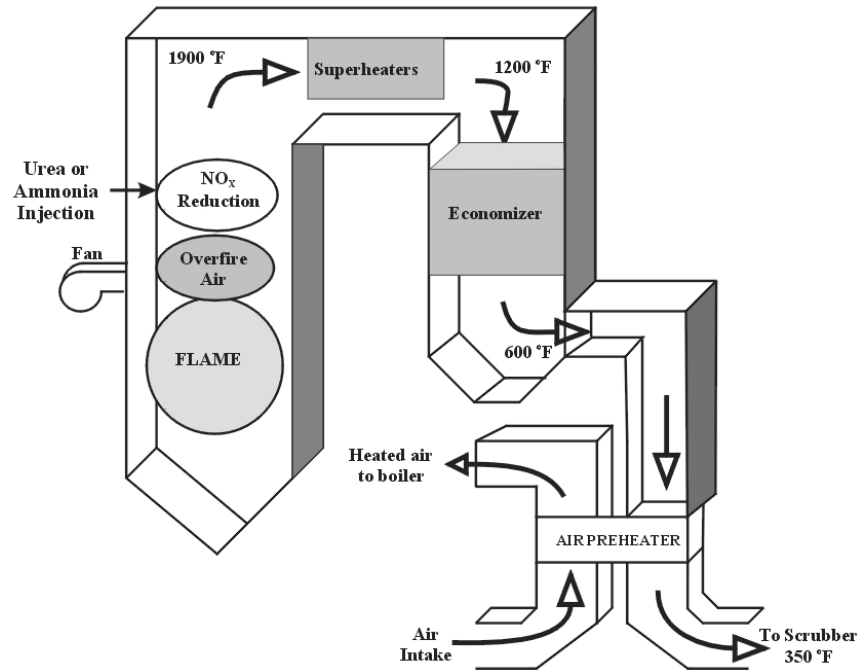
Figure 2. SNCR system for NO$_X$ control in a coal fired boiler. (U.S. DOE, 2004)

2.1.2.2.3 Aerobic/Anoxic Biofiltration. Biofilters and biotrickling filter bioreactor configurations have been proposed for removal and treatment of NO$_X$ present in combustion flue gas. Biofilters employ microorganisms that are immobilized on a matrix to biodegrade contaminants present in the gas phase or present in vapor. Contaminants are absorbed from the gas phase into the thin aqueous film present on the surface of the active biofilter. Absorbed contaminants then diffuse through the thin liquid film and are degraded by bacteria present both at the biofilm surface and at depth within the biological layer. Therefore, biofilter technology can be effective for contaminants that are sufficiently soluble and biodegradable to allow diffusion and treatment to occur in a relatively short time. Biofilter technology has been demonstrated both on the laboratory scale and in field application for such contaminants as: alcohols, gasoline vapors, the benzene, toluene, ethylbenzene and toluene (BTEX) class of compounds, and reduced sulfur compounds such as hydrogen sulfide (du Plessis *et al.*, 1988). Several researchers have considered treating flue gas NO$_X$ using biofilter technology, by employing anoxic reduction based on denitrification. This method has been demonstrated successfully, but mass transfer limitations related

to the low solubility of nitric oxide prevent it from being seriously considered for large-scale implementation (Breckenridge, 2000).

Ultimately, application of biofilter technology for NO_X removal and treatment from waste gas streams will depend on advancing removal efficiency, decreasing gas residence time, and decreasing gas pressure drop (Flanagan *et al.*, 2002).

2.1.2.2.4 NO_X Absorption. Nitric oxide is only sparingly soluble in water, with a Henry's Law coefficient of 1.9×10^{-3} M/atm at 25 °C (Perry, 1963). By amending scrubber solution in an absorption column with the ferrous chelate of ethylenediaminetetraacetic acid (EDTA), this solubility limitation can be overcome. Dissolved NO in bulk solution reacts with ferrous EDTA chelate, effectively removing it from bulk solution and allowing the dissolution of more NO. The reaction between dissolved NO and the ferrous EDTA chelate is described in Equation 5.

$$Fe(II)EDTA]^{2-} + NO \longleftrightarrow NO\bullet Fe(II)EDTA^{2-} \qquad (5)$$

The product of this reaction is a reversible adduct between the NO molecule and the ferrous EDTA molecule, also referred to as a nitrosyl adduct to the ferrous EDTA complex. Scrubbing solution capacity is, therefore, a function of ferrous EDTA concentration, with the theoretical scrubbing capacity a 1:1 molar ratio of ferrous EDTA to NO. Following adduct formation, the nitrosyl adduct must be removed from spent scrubber solution in order to regenerate scrubbing capacity. In addition, any ferrous EDTA that was oxidized to ferric EDTA as a result of exposure to oxygen during the absorption process will also have to be reduced back to the ferrous form, as NO will not form a reversible adduct with ferric EDTA. Several possible reducing mechanisms have been explored and are reported on in the literature. Those mechanisms are discussed in Chapter 3.

2.1.3 Overview of Sulfur Dioxide Scrubbing

In conventional treatment of sulfur-bearing flue gas from coal combustion, sulfur dioxide is removed from flue gas by a scrubbing process employing "throw-away" or regenerated scrubbing slurries (Cooper and Alley, 1994).

Limestone scrubbing is the simplest sulfur removal technique, due to the availability and inexpensive cost of limestone in many areas. Limestone slurry is contacted with flue gas in a spray tower.

In the tower, SO_2 is absorbed, neutralized, and partially oxidized to calcium sulfite and calcium sulfate, represented by:

$$CaCO_3(s) + H_2O + 2SO_2 \longrightarrow Ca^{+2} + 2HSO_3^- + CO_2(g) \tag{6}$$

$$CaCO_3(s) + 2HSO_3^- + Ca^{+2} \longrightarrow 2CaSO_3 + CO_2 + H_2O \tag{7}$$
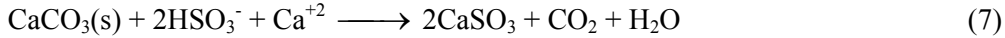
Scrubbing can also be carried out with lime (CaO, quicklime or hot lime), which is considerably more reactive than limestone. Net reactions for this process are:

$$CaO + H_2O \longrightarrow Ca(OH)_2 \tag{8}$$

$$SO_2 + H_2O \longleftrightarrow H_2SO_3 \tag{9}$$

$$H_2SO_3 + Ca(OH)_2 \longrightarrow CaSO_3 \cdot 2H_2O \tag{10}$$

$$CaSO_3 \cdot 2H_2O + \tfrac{1}{2} O_2 \longrightarrow CaSO_4 \cdot 2H_2O \tag{11}$$
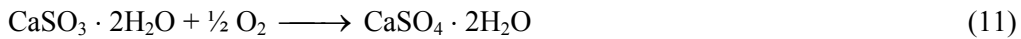
Lime scrubbing can achieve higher SO_2 removal than limestone scrubbing and allows more flexibility in operation, but has a high reagent cost (Cooper and Alley, 1994).

Dual alkali systems avoid problems with scrubber tower scaling and plugging by using sodium sulfite/sodium hydroxide solution for absorption/neutralization of SO_2 inside the scrubbing tower. Sodium sulfite/sulfate formed in the scrubber is highly soluble in water, so scaling within the scrubbing tower is not a problem. After leaving the scrubbing tower, this solution is treated with lime or limestone and makeup sodium hydroxide or soda ash (Na_2CO_3), resulting in sulfite/sulfate precipitation (Cooper and Alley, 1994).

Forced oxidation system employ conventional limestone scrubbing followed by oxidation of $CaSO_3$ slurry to produce gypsum ($CaSO_3$) sludge. This sludge can be dewatered and used to produce gypsum wall-board.

Magnesium oxide (MgO) processes have an absorption step similar to that of lime or limestone scrubbing. Wet scrubbing with a $Mg(OH)_2$ slurry produces $MgSO_3/MgSO_4$ solids, which is then fired in a high-temperature calciner (kiln in the presence of coke or some other reducing agent) to regenerate MgO and a 15% SO_2 gas stream, which can be used to make sulfuric acid (Cooper and Alley, 1994).

2.2 OXIDATION REDUCTION POTENTIAL

2.2.1 Electron activity (pε) and redox potential (EH)

Aqueous systems contain no free electrons, but the relative electron activity, as an intensity parameter, can still be defined (Stumm and Morgan, 1996).

$$p\varepsilon = -log\ \{e^-\} \tag{12}$$

pε is the hypothetical electron activity ($\{e^-\}$) and measures the tendency of a system to accept or transfer electrons. In a highly reducing system, the tendency to donate electrons (i.e., the hypothetical "electron pressure" or electron activity) is relatively large and pε is low. In contrast, high pε values indicate a relatively low electron activity and a relatively oxidizing system. Any reduction reaction can be written as:

$$Ox + ne^- \rightarrow Red \tag{13}$$

In this reaction, an oxidized species (Ox) reacts with n electrons to form the reduced species (Red). The Law of Mass Action defines the constant K^* as:

$$\{Red\}/\{Ox\}\ e^{-n} = K^* \tag{14}$$

This leads to:

$$p\varepsilon = (1/n)log\ K^* +\ (1/n)log\ [\{Red\}/\{Ox\}] \tag{15}$$

Since no free electrons are present in the system, the shown reduction reaction must be linked to an oxidation reaction. For reference purposes, the oxidation of hydrogen is used leading to the equation:

$$p\varepsilon = p\varepsilon^\circ + (1/n)log\ [\{Red\}/\{Ox\}] \tag{16}$$

Here, pε° is the standard electron activity of the actual reduction half reaction when coupled to the oxidation of hydrogen under standard conditions. The electron activity is, via the Nernst equation, linked to the redox potential, E_H

$$p\varepsilon =\ E_H / (2.3RTF^{-1}) \tag{17}$$

or:

$$E_H = E_H^O + \left(2.3RT/nF\right)log\left[\{Ox\}\Big/\{Red\}\right] \tag{18}$$

where:

T is the absolute temperature in Kelvin

R is the gas constant

F is Faraday's number

At 25°C, 2.3 RTF^{-1} = 0.059 V mol^{-1} (Snoeyink and Jenkins, 1980).

The redox potential is a measure of a solution's affinity to accept or donate electrons. When the E^0 for a given reaction is positive, the reaction will proceed spontaneously. E_H and E^0 values are reported in units of volts or millivolts.   Extensive reference tables are available in the literature that provide lists of half-reactions and their corresponding standard potentials at 25ºC . Table 2 lists half-reactions and standard potentials for several reactions of interest.

Table 2. Standard electrode potentials at 25ºC for half-reactions of interest.

Half Reaction	E_H (volts)	Source
$H_2 \longrightarrow 2H^+ + 2e^-$	0	(Krauskopf, 1967)
$AgCl(s) + e^- \longrightarrow Ag(s) + Cl^-$	+0.222	(Krauskopf, 1967)
$SO_4^{2-} + 10H^+ + 8e^- \longrightarrow H_2S_{(g)} + 4H_2O$	+0.34	(Snoeyink and Jenkins, 1980)
$SO_4^{2-} + 9H^+ + 8e^- \longrightarrow HS^- + 4H_2O$	+0.24	(Snoeyink and Jenkins, 1980)
$SO_4^{2-} + 8H^+ + 8e^- \longrightarrow S^{2-} + 4H_2O$	+0.16	(Krauskopf, 1967)
$S_{(s)} + 2H^+ + 2e^- \longrightarrow H_2S_{(g)}$	+0.17	(Snoeyink and Jenkins, 1980)
$SO_4^{2-} + 2H^+ + 2e^- \longrightarrow SO_3^{2-} + H_2O$	-0.04	(Snoeyink and Jenkins, 1980)
$Fe^{+3} + e^- \longrightarrow Fe^{+2}$	+0.77	(Krauskopf, 1967)
$Fe^{+3} EDTA + e^- \longrightarrow Fe^{+2}EDTA$	+0.12	(Stumm and Morgan, 1996)
$Fe^{+3} EDTA + e^- \longrightarrow Fe^{+2}EDTA$	+0.096	(Straub, et. al, 2001)
$Pt^{2+} + e^- \longrightarrow Pt^0$	+1.20	(Snoeyink and Jenkins, 1980)
$2NO^{3-} + 12H^+ + 10e^- \longrightarrow N_{2(g)} + 6H_2O$	+1.24	(Snoeyink and Jenkins, 1980)
$6CO_2 + 8H^+ + 8e^- \longrightarrow CH_{4(g)} + 2H_2O$	+0.17	(Snoeyink and Jenkins, 1980)
$2NO + 2H^+ + 2e^- \longrightarrow N_2O + H_2O$	+1.766	(Lide and Frederikse, 1995)
$N_2O + 2H^+ + 2e^- \longrightarrow N_{2(g)} + H_2O$	+1.591	(Lide and Frederikse, 1995)
$2NO + 4H^+ + 4e^- \longrightarrow N_{2(g)} + 2H_2O$	+1.678	Calculated from previous two
$2CO_2 + 7H^+ + 8e^- \longrightarrow CH_3COO^- + 2H_2O$	-0.28	(Rittmann and McCarty, 2001)
$^1/_6CO_2 + H^+ + 2e^- \longrightarrow {}^1/_{12}CH_3CH_2OH + ¼H_2O$	-0.32	(Rittmann and McCarty, 2001)
$O_{2(aq)} + 4H^+ + 4e^- \longrightarrow 2H_2O$	+1.27	(Snoeyink and Jenkins, 1980)

Typically, all half reactions are listed as reduction reactions, with a free electron present as a reactant. As discussed earlier, free electrons can not exist in solution, so listed reduction reactions must be coupled with an oxidative half-reaction so that all electrons are exchanged between the oxidized and reduced species. By reversing the direction of listed reduction half reactions, and reversing the sign (positive or negative) of the corresponding E_H value, oxidative reactions and corresponding standard

oxidation-reduction potential values can be determined. Two half reactions can then be added and balanced such that electrons cancel, and no free electrons are listed in the final redox reaction. E_0 can only be added if all electrons cancel, so that the nF components of the free energy terms are identical for both half reactions. When calculating ORP for a new half-reaction by adding two half-reactions, the E_0 values is not correct if the number of electrons transferred in each half-reaction does not match.

2.2.2 Gibb's Free Energy

In contrast, addition of Gibb's free energy values, which takes into account the number of electrons transferred, is always allowed. Gibbs free energy is defined as:

$$\Delta G = - nFE_H \tag{19}$$

where ΔG is Gibb's energy of the reaction, defined as:

$$\Delta G = \Delta H - T\Delta S \tag{20}$$

where:

       T = absolute temperature in Kelvin

       ΔH = change in enthalpy

       ΔS = change in entropy

Combining the two previous equations yields an equation that can be used to calculate the actual energy yield, ΔG_r, for a given redox reaction at in-situ conditions.

$$\Delta G_r = \Delta G^0 + 2.3RT \log\left[\frac{\{Ox\}}{\{Red\}} \right] \tag{21}$$

where $\Delta G°$ is Gibb's energy of the reaction at standard conditions. When the $\Delta G°$ of a reaction is negative, the reaction will proceed spontaneously as written (Snoeyink and Jenkins, 1980). Table 3 lists several redox reactions and calculated $\Delta G°$ values relevant to the process described herein.

Table 3. Summary of several oxidative and reductive reactions of interest, including calculated or reported Gibb's energy at standard conditions.

Oxidation (electron donating reactions)		ΔG_o, kJ
Ethanol $\rightarrow$ Acetate Acetate $\rightarrow$ Methane Fe(II)L $\rightarrow$ Fe(III)L(**) Sulfite $\rightarrow$ Sulfate	$CH_3CH_2OH + H_2O \longrightarrow CH_3COO^- + H^+ + 2H_2$ $CH_3COO^- + H_2O \longrightarrow HCO_3^- + CH_4$ $2[Fe(II)EDTA]^{2-} + \frac{1}{2} O_2 + 2H^+ \longrightarrow 2[Fe(III)EDTA]^- + H_2O$ $SO_3^{2-} + \frac{1}{2} O_2 \longrightarrow SO_4^{2-}$	+9.6 -31.0 -86.195 -171.85
Respirative (electron accepting reactions)		
$HCO_3^- \rightarrow$ Acetate $HCO_3^- \rightarrow$ Methane Sulfate $\rightarrow$ Sulfide Nitrate $\rightarrow$ Nitrogen gas	$2\,HCO_3^- + 4\,H_2 + H^+ \rightarrow CH_3COO^- + 4\,H_2O$ $HCO_3^- + 4\,H_2 + H^+ \rightarrow CH_4 + 3\,H_2O$ $SO_4^{2-} + 4\,H_2 + H^+ \rightarrow HS^- + 4\,H_2O$ $CH_3COO^- + SO_4^{2-} + H^+ \rightarrow 2\,HCO_3^- + H_2S$ $2\,NO_3^- + 5\,H_2 + 2\,H^+ \rightarrow N_2 + 6\,H_2O$	-104.6 -135.6 -151.9 -59.9 -1120.5
NO $\rightarrow$ Nitrogen gas (*) Fe(III)L $\rightarrow$ Fe(II)L(**)	$1/6\,CH_3CH_2OH + [NO\bullet Fe(II)EDTA]^{2-} \longrightarrow [Fe(II)EDTA]^{2-} + \frac{1}{2} N_2 + 1/3\,CO_2$ $\left[NO\bullet Fe(II)EDTA\right]^{2-} + \frac{1}{4} H^+ + \frac{1}{4} CH_3COO^- \longrightarrow \frac{1}{2} N_2 + \left[Fe(II)EDTA\right]^{2-} + \frac{1}{2} H_2O + \frac{1}{2} CO_2$ $\left[NO\bullet Fe(II)EDTA\right]^{2-} + H_2 \longrightarrow \frac{1}{2} N_2 + \left[Fe(II)EDTA\right]^{2-} + H_2O$ $[Fe(III)EDTA]^- + 1/12\,CH_3CH_2OH + \frac{1}{4} H_2O \longrightarrow [Fe(II)EDTA]^{2-} + 1/6\,CO_2 + H^+$ $[Fe(III)EDTA]^- + 1/8\,CH_3C00^- + 1/4\,H_2O \longrightarrow [Fe(II)EDTA]^{2-} + \frac{1}{4} CO_2 + 7/8\,H^+$ $[Fe(III)EDTA]^- + \frac{1}{2} H_2 \longrightarrow [Fe(II)EDTA]^{2-} + H^+$ $[Fe(III)EDTA]^- + \frac{1}{2} SO_3^{2-} + \frac{1}{2} H_2O \longrightarrow [Fe(II)EDTA]^{2-} + \frac{1}{2} SO_4^{2-} + H^+$	-446.53 -331.53 -324.11 -42.191 -13.018 -10.078 -11.758

(*) present as adduct of $[Fe(II)EDTA]^{2-}$
(**) Ligand (L) in all cases is $EDTA^{4-}$

2.3 MICROBIALLY-MEDIATED REDOX PROCESSES

Several of the reactions listed in Table 3 will not proceed to a significant extent spontaneously, but, rather, require the presence of a non-reacting catalyst to decrease the activation energy threshold and allow the described reaction to proceed. In the case of this research, the catalyst is introduced as the active enzymes of bacteria that facilitate or mediate the redox reactions of interest. The reduction reactions of interest in this study are variations on microbially-catalyzed reduction reactions that are ubiquitous in the natural environment. The following general description of microbially-mediated anoxic/anaerobic reduction reactions and the properties of microorganisms that catalyze them provides context for the industrial biological treatment process considered herein.

2.3.1 General Description of Microorganisms

Microorganisms, as with all living organisms, require a source of energy, a source of carbon, and inorganic nutrients (including nitrogen, phosphorus, sulfur, and metallic elements such as sodium, potassium, calcium, magnesium, manganese, iron, zinc, and cobalt) to sustain life and proliferate their species. The method by which microorganisms access energy and carbon varies significantly. It is useful, therefore, to classify microorganisms by the carbon that they utilize and their source of energy.

The vast majority of all microorganisms utilize carbon from either carbon dioxide or organic compounds found in their environment. Microorganisms that depend on organic compounds for carbon are called heterotrophs. Those that use carbon dioxide for their carbon are called autotrophs. Because energy is required to drive the reductive reaction in which CO_2 is converted to organic cell tissue, autotrophs use more energy for cell production and, in general, have a lower cellular yield than do heterotrophs (Metcalf and Eddy, 1991).

In addition to carbon source, bacteria are distinguished based on the source of reducing equivalents that they use (their electron source) for metabolism. Organisms that utilize energy from sunlight (photosynthesis) are called phototrophic and those that use chemicals from their environment for energy are referred to as being chemotropic. Chemotrophic microorganisms can be further subdivided based on the type of compounds from which they derive energy. Those microorganisms that oxidize inorganic compounds (*e.g.*, water, hydrogen, sulfide or ammonia) for this purpose are called lithotrophs,

and those that utilize organic compounds (*e.g.*, sugars or organic acids) as their source of reducing equivalents are called organotrophs (Voet *et al.*, 2002).

Dissimilatory reduction reactions generate energy for use by the microorganisms (as electron acceptors in energy metabolism), while assimilatory reduction processes reduce oxidized inorganic species for incorporation into biological compounds (cellular nutrients). Microorganisms can also be placed into one of three groups, based on their response to the presence of oxygen. Bacteria that can only grow in the presence of oxygen are called aerobes, those that grow only in the absence of oxygen and are called strict anaerobes; and bacteria that can grow in the presence of low levels of oxygen and are called facultative anaerobes.

2.3.2 Ecological Succession Based on Thermodynamic Preference

In general, microbially-catalyzed reduction reactions proceed in order of thermodynamic preference, with the higher energy yielding reactions proceeding to near completion before less energy yielding reactions (Lensing *et al.*, 1994). Among reactions that occur in the environment, the commonly-observed progression of reduction of oxidized species is as follows:

- Aerobic respiration
- Anoxic denitrification
- Dissimilatory ferric iron/ Mn(III) reduction
- Dissimilatory sulfate reduction
- Anaerobic Methanogenesis (Pohland and Kim, 2000)

Because of this thermodynamically regulated reductive succession, a parallel hierarchy of ecological succession manifests, in which bacteria capable of utilizing energy from more energy yielding reducing reactions thrive before those bacteria deriving trophic activity from lower energy yielding reactions. This ecological succession has been observed in such diverse environments as eutrophic lakes, engineered bioreactors, and groundwater contamination plumes (Christensen *et al.*, 2000).

When we consider reduction of oxidized species in a plug flow reactor configuration, it is expected that reduction would also proceed spatially in this manner. In the case of attached growth systems, it is believed that this ecological succession will express itself as zones of distinct or semi-distinct biological activity. That is to say, the region nearest the influent of the reactor will be predominated by aerobic bacteria, followed by denitrifying bacteria, and ferric iron /Mn(IV) reducers. Finally sulfate reduction and methanogenesis will predominate in the remainder of the reactor. These

zones of activity should be discernable by measurement of oxidation-reduction potential as well as by observation of relative activity of bacteria from different locations in the reactor (Sam-Soon, *et al.*, 1990).

2.3.3 Characteristics of Aerobic Microorganisms

Aerobic organisms are capable of oxidizing a wide variety of organic compounds and expressing alternative terminal oxidases. Aerobic bacteria are, generally speaking, excellent scavangers of dissolved oxygen, and can function at dissolved oxygen concentrations as low as 1 mM. Aerobic bacteria use diatomic oxygen or peroxide as reactants in which one or more oxygen atoms are incorporated into an organic carbon molecule. Using oxygenase and peroxidase enzyme activity, aerobic bacteria can successfully oxidize simple organics, as well as more complex molecules such as aliphatic and aromatic hydrocarbons and lignin (Voet *et al.*, 1994).

2.3.4 Fermentation, Hydrogen Partial Pressure, and Anaerobic Syntrophy

In anaerobic ecosystems, organic matter is generally degraded by consortia of microorganisms. Fermentive bacteria often produce fermentation acids, H_2 and formate. These fermentation products are then oxidized in completion of any of a wide variety of reduction reactions. However, anoxic oxidation of acids such as propionate and butyrate, with H_2 or formate as reduced product, has positive standard free-energy change. These oxidations are exergonic (energy releasing) only when H_2 partial pressure is extremely low (Harper and Pohland, 1986). Bacteria can grow on these substrates only when co-cultured with H_2-using organisms. Bacterial H_2 oxidation is carried out by all major respiratory groups of bacteria and archaea, including nitrate reducers, denitrifiers, SRB, and methanogens. Many hydrogen oxidizers are autotrophic. This syntrophy is a vital relationship by which anaerobic consortia thrive. Following is a more detailed consideration of several microbially-mediated reduction reactions that are relevant to the current study (McCarty and Smith, 1986).

2.3.5 Microbially-Mediated Oxidation and Reduction of Nitrogen

Denitrification is an important step in the global nitrogen cycle, reducing nitrate in surface water, groundwater, and wastewater streams to insoluble nitrogen gas that can be removed from aqueous systems. In order to understand implications of denitrification of a process stream carrying ferrous

EDTA-nitrosyl complexes, it is necessary to first understand phenomena of standard nitrate denitrification. Chemical, biological, and process aspects of denitrification are summarized herein.

2.3.5.1 Nitrogen Cycle. The nitrogen cycle is a series of chemical reactions, many of which are biologically mediated, that oxidize and reduce nitrogen through various chemical forms as a function of environmental conditions. The oxidation reactions result in the conversion of NH_4^+ to NO_2^- and then ultimately to NO_3^-, known as nitrification. The reduction reactions taking nitrate to nitrite and then to the ammonium ion are collectively referred to as nitrate reduction. Reduction of nitrate to nitrogen gas (denitrification), and reduction of nitrogen gas to ammonium ion (nitrogen fixation) can also occur. In addition to these oxidation/reduction reactions, incorporation of ammonium ions into nitrogen-containing organic matter (amination) or release of ammonium ion from organic matter (deamination or ammonification) also play a role in the natural nitrogen cycle. The nitrogen cycle is summarized in Figure 3.
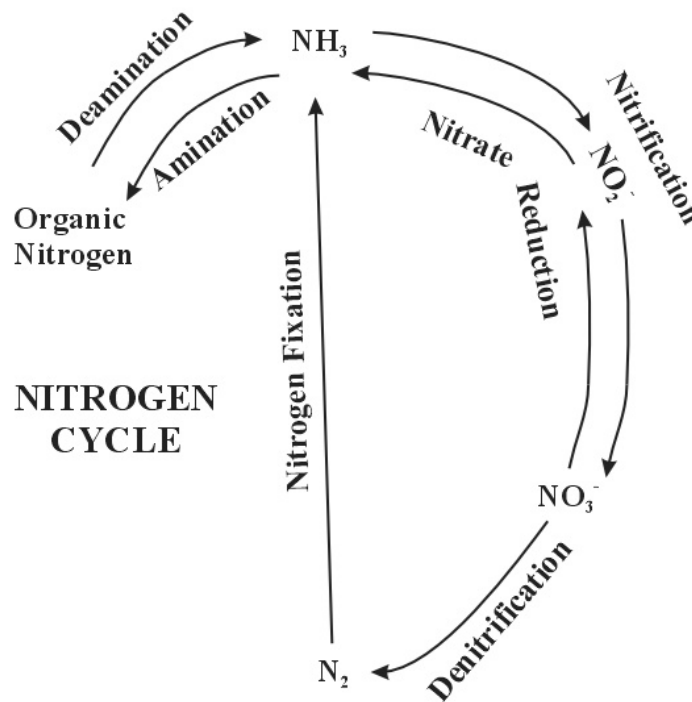
Figure 3. Reactions involved in the nitrogen cycle (Snoeyink and Jenkins, 1980)

2.3.5.2 Nitrification. Nitrification is the biological oxidation of ammonia to nitrate (NO_3^-) via formation of nitrite (NO_2^-) intermediate. The autotrophic bacteria that carry out this oxidation are of the genera *Nitrosamonas* and *Nitrobacter*. *Nitrosamonas* is responsible for oxidizing ammonia to the intermediate

nitrite, which is then converted by *Nitrobacter* to nitrate. Because no nitrite build up is observed during nitrification, conversion of nitrite to nitrate is generally acknowledged to be the rate-limiting step in the overall nitrification process. These reactions may be written as:

Nitrosamonas oxidation of ammonium ion:

$$55\ NH_4^+ + 76\ O_2 + 109\ HCO_3^- \rightarrow C_5H_7O_2N + 54\ NO_2^- + 57\ H_2O + 104\ H_2CO_3 \quad (22)$$
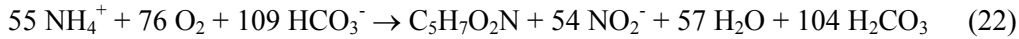
and *Nitrobacter* oxidation of nitrite to nitrate:

$$400\ NO_2^- + NH_4^+ + 4\ H_2CO_3 + HCO_3^- + 195\ O_2 \rightarrow C_5H_7O_2N + 3\ H_2O + 400\ NO_3^- \quad (23)$$
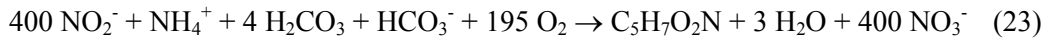
or, further simplified to:

$$2NH_4^+ + 3O_2 \rightarrow 2NO_2^- + 4H^+ + 2H_2O \quad (24)$$

and

$$2NO_2 + O_2 \rightarrow 2NO_3^- \quad (25)$$

respectively (Metcalf and Eddy, 1991).

2.3.5.3 Denitrification (Dissimilatory Nitrate Reduction). Denitrification is the reduction of NO_3 to N_2, and is carried out by facultative anaerobes that substitute NO_3 for O_2 as the terminal electron acceptor. This substitution requires use of an alternate terminal reductase to allow the stepwise reduction of nitrate to nitrogen gas via nitrite, nitric oxide and nitrous oxide. Nitrate is a thermodynamically less favorable terminal electron acceptor, as compared to oxygen, and has been reported to result in 40% lower biomass yield (Ka *et al.*, 1997). Denitrifiers are capable of oxidizing complex organic carbon compounds directly to CO_2. There are several genera of bacteria capable of reducing nitrate and nitrite under anoxic conditions, including *Achromobacter*, *Aerobacter*, *Alcaligenes*, *Bacillus*, *Brevibacterium*, *Flavobacterium*, *Lactobacillus*, *Micrococcus*, *Proteus*, *Pseudomonas*, and *Spirillum (Etchebehere et al., 2001)*. In practice, denitrifying reactors generally employ a consortium of bacteria of these genera .   The number of identified denitrifiers is second only to aerobic heterotrophs.

A theoretical stoichiometric equation for denitrification with ethanol as the carbon source was reported by Constantin and Fick (Constantin and Fick, 1997) as follows:

$$5\,C_2H_5OH + 12\,NO_3^- + 12\,H^+ \longrightarrow 10\,CO_2 + 21\,H_2O + 6\,N_2 \quad (26)$$

Research suggests that ethanol and other more complex organics must first be converted by to volatile organic acids (such as acetate) and H_2 (Æsøy and Ødegaard, 1994). Acetic acid is directly utilized by bacteria in the tricarboxylic cycle as acetate (Voet *et al.*, 2002).

Payne (1981) proposed that anoxic denitrification occurs by the sequential reduction of nitrate (NO_3^-), nitrite (NO_2^-), nitric oxide (NO), and nitrous oxide (N_2O) to molecular nitrogen (N_2) (Copp and Dold, 1998). It is generally accepted that denitrifying bacteria have nitric oxide reductase activity and that a

substantial fraction of reduction of nitrate proceeds through this stepwise pathway with NO as an intermediate (Feurhacker, et al., 2001; Schulthess et al. 1995).
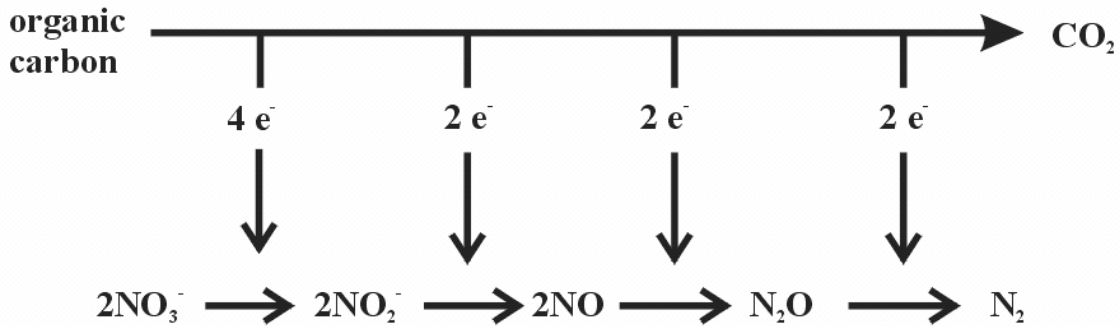
Figure 4. Stepwise reduction of nitrate by denitrifying bacteria (Fuerhacker *et al.*, 2001).

2.3.5.4 Denitrification Unit Operations. A number of unit processes for wastewater denitrification have been designed based on the environmental conditions under which microbially-mediated denitrification may proceed. Many of these processes integrate nitrification and denitrification of wastewater in an effort to maximize organic nitrogen removal at the lowest operation expense. In aerobic treatment of wastewater (*i.e.*, activated sludge processes), nitrogen is transformed from ammonia-N to nitrate-N with no significant net denitrification (Metcalf and Eddy, 1991). In addition, aerobic wastewater treatment processes consume most of the available soluble organic substrate, leaving only a small amount of organic substrate trapped in the biomass.

While organic matter trapped inside the cells can be released through hydrolysis (the microbial process of breaking particulate and high molecular weight soluble organic compounds into smaller components), kinetics are slow and very large anoxic bioreactors would be required to achieve even partial denitrification with hydrolysis products as the sole carbon (Grady *et al.*, 1999). One alternative is to add a more readily available electron donor/carbon source to the bioreactor (*e.g.*, ethanol or methanol). While this would overcome the slow kinetics of using cellular material as the carbon source for denitrification, constant addition of electron donor would be cost prohibitive for most applications. As a result, processes have been developed that use raw wastewater as the primary carbon source while also achieving aerobic nitrification and anoxic denitrification.

2.3.5.4.1 Combined Nitrification/Denitrification. In combined nitrification/denitrification processes, the raw wastewater and cell tissue fragments from endogenous decay of biomass is used as the primary source of carbon for the process. These systems are based on aerobic conversion of ammonia to nitrate and subsequent denitrification using raw sewage/hydrolyzed biosolids as the carbon source. One example is the proprietary, four-stage Bardenpho Process, which employs separate reaction zones for carbon oxidation, and aerobic nitrification, and anoxic denitrification. Influent wastewater passes initially through an anoxic denitrificaiton zone with recycled mixed liquor from a subsequent aerobic nitrification zone. This allows nitrate that is formed in and recycled from the subsequent aerobic reactor to be reduced under anoxic conditions to nitrogen gas with raw sewage as a free and readily degradable carbon source/electron donor (Siegrist and Gujer, 1994).

The effluent of the anoxic reactor then enters the aerobic reactor where ammonia from the influent feed is oxidized to form nitrate and organic matter is partially oxidized (*i.e.* activated sludge process). Some of this mixed liquor is recycled back to the first anoxic zone as previously described, while the remaining fraction of the aerobic reactor effluent continues on to a subsequent anoxic zone where remaining nitrate is reduced to nitrogen gas (Ra *et al.*, 2000). Following this second anoxic zone is a second aerobic reactor that completes microbially-mediated oxidation of organic waste material. Finally, biosolids are removed through a clarification process and some of the biosolids are recycled to the first anoxic reactor. Figure 5 illustrates the Bardenpho process.

```
Influent → [Anoxic Denitrifi-cation Zone] → [Aerobic combined oxidation nitrification zone] → [Anoxic denitrific-ation zone] → [Aerobic Zone] → (Secondary Clarifier) →
```

Mixed Liquor Return

Sludge Return   Waste Sludge
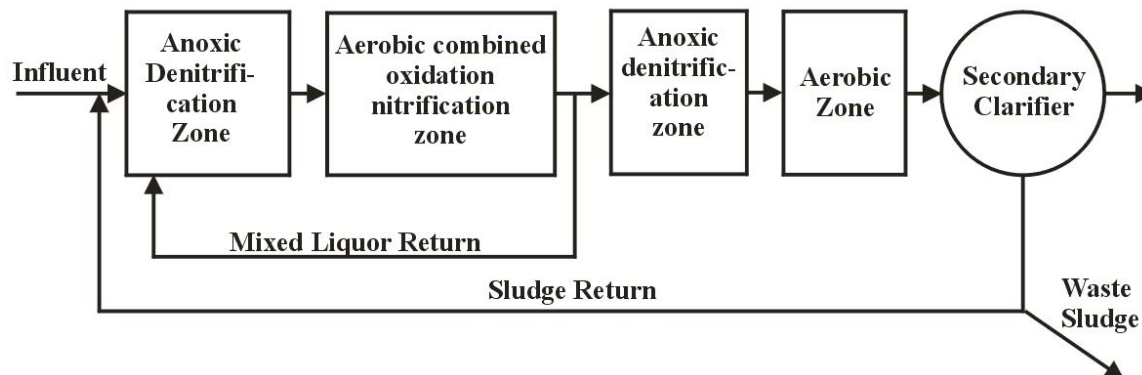
Figure 5. Schematic of the patented Bardenpho process for denitrification

A second, simpler combined nitrification/denitrification process is the oxidation ditch. An oxidation ditch is based on a loop-flow configuration in which wastewater enters a ditch and flows through a channel, entering initially into an anoxic zone. This allows nitrate-rich wastewater that has finished one cycle through the loop to contact with a readily-available carbon source (*i.e.*, sewage) promoting reduction of nitrate to nitrogen gas in the anoxic zone. After flowing approximately half way through the loop, the wastewater is mechanically aerated, marking the beginning of the reactor aerobic zone. This aerobic zone allows oxidation of ammonia from the wastewater as well as microbially-mediated oxidation of organic waste. After completing the first cycle through the loop, some fraction of the wastewater flow (equivalent to influent flow plus return sludge flow) leaves the reactor, is clarified and supernatant is discharged from the oxidation ditch process. Some biosolids that are removed from the clarifier bottom are recycled back to the beginning of the anoxic stage of the oxidation ditch (Metcalf and Eddy, 1991). Figure 6 illustrates the oxidation ditch nitrification/denitrification process.
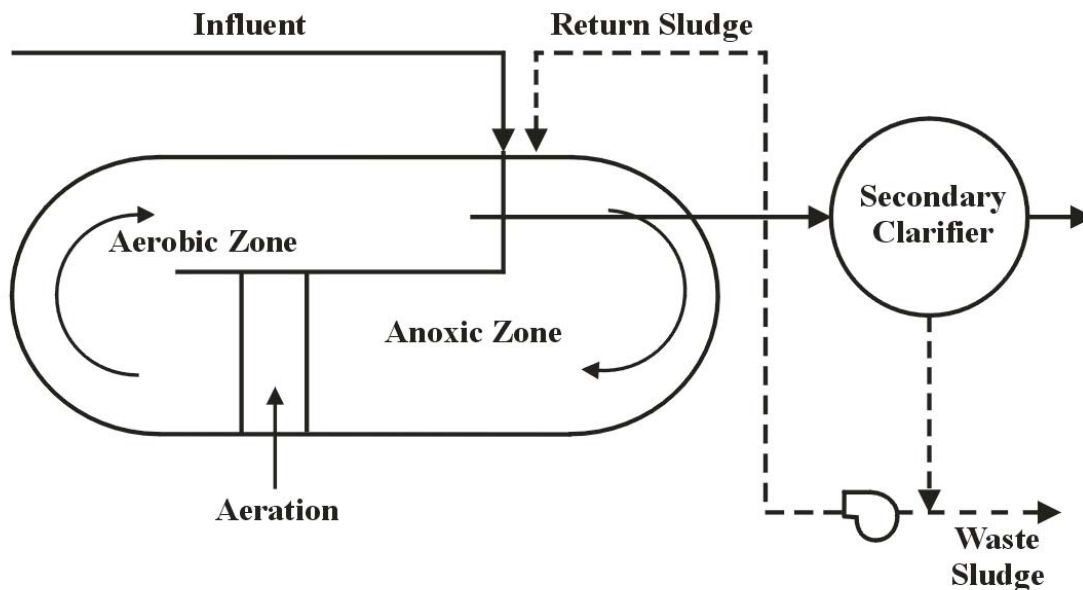
Figure 6. Oxidation ditch with secondary clarification and sludge recycle for denitrification of wastewater.

2.3.5.4.2 Separate-Stage Denitrification. In a separate-stage denitrification process, a simple, readily bioavailable carbon source/electron donor such as methanol or ethanol is introduced to the beginning of an anoxic reactor to support anoxic denitrification of a nitrified waste stream (Christensson *et al.*, 1994; Constantin and Fick, 1997). This type of process is used after oxidation of ammonia to nitrate in an aerobic reactor. Because aerobic processes quickly exhaust most of the readily bio-available organic matter, denitrification subsequent to aerobic reactors often requires a carbon source/electron donor for microbially-mediated denitrification to proceed. Unless the carbon source/electron donor being used is a waste stream from another industrial process, the cost of separate-stage denitrification is often too expensive to consider. Any anoxic reactor configuration can be successfully applied to separate-stage denitrification. Figure 7 is an example, with denitrification occurring in an attached growth bio-filter with methanol as the added carbon source/electron donor (Lemmer *et al.*, 1997).
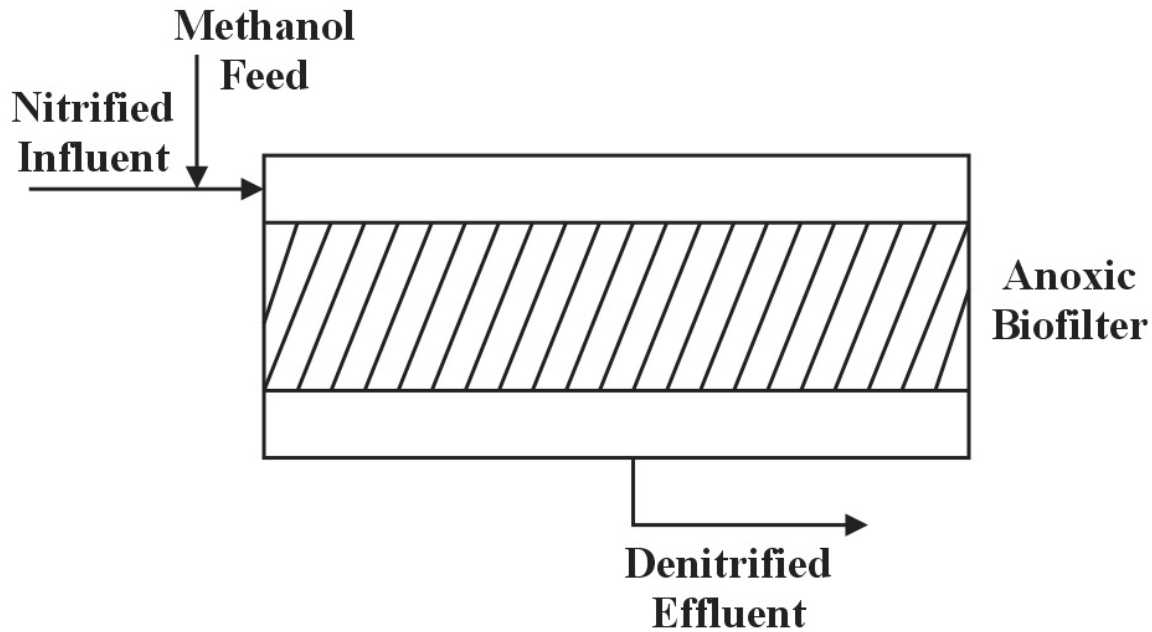
Figure 7. Schematic of an attached growth bio-filter with methanol addition for the separate stage denitrification of wastewater.

2.3.5.4.3 Single Reactor Nitrification/Denrification (Aerobic Denitrification). In a number of species of bacteria, denitrification has been observed to proceed at substantial rates under aerobic conditions (Patureau *et al.*, 1998) even though denitrification has been generally believed to be an anoxic process. Co-respiration of oxygen and nitrogen oxides under full-aerobic, continuously-cultured conditions has been demonstrated by investigators for *Thiosphaera pantotropha*, *Alcaligenes faecalis*, and *Pseudomonas nautical* (Patureau *et al.*, 1998). The recently isolated Gram-negative bacterium *Microvirgula aerodenitrificans* was also shown to aerobically catalyze denitrification through use of a periplasmic reductase (Patureau *et al.*, 1994).

The ability of some bacteria to catalyze denitrification aerobically allows consideration of single reactor processes for nitrification/denitrification of wastewater. Because such a reactor would require a relatively pure population of aerobic denitrifiers, such a process has not been successfully applied to reactors larger than bench-scale. Inorganic nitrogen (*i.e.*, ammonia) is often produced through anaerobic treatment of wastewater, and is typically removed through some post-treatment process involving separate nitrification and denitrification. A modification of this process described recently (Akunna *et al.*, 1992; 1994, Garuti *et al.*, 1992; Tilche *et al.*, 1994) involves denitrification and anaerobic digestion in the same bioreactor, with subsequent aerobic nitrification of ammonia to nitrate. This nitrate is then recycled back to the head of the anoxic/anaerobic bioreactor for denitrification. This process has proved successful, with nitrogen removals as high as 90% (Garuti *et al.*, 1992; Tilche *et al.*, 1994).

2.3.5.5 Inhibition of Denitrification. A brief discussion of environmental parameters that affect denitrification rate, including pH, sulfide concentration, dissolved oxygen concentration, and dissolved nitric oxide concentration follows.

2.3.5.5.1 Effect of pH on Anoxic Denitrification. A study by Glass and Silverstein (1998) investigated the effect of pH on anoxic denitrification of a high nitrate wastewater (2700 mg/l NO_3-N) in sequencing batch reactors. The study found that significant inhibition of denitrification occurred in the pH range of 6.5 – 7.0. Above pH 7.0, denitrification proceeds, but as pH increased, increased concentrations of nitrite were observed. The specific rate of nitrate reduction to nitrite (via nitrate reductase) increased with increasing pH. In the absence of nitrate, nitrite reductase specific activity was found to increase with increasing pH. However, in the presence of nitrate, the specific rate of nitrite reduction was found to remain the same with increasing pH. While intermediate nitrate concentration was found to vary between pH of 7.5 and 9.0, the overall specific denitrification rate remained the same independent of pH.   It should also be noted that because of the denitrification reaction (using acetate as an example carbon source):

$$0.625 \; CH_3COO^- + 1 \; NO_3^- + 0.375 \; H^+ \rightarrow 1.25 \; HCO_3^- + 0.5 \; N_2 + 0.5 \; H_2O \qquad (27)$$
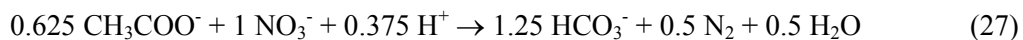
the net denitrification reaction consumes 0.375 equivalents of acidity per mole of nitrate reduced to N_2, and alkalinity is produced as a result of denitrification.   Therefore, if the system is inadequately buffered at the beginning of denitrification, pH will rise during denitrification until sufficient alkalinity is produced to buffer the system from further pH rise. Therefore, if the influent to an anoxic denitrification reactor is pH-neutral and non-buffered, denitrification will proceed without observable inhibition due to pH (Glass and Silverstein, 1998).

2.3.5.5.2 Sulfide Toxicity to Denitrifiers. Free dissolved sulfide in the form of H_2S or HS^- exhibits a toxic effect on biological denitrification. In particular, H_2S strongly inhibits the function of nitrous oxide reductase (Schoharting *et al.*, 1998). Because of this, even small concentrations of free dissolved HS^- result in accumulation of nitrous oxide in nitrate reducing environments. However, because of the thermodynamic advantage of denitrification over sulfate reduction (described in detail above), sulfide should not be present in a denitrifying process. Because sulfate reduction will proceed only after nitrate reduction is complete and because sulfide is a product of sulfate reduction, nitrate-reducing bacteria should have limited, if any, contact with free dissolved sulfide. However, in a completely-mixed reactor,

increased contact between sulfide and nitrate will occur, allowing inhibition of nitrate reduction (Speece, 1996).

2.3.5.5.3 NO Inhibition and Enzyme Activity of Denitrifiers.
Free dissolved NO and NO_2^- may also inhibit microbial growth due to their high affinity to metal ions located in the active sites of enzymes. NO in particular shows strong affinity to ferrous haem (similar binding geometry to O_2) the active group in cytochromes (Watmough *et al.*, 1999). However, the low solubility of NO prevents the accumulation of substantial concentrations of dissolved NO under most conditions.

2.3.5.5.4 Dissolved Oxygen Inhibition of Denitrification.
Denitrifying bacteria have demonstrated significant variability in their tolerance of dissolved oxygen (Ka *et al.*, 1997). Ludzack and Ettinger (1995) first described utilization of available soluble organic substrate from the beginning of the process.

$$U'_{DN} = U_{DN} \times 1.09^{(T-20)}(1-DO) \tag{28}$$

where:

   U'_{DN} = overall denitrification rate

   U_{DN} = specific denitrification rate, lb $NO_3 - N$/lb mixed liquor VSS*d

   T = wastewater temperature (°C)

   DO = dissolved oxygen concentration in solution

Based on this equation, it can be seen that at dissolved oxygen concentrations of 1 mg/l or greater, no denitrification will occur. Other researchers have described DO threshold concentrations around 0.2 mg/l above which denitrification is poor (Chan and Campbell, 1980; Knowles, 1982).

2.3.5.5.5 Oxidation-Reduction Potential Influence on Denitrification Rate.
Even at concentrations too low to be measured with a dissolved oxygen probe (< 0.1 mg/l), dissolved oxygen was found to have a significant effect on denitrification rate. Denitrification rate was found to decrease linearly with increasing oxidation reduction potential; a result that may be explained by the thermodynamic preference of aerobic over anoxic reactions. An example plot of data collected by Lie and Welander (1994) shows the linear decrease in denitrification activity with increasing oxidation reduction potential. A cycled aerobic/anoxic biological nutrient removal process for the treatment of piggery waste was shown to cycle between ORP values of –360 and +50 mV, ostensibly versus a standard hydrogen electrode (SHE). Authors describe the observation of a "nitrate knee" indicative of denitrification at an ORP of –200 mV (vs. SHE) (Ra *et al.*, 2000).

2.3.6 Dissimilatory Mn(IV) and Ferric Iron Reduction

Dissimilatory iron and manganese reduction occurs under similar redox conditions (Lensing *et al.*, 1994). These reduction reactions are carried out by strict and facultative anaerobes that oxidize organic acids and H_2, endproducts of hydrolysis and fermentation. Both soluble and insoluble forms of oxidized iron and manganese can be utilized, but must first be solubulized before they are available for microbial catalysis. Reactivity of the oxidized species is a function of such properties as particle size, solubility and surface area and greatly impacts reducibility of mineralized forms of the oxidized species. For example ferric iron exists as an insoluble mineral at neutral pH, but is more soluble and therefore more easily reduced at lower pHs. Bacteria access insoluble forms of iron and manganese using exogenous and endogenous extracellular electron shuttles to carry electrons to the minerals. An example of an exogenous electron shuttle commonly observed to chelate iron in the natural environment is humic acid. Endogenous electron shuttles include soluble cytochrome c or other microbially-generated molecules such as quinones or meanquinones (Lovely and Woodward, 1996). All serve to increase iron solubility and facilitate the transfer of electrons to the oxidized species. The physiology and biochemistry of dissimilatory iron and manganese reduction is relatively poorly understood.

Dissimilatory ferric iron-reducing bacteria couple the oxidation of organic compounds or hydrogen to the reduction of ferric iron, present in the environment as oxides or as the metal center in a chelate or enzyme. The observation and study of microbially-catalyzed ferric iron is well established. However, the biogeochemical significance of microbial ferric iron reduction was recognized only in the last 10 years.

Sediments and soils can contain iron minerals at quantities in the range of several 10 mmol per kg dry matter, and ferric iron is by mass the most important electron acceptor in such environments. Only in marine sediments, the high sulfate content (28 mM in seawater) counterbalances the dominance of ferric iron as electron acceptor. Numerous dissimilatory ferric iron-reducing bacteria belonging to different phylogenetic groups have been isolated from marine and freshwater sediments. Further novel strains of ferric iron-reducing bacteria were obtained from the deep terrestrial subsurface, a petroleum reservoir, a continental hot spring, and from a hydrothermal event system. An example of heterotrophic iron reduction using acetate as the electron donor is shown in Equation 29 (Nielsen, 1996).

$$. CH_3COO^- + 8\,Fe(III) + 4\,H_2O \rightarrow 2\,HCO_3^- + 9\,H^+ + 8\,Fe(II) \tag{29}$$
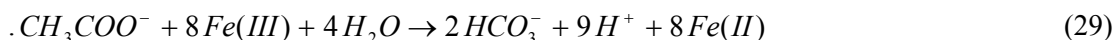
2.3.7 Biological Reduction of Sulfate

Microbially-mediated reduction of sulfate is carried out by a group of bacteria, commonly referred to as sulfate-reducing bacteria or SRB, that share the ability to reduce sulfate as the primary bioenergetic electron accepting reaction (Hansen, 1993). These bacteria employ sulfate as the primary terminal electron acceptor in the oxidation of a wide variety of organic and/or inorganic electron-donating compounds. Dissimilatory sulfate seduction is carried out primarily by strict anaerobes which oxidize organic acids and H_2. Partially reduced sulfur compounds such as $S_2O_3^{2-}$ (thiosulfate), SO_3^{2-} (sulfite), and S^o (elemental sulfur) may also be reduced to HS^-. Some SRB can also utilized NO_3^-, Mn(IV), Fe(III), and other oxidized metals as electron acceptors for generation of energy. The product of complete reduction of sulfate is sulfide ion. The chemistry of the microbially catalyzed reduction of sulfate is summarized by the following general reaction:

$$4AH_2 + SO_4^{2-} + H^+ \rightarrow 4A + HS^- + 4H_2O \tag{30}$$
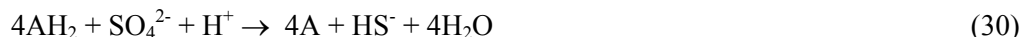
where AH_2 represents a generic electron donor (De Vegt and Buisman, 1996).

The general label SRB applies to many different types of bacteria that are capable of functioning under a wide variety of environmental conditions and utilizing a wide variety of energy and carbon sources. As of 1993, over 14 genera and 40 species of SRB had been identified. However, no species of SRB identified that is capable of surviving in an aerobic environment.

In order for microbially-catalyzed sulfate reduction to proceed, the bacteria require a strictly anaerobic aqueous environment. There are several literature sources that, in composite, describe a wide variety of oxidation reduction potential (ORP) conditions under which sulfate reduction has been observed to proceed. There seems to be consensus that ORP values of –100 mV (vs. standard hydrogen electrode) appears to be the upper threshold above which bacteria will fail to effectively catalyze the reduction of sulfate to sulfide. The existence of facultative anaerobic or aerobic sulfate reducing bacteria has, as yet, not been proven. Bioenergetics suggests that such bacteria should not be able to thrive, or at best would have long ago lost out in the ongoing competition of natural selection.

2.3.7.1 Sulfide Production. Hydrogen sulfide acts as a strong reducing agent that readily reacts with dissolved divalent metals to form highly insoluble metal sulfide precipitates.

$$H_2SO_4 + 4H_2 \rightarrow H_2S + 4H_2O \tag{31}$$

High sulfate waste streams can come from a number of industrial processes, including alcohol distilleries, yeast production plants, petroleum refining, mine drainage, and industrial production of fatty acids.

The product of methanogenic anaerobic fermentation, is odorless, non-toxic to microbial consortia, and very insoluble (about 18 mg/l at 35 °C). H_2S, in contrast, is malodorous, strongly corrosive, very soluble in water, inhibits microbial activity even at relatively low concentrations, and can be fatal to humans at concentrations as low as 800 to 1000 ppm with only 30 minutes of exposure. At high concentrations, it can be fatal immediately (Hansen, 1993; Rittmann and McCarty, 2001).

Methanogenesis and sulfate reduction proceed under strictly anaerobic conditions and both require strictly anaerobic environment to survive. Because they operate under very similar thermodynamic conditions (very negative oxidation-reduction potential), they often are active at the same time and in the same space, and therefore compete for substrate. Several factors affect the balance between MPB/SRB competition (Spanjers *et al.*, 2002). These factors include organic substrate concentration and type, maximum specific utilization rate (k_{max}), half velocity constant (k_s), nutrient availability, temperature, and biomass structural properties. Another factor influencing the balance between sulfate reduction and methanogenesis is the concentration of sulfate in solution. In general, high influent sulfate concentration will impact the overall thermodynamics of sulfate reduction (by increasing reactant concentration) to the extent that sulfate reduction should predominate over methanogenesis, which would otherwise have very similar thermodynamic properties to sulfate reduction (Speece, 1996).

In sulfate reducing systems, the fate of sulfur in solution can often be identified because of the strong characteristics of the products of sulfate reduction. Reduction of sulfate/sulfite in solution will result in generation of sulfide ions, per Equation 31. Sulfide in solution and headspace above the solution will speciate as a function of solution temperature, pH, and ORP (Speece *et al.*, 1997). Total dissolved sulfide in solution will be present either as S^{2-}, HS^-, or dissolved H_2S. The concentration of H_2S in head space is a function of solution temperature and the concentration of free dissolved H_2S in solution. If there are divalent metal ions in solution, they will rapidly react with dissolved sulfide ions to form metal sulfide precipitates, which typically have very low solubility. Table 4 lists the solubility of several commonly formed metal sulfide compounds. In addition to these possibilities, some sulfur may be integrated into microorganisms as a function of assimilatory reduction. Finally, dissolved sulfur compounds can, in certain conditions, react with nitrogen compounds to form sulfur-nitrogen species (Dravo Lime, 1992).

Table 4. Solubility of several metal sulfide compounds of interest.

Metal	Metal Sulfide	Solubility (mg/L)
Copper	Cu_2S	3×10^{-11}
	CuS	3×10^{-18}
Lead	PbS	4×10^{-9}
Cobalt	CoS	2×10^{-8}
Nickel	NiS	1×10^{-7}
Zinc	ZnS	3×10^{-7}
Iron	FeS	5×10^{-5}
Mercury	HgS	4.47×10^{-27}

The concentration of H_2S in the off-gas can be used to determine the dissolved sulfide concentration in the liquid at a given temperature and pH. Reactor pH affects the ratio of sulfide ion concentration in each ionization state (H_2S and HS^-). This in turn affects the gas concentration of H_2S according to Henry's Law. Aqueous H_2S is far more toxic to bacteria than is dissolved HS^-.

$$H_2S \longleftrightarrow HS^- + H^+ \tag{32}$$

$$K_1 = \frac{\{HS^-\}\{H^+\}}{\{H_2S\}} = 10^{-7.0} \quad , \quad pK_1 = 7.0 \tag{33}$$

This ionization value (pK) is strongly affected by temperature as illustrated in Table 5.

Table 5. Ionization value for the dissociation of dissolved H_2S as a function of temperature (Speece, 1996).

Temperature (°C)	K_1 for sulfide	pK_1
18	9.1×10^{-8}	7.04
25	11.2×10^{-8}	6.95
35	14.9×10^{-8}	6.82
45	19.4×10^{-8}	6.71
55	24.7×10^{-8}	6.61

The fraction of un-ionized H_2S is described in Equation 35.

$$H_2S = \frac{1}{1 + (K_1 / 10^{-pH})} \tag{35}$$

Solubility of H_2S is also a function of temperature, with decreasing solubility as temperature increases, as shown in Table 6.

Table 6. Solubility of H₂S decreases with increasing solution temperature (Speece, 1996).

Temperature (°C)	$[H_2S]$ (mg/l per atm of H₂S in gas)
15	4410
20	3850
25	3380
30	2980
35	2650
40	2360
45	2100
50	1880
60	1480

Un-ionized sulfide (H_2S) in liquid phase can be determined by measuring $[H_2S]_{gas}$. As a rule of thumb, there is about 26 mg/l $[H_2S]_{aq}$ for every 1 percent of H₂S in gas at 35°C.

2.3.7.2 Sulfide Toxicity. For granular biomass precultivated in the presence of sulfate, the inhibition caused by H_2S is dependent on the pH. At alkaline pH, the inhibitory effect of H_2S has been shown to be higher than at neutral or acidic pH. Distinction between granulated and suspended biomass (for methanogenic bacteria) is attributed to the development of different active populations of bacteria, and/or to the existence of pH and sulfide gradients in the granule (Visser et al., 1993) (Speece, 1996) Several studies have shown H_2S inhibition to be reversible (Parkin *et al.*, 1990).

2.3.8 Methanogenesis

Methanogenesis is carried out by strictly anaerobic *Archaea* commonly referred to as methanogens (Harper and Pohland, 1986). Methanogenic consortia are analogous to sulfate-reducing consortia, but are more restricted in their ability to utilize organic substrates. Most fermentation acids (lactate, propionate, and butyrate) cannot be catabolized by methanogens directly. Other organisms (acetigens) oxidize these acids to acetate while producing H_2 or formate as a reduced product. Hydrogenotrophic methanogens are capable of using H_2 or formate.

$$H_2 + CO_2 \rightarrow CH_4 \tag{34}$$

H_2 oxidizers are autotrophic (CO_2 reducing).

Aceticlastic methanogens convert acetate to CO_2 and CH_4 (Pohland and Kim, 2000).

$$CH_3COO^- \rightarrow CH_4 + CO_2 \qquad\qquad\qquad\qquad (35)$$

2.4 KINETICS OF MICROBIALLY-MEDIATED REDUCTION REACTIONS

Principles of microbial growth and microbially catalyzed substrate utilization were developed between 1940 and 1970. Microbial growth kinetics were initially defined by the famous Monod expression (Monod, 1949), and by the linear relationship between bacterial specific growth rate and specific substrate utilization rate, as applied to steady-state chemostat operation.

2.4.1 Monod Kinetic Model of Substrate Limited Growth

The effect of change in the concentration of limiting substrate on bacterial growth rate can be defined using the following expression, commonly known as the Monod Equation:

$$\mu = \mu_m \frac{S}{(K_S + S)} \qquad\qquad\qquad\qquad (36)$$

where:

μ = specific growth rate, (time^{-1})

μ_m = maximum specific growth rate, (time^{-1})

S = concentration of growth limiting substrate in solution,

(mass/(unit volume))

K_S = half velocity constant, substrate concentration @ ½ the max growth rate,

(mass/unit volume)

This expression defines a rectangular hyperbolic curve as shown in Figure 8. The maximum height of the curve is established by the maximum specific growth rate, while the pitch of the curve is established by the half velocity constant, the substrate concentration at which the observed growth rate is one half of the maximum specific growth rate (Metcalf and Eddy, 1991; Grady *et al.*, 1999; Rittmann and McCarty, 2001).
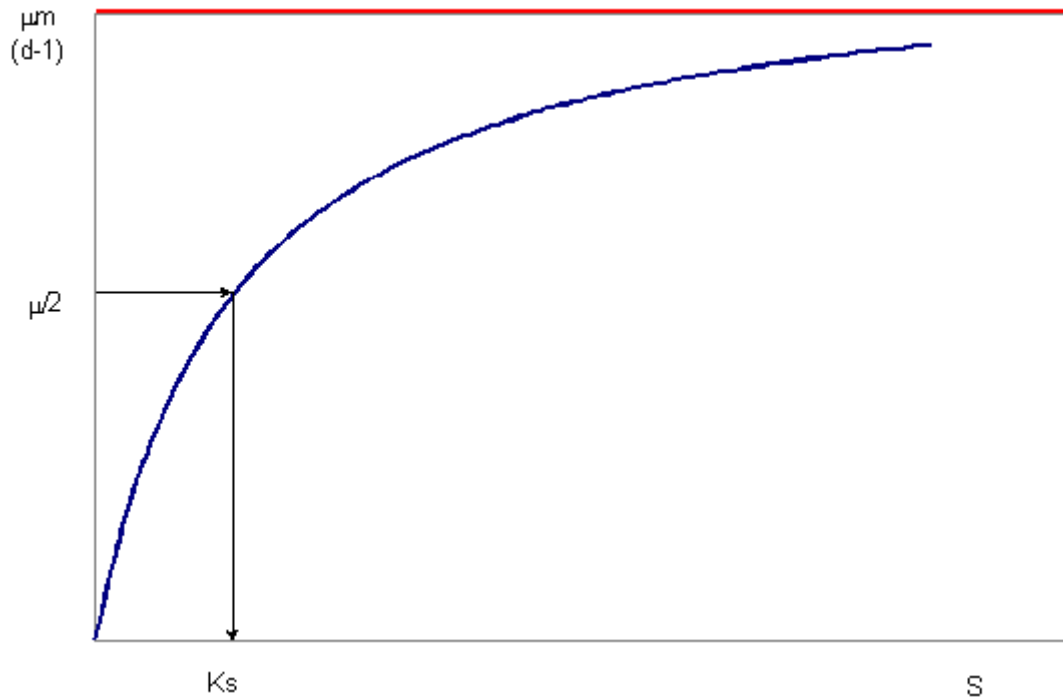
Figure 8. Definition of the half velocity constant and the maximum specific velocity

In batch and continuous culture systems, rate of bacterial growth (cell growth) can be defined by the following relationship:

$$r_g = \mu X \tag{37}$$

where:

r_g = rate of bacterial growth, (mass/(unit volume·time))

μ = specific growth rate, (time^{-1})

X = concentration of microorganisms, (mass/unit volume)

By combining the previous two reactions, we can develop a new expression for substrate limited biomass growth is developed:

$$r_g = \frac{\mu_m X S}{(K_S + S)} \tag{38}$$

Because quantity of new cells produced is proportional to the quantity of substrate utilized:

$$r_g = -Y r_{SU} \tag{39}$$

where:

Y = ratio of mass of cells formed to the mass of substrate consumed, measured

during any finite period of logarithmic growth, or maximum yield coefficient, (mg/mg)

r_{SU} = substrate utilization rate, (mass/unit volume·time)

r_g = rate of bacterial growth, (mass/(unit volume·time))

Biomass yield is a function of several factors, including the oxidation state of the carbon source, presence of nutrients and growth factors, the degree of substrate polymerization, complexity of metabolic pathway, the intrinsic growth rate of the bacteria, and the specific physical parameters of the cultivation (Metcalf and Eddy, 1991).

Combining the previous two reactions, gives:

$$r_{SU} = \frac{\mu_m X S}{Y(K_S + S)} \tag{40}$$

μ_m/Y is often replaced with k

k = maximum rate of substrate utilization per unit mass of microorganism

$$r_{SU} = \frac{k X S}{(K_S + S)} \tag{41}$$

In a biological reactor, not all cells in the system are in log-growth phase. Some cells are older and grow more slowly or not at all. To account for energy required for cell maintenance, cell death, and predation, a lumped expression know as endogenous decay is added to this rate equation.

$$r_d = -k_d X \tag{42}$$

where:

k_d = endogenous decay coefficient, (time^{-1})

X = concentration of cells, (mass/unit volume)

$$r_g' = \frac{\mu_m X S}{(K_S + S)} - k_d X \tag{43}$$

$$r_g' = -Y r_{SU} - k_d X \quad = \text{net rate of bacterial growth, (mass/unit volume · time)} \tag{44}$$

$$\mu' = \mu_m \frac{S}{(K_S + S)} - k_d \quad = \mu' = \text{net specific growth rate, (time}^{-1}) \tag{45}$$

and,

$$Y_{obs} = \frac{r_g}{r_{SU}} \quad = \text{observed yield} \tag{46}$$

40

Temperature affects the rate of bacterial production and substrate consumption. One equation developed to approximate biological reaction rate at a different temperature than that used to conduct kinetic data collection experiments is:

$$r_T = r_{20}\, \theta^{(T-20)} \tag{47}$$

where θ is the temperature activity coefficient. However, because of the desire to minimize the "extrinsic" properties of kinetic parameters, it is best to operate laboratory scale kinetic investigations at temperatures comparable to those expected of a full-scale implementation (Snoeyink and Jenkins, 1980).

Choosing the proper rate expression is important in order to conduct a mass balance analysis. So it is important to ensure that the rate expression effectively defines the observed phenomena. It is not always meaningful to apply rate equations generally to other reactor conditions not used for initial rate expression development. Grady (1996) described the importance of properly simulating the environmental conditions expected of full-scale implementation when conducting kinetic investigations. He explained that a change in the physiological state of a culture may lead to a significant change in culture's kinetic performance, and indeed may change the composition of the microbial population itself.

2.4.1.1 Toxicity and Inhibition. Inhibition occurs when a substance reduces a microorganism's ability to perform a metabolic reaction. Impairment of bacterial function occurs when the inhibiting molecule binds to an active enzyme site, which prevents substrate from binding to the enzyme - thereby preventing normal enzymatic function and inhibiting metabolism.

There are several different substances and environmental conditions that can cause inhibition. Substances that decrease the rate of a reaction when present in the reaction mixture are called inhibitors. Presence of various non-metallic cations in solution (Ca^{2+}, K^+, Na^+, etc.) has been reported by Speece (1996) to cause inhibition in MPB. Similarly, cyanide and heavy metals (Cu^{2+}/Cu^+, Hg^+, Pb^{2+},etc.) have been linked to inhibition of an assortment of enzymes. The most common causes of inhibition, however, are substrate and product inhibition.

In substrate toxicity, substrate concentrations become too high to support continued microbial activity. Mechanisms that exist to address substrate inhibition include recycle of reactor effluent to the beginning of the process, or utilizing a completely mixed reactor to maintain lower concentrations of the toxic substrate that is in contact with active biomass. At lower concentrations, toxic substrates are often more easily biodegraded (Speece, 1996).

In product inhibition, product(s) of substrate consumption build-up to a maximum limit concentration above which the process cannot proceed effectively. One common example of this is wine fermentation. When ethanol (a product of fructose consumption) reaches a concentration of approximately 12% by

volume, fermentation reactions no longer proceed. Product toxicity is not observed when the product being formed is insoluble as in the case of methanogenesis and methane production. Nitrogen gas, the final product of biological denitrification, is another highly insoluble benign gas that has no observable toxicity. H_2S formed as a product of sulfate reduction is soluble in water, and can build to toxic concentrations under anaerobic conditions. Elevated sulfide concentration has been shown to inhibit sulfate reduction, nitrate reduction, methanogenesis, and most other biological activity (Levenspiel, 1980).

2.4.1.2 Modeling of Inhibition. There are three general categories of inhibition, each described by a slightly different kinetic model. In irreversible inhibition, an inhibiting substance irreversibly binds to the active site of an enzyme, thereby rendering it permanently inactivated. Irreversible inhibition is usually established by a covalent bond between part of the enzyme and the inhibitor. Tight binding inhibition occurs when a reaction between the enzyme molecule and the inhibiting molecule occurs. These reactions have such high stability (*i.e.*, slow dissociation rates) that they are, for all intents and purposes, permanently and irreversibly bound. More commonly, reversible inhibition occurs, in which a reversible, non-covalent bond between the enzyme and inhibitor is formed. Such a bond is reversible, and has lower stability. Reduction of the inhibitor concentration in bulk solution is typically sufficient to drive the dissociation of enzyme and inhibitor.

Binding capacity, or stability or dissociation constant, is used as the measure of an enzyme's strength and inhibition reversibility.
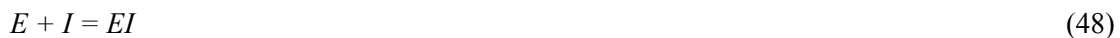
$$E + I = EI \tag{48}$$

$$K_i = \text{dissociation constant} = [E]*[I]/[EI] \tag{49}$$

One of the most employed inhibition models is the Haldane expression for substrate inhibition. The Haldane model is based on a modification to the standard Monod model that is based on the assumption of formation of an inactive enzyme-substrate-substrate (ESS) complex. In this model, Enzyme (E) combines with a substrate molecule (S) to form an enzyme-substrate (ES) complex, which is an intermediate product in the final formation of product (P) and free enzyme. In addition to these reactions, free S can also react with the ES complex to form an enzyme-substrate-substrate (ESS) complex that is inactive, which will not result in P formation. Formation of this inactive ESS complex is reversible. This description can be summarized in Equation 50.

$$k_1 \qquad k_2$$
$$E + S <==> ES <==> P + E \tag{50}$$
$$k_i \quad +$$
$$S$$
$$k_3 \downarrow\uparrow k_4$$
$$ESS \text{ (inactive)}$$

Based on the rate of product formation (Equation 51), the assumption that rapid equilibrium is achieved (Equations 53 and 54), and on the fact that enzyme species are conserved in the system (Equation 52), a system of four equations can be solved in parallel, resulting in Equation 55.

$$\frac{d[P]}{dt} = rate = v = k_2[ES] \tag{51}$$

$$[E_0] = [E] + [ES] + [ESS] \tag{52}$$

$$k_1[S][E] = k_i[ES] \tag{53}$$

$$k_3[S][ES] = k_4[ESS] \tag{54}$$

$$v = \frac{k_2}{(k_1[S]k_4 + k_4k_i + [S]^2k_3k_1)} k_4k_1[S][E_0] \tag{55}$$

By defining equilibrium constants as described in Equations 56 (maximum velocity constant), Equation 57 (half-velocity constant), and Equation 58 (Haldane inhibition constant), the Haldane expression for substrate-inhibited substrate-limited growth can be simplified to the more recognizable form shown in Equation 58.

$$v_m = k_2[E_0] \tag{56}$$

$$K_m = \frac{k_i}{k_1} \tag{57}$$

$$K_i = \frac{k_4}{k_3} \tag{58}$$

Using these definitions, Equation 55 is simplified to Equation 59.

$$v(s) = \frac{v_m s}{K_m + s + \dfrac{s^2}{K_i}}$$ (59)

Therefore, at high values of K_i (k_4/k_3), the right-most expression in the denominator approaches zero and the effect of substrate inhibition is negligible as compared to the Monod model. At low values of K_i, the rate of ESS dissociation is much slower than that of ESS formation, K_i is small, and the third term in the denominator becomes large at high substrate concentrations. In the case of small K_i, the kinetics differs significantly from the Monod model at higher substrate concentration. An application of the Haldane inhibition model is shown in Chapter 6, Figure 47.

2.4.2 Sludge age and bioreactor stability

In a suspended growth bioreactor, with no sludge recycle, mean cell detention time (θ_C, often referred to as "sludge age) is equal to hydraulic residence time. For this study, the specific utilization rate (U) is a measure of the rate of ethanol utilization by a unit mass of organisms, which is a function of ethanol concentration and sludge age. The relationship between these parameters is summarized in Equations 60 and 61.

$$\frac{1}{\theta_C} = YU - k_d$$ (60)

$$U = \frac{S_0 - S}{\theta_C}$$ (61)

By specifying any one of U, S_0, or θ_C, the other two parameters are set and the overall ability of the bioreactor to remove COD (and concomitantly reduce oxidized species in solution) is established.

The critical sludge age at which washout occurs can be estimated using Equation 62.

$$\frac{1}{\theta_C^M} = Y \frac{k S_0}{K_S + S_0} - k_d$$ (62)

where:

S_0 is the ethanol concentration, g COD/liter

Y is the maximum observed yield coefficient, mg/mg

θ_C^M is the minimum sludge age at which washout occurs, days

K_S is the Monod half velocity constant, g COD/liter, and

k_d is the endogenous decay coefficient, days^{-1}

44

Solids retention time (SRT) is characterized by biomass concentration and mean cell age. Increased solids retention time (SRT) can help to prevent process failure due to toxicity. One study by Bhattacharya and Parkin (1988) showed that at toxic concentrations of ammonium ion (7000 mg/l), process failure was observed to take longer with increased SRT, and no tendency toward failure was observed with long SRT. A similar study by Speece and Parkin (1996) showed increased reduction of biogas production with decreased SRT for the same chloroform concentration.

Because bacteria in attached-growth systems are fixed in the reactor, their detention time is independent of hydraulic flow conditions and mean cell detention times on the order of 100 days can be obtained. Thus attached growth treatment is ideal for processes requiring large sludge ages, such as the process under consideration.

3.0 LITERATURE REVIEW

3.1 NO$_X$ ABSORPTION COUPLED WITH MICROBIALLY-CATALYZED TREATMENT AND REGENERATION

In addition to the commonly applied NO$_X$ control technologies described earlier, post-combustion NO$_X$ absorption has also been investigated extensively by industry and government organizations. NO$_X$ absorption involves physical/chemical absorption of NO$_X$ into liquid scrubber solutions which are amended with chemicals that increase the solubility of nitric oxide (NO), which typically, makes up over 90% of the flue gas NO$_X$. As yet, such technologies have not found large-scale application in the U.S. for flue gas treatment because of operational difficulties.

The most notable example of such a scrubber solution additive is ferrous ethylenediaminetetraacetic acid (or Fe(II)EDTA^{2-}). EDTA is the most commonly used polyaminocarboxylate ligand. It is highly labile (has a fast coordination rate), and forms a strong bond with divalent and trivalent metals using six coordination sites - free electron pairs on the molecule (Snoeyink and Jenkins, 1980). Figure 9 illustrates the EDTA molecule, and Figure 10 shows EDTA coordinated with a metal center.
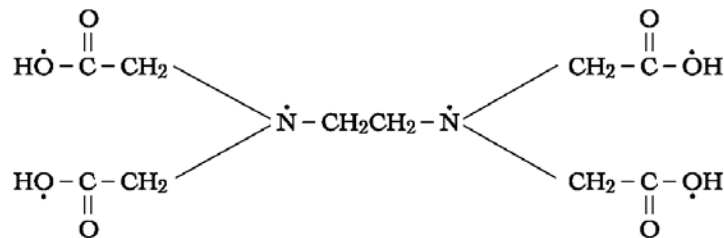
Figure 9. EDTA molecule illustrating free electron pairs that act as coordination sites for chelation of metal ions (Dow, 2004).
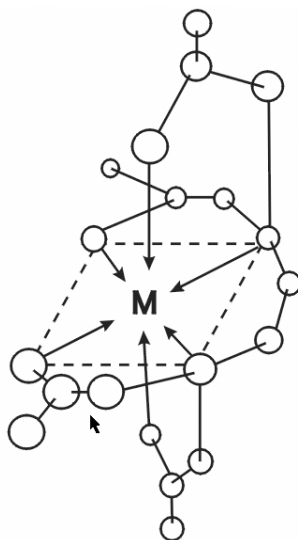
Figure 10. Six points at which the EDTA molecule coordinates with the chelated metal (Snoeyink and Jenkins, 1980; Dow, 2004).

Figure 11 illustrates relative stability of the chelate of several metal ions. Chelate stability is another name for the equilibrium constant of the chelate formation reaction. The stability of ferrous EDTA and ferric EDTA are both quite large: $10^{14.3}$ and 10^{25}, respectively (Martel and Calvin 1953). Metals with higher chelate stability can, over time, displace less stable chelated metals. Metal-EDTA complexes have been shown to be poorly degraded in traditional aerobic wastewater treatment processes (Kaluza, et al., 1998).
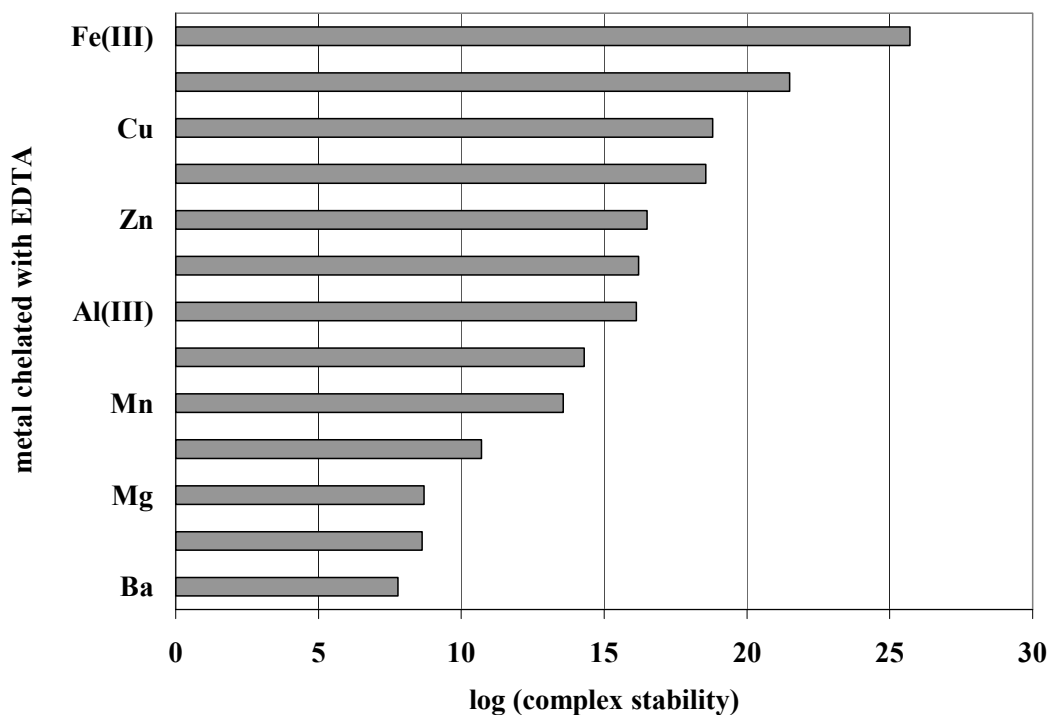
Figure 11. Relative stability and the displacement hierarchy of several metal EDTA ligands (Dow, 2004).

Scrubbing of NO_X from the gas phase with ferrous EDTA has been shown to be highly effective (Weisweiler *et al.*, 1986). Figure 12 illustrates the ability of ferrous EDTA to absorb NO, as compared with the same concentration of the oxidized ferric EDTA. Extensive research has been conducted to evaluate and model scrubber treatment efficiency as a function of such variables as ferrous iron concentration, packing material properties, liquid loading rate, gas loading rate, and scrubber geometry (Dravo Lime, 1992; Livengood and Mendelsohn, 1998). These models are based on two-film theory, as derived by Li et al. (1996) and summarized in Appendix D. Despite the large NO absorption capacity of ferrous EDTA solutions, removal of the nitrosyl adduct of ferrous EDTA (shown as $NO \bullet Fe(II)EDTA^{2-}$) and regeneration of ferrous EDTA from the oxidized ferric EDTA has proven to be difficult. Chemical or electrochemical reduction techniques have been demonstrated to be effective, but issues related to rate, cost, and additive degradation prohibits their full-scale application (Saito *et al.*, 1976; Sada *et al.*, 1984; Dravo Lime, 1992; Kleifges, 1997). Because of the difficulty in addressing both the technical issues as well as demonstrating economic feasibility, the NO_X scrubbing approach has remained unimplemented for full-scale industrial application.

More recently, reduction of the nitrosyl adduct of $[Fe(II)EDTA]^{2-}$ has been shown to be achievable through treatment with NO reducing bacteria. By providing an anoxic environment, an electron donor for the reduction of NO, a carbon source, and nutrients to promote new cell growth, NO reducing bacteria will successfully and efficiently treat the spent scrubber solution. Similarly, there are bacteria in solution that will, given the proper nutrients, reduce Fe(III)EDTA$^-$ to Fe(II)EDTA^{2-} (Brooks *et al.*, 1999; Buisman *et al.*, 1999; Buisman *et al.*, 2001; van der Maas *et al.*, 2002; van der Maas *et al.*, 2003).

While these investigations provide important insight into the fundamental reactions involved with a closed-loop NO$_X$ absorption process, no known literature evaluates the kinetics of microbially-mediated reduction of primary constituents of this process. Included in the current investigation is a preliminary evaluation of the kinetics of reduction of the nitrosyl adduct of ferrous EDTA, information that should provide insight into process configuration and operation of biological treatment and regeneration of spent NO scrubbing process waters.

3.1.1 Oxidation of Ferrous EDTA in the Scrubbing Process

In addition to the desired absorption of NO from industrial flue gas, the undesirable oxidation of the ferrous EDTA chelate to ferric EDTA also occurs. The oxidation of ferrous EDTA has been described to proceed via a complex multi-step mechanism that is summarized by the following equation (Engelmann *et al.*, 2003):

$$2\,Fe(II)EDTA^{2-} \;+\; \tfrac{1}{2}O_2 \;+\; 2\,H^+ \;\rightarrow\; 2\,Fe(III)EDTA^- \;+\; H_2O \tag{63}$$
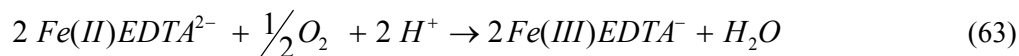
NO does not form an adduct with ferric EDTA, and, therefore, the presence of ferric EDTA corresponds with decreased scrubber solution capacity. Figure 12 illustrates the substantial difference in time to breakthrough of a 1500 ppm NO gas stream (balance of N$_2$ gas) between 100 ml of 0.045 M solutions of ferrous and ferric EDTA.
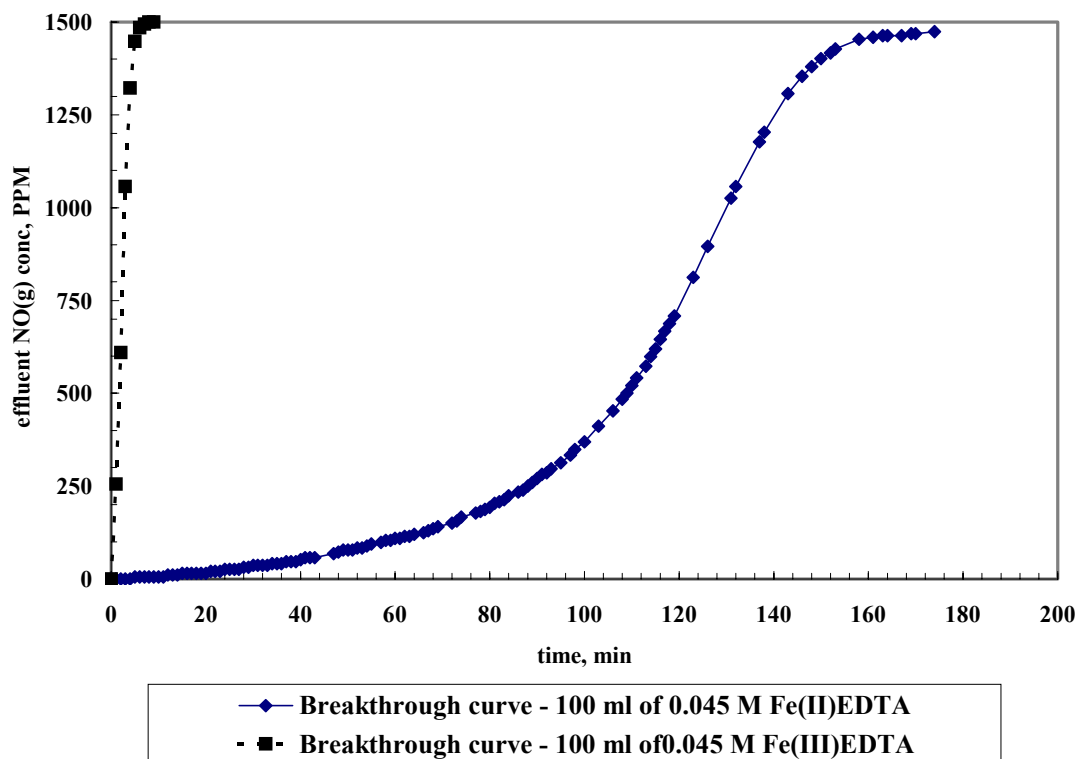
Figure 12. Breakthrough of 1500 ppm nitric oxide (0.7 liters per minute) in 0.045 M solutions of ferrous and ferric EDTA.

Theoretical scrubbing capacity was verified experimentally through saturation of ferrous EDTA solution with NO. A brief description of this experiment, sample data, and calculations are shown in Appendix B. A more extensive discussion of NO_X scrubbing and biological treatment of spent scrubber process water is discussed in Chapter 5.

3.1.2 Microbially-Mediated Reduction of Oxidized Species in Process Solution

Microbially-mediated reduction of the nitrosyl adduct of ferrous EDTA (NO•Fe(II)EDTA^{2-}) has been observed to occur using ethanol as the primary electron donor. A reported reaction that describes the reduction of the nitrosyl adduct to nitrogen gas using ethanol as the primary electron donor is listed in Equation 54 (Buisman *et al.*, 1999).

$$1/6\,CH_3CH_2OH + NO\bullet Fe(II)EDTA^{2-} \longrightarrow Fe(II)EDTA^{2-} + \tfrac{1}{2}\,N_2 + 1/3\,CO_2 + \tfrac{1}{2}H_2O \qquad (64)$$

It should be noted that, as with standard denitrification, alkalinity is also generated as a result of dissimilatory NO adduct reduction.

3.1.2.1 Reduction of Ferric EDTA to Ferrous EDTA. In the event that some of the ferrous EDTA in the process liquor is oxidized to ferric EDTA, the bioreactor will be operated to promote microbially-mediated reduction of ferric EDTA. Reduction of ferric EDTA back to the ferrous form will effectively regenerate the spent scrubber solution to its active form so that it can be reused in the scrubbing process. The reduction of ferric EDTA to ferrous EDTA using ethanol as the primary electron donor is proposed to proceed according to the reaction listed in Equation 52 (Buisman *et al.*, 1999).

$$Fe(III)EDTA^- + 1/12\ CH_3CH_2OH + \tfrac{1}{4}\ H_2O \longrightarrow Fe(II)EDTA^{2-} + 1/6\ CO_2 + H^+ \tag{65}$$
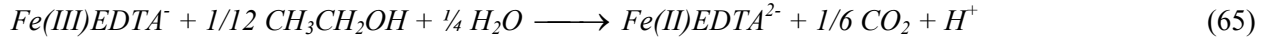
While acidity is generated during this reaction, the oxidation reaction listed in Equation 53 consumes equivalent H^+ per mole of Fe(III)EDTA oxidized. As a result, the net change in pH resulting from iron EDTA oxidation and reduction in a closed-loop system is negligible.

3.1.2.2 Intermediate Products of Ethanol Oxidation. It is also possible that some of the bacteria responsible for catalyzing reduction of oxidized species in solution are incapable of utilizing ethanol directly and instead utilize products of ethanol oxidation (Harper and Pohland, 1986). Ethanol oxidation is reported to proceed according to the following reactions:

$$CH_3CH_2OH \rightarrow CH_3CHO + H_2 \tag{66}$$
$$CH_3CHO + H_2O \rightarrow CH_3COO^- + H^+ + H_2 \tag{67}$$

with the overall oxidation reaction proceeding as:

$$CH_3CH_2OH + H_2O \rightarrow CH_3COO^- + H^+ + 2H_2 \tag{68}$$

Using these products of ethanol oxidation (H_2, acetaldehyde, and acetate), microbially-mediated NO reduction is proposed to proceed by the following reactions, respectively (with the exception of the reaction with H_2, which was described previously by (Buisman *et al.*, 1999)):

$$NO \bullet Fe(II)EDTA^{2-} + H_2 \longrightarrow \tfrac{1}{2}N_2 + Fe(II)EDTA^{2-} + H_2O \tag{69}$$

$$NO \bullet Fe(II)EDTA^{2-} + CH_3CHO \longrightarrow \tfrac{1}{2}N_2 + Fe(II)EDTA^{2-} + CH_3COO^- + H^+ \tag{70}$$

$$NO \bullet Fe(II)EDTA^{2-} + \tfrac{1}{4}H^+ + \tfrac{1}{4}CH_3COO^- \longrightarrow \tfrac{1}{2}N_2 + Fe(II)EDTA^{2-} + \tfrac{1}{2}H_2O + \tfrac{1}{2}CO_2 \tag{71}$$
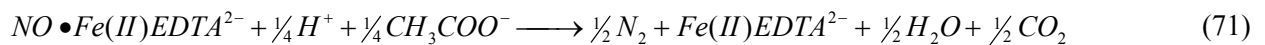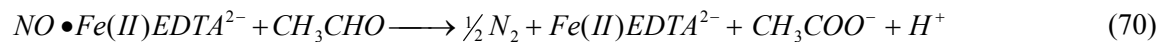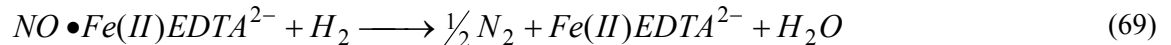
Again, iron-reducing bacteria that are not capable of utilizing ethanol directly as an electron donor may instead use the products of ethanol oxidation – hydrogen, acetaldehyde and acetate. Proposed reactions describing ferric EDTA reduction are, respectively:

$$Fe(III)EDTA^- + \tfrac{1}{2}H_2 \longrightarrow Fe(II)EDTA^{2-} + H^+ \tag{72}$$

$$Fe(III)EDTA^- + \tfrac{1}{2}CH_3CHO \longrightarrow Fe(II)EDTA^{2-} + \tfrac{1}{2}CH_3COO^- + 3/2\ H^+ \tag{73}$$

$$Fe(III)EDTA^- + 1/8\ CH_3COO^- + \tfrac{1}{4}H_2O \longrightarrow Fe(II)EDTA^{2-} + \tfrac{1}{4}CO_2 + 7/8\ H^+ \tag{74}$$
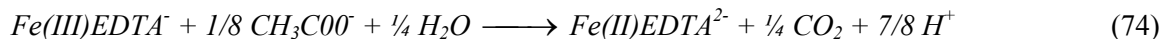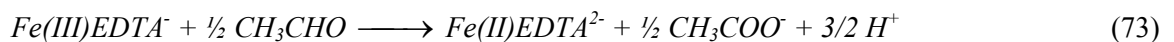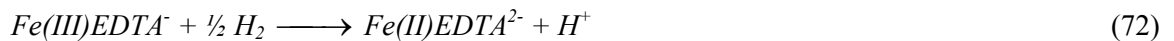
3.1.2.3 Chemical Reduction of [NO•Fe(II)EDTA]²⁻. Two additional chemical mechanisms for the reduction of the nitrosyl adduct of ferrous EDTA have been described in the literature. Following the scrubbing of NO using an aqueous solution of ferrous EDTA, the NO reacts with sulfite present in solution as a result of simultaneous SO_X scrubbing. Sulfite is then oxidized to sulfate and NO is reduced to nitrogen gas, according to the reaction listed in Equation 62 (Sada *et al.*, 1984).

$$NO \cdot Fe(II)EDTA^{2-} + SO_3^{2-} \rightarrow Fe(II)EDTA^- + \frac{1}{2} N_2 + SO_4^{2-} \tag{75}$$
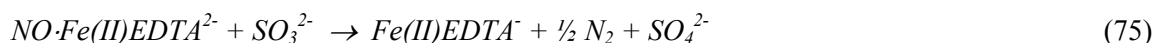
Recently, researchers have identified an additional pathway for the reduction of NO present as the adduct of ferrous EDTA. Ferrous EDTA itself has been identified as an available electron donor that is utilized in the reduction of the nitrosyl adduct of ferrous EDTA. Therefore, a free ferrous EDTA molecule without a nitrosyl adduct will give up an electron to reduce the NO adduct of another ferrous EDTA molecule (van der Maas *et al.*, 2002). This reaction is described as follows:

$$NO \cdot Fe(II)EDTA^{2-} + Fe(II)EDTA^{2-} + 2 H^+ \leftrightarrow 2 Fe(III)EDTA^- + \frac{1}{2} N_2 + H_2O \tag{76}$$
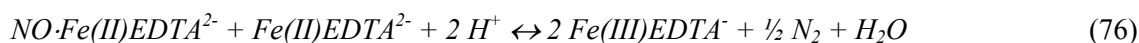
and was observed to proceed even under sterile conditions, suggesting that some portion of the nitrosyl adduct reduction is chemically rather than microbially-mediated (van der Maas *et al.*, 2002). However, this reaction was not observed in the experiments described herein.

3.2 VOLTAMMETRIC METHODS - VOLTAGE SWEEP ELECTROCHEMICAL TECHNIQUES

Several analytical methods were employed in an attempt to quantify the observed reactions and process performance observed in this study. Many of the methods are straightforward and commonly applied in the field of environmental engineering. One notable exception is the application of scanning voltammetry for the quantitative evaluation of the oxidation state and concentration of species of the ferrous/ferric EDTA complex. Because this method is relatively novel in its application in the field of environmental engineering, a brief summary of the theory and practical considerations of voltammetric electro-analytical methods will be provided.

Voltammetry is a term used to describe the general category of electroanalytical methods in which current is recorded as a function of applied potential (Skoog, et al., 1997). In voltametric methods, an external potential is applied to the cell, and the current response is measured. Precise control of the external applied potential is required, which is not possible with a two electrode system, as a result of the potential drop across the cell caused by solution resistance (potential drop (E) = current (i) x solution resistance (R)) and polarization of the counter electrode that is required to complete the current measuring

circuit. A third electrode relieves the reference electrode from carrying the applied current, and allows accurate potentiometric measurement coincident with application of current (Skoog *et al.*, 1997).

3.2.1 Three Electrode System

In a three electrode system, the potential of one electrode - the working electrode - is controlled relative to the reference electrode, with the current passing between the working electrode and a third electrode - the auxiliary or counter electrode. In such methods, the potential may be maintained constant or changed over time according to an applied waveform. The potentiostat measures the current flow between the working and auxiliary electrodes. The controlled variable in a potentiostat is the cell potential and the measured variable is the cell current. Using a three electrode system and a potentiostat, better potential control can be achieved. Figure 13 shows the general configuration of a three electrode system (Gorby, 2001).
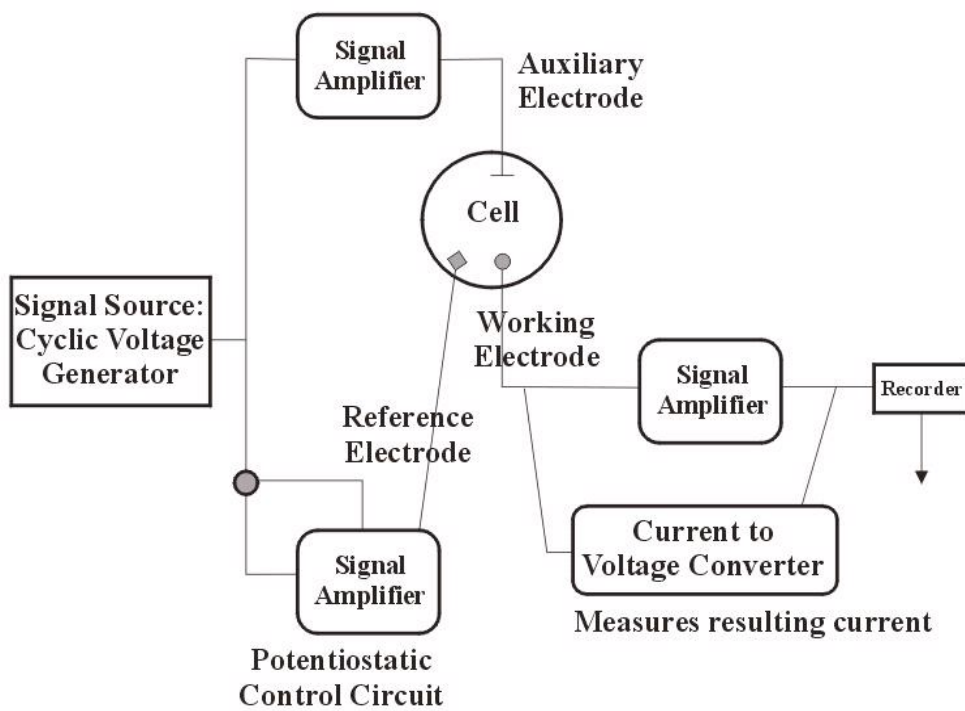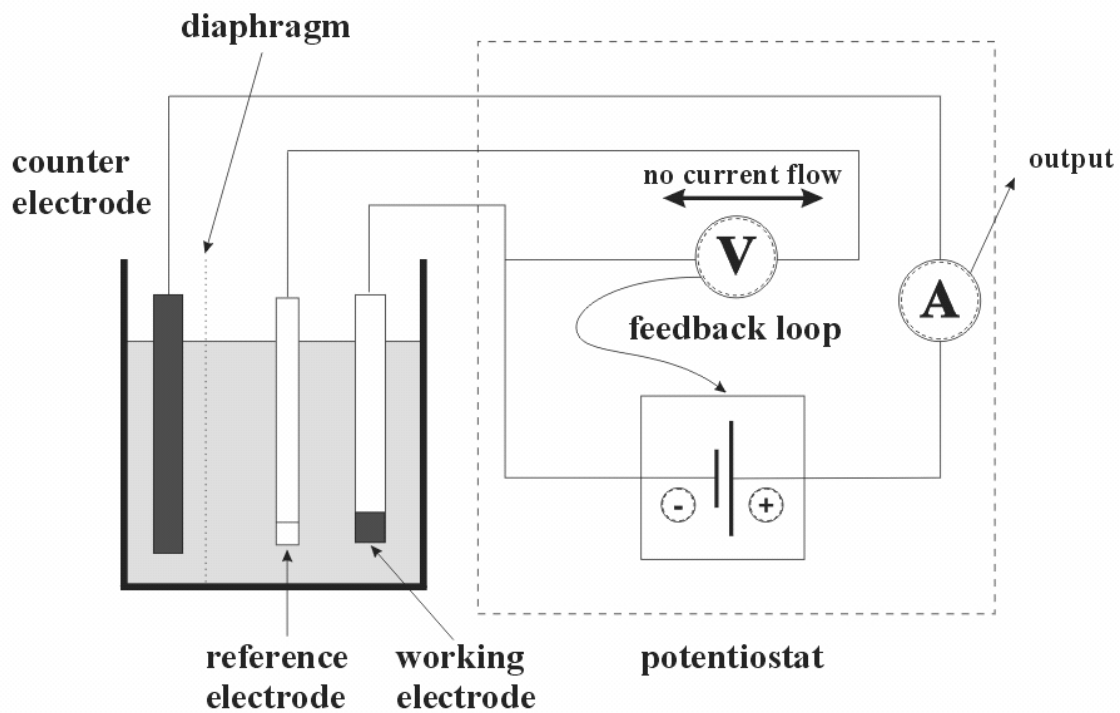
Figure 13. Three electrode system apparatus (top) and a simplified system schematic (bottom).

Following is a description of the parts of a three-electrode system, a summary of their function and their physical properties.

3.2.1.1 Working Electrode. The potential is controlled and the generated current is measured at the working electrode. The working electrode is made of a conductive material that is electrochemically inert (i.e., does not generate a current in response to an applied potential) over the potential range of the study. Common examples of working electrode materials include gold, platinum, and glassy carbon. Also of concern is the rate at which the electrode transfers electrons. Slow electron transfer kinetics can affect the observed reversibility of the redox system being studied. The working electrode serves as a surface on which the electrochemical reaction of interest takes place.   Dimensions of standard working electrodes for voltammetry are either a disk electrode with a diameter of 1.6 – 3 mm or a wire foil electrode with a 0.5 mm diameter and a length of approximately 20 mm (Gorby, 2001).

3.2.1.2 Reference Electrode. The reference electrode is used in measuring the working electrode potential. A reference electrode should have a constant, known electrochemical potential. Examples of common reference electrodes are the saturated calomel electrode (SCE) and silver/silver chloride (Ag/AgCl) electrodes. Both of these reference electrodes function by the redox reaction between a sparingly soluble chloride and the metallic element that is in the aqueous chloride solution. Either reference electrode can be used in voltammetric experiments; however, results of experimentation are meaningless if the reference electrode is not listed with the data.   These two electrodes have different potentials with respect to the standard hydrogen electrode. Because reported potential measurements are relative to the reference electrode, quoted potentials are meaningless without specification of the employed reference electrode. A pseudo-reference, a reference electrode made of a piece of the working electrode material, can also be used (Sharma, 1995; Gorby, 2001).

3.2.1.3 Auxiliary (Counter) Electrode. The auxiliary electrode is a conductor that completes the cell circuit. The electrical current that flows into the cell solution (sample being analyzed) via the working electrode exits the solution via the auxiliary electrode. In other words, the auxiliary electrode provides a surface at which a redox reaction occurs in order to balance the redox reaction that is occurring at the surface of the working electrode. The auxiliary electrode is generally made of an inert conductor such as a platinum foil or graphite electrode (Sharma, 1995). The surface area of the auxiliary electrode should be

equal to or larger than that of the working electrode in order that the current generated at the working electrode may be accommodated. In some electrochemical experiments, the products of the reaction occurring at the auxiliary electrode can diffuse to the working electrode and interfere with the redox reaction occurring at that site (Gorby, 2001). Typically, the duration of electroanalytical experiments such as cyclic voltammetry, is sufficiently short that this diffusion will not result in significant interference, but in order to ensure that such interference is not an issue, the auxiliary electrode can be placed in a separate (yet electrochemically available) compartment. For example, the auxiliary electrode can be placed in a glass compartment that is connected to the redox system being analyzed by a permeable glass frit or separated by the other two electrodes by a permeable diaphragm as shown in Figure 14 (Sharma, 1995; Skoog *et al.*, 1997; Gorby, 2001).
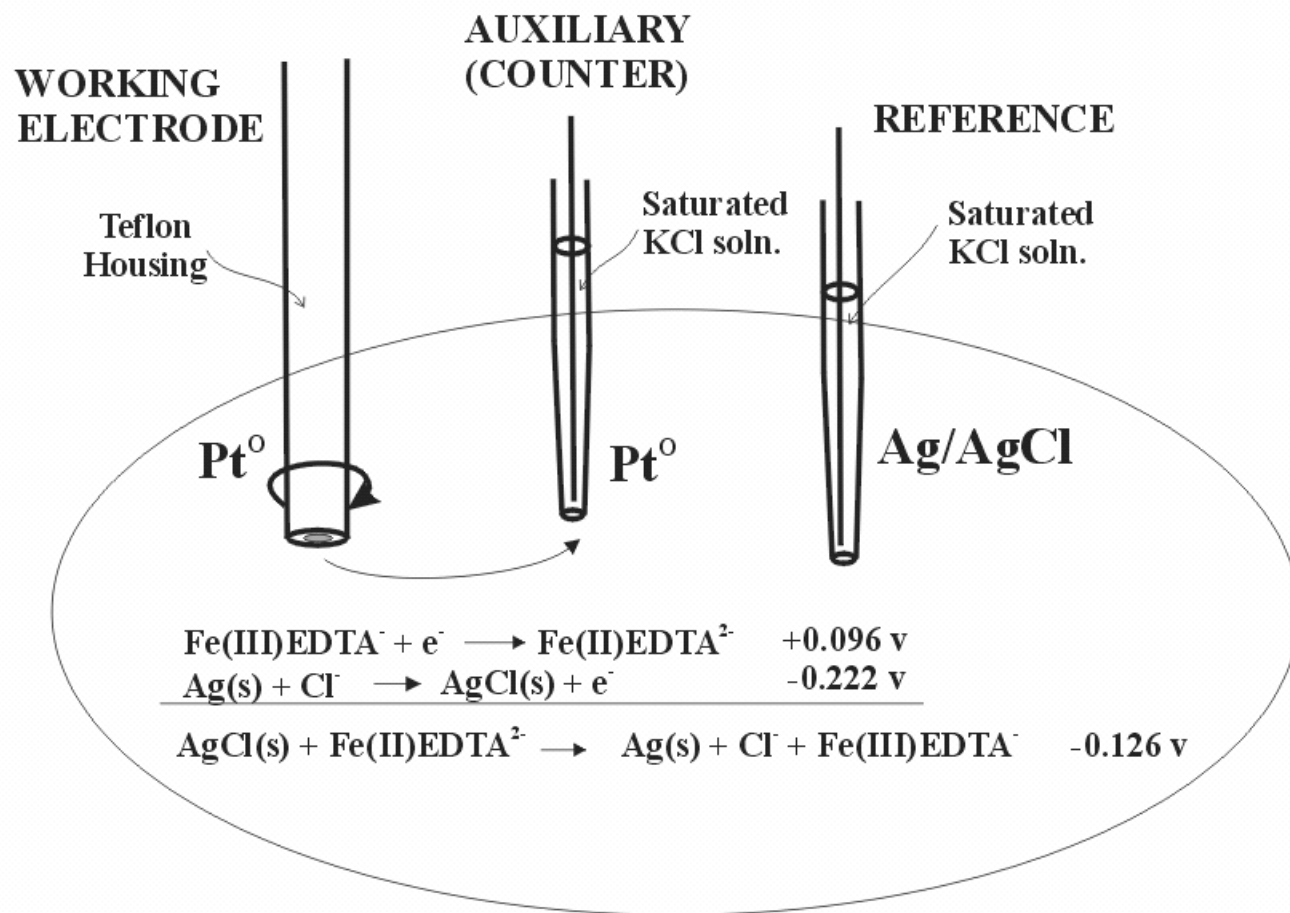
Figure 14. Three-electrode configuration and example of observed redox conditions associated with reduction of ferric EDTA.
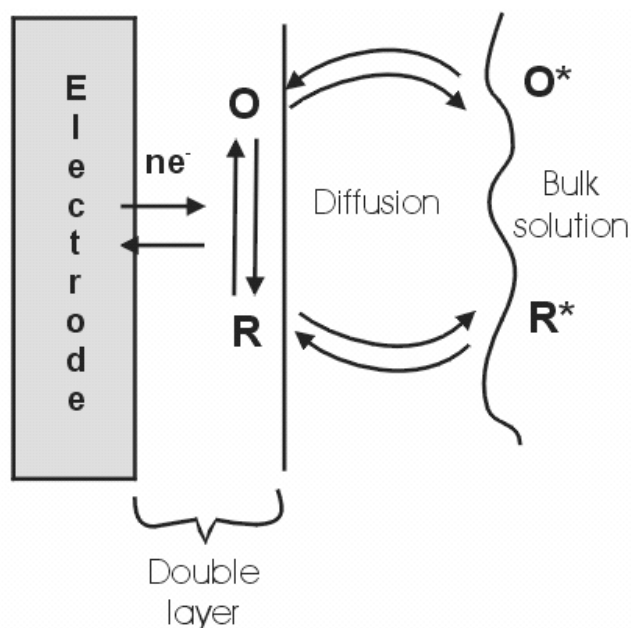
Figure 15. Mechanisms involved in electrochemical oxidation/reduction at an electrode surface.

In a three-electrode system, several factors affect the observed current response. Limitations in mass transfer from bulk solution to the electrode surface can significantly slow overall current response. Electron transfer rate at the electrode surface is a function of electrode composition. Chemical reactions other than the electrochemical reaction being studied can occur before or after the redox reaction takes place. Such reactions can slow the overall current response, or even affect overall redox reaction reversibility. Finally, reactions taking place at the electrode surface other than the redox reaction can significantly affect the current response. Such surface reactions include adsorption, desorption, and electrodeposition (Gorby, 2001). Steps can be taken to minimize these factors that affect current response so that current response of the Nernstian system can be isolated. To minimize the effect of mass transfer from bulk solution to the electrode surface, the solution can be agitated to minimize the double layer that builds up at the electrode surface, thereby decreasing the effect of diffusion. By choosing a highly conductive electrode material, such as platinum, the current effects of slow electron transfer can be minimized. By conducting electrochemical experiments in a relatively short period of time, the impact of slower chemical reaction of reactants or products in the Nernstian system can often be minimized (Gorby, 2001). In systems where both oxidized and reduced species of the Nearnstian system are soluble, the effects of adsorption and deposition can be avoided. Electrochemical experiments should be designed to avoid conditions under which electrodeposition occur.

3.2.2 Linear Sweep Voltammetry (LSV)

In linear sweep voltammetric experiments, the potential is changed by the potentiostat at a constant rate from an initial potential (E_{START}) to a prescribed final potential (E_{END}). The rate at which the linear voltage is changed is referred to as the scan or sweep rate. E_{START} and E_{END} are defined such that the E^0 of the redox reaction under consideration is between the extreme potentials of the scan. At the inflection point of the resulting voltammagram, $E\frac{1}{2}$ of the analyte is approximately equal to the E^0 of reversible Nernstian systems. The observed peak current of the voltammagrams is directly proportional to the rate of electrolysis at the electrode surface. Electrolysis occurs at the electrode surface in response to a change in potential (the sweeping potential) so that it can maintain the surface concentrations of the oxidized and reduced species at the values required by the Nernst equation. As sweep rate increases, the rate of electrolysis increases, and greater current is generated.

Important parameters of a linear sweep voltammogram are:

i_p – magnitude of the peak current

E_p – peak potential

According to the Randles-Sevcik equation, the peak current is directly proportional to the analyte concentration and the square root of the linear sweep scan rate.

$$i_p = nFAC\left(\frac{nFvD}{RT}\right)^{\frac{1}{2}} \tag{77}$$

where:

i_p = magnitude of peak current, A

n is the number of electrons appearing in half-reaction for the redox couple,

v is the rate at which the potential is swept (V / sec),

F is Faraday's constant (96485 C / mol),

A is the electrode area (cm^2),

R is the universal gas constant (8.314 J / mol K),

T is the absolute temperature (K), and

D is the analyte's diffusion coefficient (cm^2/sec).

Note that if the temperature is assumed to be 25°C (298.15 K)

$$i_p = \left(2.687 \times 10^5\right) \times n^{\frac{3}{2}} A D^{\frac{1}{2}} C v^{\frac{1}{2}} \tag{78}$$

Therefore, at constant scan rate, and area, we would expect a linear increase in peak current magnitude with a linear increase in analyte concentration (Verma, 1997). Solution species can be quantitatively measured using linear sweep voltammetry.

3.2.2.1 Cyclic voltammetry. Similar to linear sweep voltammetry, cyclic voltammetry involves the linear scan from an initial excitation potential to a second excitation point. However, as opposed to the linear sweep scan, in cyclic voltammetry the scan direction is then reversed and continues to a third potential. Scan setup therefore involves designation of initial, high and low excitation potentials (Gorby, 2001). These high and low excitation potentials are often referred to as switching potentials because they represent the potential at which the scan direction switches. One or more cycles of this excitation waveform can be conducted. That is to say, the instrument can conduct one or more waveform "cycles." Cyclical scans allow the generation of a new redox species in one scan, the fate of which can be observed in the reverse and subsequent scans. Because cyclic voltammetry is merely a series of continuous linear sweep voltammograms, the Randles-Sevcik equation remains valid. In an electrochemically reversible system, it is common to quote the mean of the cathodic and anodic peak potentials as the redox potential. If the diffusion coefficients of the oxidized and reduced species are comparable, this provides a reasonable approximation of the formal redox potential. If the system is irreversible, this approximation can not be used to determine the system's formal redox potential.

For a redox reaction to be reversible, the concentrations of the oxidized and reduced species at the electrode surface must be maintained at the values required by the Nernst equation. In cyclic voltametric experiments, a redox reaction is said to be practically reversible if the rate of electron transfer is fast relative to the voltage scan rate (the rate of change of potential) and if the oxidized and reduced species do not undergo significant chemical reaction on the experimental time scale. By employing cyclic voltammetry, it is readily discernable whether or not a system is electrochemically reversible. The system is said to be reversible if the peak potential difference of the generated voltammogram is near the theoretical value of about 58–59 mV, depending on the temperature and the switching potential, and the heights of the cathodic and anodic peaks (peak currents) are equal. Finally, the peak potential difference of a reversible system should not change with changing voltage scan rate (Sharma, 1995; Skoog *et al.*, 1997; Gorby, 2001).

3.2.2.2 Description of a reversible cyclic voltammogram. The following description of the response of a reversible Nernstian system to an applied voltage cycle refers to the sketches of the applied waveform and the corresponding cyclic voltammagram shown in Figure 16. Starting at an initial voltage (A), the potential is scanned in the negative direction. At the point marked (B), the potential has become negative

60

enough to start a cathodic current between the species, reducing the analyte at the working electrode. The reaction continues at the electrode until most of the species has been reduced, peaking the cathodic current at (D). The current then decays for the rest of the forward scan until the potential scan is reversed (F). The scan in the positive direction proceeds similarly to that of the negative scan. The cathodic current continues to slowly decay until the potential nears the standard reduction potential of the Nearnstian system being analyzed at which point oxidation of the solution begins and a current is generated at the surface of the working electrode (H). The peak anodic current generated as a result of the applied current (J) is proportional to the concentration of the reduced species in solution. The anodic current then decays from this peak, and the potential completes its cycle (K) (Skoog, *et al.*, 1997).
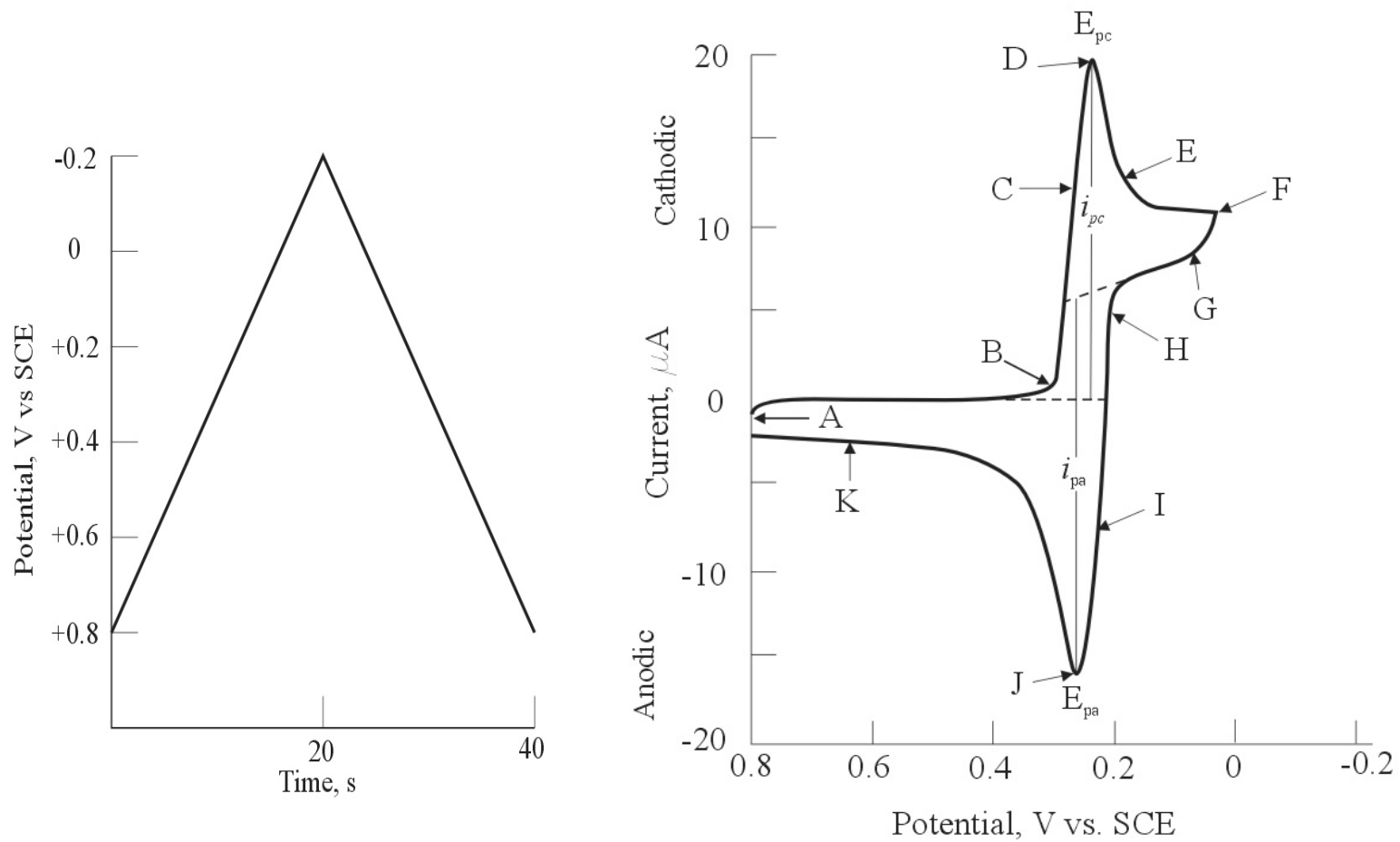
Figure 16. Potential sweep used in cyclic voltammetry analysis and corresponding current response (cyclic voltammagram) (Skoog *et al.*, 1997)

Important parameters of cyclic voltammograms are similar to those of linear sweep voltammogram:

E_{pc} - cathodic peak potential – voltage at which current is highest

i_{pc} - highest current value

E_{pa} - anodic peak potential, voltage at which current is lowest

i_{pa} - lowest current value

A redox couple exhibiting the characteristics of reversibility and rapid electron exchange with the working electrode is referred to as an electrochemically reversible couple. The formal reduction potential ($E^{o'}$) for an electrochemically reversible couple is centered between E_{pa} and E_{pc}.

$$E^{o'} = \frac{E_{pa} + E_{pc}}{2} \tag{79}$$

The separation between the cathodic and anodic peak potentials can also be used to calculate the number of electrons transferred during the electrode reaction of a reversible couple.

$$E_p = E_{pa} - E_{pc} = \frac{0.058}{n} \tag{80}$$

In addition to these simple quantitative relationships of electrochemically reversible couples, cyclic voltammetry can also be used to gain insight into intermediates of electrochemical reactions as well as the kinetics of electrochemical reactions (Verma, et al., 1997).

3.2.2.3 Cyclic Voltammetry with Rotating Disc Electrode. In rotating disc electrode techniques, an electrode rotates around its central vertical axis, as shown in Figure 14. Electrode rotation results in convective forces increasing mass transport to the electrode surface. At sufficiently high rotation speeds and sufficiently low voltage scan rates, the hydrodynamic transport results in decrease of the double layer, resulting in steady state behavior at the electrode surface. The Levich equation describes the limiting current in voltammograms generated by rotating disc electodes, and was found to be a function of electrode area, solvent viscosity, and angular velocity of the working (rotating) electode (Ogura and Ozeki, 1981; Ogura and Watanabe, 1982; Ogura and Ishikawa, 1983; Schneppensieper, 2000; Schneppensieper *et al.*, 2002).

$$i_L = 0.620\, n\, F\, A\, D^{\frac{1}{3}}\, c_0\, v^{-\frac{1}{6}}\, \omega^{-\frac{1}{2}} \tag{81}$$

where:

A is the electrode surface area, cm^2

v = solvent viscosity, $cm^2\ sec^{-1}$

ω = angular velocity of the electrode, s^{-1} ($\omega = 2\pi f$, f is frequency of rotation)

3.2.2.4 Cyclic Voltammetry of Ferric EDTA Solutions. Several sources describe the application of cyclic voltammetric and rotating disc electrode voltammetric methods for the quantitative evaluation of solutions of iron EDTA (Shepherd, 1996; Verma et al., 1997; Engelmann, et al., 2003). Figure 17 illustrates an example of a CV experiment conducted with a rotating disc electrode. For the voltammogram shown in Figure 17, the scan rate was 15 mVs^{-1}, starting from –450 mV and progressing in a positive direction until reaching the switching voltage of 1.1 V. The rotation speed was 1000 rpm, and the solution pH was 7 (Ogura and Ishikawa, 1983). Because the concentrations and other conditions under which the voltammetric evaluation of the solution were quite different, current responses are quite different than those described herein. However, the trends of the experiments were the same. As mentioned, the mean of E_{pa} and E_{pc} (-73 mV in the figure shown) approximates the formal reduction potential of the ferrous/ferric EDTA Nearnstian couple.
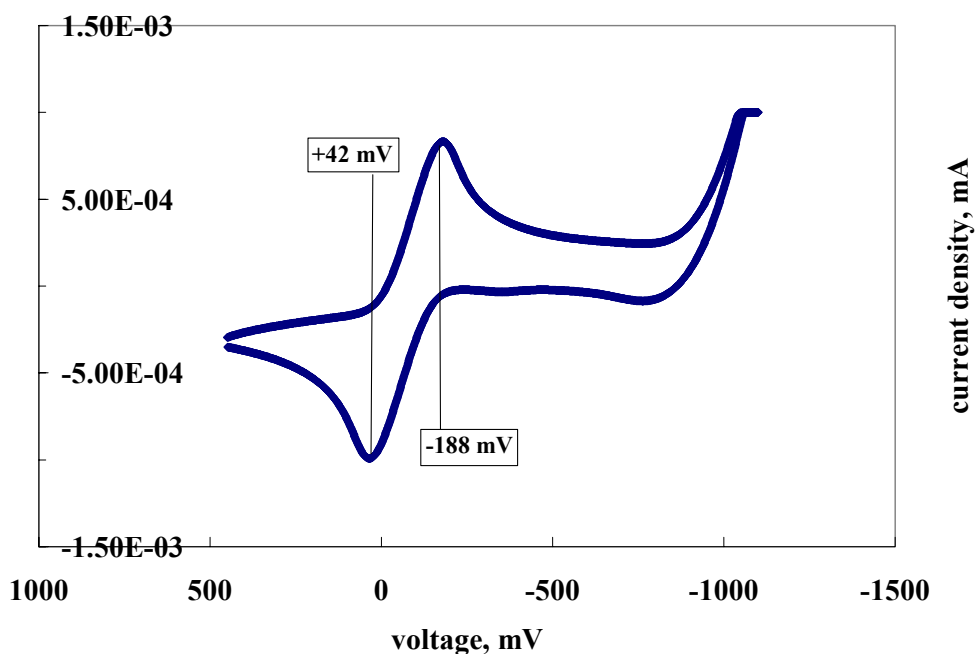
Figure 17. Cyclic voltamagram of a solution of 10 mM ferrous EDTA.

Some studies attempt to use cyclic voltammetric methods to evaluate the concentration of the nitrosyl adduct of ferrous EDTA. These methods provide results that are more subtle and less reliable than those of the ferrous/ferric EDTA complex, and were not used in quantitative evaluation of process waters. It should also be noted that no literature source was identified where cyclic voltametric methods were applied for determination of Fe(III)EDTA/Fe(II)EDTA concentrations in biologically active systems.

4.0 MATERIALS AND METHODS

This chapter provides an overview of the methods and materials used in meeting the objectives of the outlined research. All experiments were conducted at the Pittsburgh, Pennsylvania campus of the United States Department of Energy's National Energy Technology Laboratory (NETL). Research was conducted by the author in conjunction with research coordinators at the National Energy Technology Laboratory and the University of Pittsburgh Department of Civil and Environmental Engineering.

4.1 PROTOTYPE SCALE APPARATUS

4.1.1 Process Overview

Researchers at the United States Department of Energy National Energy Technology Laboratory (NETL) Division of Environmental Science and Technology investigated application of anaerobic biological treatment and regeneration of spent flue gas scrubber solution in a prototype scale upflow anaerobic reactor. Operation of the system can be summarized as follows:

- Absorption of nitric oxide into scrubber solution amended with ferrous EDTA
- Spent scrubber conditioning for bioreactor by pH neutralization and nutrient solution/ethanol addition
- Treatment of spent scrubber solution by reduction of nitric oxide present as the nitrosyl adduct of ferrous EDTA to N_2 gas
- Regeneration of spent scrubber solution by reduction of oxidized iron EDTA (ferric EDTA) present in the scrubber solution
- Recycling of treated and regenerated scrubber solution to the absorption stage

For the purposes of the proposed research, a simplified process included a packed absorption column for the removal of nitric oxide from NO balanced in nitrogen gas, followed by a bioreactor where scrubber solution was treated and regenerated. The regenerated scrubber solution is then recycled back to the absorption column. Figure 18 illustrates a schematic of the prototype process configuration. The prototype apparatus was assembled by NETL researchers using process components from a prototype apparatus that was previously used for evaluation of a sulfate reducing biological process for metal and sulfate bearing mine water (Hammack et al., 1998).

A scrubber solution amended with the chelate ferrous ethylenediaminetetraacetic acid $[Fe(II)EDTA]^{2-}$ was used to scrub nitric oxide (NO) from a synthetic flue gas. The scrubbed solution containing the adduct $[NO\bullet Fe(II)EDTA]^{2-}$, free ferrous EDTA, and ferric EDTA - was then transported to a continuously stirred tank reactor, where it was pH adjusted to neutral pH. The process water was amended with an ethanol/nutrient solution as it was fed to a bioreactor that was arranged in an up-flow configuration. The bioreactor was operated under high-mesophilic/low-thermophilic conditions (35 ºC) and in the absence of oxygen.

In the presence of a solution of nutrient amended carbon source/electron donor (ethanol) oxidized species present in solution were biologically reduced. Reduction of the nitrosyl adduct of ferrous EDTA to nitrogen gas removed the NO molecule from the weak electron sharing bond with the ferrous EDTA, allowing for subsequent reloading of the free ferrous EDTA with nitric oxide when recycled to the scrubber. Reduction of ferric to ferrous iron returns the iron chelate to the ferrous form that is active for NO adsorption.
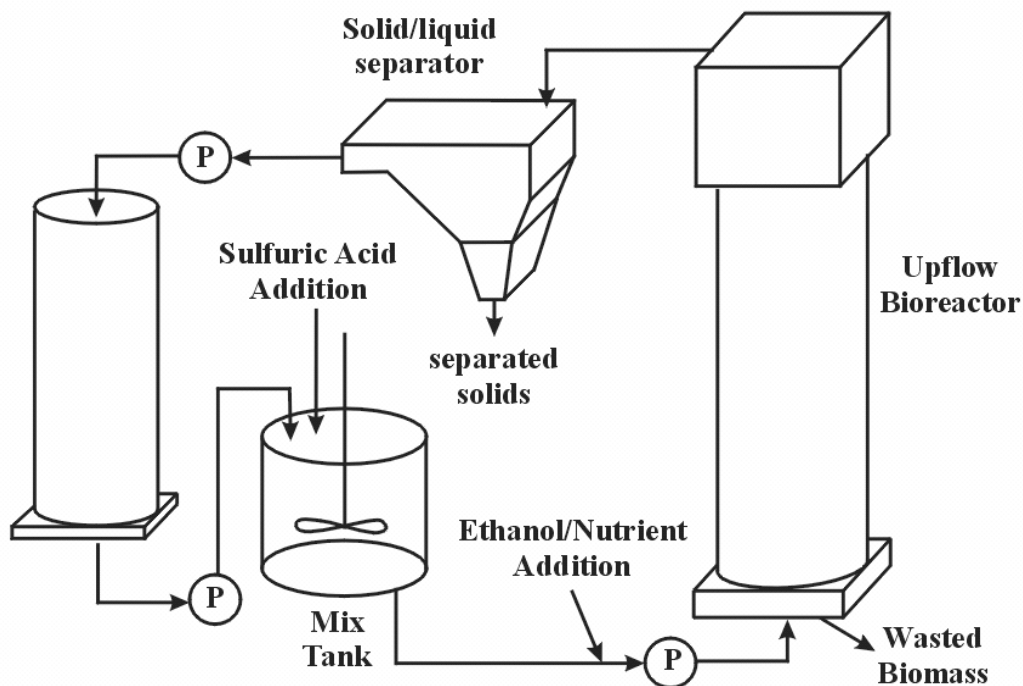
Figure 18. Prototype NO$_X$ adsorption and spent process water treatment and regeneration process.

A more detailed description of each of the components of the system of Figure 18 is provided below.

4.1.2 Scrubber Description

During Phase II of process operation, process water is passed through a small packed bed counter-flow absorption scrubbing tower. The scrubbing tower has an internal diameter of 8.5 inches and an effective depth of 21 inches. It is packed with 1-inch plastic pall rings. The system was operated using a target concentration of 0.045 M iron EDTA solution for scrubbing of nitric oxide. Scrubber solution was fed into the top of the scrubbing tower, and trickled through the pall rings to increase surface area that is in contact with the gas stream. The gas was introduced into the bottom of the scrubbing tower and traveled up through the tricking scrubber liquor. Liquid and gas flows could be manipulated to increase or decrease scrubber efficiency. Typically, flue gas flow rate was maintained near 3.2 liters per minute with a typical scrubber solution flow rate of approximately 0.19 liters per minute. The scrubber was operated at ambient temperature (20 ºC). After [NO•Fe(II)EDTA]$^{2-}$ adduct formation, spent scrubber solution was then pumped to a small CSTR, referred to herein as the mix-tank.

4.1.3 Mix Tank

Spent process water pumped from the absorption tower effluent to a mix-tank with a maximum capacity of 59 liters. The mix tank served as a storage vessel where process water was conditioned prior to biological treatment and regeneration, as an equalization-tank controlling process hydraulic balance, and as a preliminary bioreactor before process water was pumped to the up-flow reactor. Spent process water conditioning included pH adjustment to maintain spent scrubber solution pH at circum-neutral conditions and heating to maintain a solution temperature of 35 ºC. Process water pH drifted up as a function of the generation of alkalinity associated with denitrification of the process water, as is described in Chapter 2 above. Mix-tank effluent was amended with ethanol/nutrient solution just before entering the upflow biological reactor to promote growth and metabolic activity of nitric oxide and ferric EDTA reducing in the upflow bioreactor. Finally, the mix tank was equipped with a float gauge to monitor the level of process water in the tank. By observing trends of fluctuation in the process water level in the mix tank, the flows of the pumps feeding into and drawing from the mix tank could be adjusted to control hydraulic balance in the system. Finally, the prototype apparatus was monitored using a simple processor unit that provided basic process control. In particular, the processor identified when conditions breached predetermined thresholds for process water temperature, pH, and tank level (high and low) and shut down all pumps, the mixer, and the heating element.

4.1.4 Biological Reactor Description

The prototype scale reactor is an up-flow reactor that was originally designed to operate as a sulfate reducing upflow anaerobic sludge-blanket (UASB) reactor. The reactor has an empty bed volume of 42.5 liters and is fitted with a water jacket that maintains the reactor at low-thermophilic conditions (35-40°C). Spent scrubber solution was combined with ethanol/nutrient solution and fed into the bottom of the reactor. In the bioreactor, the spent scrubber liquor/nutrient solution mixture was exposed to populations of bacteria capable of performing the desired reduction reactions. The bioreactor VSS reached concentrations of up to 2.7 grams per liter at the bottom of the bioreactor and 1.01 grams per liter in the bioreactor effluent. Qualitative observation of the biomass showed that granulation of biomass was never achieved, and biomass maintained flocculent characteristics throughout process operation. Granulation of biomass is often observed in strictly anaerobic bioreactors operating in an upflow configuration and

consistently under sulfate reducing and methanogenic oxidation reduction conditions. This matter is discussed in further detail in Chapter 5.

Prior to upflow reactor inoculation and loading, a tracer study was conducted to determine the hydrodynamic characteristics of the upflow reactor. A step-input tracer study was performed using methyl orange as the chemically inert indicator and a spectrophotometric method was used to determine methyl orange concentration. The geometry of the upflow reactor suggests that it would perform in a manner approaching that of an ideal plug-flow reactor. The tracer study showed that the upflow reactor performed as four continuously-stirred-tanks connected in series. Details of the tracer study experiment and description of the subsequent calculations are provided in Appendix A.

4.1.5 Reactor Inoculation

The bioreactor was initially inoculated with biomass from two distinct stages of two publicly owned wastewater treatment plants located in western Pennsylvania. Approximately five liters each of mixed liquor from an anaerobic digester and from an anoxic denitrification basin were added to the prototype upflow bioreactor with the balance of the volume filled with 0.045 M ferrous EDTA solution. The anoxic denitrifying seed bacteria came from the Unity Township Municipal Authority Pleasant Unity Sewage Treatment (NPDES PA 0092274), Unity Township, Westmoreland County, PA. The plant permit allows for a 0.95 MGD discharge to an unnamed tributary of the Sewickley Creek. The anaerobic digester biosolids were taken from the Pleasant Hills Authority Wastewater Treatment Plant (NPDES PA 0027464), located in Pleasant Hills, Allegheny County, PA. This plant has an approximate treatment capacity of 20 MGD and discharges to Lick Run, a tributary to Peters Creek. Details of reactor inoculation and reactor startup are provided in Chapter 5.

4.1.6 Prototype Process Operation

The prototype process was operated in two distinct stages. Following is a brief description of the general operation scheme applied in each phase.

4.1.6.1 Phase I of Operation – Biomass Cultivation. During the first 42 days of process operation, the absorption step was absent from the process. The process was loaded with iron EDTA solution and nitrate was added to the solution as a surrogate for the nitrosyl adduct of ferrous EDTA. After initial nitrate addition and addition of nutrient/ethanol solution, biomass in the upflow bioreactor began to perform denitrification (reduction of nitrate to nitrogen gas) as evidenced by observed generation of biogas. Volume and mean composition of biogas is described in Section 5.2.2. In addition to the formation of biogas, denitrification also generates alkalinity, and as such a gradual increase in pH was observed in the mix tank. As the pH increased above the designated high pH threshold (7.1), nitric acid was fed to the system to decrease the pH to near neutral. As a result, additional nitrate ion was added to the solution allowing additional denitrification to take place. In this manner, denitrifiation was promoted throughout the first 42 days of process operation, and a substantial population of denitrifying bacteria was developed throughout the closed-loop process. In addition to denitrification, iron reduction was observed to occur and a population of bacteria capable of reducing iron present in the iron EDTA chelate was cultivated.
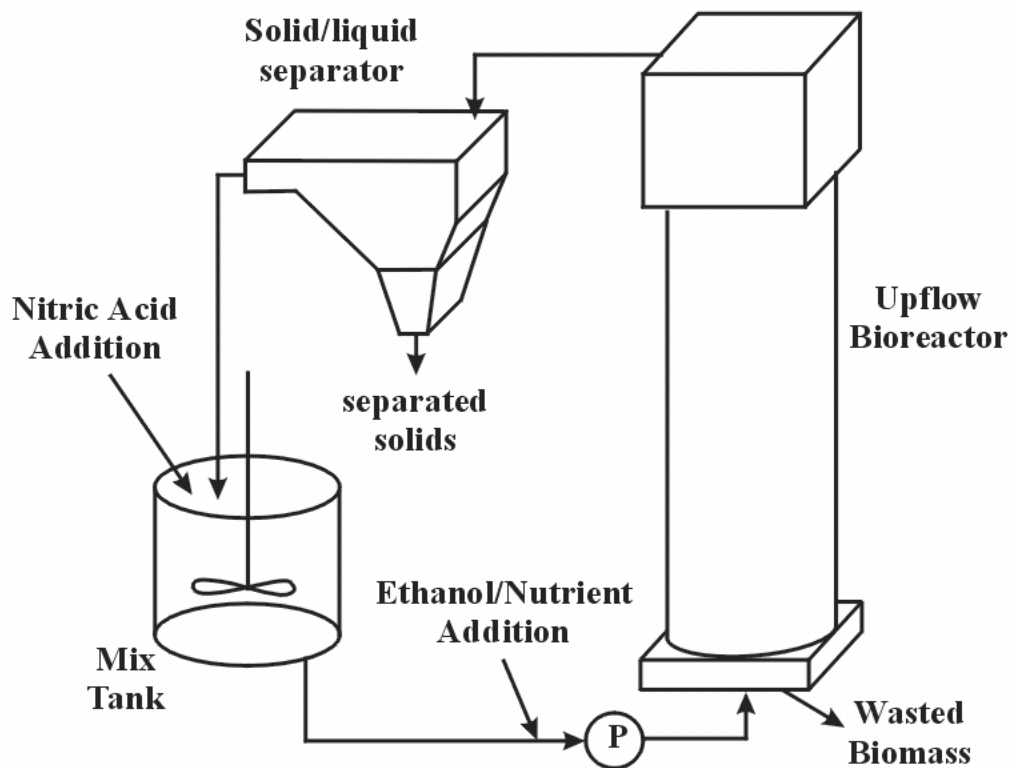
Figure 19. Prototype process as operated in Phase I, with nitric acid addition used as both a nitrate source and means of pH adjustment.

4.1.6.2 Phase II of Operation – Addition of NO scrubbing. Following this initial period of biomass cultivation, nitrate addition was terminated and was replaced with NO addition as the oxidized nitrogen electron acceptor in the system. The absorption stage was initiated for the scrubbing of nitric oxide balanced in nitrogen gas.   Nitric oxide was scrubbed from the gas phase with a high degree of efficiency, and effectively all of the NO fed to the scrubber reported to the process water. In place of nitric acid, sulfuric acid solution was used to counter the pH increase resulting from NO reduction in the process water. In addition to reduction of the nitrosyl adduct of ferrous EDTA, oxidized ferric EDTA was also reduced in the biologically active process stream. In this manner, the bioreactor operated for 100 days. Further discussion of process operation and performance is described in Chapter 5.

4.2 REAGENT PREPARATION

4.2.1 Ferrous EDTA Preparation

A 0.045 M solution of ferrous EDTA was prepared using ferrous sulfate and disodium EDTA added in equimolar concentrations to distilled water that was nitrogen purged to remove dissolved oxygen. The solution was prepared in a glove bag under anaerobic conditions in order to prevent introduction of dissolved oxygen and subsequent oxidation of ferrous EDTA to ferric EDTA. After preparation, the solution was stored under a blanket of inert gas in order to prevent oxidation of the ferrous iron in the chelate.

4.2.2 Preparation of NO·Fe(II)EDTA solution

NO was bubbled through a solution of ferrous EDTA until full breakthrough of NO was observed in the sparging vessel effluent. Effluent gas NO concentration was monitored in real time using a Horiba gas analyzer (Model PG-200). The total mass of NO present in solution was determined by graphical integration of the plot of mass concentration scrubbed versus time. Concentration of NO·Fe(II)EDTA present in solution was then calculated as the difference between the total NO absorbed and the previously calculated equilibrium concentration. The remaining concentration of ferrous EDTA present in solution without nitrosyl adduct was calculated as the difference between initial ferrous EDTA concentration (0.045 M) and the concentration of NO·Fe(II)EDTA. After this solution was prepared, it remained in a glove bag under N_2 positive pressure in order to avoid oxidation of ferrous EDTA in solution. Batch tests were initiated as soon as possible after NO·Fe(II)EDTA solution preparation in order to minimize loss of nitrosyl adduct resulting from adduct breakdown. However, observation of a saturated solution of the nitrosyl adduct of ferrous EDTA for six weeks showed that, when contained under a blanket of inert gas, in the absence of light, under sterile and quiescent conditions, the saturated solution exhibited negligible break down over a period of a month.

4.2.3 Ethanol/Nutrient Solution Preparation

The nutrient solution used in the UASB reactor was made up of 1.887 moles/liter of ethanol (181.2 grams of COD per liter), 0.20539 moles/liter of ammonium chloride (NH_4Cl), and 0.01936 moles per liter of potassium phosphate (KH_2PO_4). Deionized water was then used to bring the solution to volume. The carbon to nitrogen to phosphorus molar ratio of the nutrient solution being used in the reactor initially was 200:10.6:1. Nutrient solution was amended with a small concentration of a comprehensive trace element solution in order to ensure that concentrations of those elements were not limiting to cell growth and metabolic activity. One milliliter of a stock trace element solution was added to each liter of nutrient solution used in batch tests or continuous prototype scale operation. The trace element solution composition is summarized in Table 7. In addition, two milliliters of concentrated HCl was added to one liter of trace metal solution to promote dissolution. The solution was buffered by addition of $NaHCO_3$ (5.4 g/l).

Table 7. Trace element solution micro-nutrient composition.

Constituent	Concentration (mg/L)
$FeCl_2 \cdot 4H_2O$	2000
H_3BO_3	50
$ZnCl_2$	50
$CuCl_2 \cdot 2H_2O$	38
$MnCl_2 \cdot 2H_2O$	500
$(NH_4)_6Mo_7O_{24} \cdot 4H_2O$	50
$AlSO_4$	241.3
$CoCl_2 \cdot 6H_2O$	2000
$NiCl_2 \cdot 6H_2O$	92
$Na_2SeO_3 \cdot 5H_2O$	284
$NaHCO_3$ (buffer)	5400

4.2.4 Biomass preparation

Seed inoculum for batch analyses were taken from the prototype-scale upflow bioreactor while operating under pseudo-steady state conditions. The upflow bioreactor served as the treatment and regeneration stage in the closed loop process used for the investigation of the iron EDTA solution-based NO absorption process. Biomass was cultivated over a period 100 days with ethanol as the primary electron

donor and NO·Fe(II)EDTA and Fe(III)EDTA as the primary electron acceptors. Bacteria were extracted using a syringe in order to minimize their exposure to the atmosphere. The sample was then centrifuged for 5 minutes at 4000 rpm at 4 °C, and the supernatant discarded. The remaining pellet of biomass was resuspended in a sterile 0.045 M solution of ferrous EDTA, and centrifuged as before. The supernatant was again discarded and the pellet of biomass was resuspended in a sterile 0.045 M solution of neutralized ferrous EDTA. After final centrifugation, the pellet of biomass was resuspended in a sterile 0.045 M ferrous EDTA solution. The inoculum suspension was then refrigerated (4 °C) overnight in order to exhaust biomass of internal energy stores remaining from metabolism that initiated in the bioreactor. The resulting mixture was used as seed inoculum in batch experimentation. Duplicate inoculum samples (50 ml each) were analyzed for volatile suspended solids concentration.

4.3 ANALYTICAL METHODS

Following is a summary of methods used for the quantitative analysis of pertinent phenomena observed through the course of experimental data collection. Specifically, procedures for measurement of oxidized and reduced species contributing to the microbially-catalyzed reactions of interest are outlined.

4.3.1 Ferric EDTA Concentration Determination

Ferric EDTA concentration was determined by measuring and plotting absorbance values of standard solutions of varying ferric EDTA concentration, with constant total iron EDTA concentration. Absorbance at 477 nm was found to be proportional to the concentration of ferric EDTA. De-aerated solutions of 0.045 M ferrous and ferric EDTA were combined in several different volume ratios to generate solutions of varying ferric EDTA concentration but constant total iron EDTA concentration. These samples were analyzed spectrophotometrically to measure the absorbance response. Absorbance spectroscopy is based on the difference between the incident light and the observed light transmitted through a sample. The degree of light absorbed in the sample is a function of sample thickness, concentration of absorbing compound, and the chemical nature of the compound. Absorption may be described by Beer's Law. Details of absorbance theory have been omitted from this document. Figure 20 shows the absorbance response from a spectrophotometric scan of solutions of varying concentrations of ferric EDTA, but 0.045 M of total iron EDTA. Figure 21 displays the predictable spectrophotometric response at 477 nM with varying ferric EDTA concentration. While the spectrophotometric response is

predictable, it is linear only at relatively low concentrations (below approximately 0.01 M) and therefore does not obey Beer's Law in the concentration range of interest. As a result, the spectrophotometric method of ferric EDTA concentration determination is useful only for qualitative determination ferric EDTA.
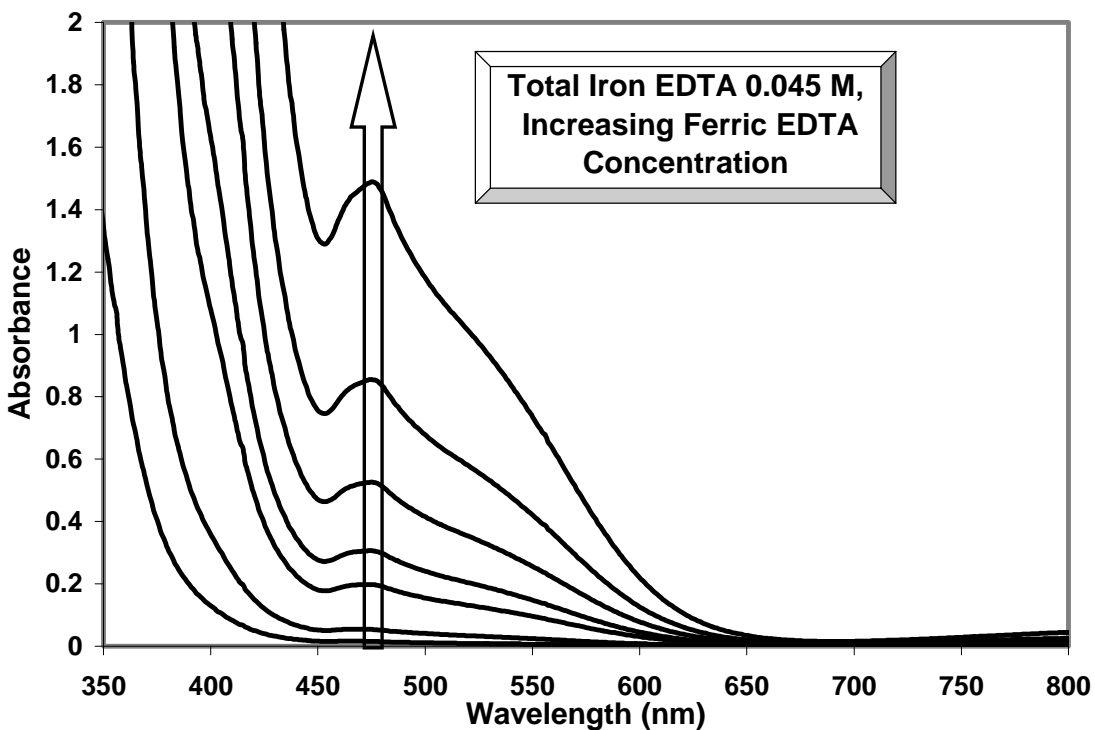
Figure 20. Spectrophotometric scans of iron EDTA solutions with varying ferric EDTA concentrations reveal a predictable absorbance peak at 477 nm.

The chart shows a curve with the equation:

$$y = 462.19x2 + 12.714x$$
$$R2 = 0.9957$$

with y-axis labeled "absorbance" (0 to 1.6) and x-axis labeled "[Fe(III)EDTA], M" (0 to 0.05).
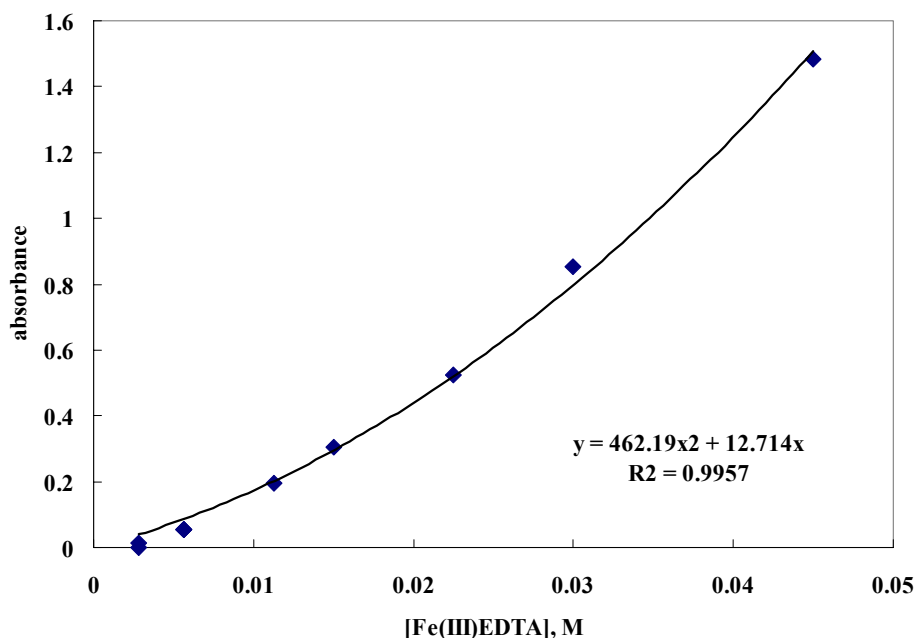
Figure 21. Increase in absorbance response (477 nm) with increasing ferric EDTA concentration in an 0.045 M Ferrous EDTA solution.

In addition to spectrophotometric analysis, samples were also analyzed using an electrochemical analyzer with rotating-disc electrode. Electrochemical measurements were conducted using a BAS100 Electochemical Analyzer with a glass cell. The working electrode was a platinum rotating disc electrode (0.33 cm^2 surface area) in a Teflon housing. A silver foil reference electrode immersed in a 2 M potassium chloride salt bridge solution and set in a glass compartment connected to the test cell through a permeable fine glass frit served as the system reference electrode. A platinum foil immersed in a KCl solution and set in a glass compartment with a fine glass frit served as the counter electrode. Instrument specifications note an absolute accuracy within 1% of the full-scale, and resolution within 0.05% of full-scale. Data collected on the BAS-100 were exported to a personal computer via serial interface. The native data format of the instrument is a hexadecimal format. Files were converted to ASCII using a BASIC routine and imported to Microsoft Excel.

Linear sweep and cyclic voltammetric methods were employed. These electrochemical methods provide a straight-forward and theory grounded means of verifying the degree to which iron in solution is oxidized or reduced. The platinum rotating-disc working electrode was operated at 700 rpm, with a voltage scanning rate of 50 mV/sec. Scans were carried out at 25° C. Figure 22 illustrates the three electrode apparatus.
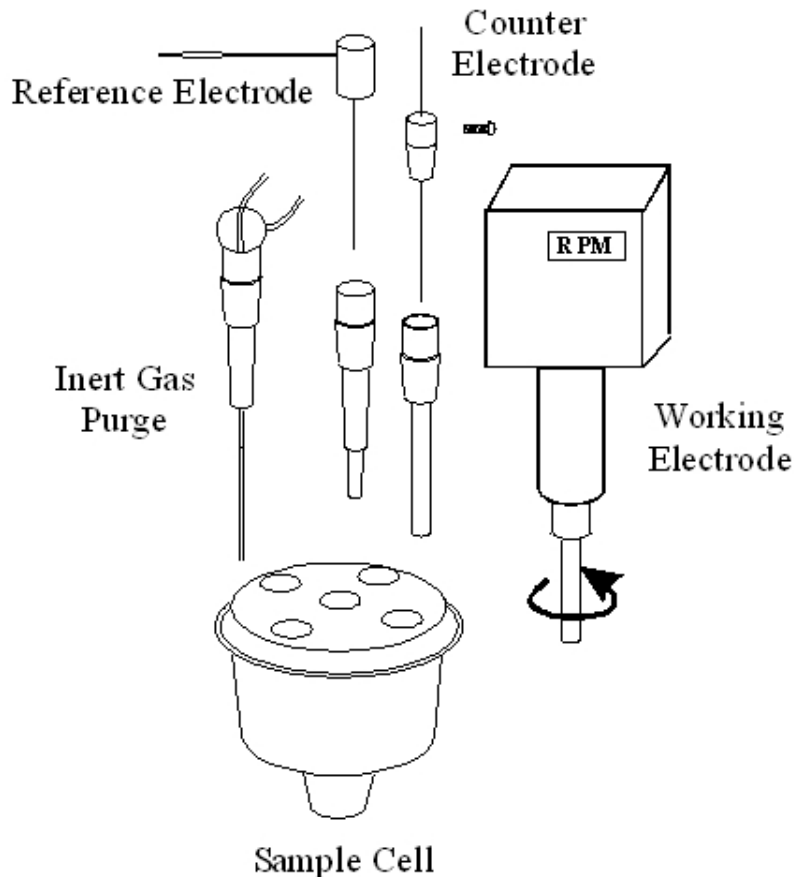
Figure 22. Three electrode apparatus compromising the BAS-100 electrochemical cell.

As described in Chapter 3, the current response generated from a linear sweep voltammetric experiment is linearly proportional to the concentration of the analyte being observed. Figure 23 shows data collected from a series of LSV experiments conducted at varying ratios of ferrous/ferric EDTA but constant concentration of total iron EDTA. Figure 24 displays the linear relationship between the current response at –400 volts (vs. Ag/AgCl electrode) and ferric EDTA concentration in an 0.045 M solution of total iron EDTA. A voltage of -400 volts (vs. Ag/AgCl reference) was sufficiently separated from the formal reduction potential of the Fe(II)EDTA/Fe(III)EDTA Nernstian couple (-126 volts vs. Ag/AgCl reference) to the induced current to fully establish. These data serve as a standard curve to which sample data are compared for quantitative determination of solution ferric EDTA concentration.
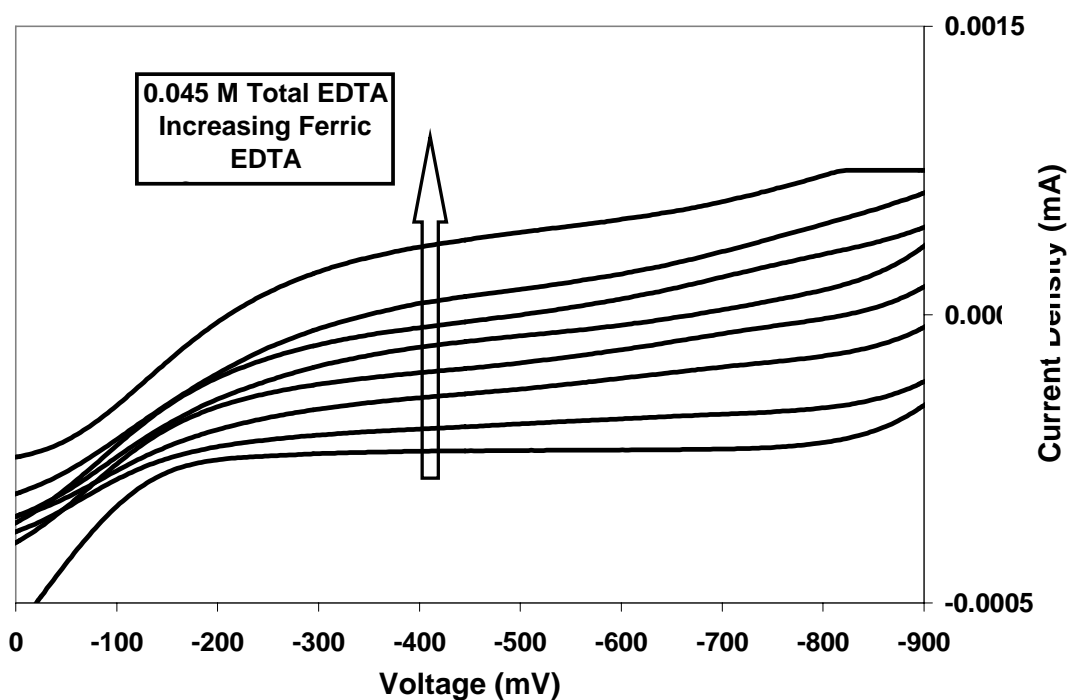
Figure 23. Increase in local current peak with increasing Ferric EDTA concentration (at a cathodic potential of -400 v. vs. Ag/AgCl reference electrode)
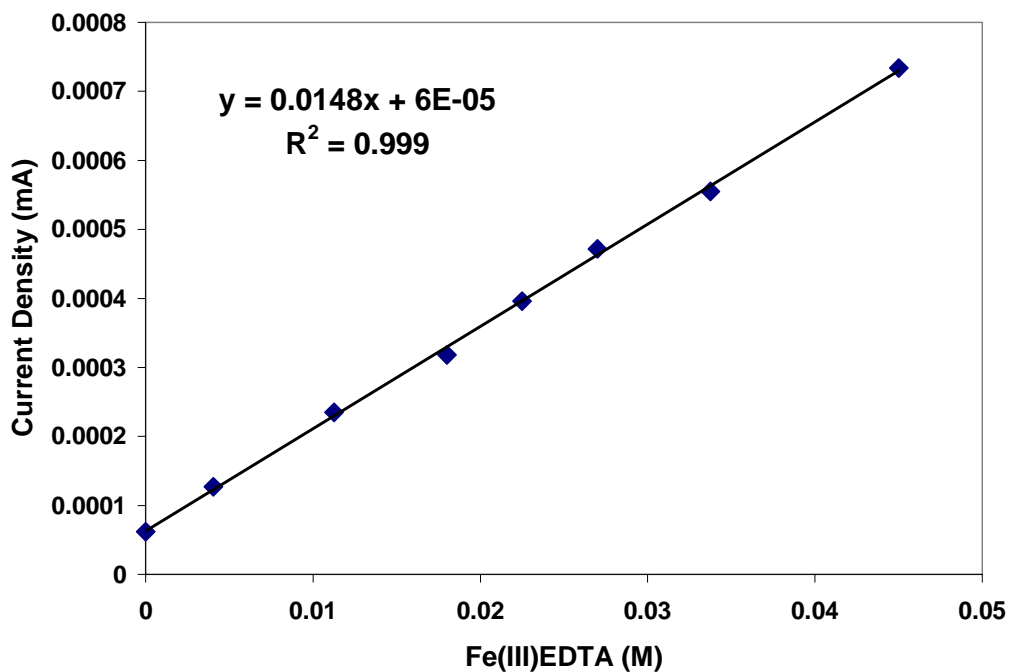
Figure 24. Linear correlation between solution ferric EDTA concentration and current at -400 mV (vs. Ag/AgCl reference)

4.3.2 NO*Fe(II)EDTA^{2-} Spectrophotometric Determination

A spectrophotometric technique was employed for the measurement of [NO•Fe(II)EDTA^{2-}]. A standard curve was developed based on magnitude of spectrophotometric absorbance responses of samples of known NO•Fe(II)EDTA^{2-} concentration. A 1:1 Fe(II)/EDTA ratio with a nitrosyl adduct exhibits peaks at wavelengths of 342, 433, and 633 nm. A peak at 433 nm shows the strongest differential absorbance, and was therefore used for quantitative determination of nitrosyl adduct concentration. This method works very well for pure solutions of NO•Fe(II)EDTA^{2-} prepared in distilled water.
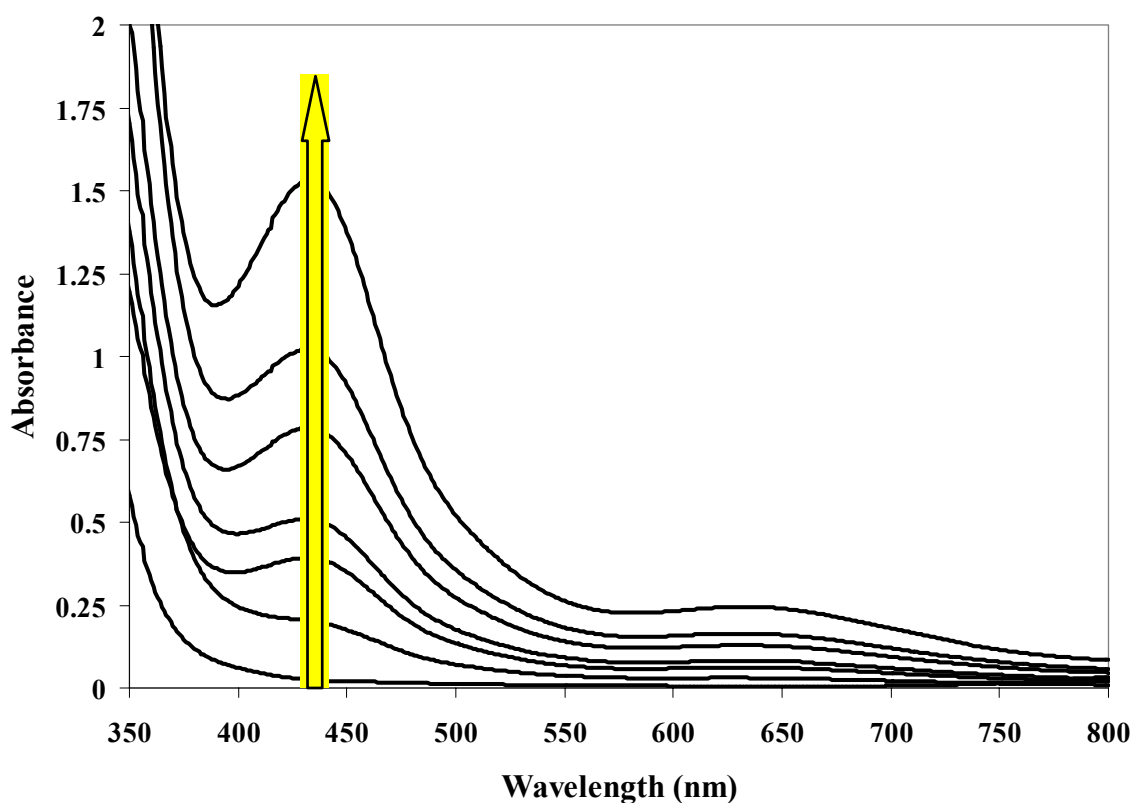
Figure 25. Spectral scan of varying concentrations of NO·Fe(II)EDTA^{2-}
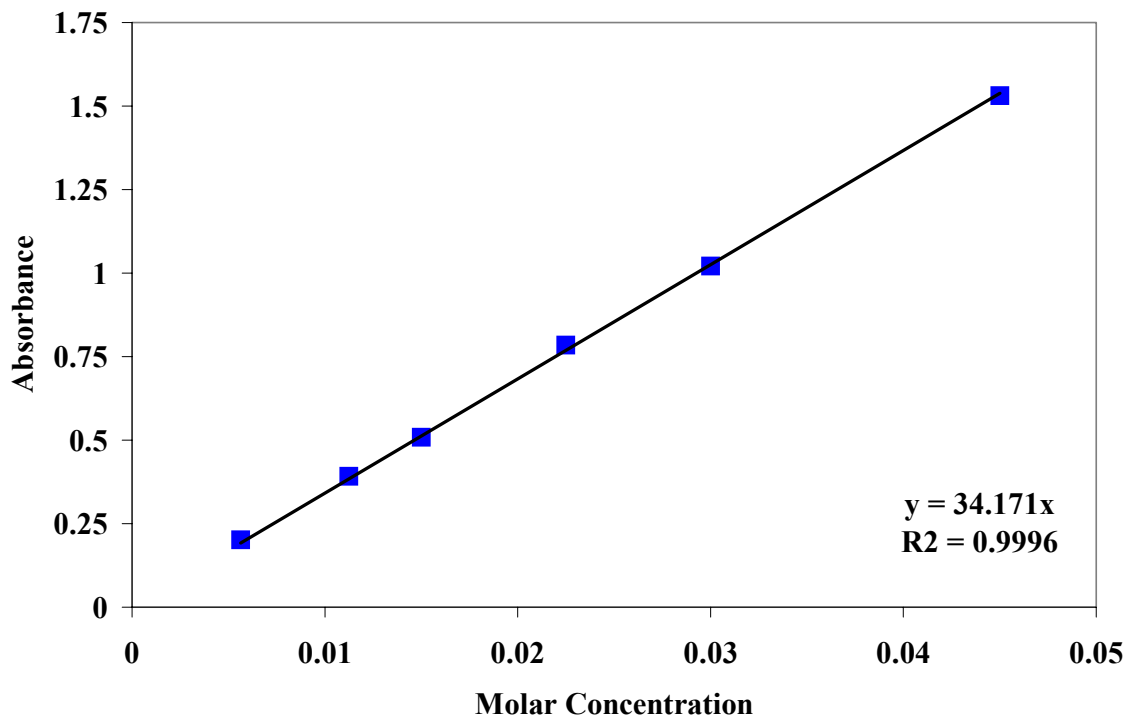
Figure 26. Absorbance at 433 nm vs. concentration of NOFe(II)EDTA

When inoculated with biomass, care must be taken to ensure that biosolids are removed from samples prior to spectrophotometric analysis. To this end, samples were both centrifuged and filtered with a 0.045 micron syringe filter before spectrophotometric analysis.

4.3.3 Total Suspended Solids, Volatile Suspended Solids, Ash Content

Samples taken from the reactor were centrifuged and the centrifugate was analyzed for total suspended solids, volatile suspended solids, and total non-volatile suspended solids (mineral ash) content based on the procedure described in Standard Method 2540. Volatile suspended solid content was used as an approximation of total biomass concentration.

4.3.4 Quantitative analysis of ethanol and products of its oxidation

Quantitative analysis of ethanol and products of its oxidation was performed using a Hewlett Packard (HP) 5890A capillary gas chromatograph equipped with a split injector held at 200 °C, and a flame ionization detector. The column used for analysis was a 60m x 0.25 mm internal diameter fused silica capillary column coated with a 0.25 μm film of a cross-linked version of SP-1000® (commercially known as Nukol®). A helium carrier gas with an average linear velocity of 30 cm/sec at 50 °C was used. The column head pressure was maintained at 270 kPa. Approximate elution times for analytes of interest are 3.5 minutes for acetaldehyde, 6.5 minutes for ethanol, and 12.5 minutes for acetic acid. Detection limits are 5, 5, and 50 parts per million by volume, respectively with R^2 values of 0.999 for all analytes in the region between 1000 ppm and detection limit.
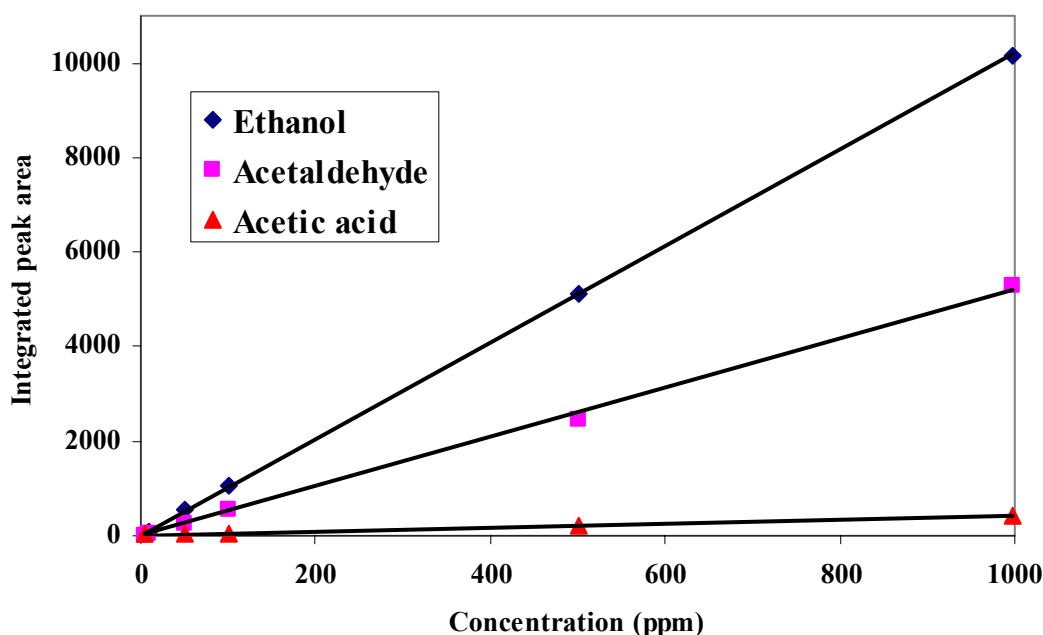
Figure 27. Gas chromatograph integration area versus analyte concentration.

One significant limitation in the application of gas chromatography as an analytical tool in the described process is the inability to resolve acetic acid generated as a product of ethanol oxidation and other acetogenic reactions from the large number of carboxylic acid groups present in the EDTA molecule. Each EDTA molecule includes four caroboxylic acid groups. These functional groups are not readily available for use by bacteria. In contrast, utilization of ethanol and products of its oxidation are significantly more available and thermodynamically favorable. As a result, it is not expected that the

caroboxylic acid groups in the EDTA molecule affected the rate of reduction of oxidized species that was catalyzed by microorganisms in the system. It does, unfortunately, prevent the observation of acetic acid accumulation in the batch reactors used for determination of kinetic constants. Attempts to subtract the known concentration of carboxylic acid introduced by the presenece of EDTA were unsuccessful. Change to the shape and area of the acetate elution peak were observed, making integration for determination of total acetate concentration problematic. However, during bioreactor operation, an external laboratory was employed for periodic analysis of reactor performance and quality control. Samples sent to this laboratory employed ion chromatography for analysis of acetate concentration in solution, and interference of acetic acid in the EDTA molecule was not problematic.

4.4 BATCH EXPERIMENTS FOR DETERMINATION OF KINETIC CONSTANTS

Batch reactor experiments were conducted in order to determine kinetic constants associated with each of the two primary microbially-catalyzed reactions of interest. Specifically, the rate at which the nitrosyl adduct of ferrous EDTA and ferric EDTA were reduced by bacteria taken from the mature prototype reactor was evaluated at several different initial ethanol concentrations. Batch tests were conducted in a series of Erlenmeyer flasks (0.5 liter). Flasks were inoculated with seed biomass cultivated from samples extracted from the prototype-scale bioreactor. Batch tests were carried out at varying ratios of ethanol: electron acceptor at ethanol concentrations above and below the stoichiometric ethanol requirement (based upon the previously described stoichiometry). All tests were conducted in triplicate.

In a few cases, one of the triplicate batch reactors did not remain airtight. Because the introduction of air resulted in the oxidation of reduced species and decreased reducing activity of anoxic/anaerobic biomass, these data were discarded and the results were not considered in kinetic evaluations. In order to maximize uniformity among several batch reactors in the same experimental series, the matrix was prepared in a single vessel and completely mixed before being distributed to serum bottles. Preparation was conducted in a glove bag under inert gas positive pressure in order to insure that anaerobic conditions were maintained. In those series where bacterial inoculation was required, the inoculum was introduced as the final step, and the time of inoculation noted as the starting time for

kinetic analyses. A 5% by volume inoculum of known volatile suspended solids concentration was transferred to Erlenmeyer flasks used for batch analysis.

Prepared inoculum was transferred into batch reactors under strict anaerobic and semi-sterile conditions.   The flasks were stoppered and flushed with argon gas before being placed on an incubator/shaker table at 35 °C and 50 rpm. Samples were analyzed for concentration of oxidized species as well as concentration of ethanol and products of its oxidation. Separate batch reactors were operated for the observation of change in solution oxidation reduction potential and pH. Solutions used in batch analyses were adjusted to an initial pH of 7.0 before inoculation using hydrochloric acid, except where noted. Batch reactors were prepared using deoxygenated solutions prepared under nitrogen or argon purge. Care was taken to prevent exposure to the atmosphere to prevent shocking of anoxic and anaerobic bacteria, and to prevent oxidation of reduced species in solution. Samples were drawn from the reactors by displacing an aliquot of reactor solution into a sample bottle using nitrogen gas pressure. Figure 28 illustrates configuration of batch reactors. Details of batch analysis design and discussion of results of kinetic analyses are discussed in detail in Chapter 6.
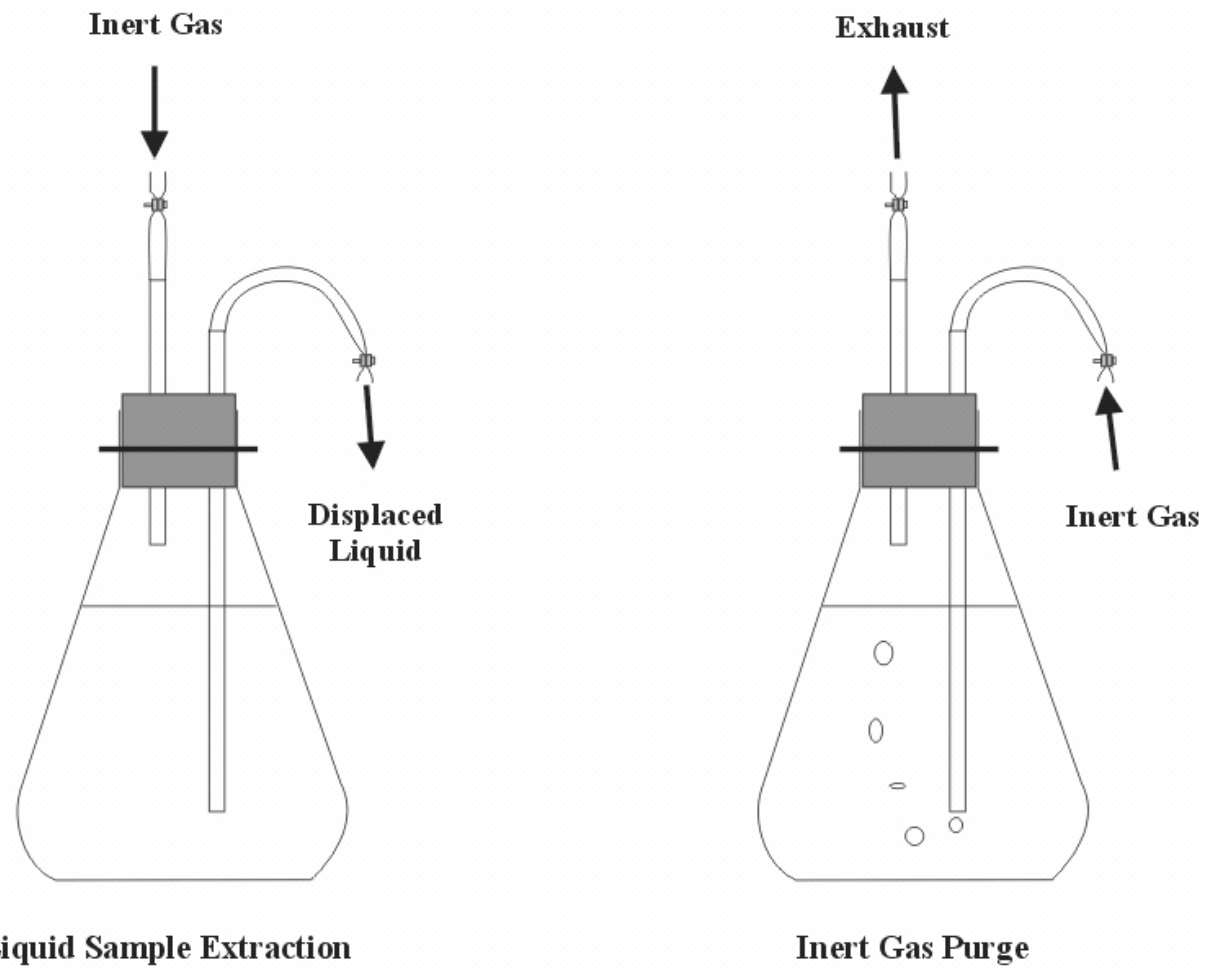
Figure 28. Bench scale batch apparatus for determination of Monod reaction constants

5.0 PROTOTYPE PROCESS OPERATION AND PERFORMANCE

Following is description of the observed performance of the prototype-scale apparatus, including an upflow bioreactor, employed to demonstrate the feasibility of the process under consideration.

5.1 PROTOTYPE PROCESS OPERATION

The prototype process was operated for a total of 149 days. As described in the materials and methods section, the prototype process was operated in two phases: an initial period of biomass development/reactor startup, referred to herein as Phase I, and a second period of prototype scrubber operation under pseudo-steady-state conditions, Phase II. Both phases of process operation will be described in detail.

According to Equation 26, denitrification using ethanol as the primary electron donor consumes one mole of protons per mole of nitrate consumed, and generates 5/6 of a mole of CO_2. Reduction of the nitrosyl adduct of ferrous EDTA using ethanol as the primary electron donor, described in Equation 54, does not consume acidity, but generates 1/3 mole of CO_2 per mole of NO reduced. Reduction of ferric EDTA with ethanol (Equation 55) generates one mole of acidity per mole of ferric EDTA reduced, and $^1/_6$ moles of CO_2. However, considering the net effect of combined oxidation of reduced ferrous EDTA (Equation 53), which consumes one mole of protons per mole of ferrous EDTA oxidized, with reduction of ferric EDTA using ethanol results in no net acidity generation and $^1/_6$ of a mole of CO_2 generation. Because the pH of the process water was maintained circum-neutral, it is possible to estimate the fraction of bicarbonate ion between H_2CO_3 and HCO_3^-. At a pH of 7, this ratio is 0.1663:0.8337, respectively. In addition, reduction of oxidized nitrogen species, results in generation of N_2 gas that is observed in the generated biogas.

Because the process water was continuously adjusted to circum-neutral conditions, with acid added to account for the increase in pH resulting from generation of alkalinity. Equivalents of acid that were added to the bioreactor can therefore be used as one indicator of biological activity of the reactor. At neutral pH and 35 ºC the Henry's Law constant for CO_2 is $10^{-1.5}$, and the dissolved CO_2 is therefore P_{CO2} * K_H.

As a result, total volume of biogas generated, volume of pH adjusting acid that is fed to the process water, and volume of ethanol serving as both oxidized species and carbon source in the microbially-catalyzed reduction reactions of interest, are useful indicators of overall bioreactor performance. Figure 29 illustrates cumulative data for addition of ethanol/nutrient solution and acid solution, as well as total volume of biogas generated in the upflow bioreactor. This figure demonstrates the strong correlation between the two independent variables, biogas production, and acid feed. Loading of ethanol to the process was controlled by the operator. Ethanol loading was based on an estimation of the loading rate of target oxidized species to the system. Specifically, the amount of ethanol loaded to the upflow bioreactor was based on the NO loaded to the system and the concentration of ferric EDTA in the process water. In addition, process water oxidation reduction potential and biogas volume and composition help to inform control of organic loading rate.
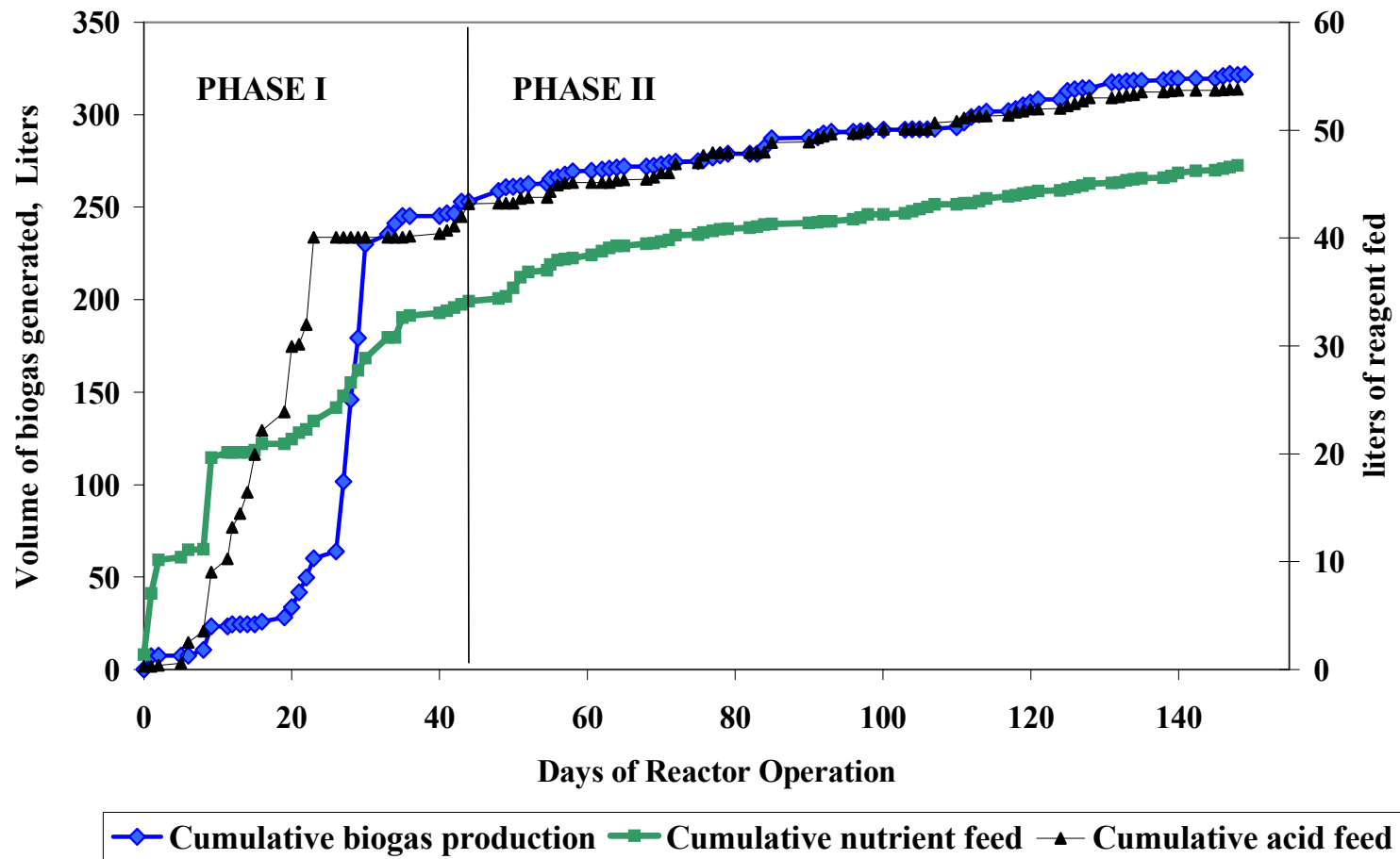
Figure 29. Cumulative ethanol/nutrient solution and acid solution loading, as well as cumulative biogas generated in the bioeractor indicates bioreactor activity.

5.1.1 Phase I – Bioreactor Inoculation and Process Start-up

Nitric oxide has been identified as an intermediate product in the stepwise biologically-mediated reduction of nitrate as carried out by denitrifying bacteria. It was assumed that by cultivating denitrifying bacteria, the ability of the microbial population in the reactor to reduce nitric oxide would also be enhanced. The prototype reactor was operated initially using nitrate as a primary electron acceptor as a means of quickly and conveniently building a substantial population of bacteria capable of reducing nitric oxide. After initial bioreactor inoculation with biomass from the denitrification stage and anaerobic digester biomass from a municipal wastewater treatment plant, bacteria were cultivated in a solution of 0.045 M iron EDTA. Use of seed biomass from municipal wastewater treatment bioreactors demonstrates that specialized bacterial strains are not required to catalyze the reactions of interest. However, without conducting microbiological molecular ecology tests on the reactor population, the relationship between species composition and diversity and biomass activity can not be studied (Grady, 1999). Without conducting such tests, it is also not possible to compare the ecological structure of the system described herein with that of similar studies conducted elsewhere, or to observe the cell population shift in the system under consideration as a function of time. Such tests, including PCR-DGGE and fluorescence *in situ* hybridization (FISH), were outside the scope of this study (Kumaraswamy *et al.*, 2004).

Iron EDTA solution was prepared under aerobic conditions; therefore, most of the iron was initially in the oxidized (ferric) form. During this period, nitric acid was added to the reactor to counteract pH increase resulting from previously described alkalinity producing reactions. In this manner, pH was maintained at approximately 7.0. As a result of the dissociation of nitric acid, a significant concentration of nitrate was also introduced to the reactor. The primary electron acceptors available for reduction were, therefore, nitrate and ferric iron present in the ferric EDTA adduct. Ethanol/nutrient solution was added to the reactor to provide electron donor/carbon source. Micronutrients required for new cellular growth were also added. The bioreactor temperature was maintained at 35ºC by a heated water jacket fitted around the bioreactor column. The bioreactor was operated under these conditions for 42 days.

A substantial population of denitrifying and iron reducing bacteria was developed during this period, with total suspended solids in the reactor bottom reaching 3.7 grams per liter and volatile suspended solids concentration of 2.6 grams per liter. Formation of biomass with a granular structure was not observed during prototype process operation, as would be expected of a upflow reactor operating under strict anaerobic conditions but were, rather, observed to develop as a bed of flocculent biomass. As a result of the lack of granule formation, a significant biomass washout was observed at the applied reactor hydraulic loading rate. The hydraulic loading rate during this period was maintained at an average

flow rate of 0.183 liters per minute (standard deviation of 0.01548 l/min). Figure 30 provides a more detailed look at the cumulative data indicative of reactor performance. Because the bioreactor was already seeded with denitrifying bacteria, prototype reactor activity was quickly established and grew rapidly. Performance was, however, not stable as a result of excessive nutrient loading, which appeared to decrease reactor NO reducing activity dramatically. On days 3 and 8, for example, excessive nutrient feeding resulted in decreased biogas generation in days 3 through 6 and 8 through 18, respectively. The period of greatest bioreactor activity was observed during the period of Day 26-30, during which the average biogas production rate reached 41 l/day. These data provide qualitative evidence suggesting that by the end of Phase I, a substantial population of denitrifying bacteria were established in the bioreactor.
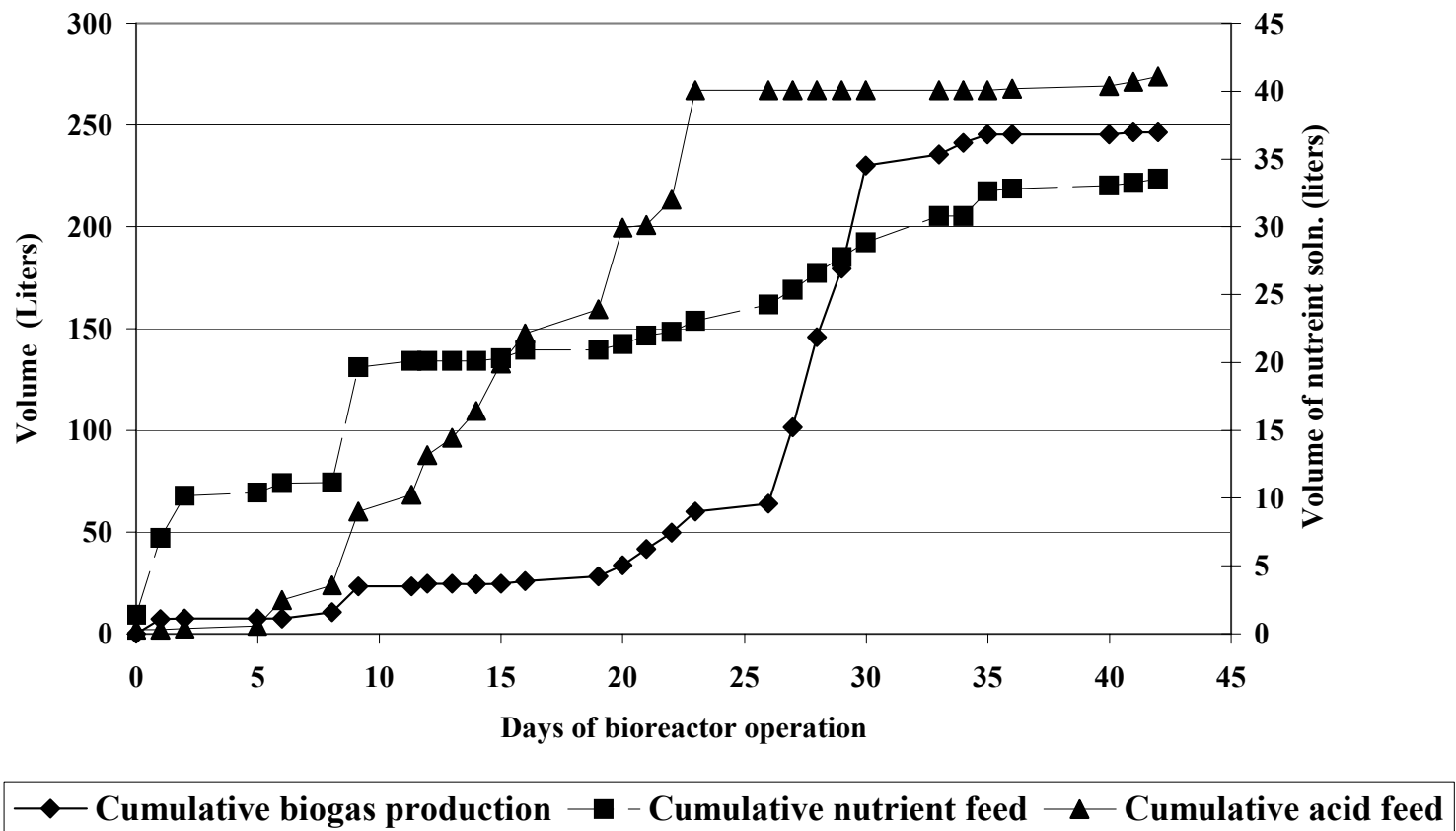
Figure 30. Cumulative data indicative of reactor performance during Phase I operation through day forty four of process operation

5.1.2 Phase II - Bioreactor / Scrubber Integration

Following the period of reactor start-up and biomass development under nitrate and iron reducing conditions, process configuration was altered such that nitric oxide, present as the nitrosyl adduct of ferrous EDTA, could be delivered to the bioreactor in place of nitrate. Instead of feeding nitrate to the system, the bioreactor was now coupled with a bench-scale gas scrubbing column to allow the absorption of nitric oxide (NO) from a gas stream of NO balanced with inert nitrogen gas. The process water was contacted with the feed gas in an adsorption column that was packed with one inch pall rings and operated in a counter-flow configuration. NO was scrubbed from the gas phase with ferrous EDTA amended solution according to Reaction 5. The spent scrubber solution, containing ferric EDTA, NO present as the adduct of ferrous EDTA, and free ferrous EDTA, was then pumped to a mix-tank. In the mix-tank, the solution pH was adjusted to neutral pH. Sulfuric acid replaced the previously described nitric acid solution so that nitrogen gas production in the bioreactor could be attributed to only NO reduction activity. The pH adjusted solution was then pumped to the bioreactor, with coincidental input of ethanol/nutrient solution. The process was operated in this manner for 100 days.

The number of moles of NO loaded to the scrubber is a function of the flow rate of gas entering the scrubber and the concentration of NO in the feed gas. Concentration of nitric oxide in the spent scrubber solution is a function of the molar loading rate of NO to the scrubber, the flow rate of the scrubber solution through the absorption tower, and the overall observed scrubber efficiency. Loading of NO to the bioreactor is a function of the concentration of NO in the spent scrubber solution and the flow rate of the solution into the bioreactor. Initially, a needle valve was used to control the flowrate of gas to the scrubber, and fine control of the gas flow rate was more difficult. Following installation of gas mass flow controllers, gas flow rate was more easily controlled. The NO loading rate was controlled by the operator in order to maintain a high degree of scrubber efficiency and a stable concentration of nitrosyl adduct loaded to the biological treatment stage of the process.

Because the active biomass in the process was constantly presented with additional oxidized species being loaded to the solution, bacteria which catalyzed the reduction of those added oxidized species thrived, while bacteria completing less thermodynamically preferable reduction reactions were, save a few exceptions, not presented with conditions under which they could thrive. Specifically, nitrate and nitric oxide reduction were thermodynamically preferred to the reduction of oxidized iron present in the EDTA chelate. Reduction of ferric EDTA was, in turn, preferred to the reduction of sulfate and methanogenesis. Continual loading of NO to the process water and partial oxidation of ferrous iron EDTA in process water limited, under most conditions, the degree to which sulfate reduction and

methanogenesis could proceed. Exceptions to this commonly observed condition occurred in two notable situations.

In the period of transition between Phase I and Phase II, the organic loading rate was not decreased adequately to allow for the decrease in molar loading of oxidized species. As a result, process water oxidation reduction potential decreased dramatically, and conditions were established where sulfate reducers and methanogens thrived. In addition, the slanted plate solid/liquid separator located after the upflow bioreactor has, by design, a region at the very base that experiences relatively quiescent conditions where settling solids collect and concentrate before being removed from the process. In this quiescent region of the settler, biomass collected and, in the presence of electron donor (ethanol/acetate) present in the bulk solution of the reactor effluent, the settling solids drifted into strictly anaerobic conditions as a result of the long residence time in that isolated region. These specific cases are described in more detail later.

5.2 PROTOTYPE PROCESS PERFORMANCE

5.2.1 Scrubber Performance

The average process water flow rate during the period of NO scrubber operation was 0.189 liters per minute (standard deviation of 0.0072 l/m). Because of limitations of available equipment, the gas loading rate to the scrubber did not exceed 4.27 liters per minute, with mean flow rate of 3.219 liters per minute (standard devation of 0.839 liters per minute) with an average NO concentration in the feed gas of 1525 parts per million (ppm) (standard deviation of 565.5 ppm). Average effluent stream NO concentration was 41 ppm (standard deviation 156 ppm). The average scrubber efficiency observed over this period of experimentation was 97.9% (standard deviation of 8.1%). With only a few exceptions, scrubber efficiency was maintained in excess of 99%. Figure 31 illustrates the efficiency of the NO scrubber throughout Phase II of process operation.

Specific instances of process failure account for most of the instances of significant scrubber efficiency decrease. For example, on Day 87 of process operation, catastrophic process failure occurred as a result of pump tubing failure. Approximately 40 liters of process water were spilled onto the laboratory floor. During this period, scrubber efficiency was essentially 0%, because no scrubber solution was being recycled to the reactor. In addition, the process water that was returned to the process spent

several hours on the floor before it was discovered and returned to the process. Because the contents were spread out as a thin film and exposed to the atmosphere during this period, the spilled process water was highly oxidized when returned to the process, and the anaerobic iron reducing bacteria contained within were shocked by the exposure to oxygen in the atmosphere. Iron reducing bacteria have exhibited significant retardation of reducing function as a result of exposure to air. Despite this fact, reducing conditions were quickly re-established in the bioreactor and scrubber efficiency was quickly returned to near 100%.

The rate at which NO was loaded to the process was limited by technical and funding constraints. The scrubber was loaded with NO from gas cylinders containing a known concentration of NO balanced in nitrogen gas. These compressed gas cylinders were expensive and gas flow rate was maintained at a relatively low value in order to keep research costs down. In addition, mass flow controllers used to control the gas loading rate to the scrubber were calibrated to work in a range of flowrates (limit for NO). It also should be noted that the focus of the research at hand was not to investigate the scrubbing portion of the process, which has already been categorized by several researchers (Li *et al.*, 1992; Dow, 1992). The scrubber was designed and operated such that nearly all of the NO being loaded to the absorption column was absorbed into solution. This allowed loading of NO to the scrubber solutions, while not wasting NO by inefficient scrubbing. A more detailed consideration of the degree to which scrubber was over-designed is provided in Chapter 7.
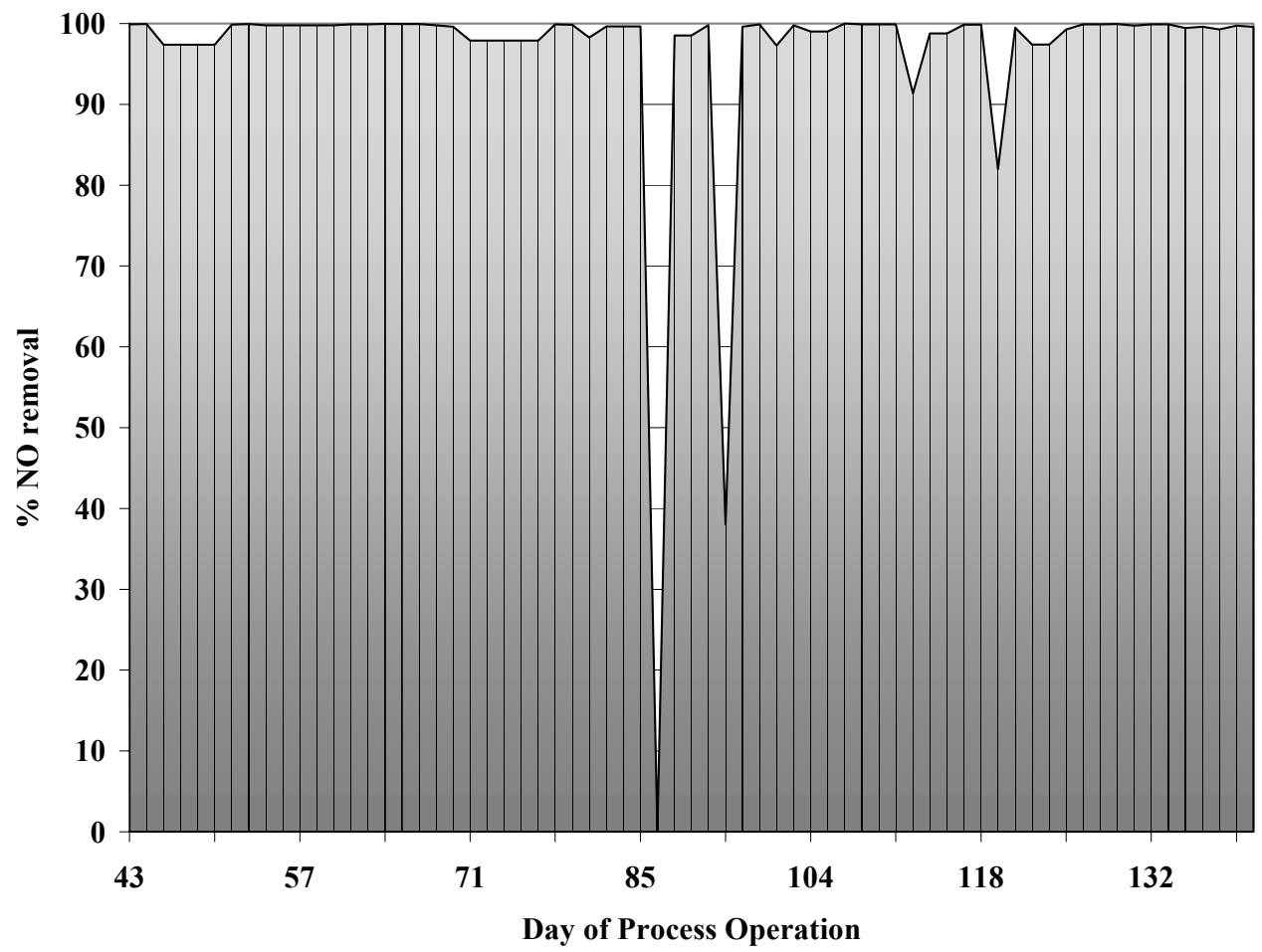
Figure 31. NO$_X$ removal efficiency of the prototype absorption column.

5.2.2 Prototype Reactor Biogas Volume and Composition.

5.2.2.1 Volume of biogas generated. During operation when nitrate was employed as the electron acceptor, a maximum gas production rate of 40.868 liters per day was observed. This observation was made over five days (n=5), with a correlation coefficient of 0.997. Over this same period, the average molar loading of nitrate to the process stream was 6.6 moles per day (standard deviation of 4.8 moles of nitrate/day). In contrast, the maximum observed gas production rate during system loading with NO was 5.879 liters per day as observed over four days (n=4) with a correlation coefficient of 0.952. The average molar loading of NO to the process stream was 0.288 moles per day with a standard deviation of 0.0001 moles per day.

Because there are the same number of moles of nitrogen in one mole of NO as there are in one mole of nitrate, the ratio of moles of nitrate fed to volume of N_2 gas generated at 35 ºC with the ratio of moles of NO fed to volume of N_2 gas generated at 35 ºC, may be compared directly. Theoretical nitrogen gas production from one liter of 0.045 M NO·Fe(II)EDTA^{2-} or 0.045 M nitrate at 35ºC is 0.284 liters. The primary difference in the volume of biogas generated in the prototype process between Phases I and II is therefore the substantial difference in total molar loading rate between NO and nitrate in Phases I and II, respectively.

5.2.2.2 Composition of biogas. As described earlier, the volume of generated biogas was used as a qualitative indicator of reactor performance. Biogas volume measurement was augmented with biogas sampling of the gas collecting in the air-tight headspace of the upflow bioreactor. During process operation, gas volume generated served as a useful qualitative indicator of process performance, and, it was hoped, would provide the opportunity to quantitatively determine NO reduction activity. However, as a result of biomass washout from the UASB, the entire closed loop process (including settlers, mixing tanks, and the absorption tower) was biologically active. Biogas was therefore generated throughout the system, making it impossible to account for all biogas generated and prohibiting successful nitrogen mass balance analysis.

A significant difference in biogas composition was noted between the period when the bioreactor was operated under denitrifying conditions and when the bioreactor was operated under NO reducing conditions. Figure 32 illustrates all collected biogas sample data. The mean gas composition of all samples analyzed during operation with nitrate and the nitrosyl adduct of ferrous EDTA as the primary electron acceptor are compared in Figure 33 and Table 8. These data show that percent N_2 composition of biogas formed while the bioreactor was operated using NO as the electron acceptor was over 9% greater than when the reactor was operated using nitrate as the primary electron acceptor. Biogas percent

composition of carbon dioxide was more than 10 percent greater under nitrate reducing conditions than under NO reducing conditions.

Table 8. Comparison of average biogas composition between period of operation with nitrate as electron donor, and with NO as electron donor.

	Average gas composition during Bioreactor Operated with Nitrate as Electron Acceptor	Average Gas Composition during Bioreactor Operation with NO as Electron Acceptor
H_2 (%)	0	0.014
O_2/Ar (%)	2.53	3.79
N_2 (%)	81.96	91.03
CH_4 (%)	0.00083	0.56
CO (%)	0	0
CO_2 (%)	15.50	4.59
C_2H_4 (%)	0	0
C_2H_6 (%)	0	0
H_2S (PPM)	47.06	0

Most of the bioreactor was maintained at oxidation-reduction potential levels less negative than those required of strictly anaerobic conditions where sulfate reduction and methanogenesis occur. However, the observation of persistent background concentrations of hydrogen sulfide and one period of significant methane production in the generated biogas suggests that such a drop in ORP and establishment of strictly anaerobic conditions remains a possibility, and can only be avoided through careful process monitoring and control. As a result of use of sulfuric acid for pH adjustment of the process water, sulfate concentrations in the bioreactor reached concentrations of greater than 10,000 mg/l. If all NO and ferric iron in solution were reduced, oxidation reduction potential could then have dropped and sulfate reduction activity increased. This would have resulted in significant sulfide production, causing obvious odor problems and sulfide inhibition of bacterial function throughout the system.
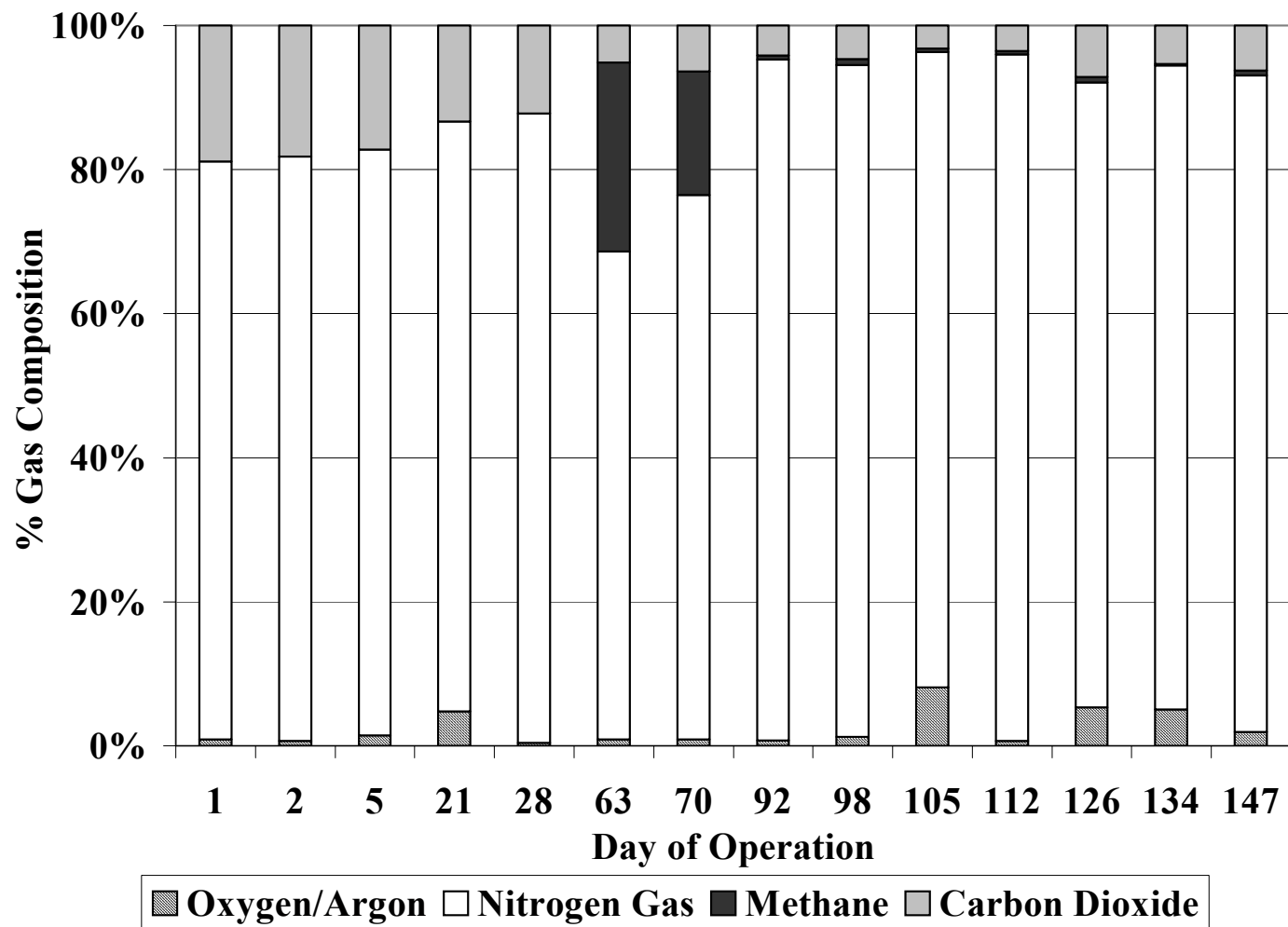
Figure 32. Gas composition of upflow bioreactor headspace at various points in process operation.

Mean Bio-Gas Composition
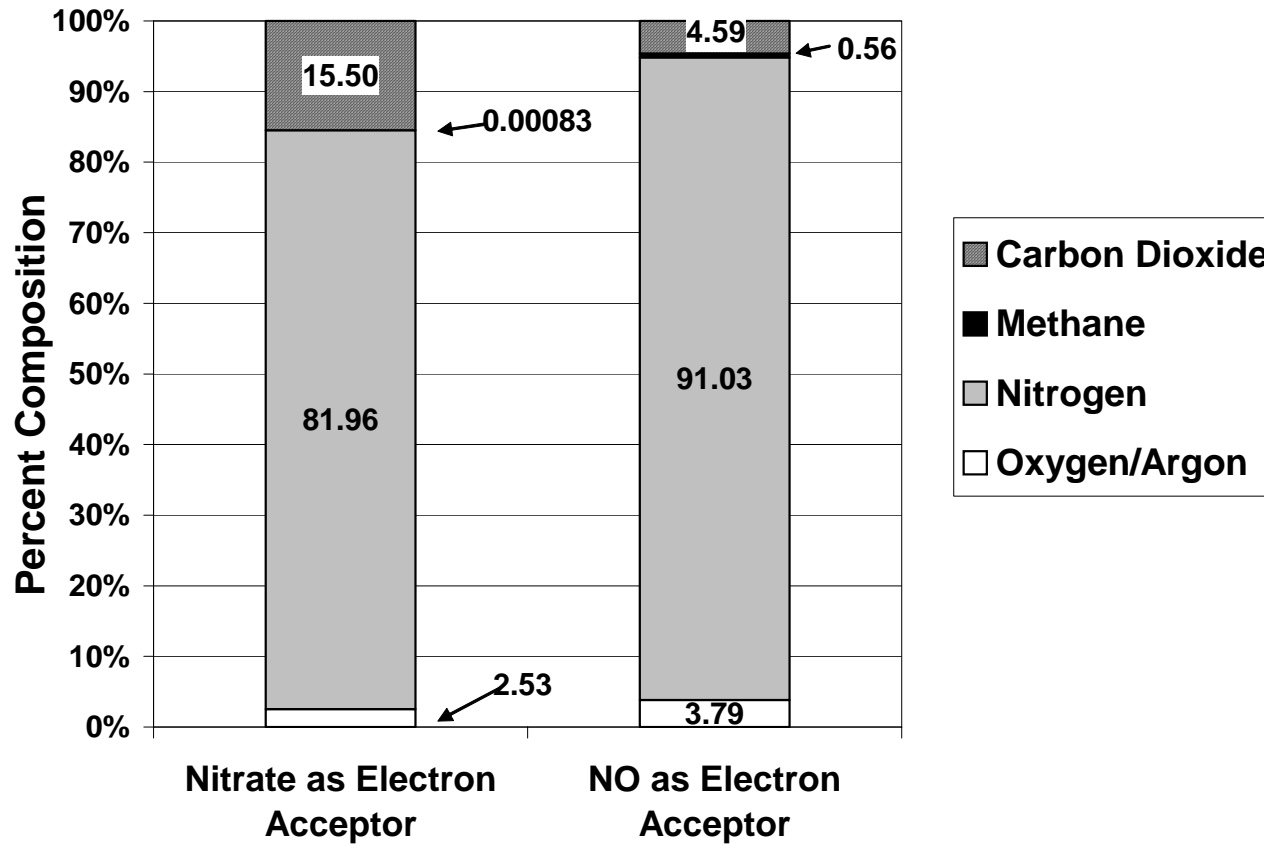
Figure 33. Average gas compositions for Phase I and Phase II of prototype process operation.

5.2.3 ORP of Biologically Active Process Waters.

Process water oxidation-reduction potential (ORP) was monitored using a silver/silver sulfide (Ag/AgCl) ORP probe. As described in Chapter 3, the probe consists of a Ag/AgCl cathode with a platinum anode. The noble metal anode is chosen so that the potential of its oxidation is less than that of any oxidizable components of the process solution. The anode serves as a site of oxidation of solution constituents without itself being significantly altered. Interpretation of oxidation-reduction potential measurements of natural and biologically active process waters is not straightforward. Voltage readings collected from an ORP cell can reflect the influence of many reactions, referred to as a "mixed potential," that can be qualitatively correlated with presence of species in solution, but not used quantitatively for solution chemical analysis.

ORP values measured in the biologically active process water were observed to drift after the probe is initially inserted into the process water. This observed behavior is attributed to polarization and fouling of the indicator electrode as a result of accumulation of oxidation products at the electrode surface. Therefore, reported ORP measurements were taken immediately (typically within 20 seconds) of insertion of the ORP probe into the process water. In cases where the ORP probe could not be inserted directly into the process stream, samples were extracted in a syringe, placed into a glove bag under nitrogen purge, transferred to a beaker and measured under inert environment as quickly as possible.

ORP measurements reflect the presence of the most easily reduced (highest half reaction E_0) species present in solution that can react at the indicator electrode surface, the electroactive species. Snoeyink and Jenkins (1980) report that iron reduction and manganese reduction are electroactive species, while several of the important redox reactions involved with the nitrogen, sulfur, and carbon cycles are not completed at the indicator electrode of ORP cells. In contrast to this statement, the literature shows several examples of application of ORP for process monitoring and control of both denitrifying and strictly anaerobic processes.

Data were collected to establish whether or not ORP was applicable for determination of spatial and temporal trends of process biological performance – for example to determine if the process water is operating under aerobic, anoxic, or anaerobic conditions. When considering the collected process ORP values, it is important to understand the reactor conditions during data collection. As described earlier, the initial stage of bioreactor operation (through day 42) involved reduction of nitrate and ferric iron present as the chelate of EDTA. Following day 42 of operation, the scrubbing stage was initiated and NO was loaded to the process water instead of nitrate. During reactor operation, process water ORP measurements were taken at several points in the process stream, as illustrated in Figure 34. Figure 35

illustrates ORP data points that were collected during the reactor start-up stage, as well as smoothed data that more clearly illustrates trends in process water ORP conditions (Figure 36). Because of the described variability and complexity of biological process waters, smoothing (moving average with a period of 6 days) of ORP data is considered to be an acceptable handling of mixed potential data.

Measurement of oxidation reduction potential was used as a means of indicating the oxidation state of the process water, and ethanol loading rate was adjusted in response. For example, if process water ORP dropped below approximately -150 mV vs. Ag/AgCl reference, it was taken as an indication that process water was overloaded with ethanol and sulfate reduction might become established if OLR conditions were maintained. Similarly, if ORP values in the upflow reactor effluent were too high (greater than approximately -90 mV vs. Ag/AgCl electrode), the process water was considered to be too oxidized and the ethanol loading rate was increased to promote NO and iron EDTA reduction.
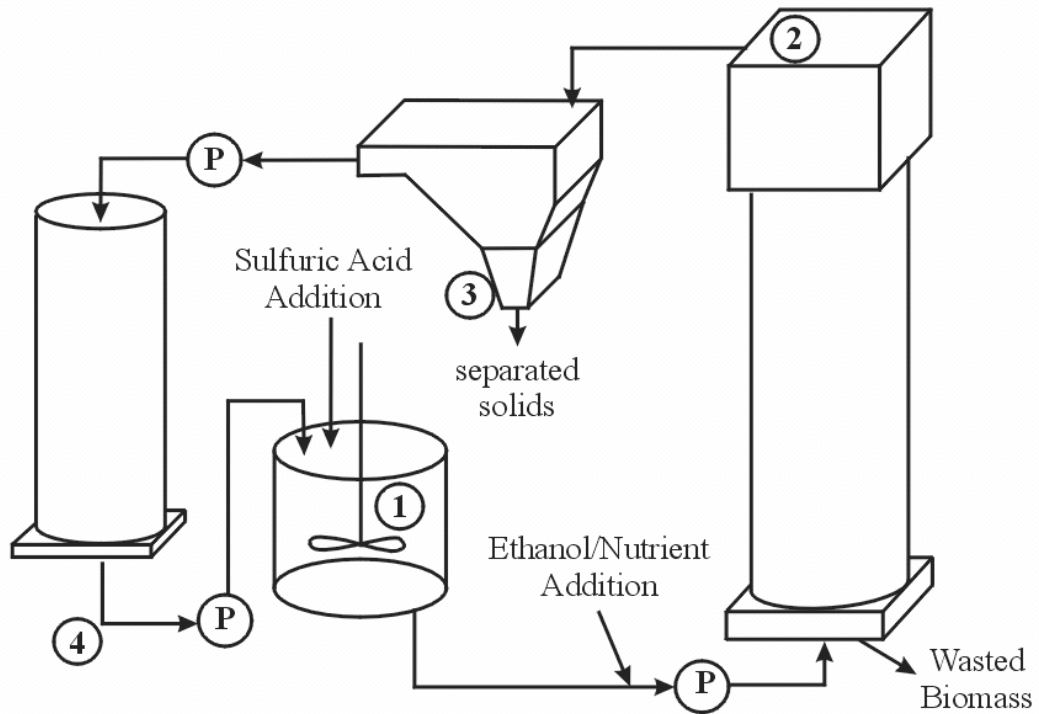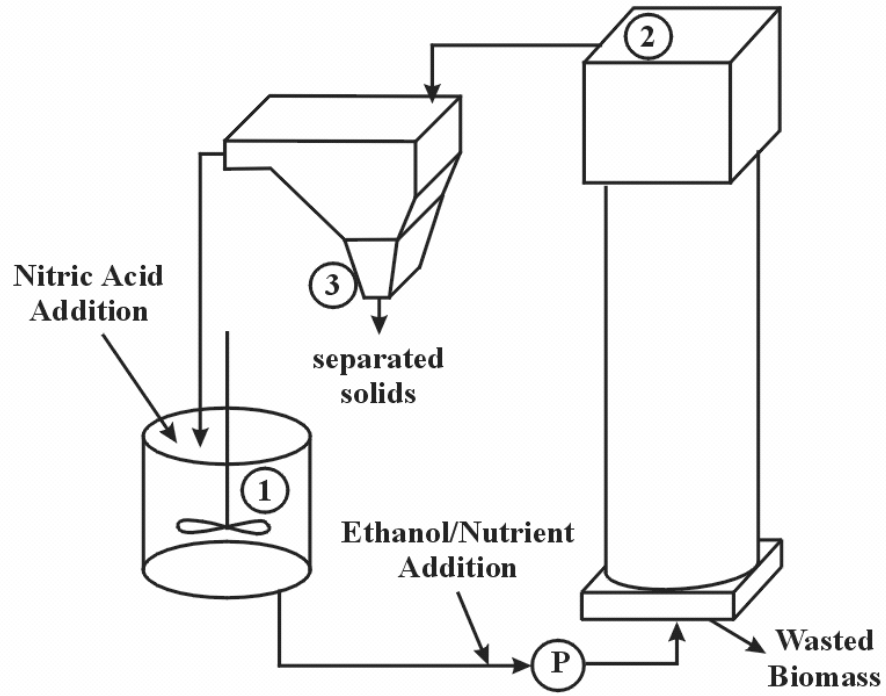
Figure 34. Locations of process water sampling: 1) mix-tank 2) upflow bioreactor effluent 3) slanted plate settler underdrain 4) scrubber effluent (Phase II only)
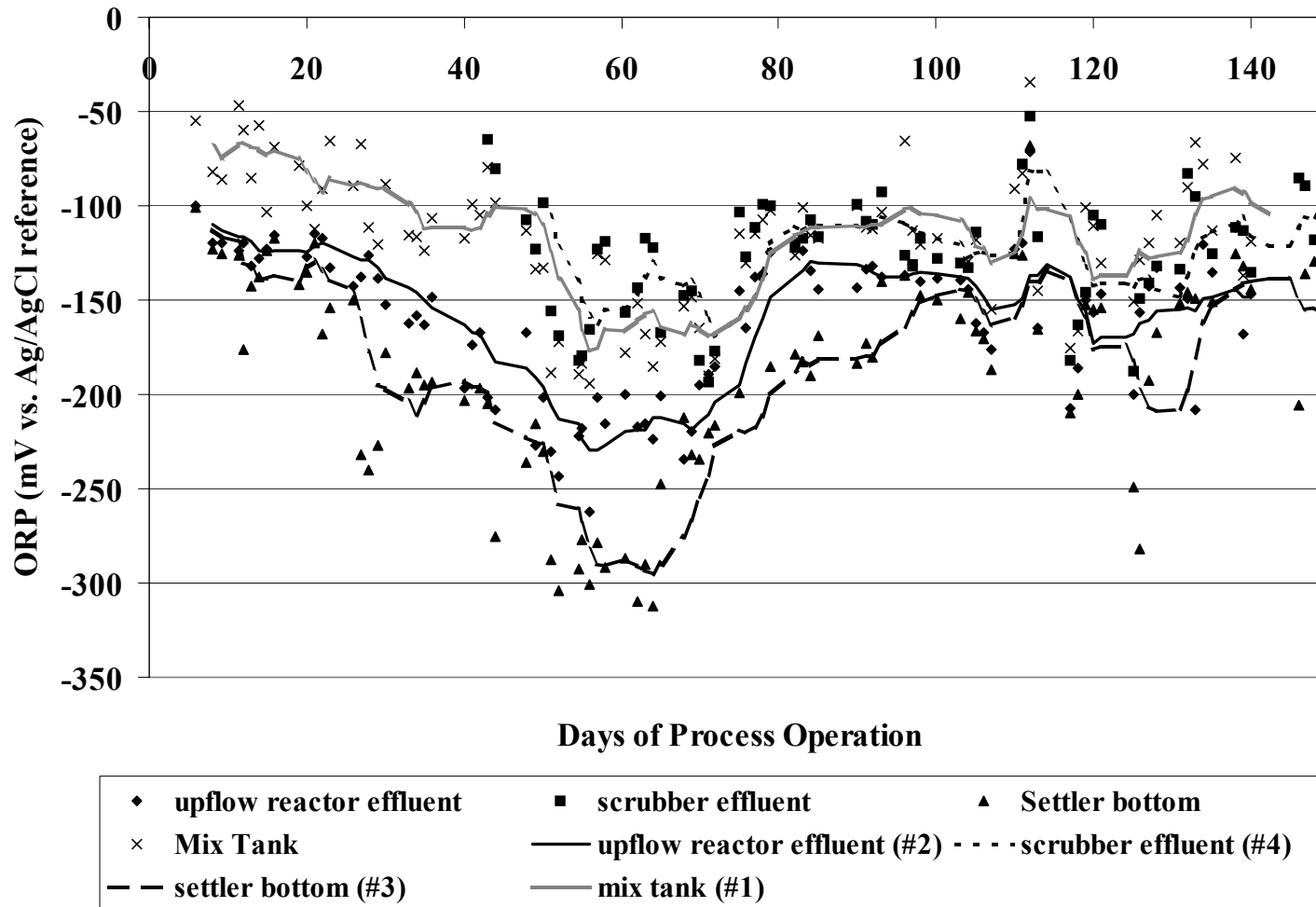
Figure 35. Oxidation reduction potential (vs. Ag/AgCl electrode) at various points in the prototype process.
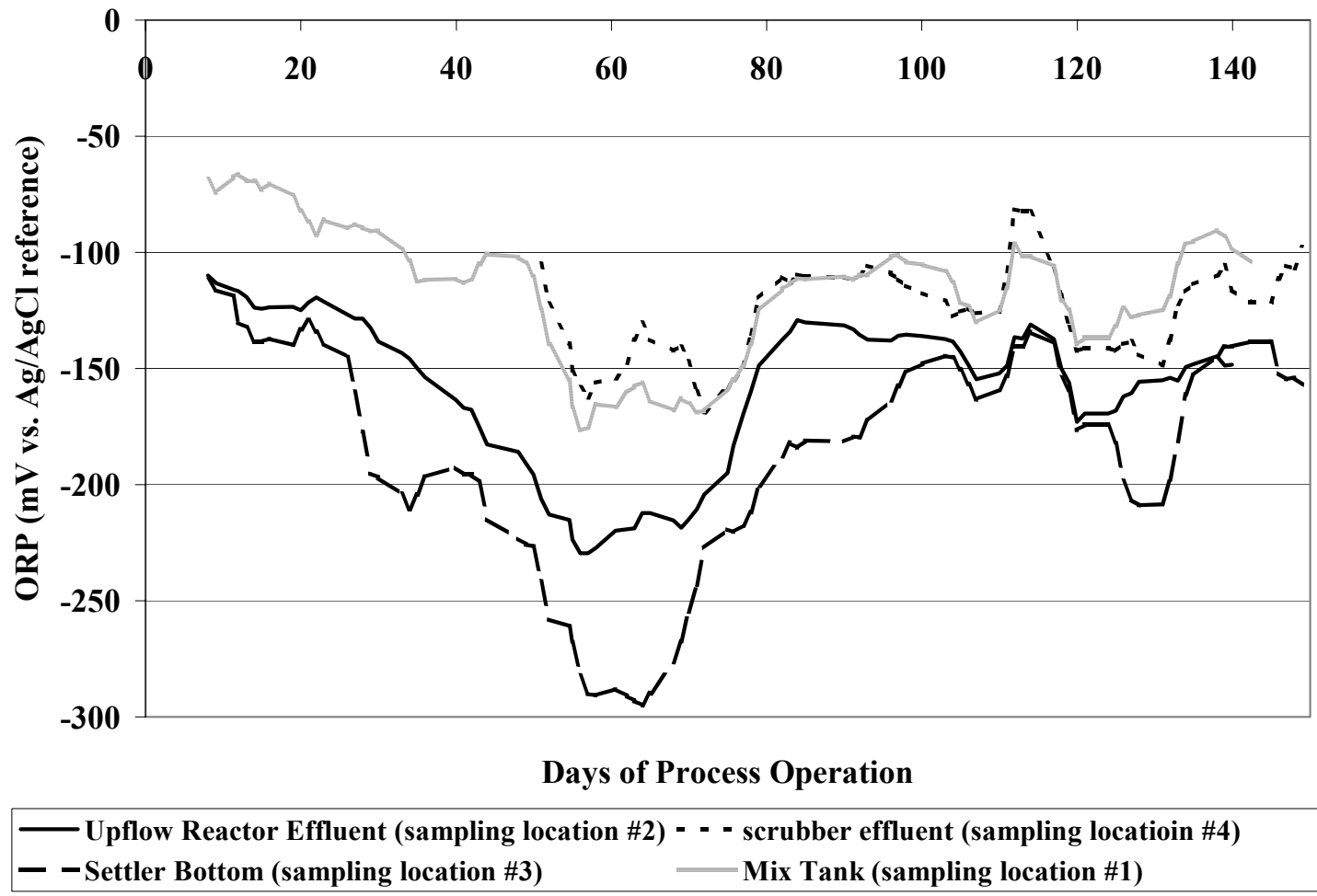
Figure 36. Six-day moving-average of ORP measurements illustrate relative trends at various points in the process.

ORP measurements at several points in the process were considered. In general, a trend was expected from higher (less negative) ORP values in the mix tank, to lower ORP values subsequent to the upflow bioreactor. In the mix tank, addition of nitrate created an electrochemical load to the system that should correspond with a demand for ethanol used by bacteria in the reduction of nitrate to nitrogen gas (denitrification). Despite the previously-described inability of the ORP probe indicator electrode to support the completion of nitrogen cycle redox reactions at its surface, it was believed that a trend in mixed potential response would qualitatively indicate the presence of that nitrate load to the system. Following nitrate reduction in the biologically active process water, the less thermodynamically-preffered reduction of ferric EDTA was expected to proceed. Ferric iron, particularly when maintained in dissolution by the chelate EDTA, should react at the ORP indicator electrode and therefore be clearly identifiable as being present or absent in reactive process waters. It should be noted that ferric EDTA reduction exhibits a significantly lower half reaction potential as compared with that of free dissolved ferric iron, as shown in Table 2 of Chapter 2.

The electrode potential for the ferric EDTA/ferrous EDTA Nernstian couple is approximately -0.126 V vs. a Ag/AgCl reference electrode. ORP measurements significantly below this expected value would suggest that, in addition to the completion of nitrate, the majority of the ferric EDTA present in solution should be reduced to the ferrous form. ORP conditions below those expected of iron EDTA reduction would also indicate that less thermodynamically-preferred electrochemical reduction reactions, in particular, sulfate reduction and methanogenesis would proceed. Because sulfate reduction and methanogenesis both occur under strictly anaerobic, relatively low ORP conditions, it would not be possible to differentiate between Fe(III)EDTA and strictly anaerobic conditions based on ORP measurements. It was expected that under low ORP conditions, sulfate reduction and methanogenesis should proceed coincidentally (ORP of -0.192 V and -0.200 V vs. Ag/AgCl reference, respectively per Table 2). Consideration of biogas H_2S and CH_4 concentration and observation of black FeS precipitate formation were used to identify the initiation of strictly anaerobic activity.

During the second phase of process operation, nitrate was replaced by nitric oxide as the oxidized species introduced to the system, and ferric EDTA remained in the process water. Continuous addition of NO in the process scrubber, as well as partial oxidation of iron EDTA in the process provided a continuous load of oxidized species in the process water to promote growth of microbial reducers in the process. A similar trend of decreasing process water following the scrubbing step of the process was expected.

As expected, process ORP was found to be highest in the mix tank, just following the scrubbing process. This is attributed to the addition of NO to the process water in the scrubber, as well as a small

degree of ferric EDTA oxidation during gas/liquid contact. The effluent of the upflow bioreactor consistently exhibited a decreased ORP as compared to that of the mix tank, consistent with the completion of NO reduction and the presence of ferric EDTA reduction conditions. Quiescent conditions at the bottom of the slanted plate settler located after the bioreactor in the process flow allow the complete reduction of ferric EDTA and progression into sulfate reducing conditions, as indicated by the formation of biogenic sulfide and subsequent ferrous sulfide formation resulting from sulfate reduction. A quantitative discussion of observed trends in ORP data is provided in Chapter 7.

5.2.4 Acetate generation.

Ethanol that is loaded to the upflow bioreactor is not necessarily consumed directly in the reduction of oxidized nitrogen species. Concentrations of acetate greater than 2500 mg/l were observed in the bioreactor effluent. As can be seen in Figure 37, the acetate concentration was typically much lower – around 500 mg/l. It is believed that ethanol is not directly used by NO reducers and furthermore may not be used directly by iron reducers. It is thought that in order for these types of bacteria to reduce the oxidized species in question, acetogenic bacteria must first cleave ethanol into acetate and hydrogen gas – both of which may be employed by NO reducers. Hydrogen was has never been observed in the reactor gas effluent. Acetate, on the other hand, was often observed to build up in concentration throughout the reactor. This suggests that the kinetics of acetate utilization is considerably slower than that of hydrogen gas, and may also relate to the fact that the bacteria derive more energy when using hydrogen gas than when using acetate as an electron donor.

The amount of energy released per electron transferred is a function of the electro-chemical properties of the electron donor and electron acceptor coupled in the redox reaction. If the electron acceptor is the same, then only the energy of the oxidation half reaction need be considered to determine the electrochemical advantage of using one electron donor over another. Considering the oxidation half-reactions of ethanol, acetate, and H_2 provides an explanation, based on energetics, as to why acetate accumulation might be observed in the reactor under consideration. The standard energies per electron equivalent for the oxidation of ethanol, acetate, and H_2 are -31.18 kJ/e$^+$ eq., -27.49 kJ/e$^+$ eq., and -39.87 kJ/e$^+$ eq. (Rittmann and McCarty, 2001). This shows that chemolithotrophic oxidation of H_2 produces more energy than either chemoorganotrophic oxidation of ethanol or acetate, and that chemoorganotrophic oxidation of ethanol yields more energy per electron equivalent than does that of acetate. Two moles of hydrogen are generated from the partial oxidation of ethanol to acetate as

described in Equation #58. Hydrogen generated as a result of the partial oxidation of ethanol in ethanol fed systems will be consumed before acetate is consumed (Harper and Pholand, 1986). Based on these thermodynamic facts, ethanol and hydrogen oxidation will be preferred to the consumption of acetate and, under certain bioreactor operation conditions, acetate accumulation would be expected.
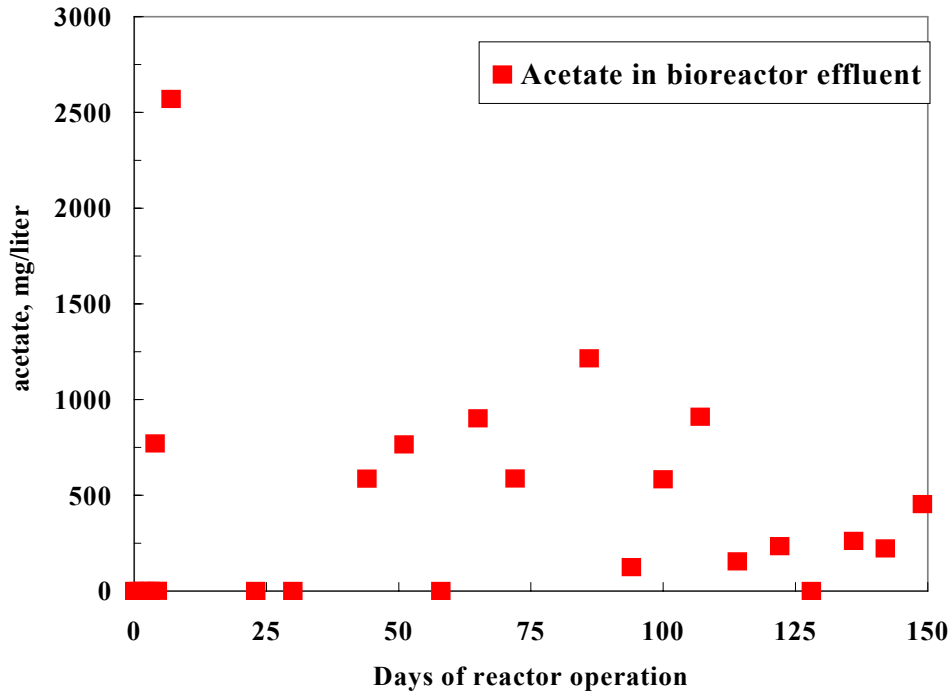
Figure 37. Acetate concentration in the upflow bioreactor effluent throughout process operation.

5.2.5 Observed Sulfate Reduction.

Formation of small amounts of fine black precipitate in the system – identified as amorphous iron sulfide – resulted from the reaction of iron present in the EDTA chelate with biogenic sulfide. The sulfide was generated as a product of microbially-catalyzed reduction of sulfate/sulfite present in the prototype process water. Figure 38 illustrates the concentration increase of sulfate in the process water as a result of addition of sulfuric acid. Sulfuric acid was loaded to the mix tank in order to counteract H^+ ion consumption that resulted from NO reduction and maintain a neutral pH in the process stream. Because most of the water in the process was maintained at ORP conditions above those required for sulfate reduction (resulting from the presence of thermodynamically preferred electron donors NO and Fe(III)EDTA), sulfate accumulated in the system.

111
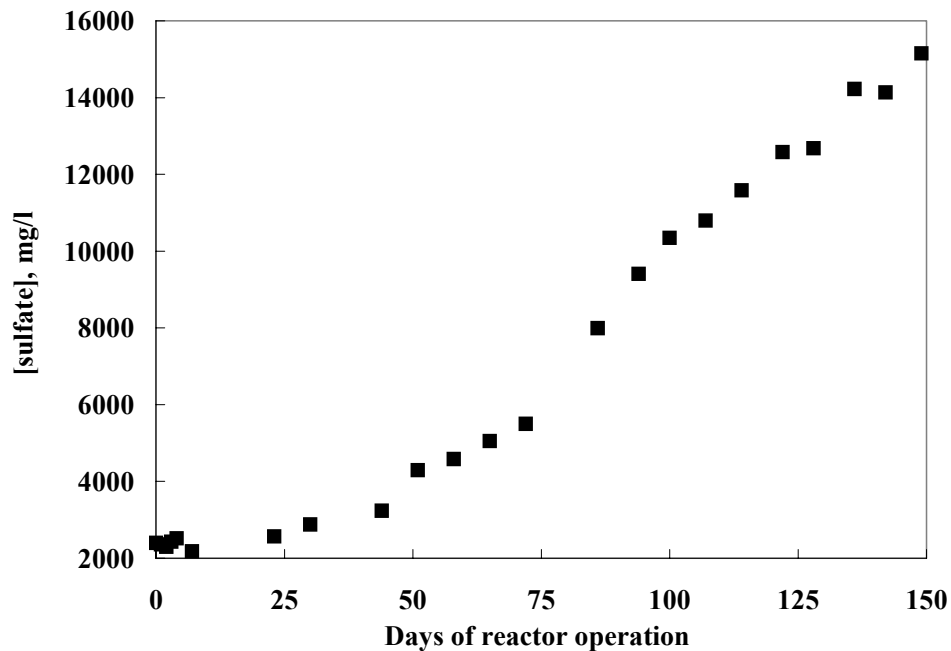
Figure 38. Accumulation of sulfate in the bioreactor.

Robbing of iron from the chelate decreases the NO scrubbing capacity of the scrubber solution. However, because of the high concentration of total iron EDTA in the process water and the limited extent of sulfate reduction in the process water, scrubber efficiency was not quantifiably impacted in the prototype process. On the other hand, presence of iron in solution has the positive effect of scavenging most of the sulfide formed in the process, which prevents sulfide toxicity from affecting activity of desired microbially-catalyzed reactions. In addition, it prevents odor problems caused by release of hydrogen sulfide to the atmosphere. Finally, both sulfide and amorphous ferrous sulfide in solution are strong reducing agents that help maintain negative ORP in process waters and have been demonstrated to promote reduction of ferric EDTA through rapid chemical reduction. Nonetheless, sulfate reduction is not a desired reaction in the biologically active process under consideration, and operation should be constrained so that it is not promoted.
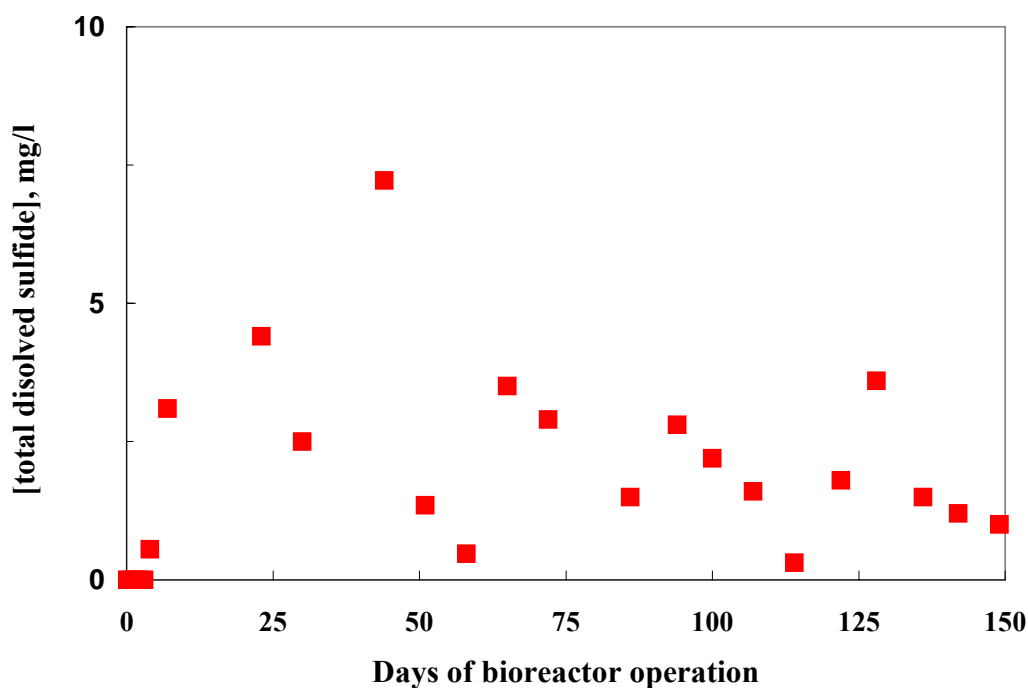
Figure 39. Free dissolved sulfide concentration in the effluent of the prototype-scale upflow reactor.

The maximum observed free dissolved sulfide in bioreactor effluent was 7.22 mg/l, mean was 1.93 mg/l (23 samples with standard deviation of 1.69 grams per liter). During operation under NO reducing conditions, maximum observed aqueous sulfide concentration was 3.6 mg/liter, with a mean sulfide concentration of 1.84 grams per liter (17 samples with a standard deviation of 1.3 grams per liter.

5.2.6 Methanogenesis.

Methanogenesis was observed in the bioreactor during the period of process transition between nitrate and NO reducing conditions, as indicated by the formation of a substantial concentration of methane in the upflow reactor biogas. After the transition from using nitrate as the primary electron donor to using NO as electron donor, the organic loading rate should have been decreased to adjust to the decreased load of oxidized nitrogen species being fed to the reactor. As a result of operator error, the decrease in electron acceptor concentration was not accompanied by a decrease in electron donor. As a result of this, there was a decrease in overall reactor oxidation reduction potential accompanied by a temporary increase in

the formation of sulfide and methane in the biologically active process water. After methane formation was observed, OLR was decreased, methane production gradually decreased, and process ORP increased.

6.0 RESULTS OF BATCH KINETIC ANALYSIS EXPERIMENTS

An important consideration in determining the ability of a microbial community or specific bacterial strain to perform desired oxidation/reduction reactions under a specified set of environmental conditions is the kinetic properties of the population. By maintaining environmental conditions similar to those observed in the system from which the population originated, the impact of extant variables on culture performance was minimized.

6.1 EXPERIMENTAL DETERMINATION OF KINETIC CONSTANTS

6.1.1 Cultivation of Biomass for Batch analyses

Biomass used in batch analyses was cultivated in the prototype reactor described in Section 5.1.1 over the 150 days of prototype process operation and demonstration of process feasibility. At the end of the approximately 100 day period of reactor operation with ferric EDTA and the nitrosyl adduct of ferrous EDTA as the primary electron acceptors, biomass was extracted from the process for use in batch experiments. The point of biomass extraction from the process was chosen based on process performance indicators, such as observed process water ORP and ferrous/ferric ratio. Bacteria used to conduct NO reduction experiments were taken from the mix tank located upstream of the upflow reactor. Biomass used to conduct iron reduction experiments were extracted from the upflow reactor. In this manner, biomass with the highest NO reducing activity were chosen for NO reducing kinetic tests, and biomass with the highest Fe(III)EDTA reducing activity were chosen for Fe(III)EDTA reducing experiments.

Following initial extraction from the system, biomass was cultivated under extant conditions over several batch tests in order to: a) increase the ratio of target bacteria : total bacteria b) remove other solids from biomass sample (*i.e.*, ferrous sulfide precipitate), and c) verify culture reducing activity. For example, biomass removed from the UASB for use in iron reducing kinetic tests initially contained a substantial population of biomass that did not contribute to the reduction of iron, such as methanogens

and sulfate reducers, as well as a significant concentration of biogenic ferrous sulfide. After the seed was removed from the bioreactor, the iron reducing biomass was cultivated in large batches under extant conditions (*i.e.*, those present in the bioreactor). At the end of each iteration of batch cultivation, suspensions were centrifuged so that biomass could be removed. During the centrifugation process, the FeS separated from the biomass in the centrifugate pellet as a result of differences in density. Before the biomass was reseeded into a new batch, FeS was removed from the pellet. After only a few iterations of batch treatment, essentially all of the FeS had been removed. In addition, repeated cultivation with Fe(III)EDTA as the primary electron acceptor promoted the growth of those microorganisms which contribute to the reduction of iron, while starving the sulfate reducing and methanogenic microorganisms. Similarly, bacteria carrying out the reduction of the nitrosyl adduct of ferrous EDTA were distilled over a series of batch cultivation iterations.

Following is a discussion of results of batch reactor kinetic tests. This discussion includes presentation of sample kinetic data, resulting plots of initial utilization rates as a function of initial ethanol concentration, as well as description of interpretation of kinetic data for the determination of kinetic model constants.

6.1.2 NO•Fe(II)EDTA^{2-} reduction batch tests

Figure 40 throgh 42 show sample results (n = 3) of kinetic batch test data for the microbially-catalyzed reduction of 0.02 M solutions of NO•Fe(II)EDTA^{2-} at initial COD concentrations of 0.345, 0.517 and 0.69 grams of COD as ethanol per liter. Concentrations of the nitrosyl adduct of ferrous EDTA was measured using the spectrophotometric technique described in the Methods and Apparatus section (Chapter 4), and ethanol concentration was measured using gas chromatography. From these plots, the initial rate of NO reduction is graphically determined as the initial slope. This is considered to be the rate of NO reduction at the initial ethanol concentration. Each plot provides one point on the Monod plot of initial reduction rate as a function of initial substrate concentration, Figure 43.
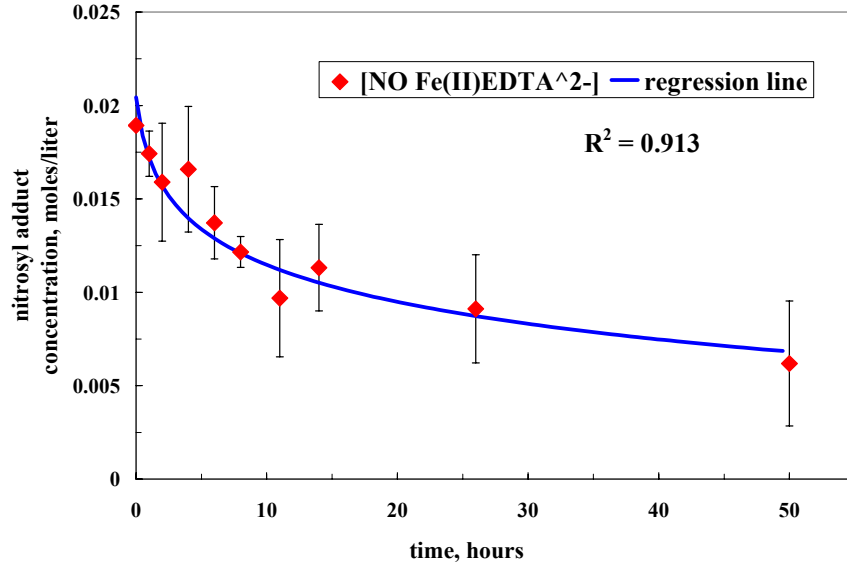
Figure 40. Change in concentration of [NO•Fe(II)EDTA^{2-}] over a period of 50 hours with an initial ethanol concentration of 0.345 grams of COD per liter.
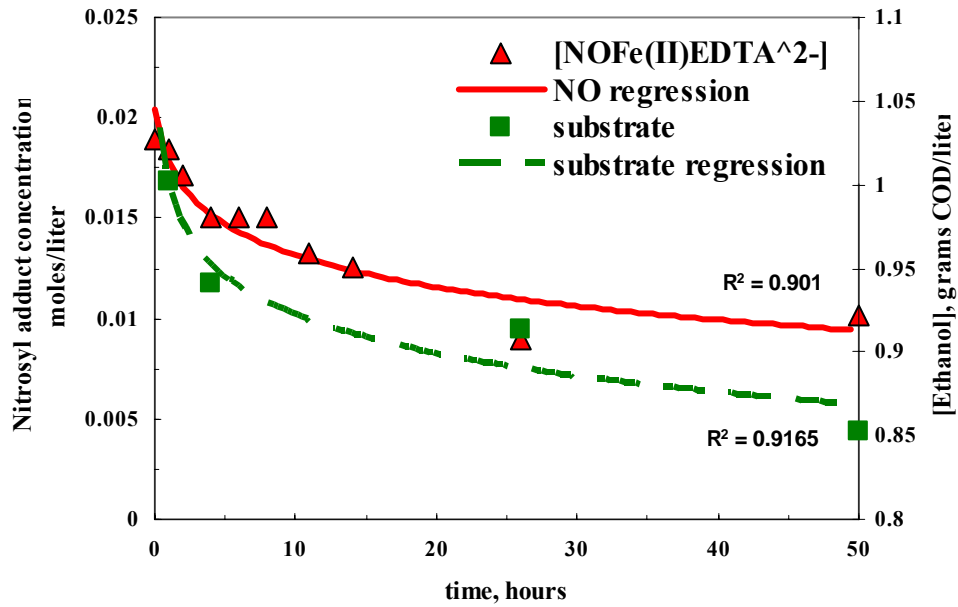
Figure 41. Change in concentration of [NO•Fe(II)EDTA^{2-}] and ethanol over a period of 50 hours with an initial ethanol concentration of 0.517 grams of COD per liter.
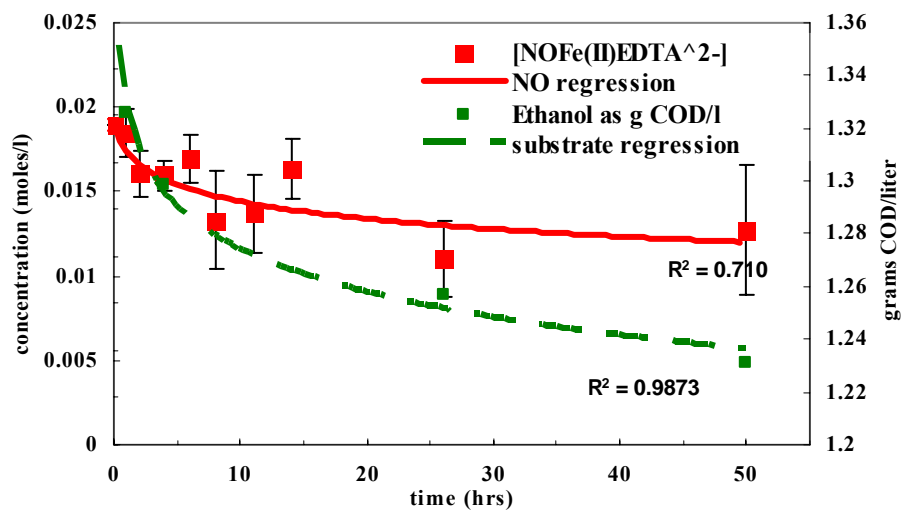
Figure 42. Change in concentration of [NO•Fe(II)EDTA^{2-}] over a period of 50 hours with an initial ethanol concentration of 0.69 grams of COD per liter.

Batch kinetic experiments were conducted over a range of ethanol concentrations, and initial rate of reduction was observed as a function of initial substrate concentrations. Resulting rate data were normalized to account for differences in initial enzyme concentration (as approximated by mixed-liquor volatile suspended solids concentration) and plotted against initial ethanol concentration. The resulting plot is displayed in Figure 43.
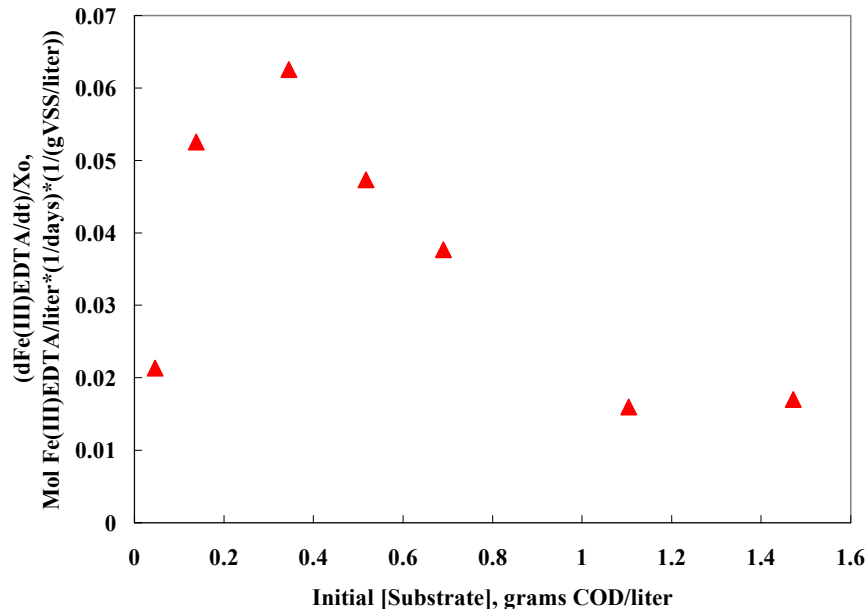
Figure 43. Specific utilization rate of the nitrosyl adduct of ferrous EDTA at various initial ethanol concentrations exhibits substrate inhibition of microbially-catalyzed reduction of NO•Fe(II)EDTA^{2-}

As can be observed in Figure 44, the reduction rate dos not approach a maximum value at higher substrate concentrations, as described by the Monod model of substrate limited growth. Decreased rate of reduction of [NO•Fe(II)EDTA^{2-}] with increasing ethanol concentration above an initial ethanol concentration of 0.33 g COD/liter suggests substrate inhibition of microbially-mediated NO reduction. Kinetic coefficients were determined by plotting the double inverse of the data plotted in Figure 44 (a Lineweaver-Burke plot). Because the microbially-catalyzed reaction no longer follows the Monod equation and does not give a hyperbolic plot, the Lineweaver-Burk plot is not linear. This increase in the inverse of the initial rate with decreasing inverse in initial substrate concentration is indicative of substrate inhibition (Levenspiel, 1980; Bailey and Ollis, 1986). However, because inhibition is limited at low concentrations of ethanol, a strait line fit to the low substrate (high 1/S) data can still be used to determine the kinetics of uninhibited NO reduction (y intercept being 1/k, and the slope being K_S/k). The linear portion of the double inverse plot was used to determine Monod kinetic constants (Figure 44). However, a modification to the Monod NO reduction rate expression must be made to properly account for the observed effect of substrate concentration on nitrosyl adduct reduction rate.
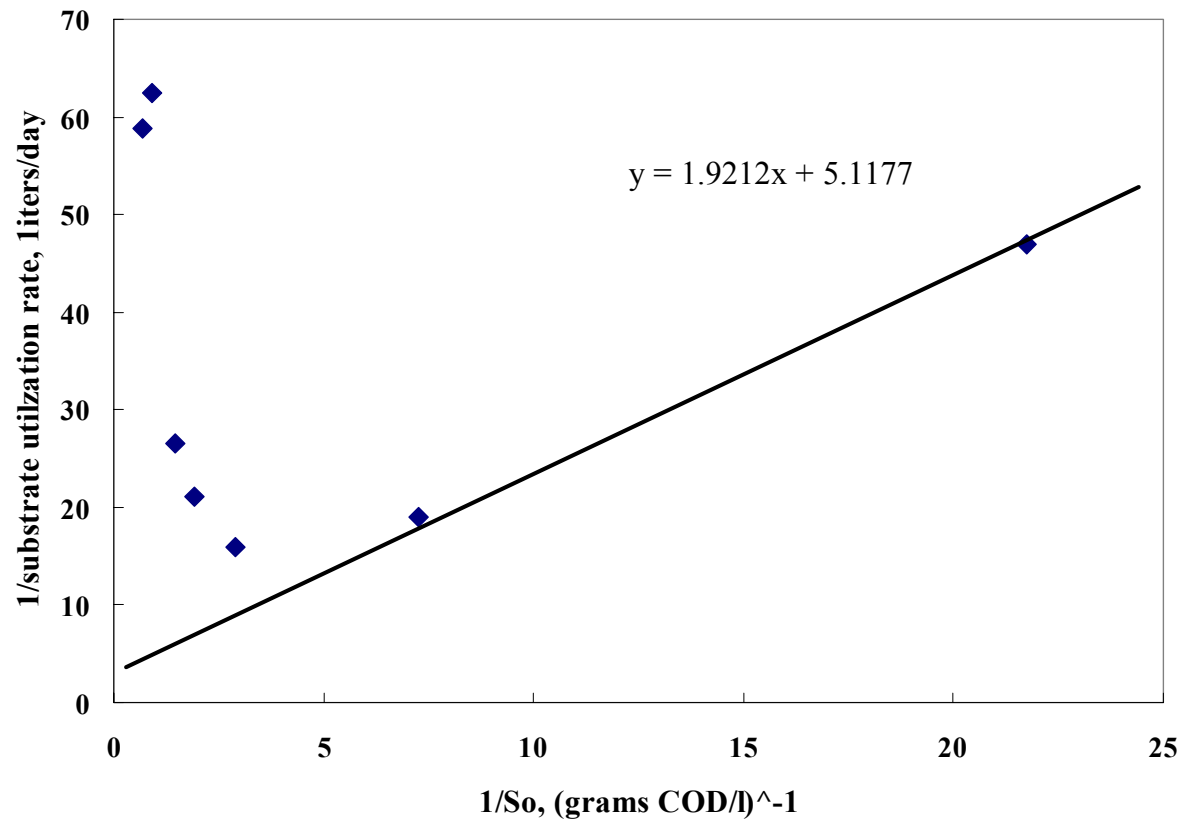
Figure 44. Lineweaver- Burke plot – inverse of reaction velocity as a function of inverse of initial substrate concentration is used to estimate Monod kinetic constants.

6.1.2.1 Inhibition Model. There are several empirical methods to describe the inhibition type and degree of inhibition of a specific inhibitor as a function of inhibitor concentration. Detailed descriptions of common theory based and empirical inhibition models have been omitted in order to maintain continuity of the manuscript, but descriptions are available in several bioengineering and biochemistry texts (Levenspiel, 1980; Bailey and Ollis, 1986; Rittmann and McCarty, 2001; Voet *et al.*, 2002). Several common substrate inhibition models were applied to the collected data of initial specific rate of nitrosyl adduct reduction as a function of initial substrate concentration. The model which best fit the experimentally derived data was a non-specific ordered model described in a thesis by (Mack, 1977). The inhibition model equation is shown in Equation 82.

$$V_0 = \frac{V_{0\,MAX}}{1 + K_S/S + (S/K_I)^n} \tag{82}$$

where:

K_I = inhibition constant

n = degree of inhibition

Based on this equation, we can see that low values of n exhibit more effect below the maximum rate (maximum utilization rate or specific growth rate or V_0^{MAX}) and less after V_0^{MAX}. Higher values of n exhibit less effect prior to V_0^{MAX} and more effect after. Figure 45 illustrates the influence that varying degrees of inhibition have on kinetics for arbitrarily chosen, but constant values of K_S, V_0^{MAX} and K_I. Increasing values of K_I while holding K_S, V_0^{MAX}, and n constant at arbitrary values shows that the overall effect of inhibition is inversely proportional to the magnitude of the inhibition constant, as illustrated in Figure 46. By manipulating both K_I and n, the described model can be manipulated to fit the experimentally collected data quite well.
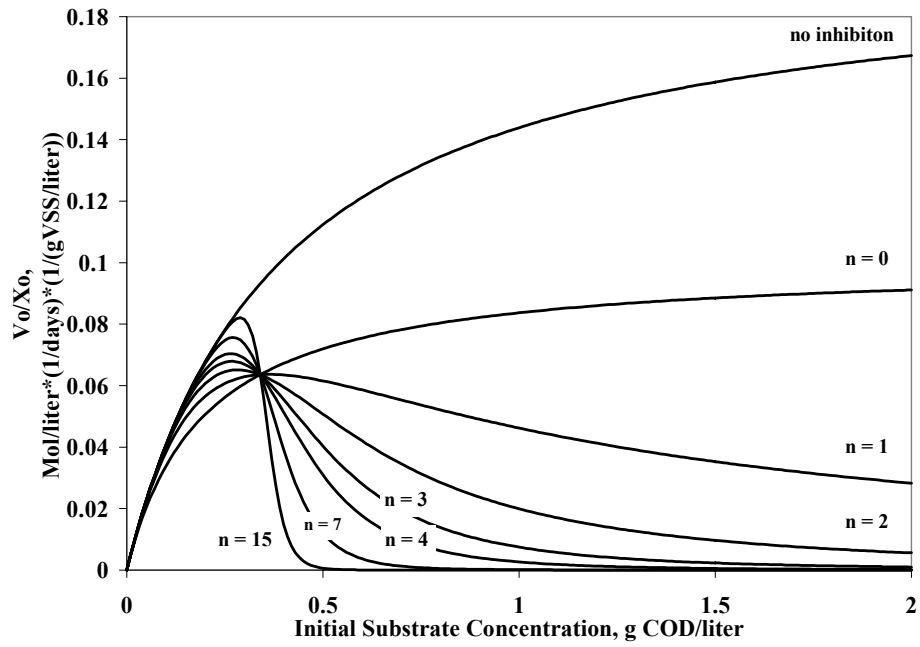
Figure 45. Response of increasing degree of inhibition with constant K_I, V_0^{MAX} and K_S.
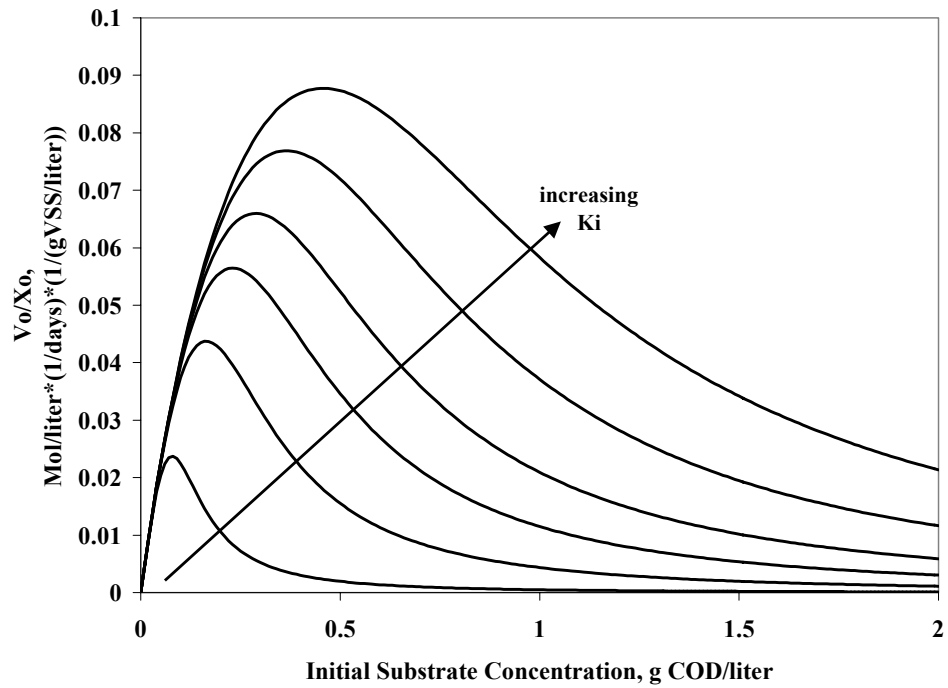
Figure 46. Response of increasing magnitude of inhibition constant with constant V_0^{MAX}, K_S, and inhibition order.

In order to determine V_0^{MAX} and K_S, we recognize that initially (at very low S values), the effect of substrate inhibition is negligible

$$\frac{1}{V_0} = \frac{1}{V_0\max} + \frac{K_S}{S}\frac{1}{V_0\max} + \left(\frac{S}{K_I}\right)^n \frac{1}{V_0\max} \tag{83}$$

At very low values of initial substrate concentration (S_0), S/K_I is very small. As S approaches zero, the $(S/K_I)^n$ approaches zero, and the last term of the previous expression can be neglected. As a result, the standard Lineweaver-Burke double reciprocal treatment of the data can be employed to determine the maximum rate and half velocity kinetic coefficients (Mack, 1977).

$$\frac{1}{V_0} = \frac{K_S}{S}\frac{1}{V_0\max} + \frac{1}{V_0\max} \tag{84}$$

$$y = mx + b$$

According to the Lineweaver-Burke method, the plot of $1/S$ versus $1/V_0$ will provide the following information:

$$\text{Slope} = \frac{K_S}{V_0\max} \tag{85}$$

$$\text{Intercept} = \frac{1}{V_0\max} \tag{86}$$

Figure 47 illustrates the experimentally determined data plotted versus the ordered inhibition model, the Haldane Inhibition Model, and the uninhibited Monod model. This plot clearly demonstrates that the ordered inhibition model best serves to describe the observed data.
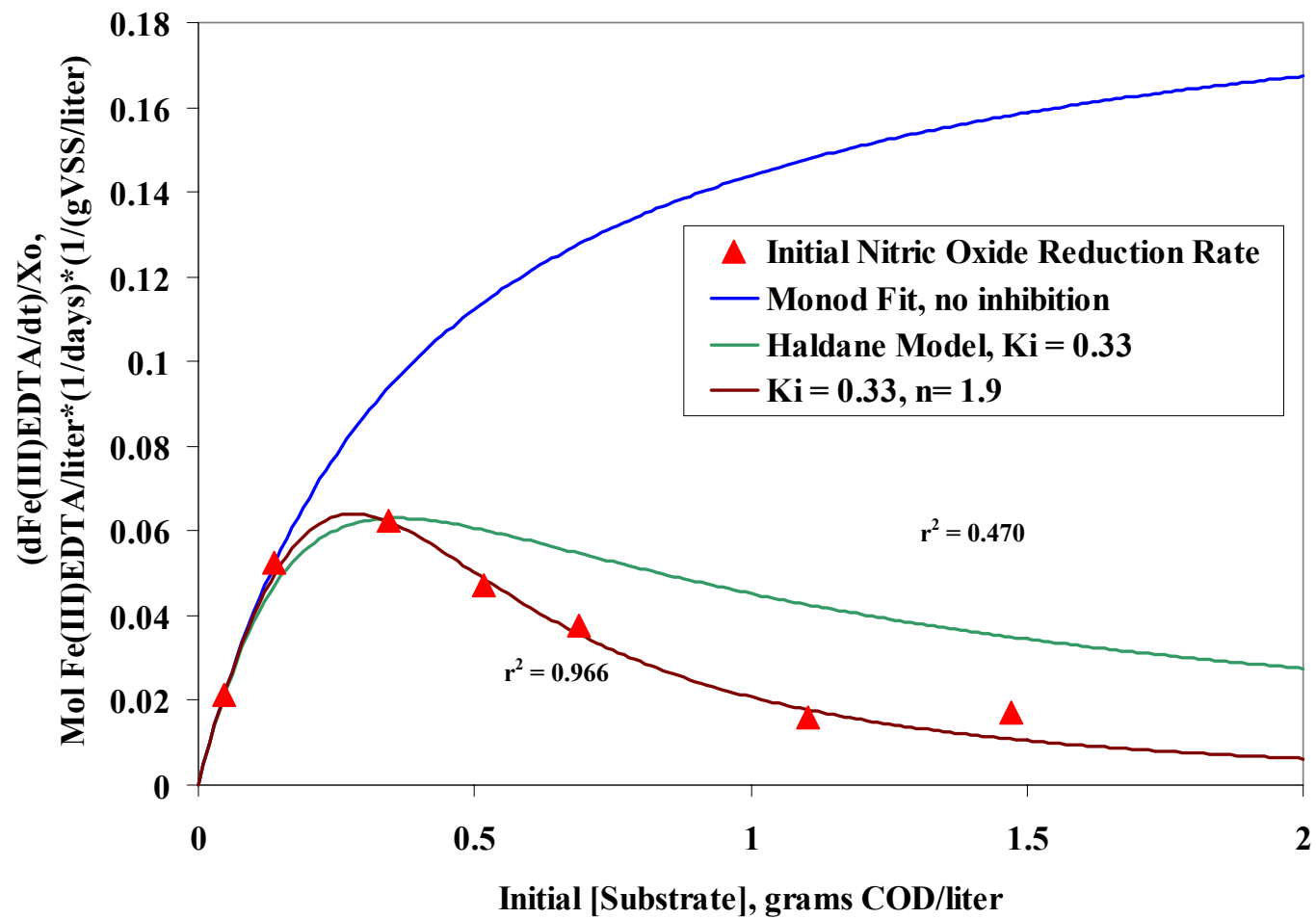
Figure 47. Best Haldane and Ordered Inhibition model fit to nitrosyl adduct reduction data.

6.1.3 Fe(III)EDTA- reduction batch tests.

Similar data were collected during ferric EDTA reduction batch. Batch tests showed that Fe(III)EDTA reduction proceeds according to the Monod kinetic expression for substrate limited growth (K_s = 0.0172 moles ETOH/l, k = 0.0141 M Fe(III)EDTA/g VSS/l*day) (Figure 48 and Figure 49).
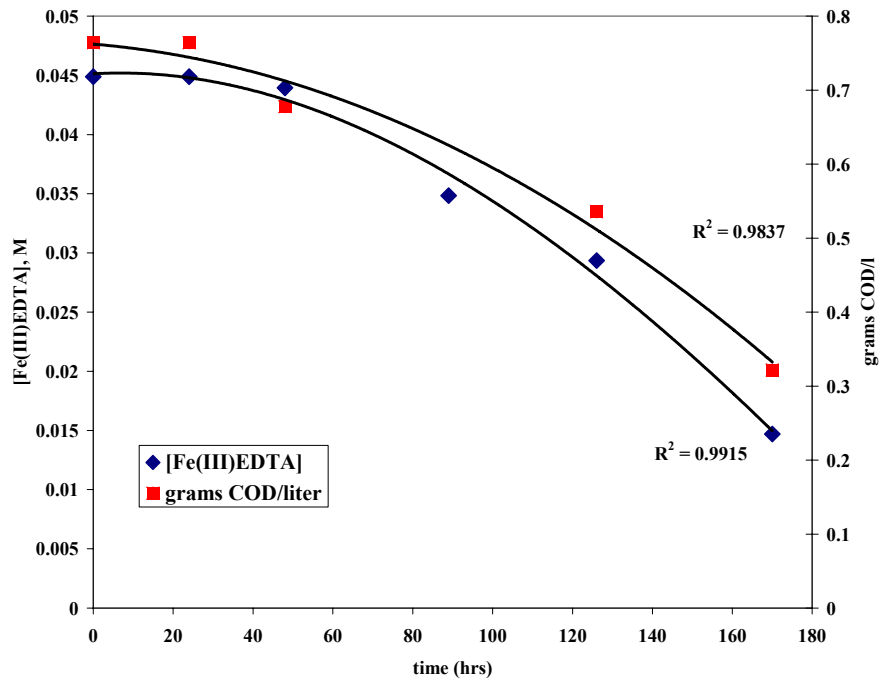
Figure 48. Representative Fe(III)EDTA reduction batch test data
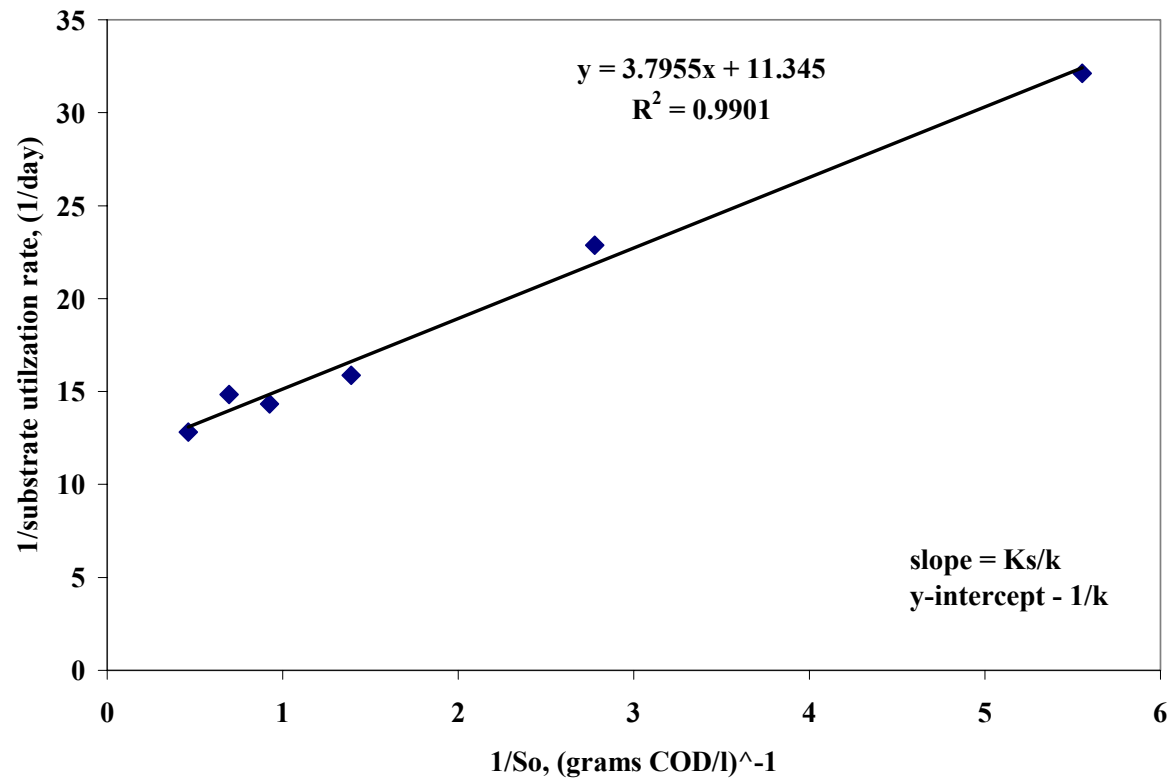
Figure 49. Lineweiver-Burke Plot of Fe(III)EDTA reduction data.
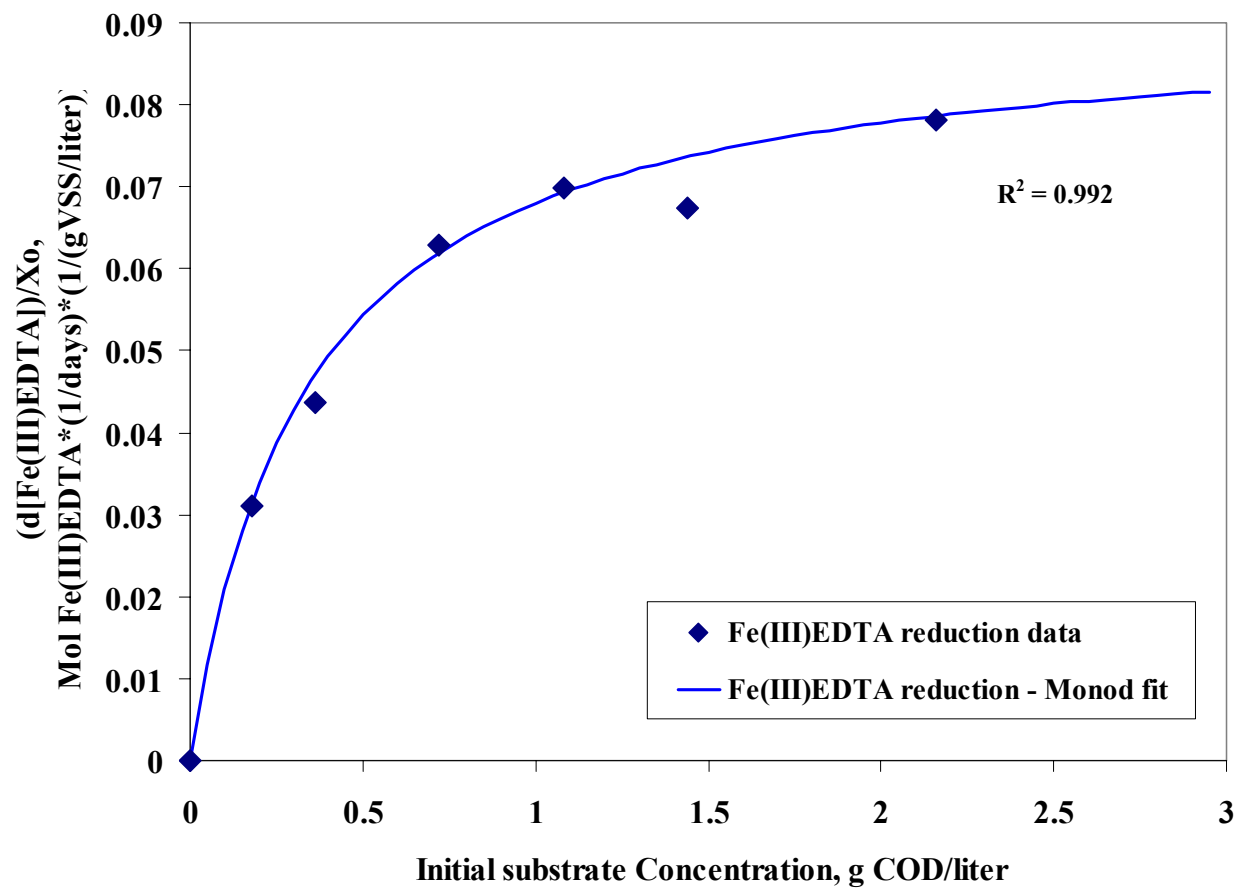
Figure 50. Rate of reduction of Fe(III)EDTA as a function of initial ethanol concentration with Monod model fit.
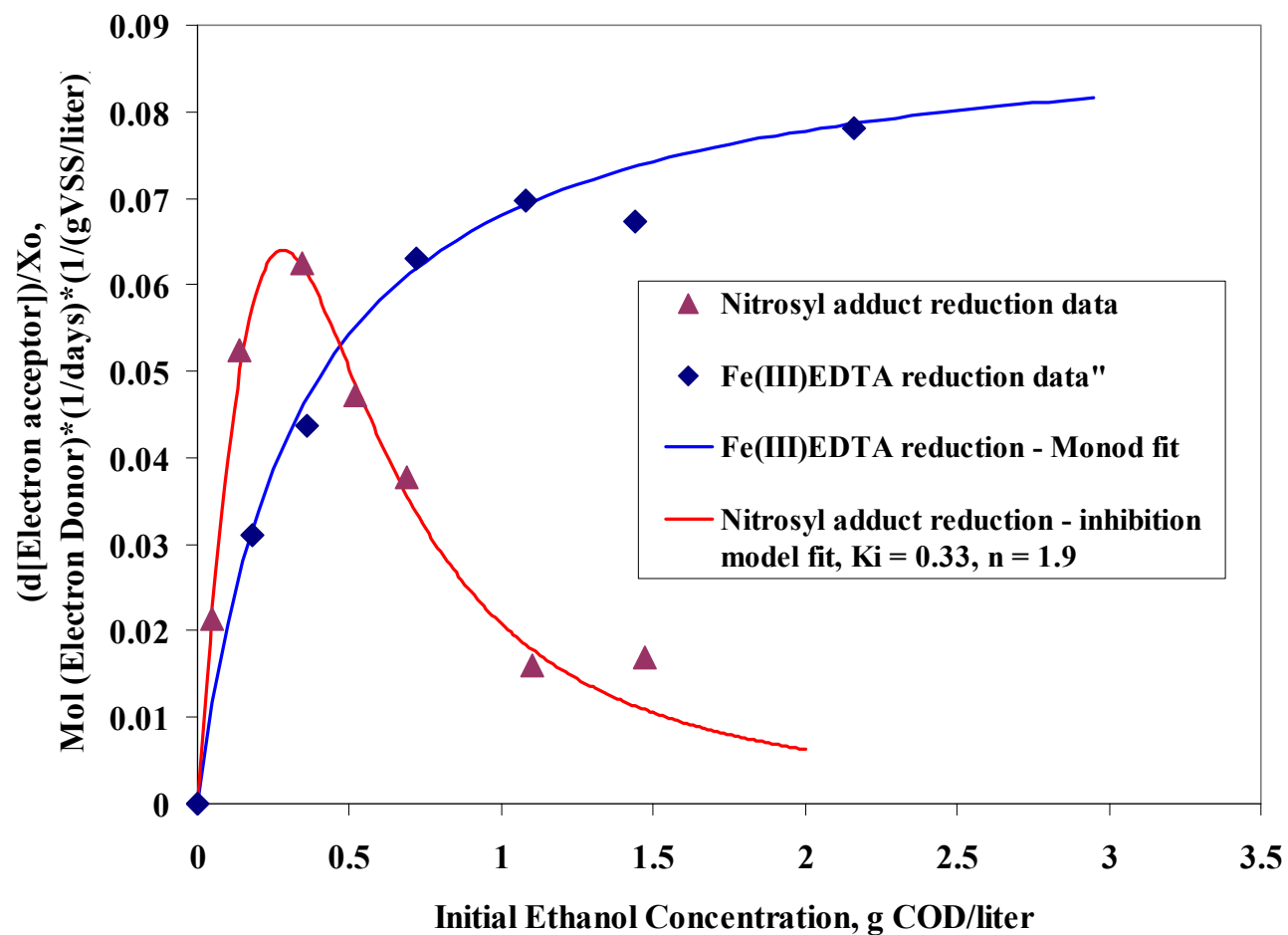
Figure 51. Summary plot of microbially-mediated reduction of the nitrosyl adduct of ferrous EDTA, and the rate of reduction of ferric EDTA as a function of initial ethanol concentration in solution (reported in g COD/liter)

6.1.4 Determination of Yield Coefficient

Yield coefficient was calculated using substrate utilization data and cell concentration data from the beginning and end of batch experiments. Because batch experiments were designed to investigate kinetics of each of the two microbially-catalyzed reactions in isolation, bacteria were exposed to conditions where the primary electron acceptor was that under consideration, and the primary electron donor was ethanol. Therefore, the yield coefficients were determined for bacteria that reduce either the nitrosyl adduct of ferrous EDTA or ferric EDTA, depending on the analyte under consideration.

In the case of NO reduction, a culture of NO reducing bacteria were exposed to a known concentration of NO*Fe(II)EDTA, and a known concentration of ethanol. Nutrients and trace metals were added in sufficient concentrations to ensure that they would not limit microbial growth. By measuring the change in total cell concentration, as estimated by g VSS/liter, as well as the change in concentration of ethanol from the beginning to the end of the batch experiment, a yield coefficient was determined. By averaging the ratio of change in g VSS/liter to the change in concentration of ethanol (recorded as g COD/liter) for all available batch experiments under all initial substrate concentrations considered, an average yield coefficient for NO reducing bacteria was determined.

The same method was employed for determining the yield coefficient for Fe(III)EDTA reducing bacteria. Calculated mean yield coefficients for NO*Fe(II)EDTA reducing bacteria as well as Fe(III)EDTA reducing bacteria are 0.259 and 0.055 g VSS/g COD, respectively. The significantly higher calculated yield coefficient of NO reducing bacteria (nearly an order of magnitude greater) is expected because the Gibb's Free Energy of the reduction of the nitrosyl adduct with ethanol (-466.53 kJ/mole as listed in Chapter 2) is approximately an order of magnitude greater than that of Fe(III)EDTA reduction using ethanol as the electron donor/carbon source (-42.191 kJ/mole). For the same reason, aerobic activated sludge processes have a substantially greater yield than do anaerobic reactors that maintain conditions under which considerably less exergonic reactions (sulfate reduction and methanogenesis) thrive.

6.1.5 Endogenous decay expression

Endogenous decay rates were determined for both nitrosyl adduct reducing bacteria and ferric EDTA reducing bacteria. The endogenous decay terms were determined by conducting batch experiments similar to those described earlier, but in the absence of the ethanol that serves both as the electron donor in the coupled redox reactions of interest and as the sole source of carbon for new cell synthesis. Under these conditions, reduction reactions will not proceed. However, when the cell walls of dead bacteria lyse, the volatile organic content of the cells was released, a small source of electron donor for the remaining active bacteria was exposed. As a result, the volatile suspended solids of the solution was observed to decrease as a function of time. The endogenous decay coefficient was determined by measuring the VSS in grams per liter of the un-fed reactor as a function of time. Figures 52 and 53 show the plots of $\ln(X/X_0)$ (unitless) vs. days. The endogenous decay coefficient for bacteria reducing the nitrosyl adduct for ferrous EDTA was found to be 0.0569 g VSS/day, and that of the Fe(III)EDTA reducing bacteria was found to be 0.0175 g VSS/day. These data show NO reducers to die more quickly than do iron reducers. One possible explanation for this observation is that NO reducers consume more ethanol per mole of oxidized species than do Fe(III) reducers, and reproduce at a greater rate. They would also be expected to live a shorter period before dying. In the absence of ethanol, NO reducers die off more quickly than do iron reducers. Cell walls of the dead bacteria lyse, and expose their volatile contents to the bulk solution. This volatile content is either consumed by the remaining living bacteria or volatilizes upon exposure to the atmosphere. The values and units of all determined kinetic coefficients are listed in Table 9.
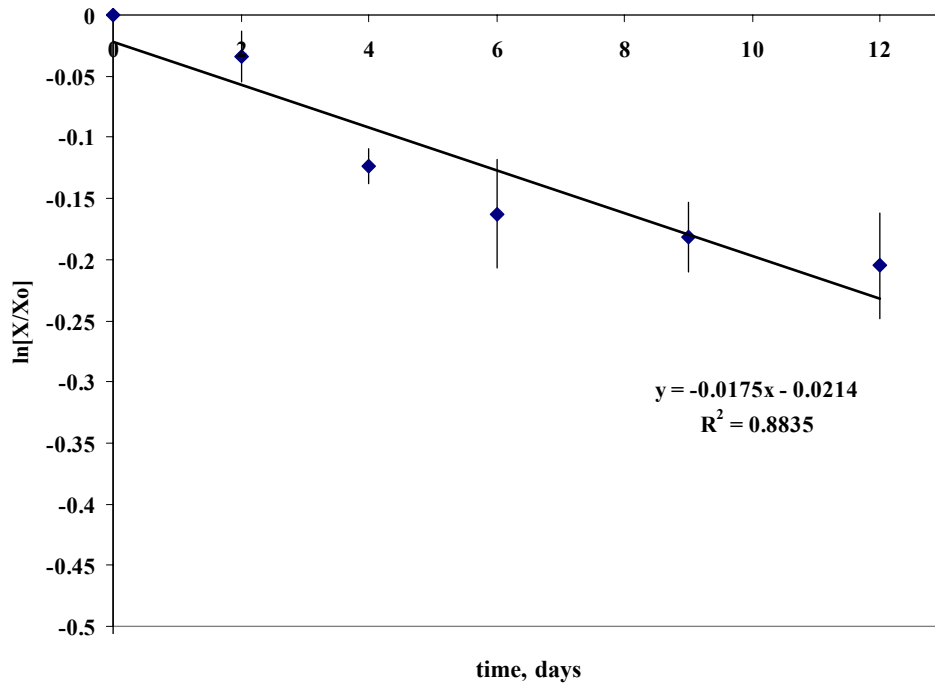
Figure 52. Endogenous Decay coefficient determination for Fe(III)EDTA⁻ reducing bacteria

On the chart:
$y = -0.0175x - 0.0214$
$R^2 = 0.8835$
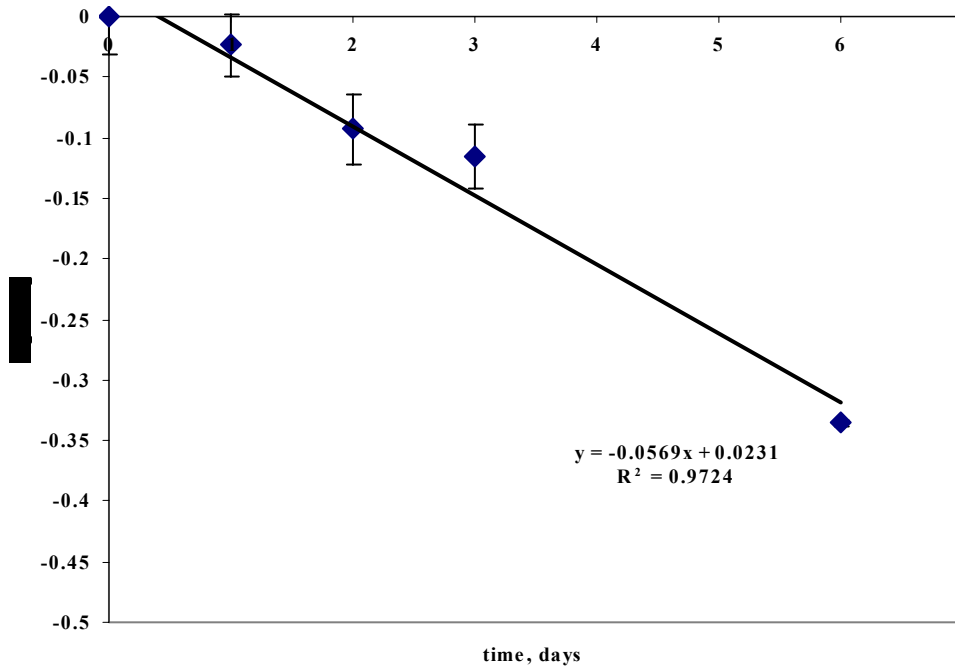
Figure 53. Endogenous decay coefficient determination for NO reducing bacteria.

On the chart:
$y = -0.0569x + 0.0231$
$R^2 = 0.9724$

Table 9. Summary of empirically derived kinetic constants.

Constant	units	Fe(III)EDTA$^-$ Reduction	NOFe(II)EDTA^{2-} Reduction
K_S	g COD/l	0.3367	0.39
k	M Ox*(g VSS/l)$^{-1}$day^{-1}	.09091	0.2
K_I	g COD/l	-	0.33
n	-	-	1.9
Y_{obs}	g VSS/g COD	0.055	0.259
k_d	1/day	0.0175	0.0569
ρ	-	1.674	1.259

7.0 DISCUSSION AND ENGINEERING CONSIDERATIONS

7.1 DISCUSSION

Following is a discussion of performance of the prototype scale apparatus, results of batch kinetic analyses, and how the process configuration and operation influenced process performance. Observations discussed herein relate to system performance of scrubbing of NO from the gas phase using ferrous EDTA, treatment of that solution in an upflow anaerobic bioreactor, and recycling of that solution to the scrubbing process.

7.1.1 Discussion of Prototype Operation

Prototype operation discussion includes consideration of the upflow bioreactor performance and NO_X scrubber performance. An effort will be made to provide an integrated consideration of factors affecting the process operated as a closed loop, as performance of these two stages are intimately linked.

7.1.1.1 Discussion of Scrubber Performance. While performance of the scrubbing column is not the focus of this research, it is useful to quantify the concentration of NO being loaded onto the ferrous EDTA scrubbing solution. To this end, a continuous gas analyzer was calibrated and used to determine the NO concentration being fed to the scrubbing unit as well as the NO concentration seen as scrubber break-through.

In the process under consideration, NO was scrubbed from the gas phase using a solution of the chelate ferrous EDTA. The primary reaction responsible for scrubbing NO from the gas phase is shown in

133

Equation 5, with NO forming a reversible adduct to ferrous EDTA. Scrubbing capacity is therefore a function of ferrous EDTA concentration, with theoretical scrubbing capacity a 1:1 molar ratio of ferrous EDTA to NO.

The system was operated with an iron EDTA solution of 0.045 mol/l, and a liquid flow rate of 0.19 l/min, giving a liquid molar loading of 0.00855 mol iron EDTA/min. By comparing NO molar loading rate to the iron EDTA molar loading rate (and assuming that all iron EDTA is in the ferrous form) ($2.475*10^{-4}$ mol NO /min : 0.00855 mol Fe(II)EDTA/min), it becomes obvious that the scrubbing unit is operating well below its theoretical (stoichiometric) capacity. Based on stoichiometry (and neglecting mass transfer and kinetic limitations), the described reactor configuration would be capable of absorbing approximately 34 times as much NO. It is believed that the excellent scrubber performance with negligible breakthrough at typical flue gas NO concentration can be attributed to the fact that the reactor is operating substantially below capacity.

It should be noted that success of the NO scrubbing process is dependent upon the success of the bioreactor. If, for some reason, the bioreactor fails to reduce a substantial portion of the ferric EDTA in solution to ferrous EDTA after having reduced the nitrosyl adduct of ferrous EDTA to N_2, scrubber performance, measured as NO scrubbing efficiency, will begin to decrease dramatically.

Dravo Lime Corporation (1992) developed a semi-empirical equation to determine the dependence of NO removal on absorber operating conditions in order to understand what conditions are necessary to remove maximum NO_X at reasonable capitol and operation costs. The mathematical model was developed to determine the dependence of NO removal on flue gas velocity, absorber liquid flowrate, ferrous EDTA concentration, absorber length, and gas-liquid contact time. The equation developed by Dravo researchers (Li et al., 1996) is shown in Equation 87.

$$\text{NTU} = -\ln(1 - (\% \text{ removal}/100)) = (k_2 [Fe^{++}] D_{NO})^{1/2} / (H/p_T) *(a*Z)/(p_M*v) \qquad (87)$$

where:

NTU = NO removal as number of transfer units (dimensionless)

K_2 = reaction rate constant for second=order reaction between dissolved (but not
yet reacted) NO and ferrous EDTA = 2.2445×10^{12} ft^3/lb mole-sec @ 122°F

$[Fe^{++}]$ = ferrous EDTA concentration in absorber liquid, mM $6.2362 *10^{-5}$ = lb
mole/ft^3

D_{NO} = diffusivity of dissolved NO in absorber liquid = 4.4×10^{-8} ft^2/sec @ 122°F

A = gas-liquid interfacial area per volume of contact zone, ft^2/ft^3

Z = length of gas-liquid contact zone, ft

p_M = molar density of flue gas = 0.00235 lb-moles/ft^3 @ 122 °F

v = flue gas velocity in absorber, ft/sec

p_T = total pressure, 1 atm

H = Henry's Law constant for NO in water = 11383.25 ft3-atm/(lb-mole) @ 122°F

   (if flue gas is saturated with water vapor, the effective solubility of NO in

   water is 12813.56 ft^3/lb-mole)

A detailed derivation of this equation, based on two-film theory and adduct formation rate is provided in Appendix C.

Based on this equation, scrubber efficiency was calculated for the set of conditions used in the prototype process scrubber, and for conditions of greater flow rates. Results (Table 10) show that the scrubber performed more poorly than predicted by the design equation, and that similar scrubber efficiency would be predicted by a four times greater gas flow rate. Because of the small dimensions and non-ideal liquid and gas flow distribution in the prototype absorption column, inaccuracy of the scrubber design equation was expected. Regardless, the comparison shown in Table 10 demonstrates that the prototype scrubber was oversized for the applied gas/liquid loading conditions. Comparison with these higher flow rates show, for example, the scrubber should have performed at the same scrubber efficiency as that which was observed in the prototype process with a gas flow rate that was three times greater.

Table 10. Comparison between prototype scrubber NO absorption efficiency and calculated scrubber efficiency based on Equation 87 (Li et al., 1996)

	Prototype Scrubber (actual)	**Prototype Scrubber (calculated)**	**3x gas flow rate**	**4x gas flow rate**
NTU	3.86	11.5431	3.8477	2.8858
% removal	97.9	99.9990	97.8671	94.4188

7.1.1.2 Biomass Characteristics. Upflow sludge blanket reactor technology is based on formulation of dense granules made up of highly concentrated biomass and inorganic precipitates (*e.g.*, ash). Granule formation is thought to begin with attached growth of biomass on these inorganic precipitates (such as calcium carbonate or metal sulfides) with further agglomeration promoted by adhesion by extracellular polypeptides excreted by bacteria. However, the majority of literature describing granule formation and UASB reactors is related to strictly anaerobic systems – typically cultivating methanogenic archaea , but occasionally with regard to cultivation of sulfate reducing bacteria (Lettinga, 1987). Work by Sam-Soon (1987, 1990, 1991) describes a mechanism of granule formation in methanogenic bacteria. According to this literature, conditions required for granule formation include presence of a high hydrogen partial pressure, high concentrations of ammonia nitrogen, and an absence of the amino acid cysteine. A bacterium is described that is capable of producing all amino acids required for new cell growth, save cysteine. Because of the lack of the essential amino acid cysteine, the bacteria cannot use produced amino acids (with production being driven by the high extracellular concentration of ammonia nitrogen). After the intracellular concentration of non-cysteine amino acids builds up, the bacteria disposes of them by excreting them in chains of extra-cellular polypeptides. These polypeptides allow large colonies of bacteria to agglomerate. These colonies are not monocultures, but groups of different types of bacteria operating in syntrophic relationships in which products generated from the activity of one microorganism is substrate for another.

The literature describing granule formation in denitrifying systems is less common (Tarre and Green, 2000; Tarre, Moshe *et al.*, 2000). The mechanism of denitrifier granulation is described in an article by Tarre and Green (2000) and is much simpler than that described for methanogenic systems, with bacteria growing on inorganic precipitate (specifically, calcium carbonate produced as a result of alkalinity production during denitrification). These denitrifying granules are smaller and less robust than those of strictly anaerobic systems, and have seldom been described in the literature.

While substantial biomass growth occurred in the prototype reactor, no granule formation was observed. Mature granule formation in an upflow reactor often takes weeks or months to establish as the predominant form of biomass in the reactor. The approximately 150 days of prototype process operation should have been sufficient to observe granulation of biomass, if conditions were sufficient to achieve granulation. However, it is believed that the cultivated biomass and the conditions under which the reactor operated would not allow granule formation. Factors contributing to the lack of granule formation include the relatively low organic loading rate to the reactor and the fact that the process was, by design, not operated to promote strictly anaerobic conditions under which granulation is typically observed.

Biomass solids analyses show that the volatile suspended solids in the bottom of the upflow reactor were consistently around 2.67 grams VSS/liter. Typical VSS values for granular biomass

produced in a methanogenic UASB are approximately 20 grams/liter. One problem associated with the lack of granule formation in the upflow reactor was that flocculent biomass has a higher rate of wash-out from the reactor. While in granule forming systems the majority of the biomass is expected to remain in the reactor (because of the high specific gravity and large particle size of the granules), the VSS in the effluent of the prototype NO/Fe(III)EDTA reducing upflow reactor was measured to be 1.25 grams/liter – almost half of that at the most concentrated point. Granules would also be desirable because the semi-attached growth characteristics of a granule in upflow reactors allow for the establishment of zones of selective growth of a certain type of bacteria and increased activity (*e.g.* NO reducers or ferric iron reducers) at a particular elevation in the reactor. When operating a fixed film reactor at steady state, conditions stabilize as a function of granule bed depth and those redox conditions will create conditions ideal for the growth of a certain type of bacteria. In the case where bacteria are non-stationary (*i.e.*, un-attached and in a mixed liquor), microorganisms float through the reactor and will be exposed to changing ORP conditions as they move. The flocculent reactor,instead, promotes growth of bacteria that can survive under the wide range of ORP conditions to which they are exposed while floating through the system. While washout and transport of bacteria throughout the process does not promote establishment of zones of activity in the upflow reactor, it does promote the cultivation of populations of bacteria that are resilient and capable of adapting and functioning under varied redox conditions.

7.1.1.3 Application of ORP for Use as an Indicator of Reactor Performance. One of the focuses of this research was to consider the usefulness of ORP in monitoring process performance for the qualitative observation of reduction reactions. Comparing observed ORP data with quantitative and qualitative process performance, such as ferrous/ferric iron concentration, biogas composition, and dissolved sulfide concentration measurements, several general trends were observed. There was a delayed response in ORP after a change in organic loading rate to the process water. This lag in response prevents the use of ORP as an indicator of short term process performance. In addition, variability in ORP measurements from one minute to the next result from the complexity of the process water and the mixed-potential response of the two electrode probe when used in situ. Consideration of smoothed data (moving average) provides a more useful interpretation of ORP results that allow observation of spatial and temporal trends that can be compared with other observed data. While the previously described mixed response makes instantaneous use of ORP data impractical, the ferrous EDTA/ferric EDTA Nearnstian couple buffers even the complex process water described in this work and provides a coarse "landmark" by which the health of process operation can be estimated.

Throughout prototype apparatus operation, ORP measurements were regularly taken at several points in the closed-loop apparatus. It was initially hoped that the ORP could be used as a direct indicator

of process performance and identify with some certainty the biologically-catalyzed reactions that predominate in the area of the process being measured. Day to day results showed substantial variability and a single data point is useful for little more than identifying whether conditions in the water are aerobic, anoxic, or strictly anaerobic. However, by smoothing ORP results over several days using a 6-day moving average, the inherent variability in ORP measurements resulting from the influence of the presence of several different species in solution is reduced and trends in ORP data can be identified. These smoothed data, shown in Figure 38, exhibit trends that are significant both temporally and spatially, corresponding significantly with reactor performance. All values are reported as mV with respect to a silver/silver chloride electrode.

Initially, after reactor start up, the process water was anoxic and relatively consistent throughout the system. By day 6, when ORP data collection began in earnest, biological activity was already significant, with both acid consumption and gas production observed. The ORP began to differentiate based on sampling location into anoxic and more anaerobic zones. In the mix tank, where nitrate was added in Phase I of operation as nitric acid, the oxidation-reduction potential achieved average levels of around –75 mV (vs. Ag/AgCl reference). In the bioreactor effluent and at the bottom of the subsequent slanted plate settler, the observed ORP was significantly lower – around –125 to –150 mV (vs. Ag/AgCl reference). Coupled with the observed biogas production and acid consumption to counteract alkalinity production, the drop in ORP was interpreted as an indicator that bacterial inoculation was successful and that biological activity was increasing. As process operation continued, ORP in the bioreactor effluent was observed to continue to decrease, with ORP values reaching approximately -175 mV (vs. Ag/AgCl reference) by day 42 when the process was modified and Phase II initiated. The ORP in the quiescent bottom of the slanted plate settler that followed the upflow anaerobic bioreactor established even lower ORP values of approximately –200 mV (vs. Ag/AgCl reference) by this point.

Conditions in the bottom of the settler were ideal for strictly anaerobic conditions to develop, with a significant sulfate concentration, anaerobic bacteria, acetate, and a long residence time. Because, in addition to being inoculated with the anoxic denitrifying bacteria, the bioreactor was also inoculated with biomass taken both a wastewater treatment plant anaerobic digester, the upflow reactor contained bacteria capable of carrying out sulfate reduction and methanogenesis from the point of reactor inoculation. However, the ORP values of the process were initially too high for these strictly anaerobic microorganisms to thrive, despite the fact that there was a significant concentration of sulfate as well as significant ethanol/acetate in the process water. By applying a significant load of nitrate to the system, establishment of sulfate reducing activity and methanogenic activity was largely avoided during Phase I of reactor operation.

After the process was converted to the Phase II configuration, and nitrate was replaced with NO as the oxidized nitrogen species being loaded to the process, conditions changed dramatically in the bioreactor, as well as the rest of the system. The dramatic decrease in the molar loading rate was not accompanied by a commensurate decrease in organic loading rate upset conditions in the bioreactor and the ORP values in throughout the process dropped quickly. By day 55 of operation, almost two weeks into Phase II of process operation, the ORP in the upflow bioreactor effluent had dropped to around –230 mV, and in the bottom of the slanted plate settler, the ORP had reached levels near –290 mV. Also, ORP conditions in the scrubber effluent (measured after process modification in Phase II) and mix tank decreased as a result of organic overloading, with values near -150 mV. Despite these low ORP conditions, no significant loss of iron (present in the chelated form with EDTA) was observed, and scrubber efficiency remained high.

It should be noted that the base of the settler where the deepest anaerobic conditions developed was not in the direct flowing stream of the active process, but rather a quiescent zone with only limited communication with the bulk of process water flow. Quiescent flow conditions are required at the base of gravity-based solid/liquid separation units, in order to promote initial settling of small particulate in the process water and subsequent under-drain thickening. These conditions were ideal for the establishment of a strictly anaerobic population. Significant sulfate reduction occurred in this settler, as evidenced by the formation of ferrous sulfide in the separated solids. Because this quiescent zone is somewhat separated from the bulk of the process water, and therefore not directly affected by changes in operation parameters, the response to modification of operation is both muted and delayed as compared to the response in other parts of the process. This is evidenced by the observation of a slower, more gradual change of ORP in this area following organic overloading. It is believed that avoiding establishment of strictly anaerobic conditions in the settler bottom would require careful monitoring and modified operation strategies.

ORP values in the upflow bioreactor, in contrast, are directly impacted by alteration of process control and operation. Even before observation of significant methane production in the bioreactor (day 63 of process operation, day 21 of Phase II operation), the organic loading rate had been decreased to more closely match stoichiometrically with NO loading. Following this decrease in organic loading rate the ORP in the bioreactor effluent began to rise, and by day 75, had risen to levels similar to those observed during the middle of Phase I (approximately –125 mV). A coincidental increase in ORP was observe in both the scrubber effluent and the mix tank located upstream of the bioreactor, with the ORP in both locations stabilizing around –115 mV.

After less negative ORP conditions were reestablished in the process, they remained relatively consistent through the remainder of process operation. This observation, coupled with observed stabilization of other indicators of process performance such as acid equivalent loading rate, biogas volume and makeup, organic loading rate, and NO loading rate, allow this period of process operation (day 75 to 149) to be considered a period of steady-state operation.

Microbially-mediated methanogenesis occurs under similar redox conditions as sulfate reduction, with methane producing bacteria (MPB) operating in competition with sulfate reducing bacteria (SRB). In most anaerobic biological reactors the goal is maximizing the conversion of organic input to methane. In the process under consideration, methane production is considered as an indicator of poor reactor performance. The primary problem associated with methane production in the upflow bioreactor considered in this study is the unnecessary consumption of ethanol. Because methanogenesis and sulfate reduction proceed under similar ORP conditions, it is accepted that sulfide formation accompanies the observed methane production. ORP values of -230 mV (vs Ag/AgCL reference) coincide with significant observed methane production (see Figure 34) in the upflow bioreactor.   However, no increase in biogas H_2S or dissolved sulfide was observed during this period. It is believed that sulfide formed in the system reacted very quickly with iron present as a chelate of EDTA, forming insoluble ferrous monosulfide. Regardless of the fate of sulfide, ORP values at this level are considered to be undesirable for the current process.

In contrast, ORP values observed during steady-state operation (days 80-149) are indicative of successful process operation. In the mix-tank where NO reduction initiated, values during steady state operation were typically around -115 mV (vs Ag/AgCl reference). In the upflow bioreactor effluent, ORP values of -125 mV were typical during steady state operation. It is worth noting that these values are both near the theoretical E_0 of the Fe(II)EDTA/Fe(III)EDTA Nernstian couple. Iron EDTA serves as both a sink for dissolved oxygen (reacts quickly with DO to prevent inhibition of anoxic/anaerobic bacteria while also helping to buffer the reduction processes to prevent process water ORP decrease into the range associated with methanogenic/sulfate reduction.

The role that the presence of iron EDTA has in moderating changes in ORP is significant. As observed in the steady-state conditions described above, ORP values in the properly functioning system to achieve biological reduction of the nitrosyl adduct of ferrous EDTA and ferric EDTA in the ethanol fed system consistently remains near an ORP value of -125 mV (vs. Ag/AgCl reference). This observed ORP value coincides with the theoretical ORP value of the ferric/ferrous Nernstian couple (-126 mV) as described in Figure 14 of Chapter 3.   Because both the oxidized and reduced species of this couple remain dissolved in solution after oxidation or reduction, the ORP influence of iron EDTA is significant.

In contrast, denitrification results in nitrogen gas production and escape of the reduced species from the system, and sulfate reduction results in formation of sulfide that immediately reacts with iron in solution and precipitation of ferrous sulfide. The reduced species of these redox couples does not stay in solution as does ferrous EDTA. In addition, it should be noted that ferrous EDTA in solution reacts readily with dissolved oxygen. Immediate removal of dissolved oxygen from bulk solution prevents the dissolved oxygen from significantly inhibiting the activity of anoxic and anaerobic bacteria functioning in the system. Therefore, not only is iron EDTA crucial because it increases solubility of NO in the process water, but it also serves, in effect, to buffer solution ORP near the E_0 of the ferrous EDTA/ferric EDTA Nernstian couple.

While the observed trends in data cannot be used for the explicit quantitative evaluation of process water ferric/ferrous ratio or other parameters of interest, it does provide some insight into process performance and zones of microbially-mediated activity. Failure to achieve a sufficiently low ORP in the effluent of the bioreactor would indicate that microbially-mediated reduction of, for example, the nitrosyl adduct of ferrous EDTA did not proceed to completion. After such an observation is made, the reason for this failure can be investigated. One possible explanation is that the ethanol (electron donor) loading rate is insufficient to allow completion of the desired reduction. Another possible explanation would be that inhibition of the microbially-mediated reduction was preventing the desired reaction from proceeding. Therefore, while ORP measurement would not provide insight into the cause of insufficient reducing capacity, it would provide a quick and inexpensive qualitative measure of process health.

On the other hand, establishment of low ORP conditions in the process water is indicative of the establishment of excessively reducing, strictly anaerobic conditions. Observation of sulfide generation or methanogenesis in the reactive process water would serve to verify this. Sulfide generation caused iron sulfide formation and precipitation of iron from solution that is used for the scrubbing of NO. Methanogenesis suggests the excessive addition, and therefore waste, of electron donor (*i.e.*, ethanol). Both observed conditions would detract from process performance, non-ideal reagent application, and therefore inefficient capital use.

7.1.2 Discussion of Batch Kinetic Analysis Results

Obtaining accurate biodegradation kinetic parameters under conditions expected of an operating treatment process is an essential step in properly predicting the performance of an engineered process. Batch experiments were designed such that they would test only the rate of the two microbially-catalyzed reactions of interest.

Because ethanol consumption is directly coupled to reduction of ferric EDTA in an ethanol-fed system, a simplified method of considering reduction of ferric EDTA was used. In this method, the rate of reduction of one substrate (the oxidized Fe(III)EDTA) is measured as a function of the concentration of the organic reducing agent (in this case ethanol). In standard Monod kinetic evaluation, the change in ethanol over time is measured as a function of initial ethanol concentration. Based on stoichiometric ratio of the reduction of ferric EDTA with ethanol (12:1), the change in ferric EDTA concentration is proportional to the change in ethanol concentration. In batch tests the observed amount of ethanol consumed in the reduction of ferric EDTA was 1.674 times greater than this stoichiometric ratio, but the ratio was predictable and consistent over the range of ethanol considered. As a result of this consistent relationship, the procedure to describe the rate of ferric EDTA reduction as a function of initial ethanol concentration is an acceptable one. A similar stoichiometric relationship was observed between microbially-mediated NO reduction and ethanol consumption, and a similar method of analyzing reduction kinetics was utilized.

The literature shows that the nitrosyl adduct of ferrous EDTA as well as oxidized ferric EDTA can be reduced by other chemical and microbially-catalyzed reactions. In particular, the autotrophic reduction of NO or Fe(III)EDTA via oxidation of reduced or partially reduced sulfur species was described by van der Maas and others (2002). One study describes the observation of microbially-catalyzed nitrosyl adduct reduction using sulfite as the sole electron acceptor. While these reactions are very interesting and could prove beneficial in industrial application because they would partially mitigate the required ethanol addition, they are not the focus of the current study.

Sulfate was present in all batch tests, but that ion is already in its fully oxidized form and could not accept electrons from NO or Fe(III)EDTA present in the batch reactors. Because ferrous sulfate was combined with tetrasodium EDTA in equimolar concentrations to make iron EDTA for all batch tests, sulfate was present at the same molar concentration as the total iron EDTA (0.045 M). Therefore, sulfate concentrations in solution remained constant in all batch tests, and did not impact relative results. The presence of sulfate also served to insure that ethanol consumption was limited to the reaction under consideration. If, for example, iron reduction had proceeded to completion and sulfate reduction started, then sulfide would have been formed in solution and black amorphous ferrous sulfide (FeS) would have been observed in the process water. That no FeS formation was observed in either NO reduction or ferric EDTA reduction experiments provides an extra verification that only the reactions of interest were observed in each batch reactor.

During the course of batch analysis, it was considered that the EDTA itself may have been consumed as an electron donor/carbon source in the reactions under consideration. However, it is believed that bacteria would oxidize ethanol or products of its oxidation before attempting to attack the

142

large EDTA molecule and that the thermodynamics of EDTA oxidation would not be favored in batch tests or in the prototype reactor. No evidence of EDTA oxidation was observed in the course of the prototype process operation.

A batch method was employed to determine the reduction kinetics of individual targeted oxidized species in the spent scrubber water. This approach allows the application of low substrate concentrations relative to the total biomass concentration in the batch bioreactor, minimizing changes to the physiological state of the biomass (*i.e.*, levels of RNA, DNA, and proteins). (Grady, 1996). Biodegradation kinetic parameters measured using low substrate to oxidized species ratios (X_0:S_0 on the order of 0.02:1) provide an accurate reflection of the actual kinetic performance of the biomass while in a physiological state consistent with that of biomass in the prototype process from which the biomass was obtained. Kinetic parameters measured under such conditions have been called "extant," implying that they are representative of existing conditions in the bioreactor (Grady *et al.*, 1995). Batch kinetic evaluations conducted at much higher biomass to substrate ratios (20:1) result in much higher observed maximum growth rates and Mechaelis-Menten half saturation coefficients, but do not accurately reflect the conditions expected in the bioreactor. This may be the result of expression of multiple enzyme systems in the larger biomass inoculum (Hwang *et al.*, 1989, Schmidt and Gier, 1990). In short, extant tests more accurately reveal the state of the biomass in the bioreactor and intrinsic tests show the ultimate biodegradable capability of the biomass. Because the purpose of the designed batch experiments was to model conditions in the prototype bioreactor, batch reactors were operated under extant conditions.

7.1 ENGINEERING CONSIDERATIONS

Consideration is given to application of apply the collected kinetic batch data and prototype process results in support of design of a process based on the described treatment concept. Data have significant implications for both process configuration and operation strategies.

7.2.1 Prototype Bioreactor Parameter Determination – Mass Balance Model

Calculations performed in order to quantify the performance of the biological reactor include determination of mean cell residence time, mean hydraulic loading rate, mean organic loading rate, and observed biomass yield coefficient. These calculations were conducted for two different mass balance

boundaries. In one set of calculations, the system boundary was drawn around the bioreactor alone.

Recognizing that the entire closed-loop system contains biomass and was therefore reactive, the second

case considers a system boundary drawn around the entire process. The boundaries of the two mass

balance systems considered are illustrated in Figure 54. The following description provides an

interpretation of prototype process steady-state performance.
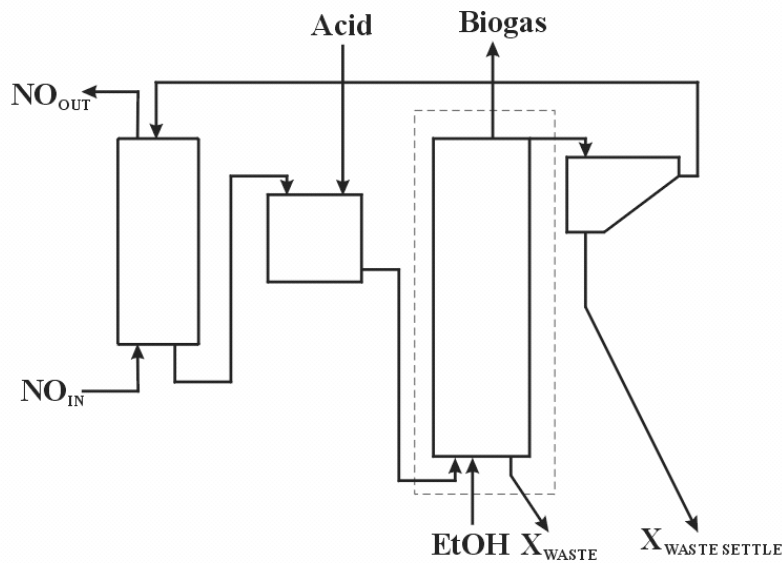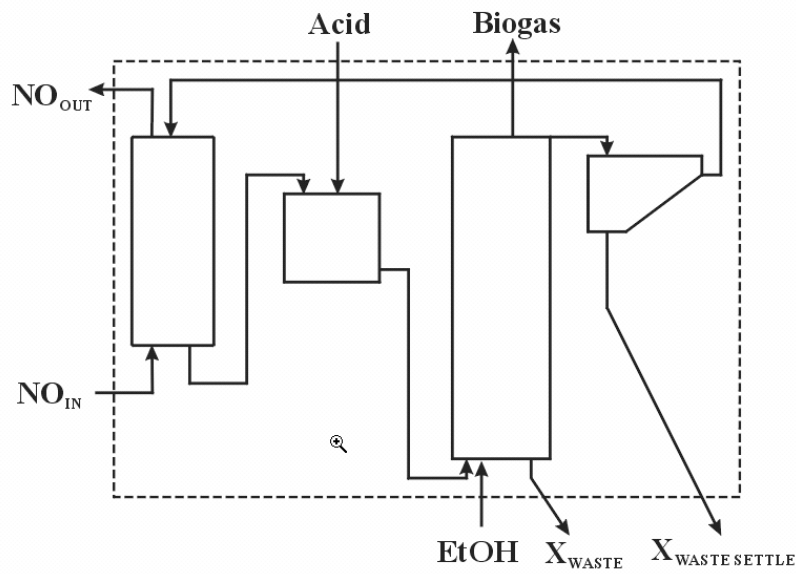
Figure 54. The two boundaries considered in the mass balance investigation.

7.2.1.2 Mass Balance on Upflow Bioreactor. Mean cell residence time is calculated as the mass of bacteria in the system divided by the rate of cell removal from the system. Mean cell residence time was calculated using mixed liquor volatile suspended solids (MLVSS) as an approximation of total biomass concentration and data on volume of biomass removed from the system throughout operation. Assuming

that the biomass concentration gradient as a function of reactor height follows a log-normal distribution, the geometric mean can be used as an approximation of mean biomass population in the reactor. The geometric mean was determined between the MLVSS concentration at the reactor bottom (X_{waste}) and the reactor effluent (X_{eff}) from the top of the upflow reactor. The geometric mean of these two values (2.67 and 1.01 g/l, respectively) was calculated to be 1.64 grams of VSS per liter. The total mass of VSS in the 42.5 liter reactor was therefore estimated to be 69.8 grams.

The rate of bacterial loss from the reactor, based on mass balance analysis is defined as the sum of the wasting rate and the biomass washout rate, minus the biomass entering the reactor suspended in the process water of the closed loop process. A mean volume of 0.4 liters per day of biomass was removed as waste from the reactor. The mean process water flow rate was 0.186 liters per minute, with influent and effluent VSS measured as 0.763 and 1.01 grams per liter, respectively. From this, the rate at which cells left the reactor was calculated to be 0.0467 grams per minute, and the mean cell residence time calculated to be 1495 minutes, just over one day. Comparing this to the hydraulic retention time in the reactor of 219.1 minutes, is observed that there is significant separation between biomass and process water in the upflow reactor.

Calculation of biomass yield in the bioreactor was also performed. Observed yield is defined as the grams of VSS generated per gram of chemical oxygen demand (COD) consumed in the reactor. In order to perform this calculation for the defined system, the following points and simplifying assumptions are noted:

- There are 96 grams of COD per mole of ethanol
- There are 64 grams of COD per mole of acetic acid
- There were 181.2 grams of organic COD as ethanol per liter of prepared nutrient solution
- Effluent COD as hydrogen gas is negligible (negligible H_2 gas observed in biogas)
- There was no ethanol in the bioreactor effluent, and therefore no effluent COD in the form of ethanol.

At steady-state, the biomass generated is assumed to be the same as the amount of biomass wasted. Therefore, the mass of VSS generated is 2.67 grams per liter times 0.4 liters per day, or 1.068 grams of VSS per day. The grams of COD destroyed is calculated as the sum of COD from ethanol entering in the nutrient solution and the COD from acetate entering in the recycled process water minus the COD from acetate leaving in the reactor effluent. The mass of COD destroyed in the bioreactor per day was calculated to be 25.1 grams. The observed yield coefficient was calculated to be 0.0426 grams of VSS generated per gram of COD consumed. By comparing the observed yield coefficient determined during batch analysis of NO reducers and Fe(III)EDTA reducers, 0.259 and 0.055 g VSS/g COD,

respectively, we see that the observed yield of the prototype reactor is similar to that of the Fe(III)EDTA reducers.

7.2.1.3 Mass Balance of Entire Process. Similar calculations were carried out for a mass balance system including the entire process. As a result, the washout of biomass from the bio-reactor was not considered as loss because that suspended biomass remains within the mass-balance system. The total biomass in the system was taken to be the sum of the biomass in the reactor and the biomass outside of the reactor. The mean biomass concentration in the non-reactor portion of the closed loop process was estimated as the arithmetic mean of the reactor effluent VSS and the reactor influent VSS. The mean cell residence time in the system is, therefore much larger. Because the total mass of active biomass is greater for this mass balance system, and because there is a low mass of biomass being wasted from the system per day, the mean cell residence time of this system was found to be much larger than that of the bioreactor alone. Calculated values for both mass balance systems are summarized in Table 11.

Table 11. Summary of the bioreactor performance parameters as determined by mass- balance on the bioreactor alone, and on the complete closed-loop process.

Parameter	Bioreactor Mass Balance	Complete Process Mass Balance
System Volume, (liters)	42.5	98.5
TotalSystem Biomass, (grams VSS)	69.79	119.5
Mean Cell Residence Time (days)	1.0	75.9
Observed Yield Coefficient (grams VSS generated/ gram of COD consumed	0.0426	0.0393

7.2.1.4 Alkalinity Production/Acid Consumption. Generation of alkalinity in the biologically-active process water was observed, with a subsequent increase in the pH of the process water. Process water was maintained at a neutral pH by the addition of acid. In Phase I of operation, nitric acid (HNO_3), with one acid equivalent per mole, was used both as the source of nitrate and as the source of acid equivalents for pH adjustment. During Phase II, nitric acid was replaced with sulfuric acid, with two acid equivalents per mole (H_2SO_4). Because the process water was maintained at a pH of 7, it was possible to determine the relative concentration of each of the bicarbonate species in solution, and the associated proton

demand. At a pH of 7 and a temperature of 35 ºC, the process water was 0.7 units above the $pK_{a,1}$ for the dissociation of $H_2CO_3^*$ to HCO_3^-, 6.3, and 3.3 units below the $pK_{a,2}$ for the dissociation of HCO_3^- to CO_3^{2-}, 10.3. As a result, it was assumed that the concentration of free CO_3^{2-} in solution was negligible. Based on this assumption, the relative ratio of $H_2CO_3^*$ to HCO_3^- was calculated. For every mole of total bicarbonate ion at neutral pH and 35 ºC, 0.1663 moles of $H_2CO_3^*$ and 0.8337 moles of HCO_3^- was produced, with essentially no CO_3^{2-}. $H_2CO_3^*$ represents the sum of dissolved and gaseous CO_2 that is generated as determined by the Henry's law coefficient. 29.76 atm/M. Finally, noting that each mole of HCO_3^- effectively removes one mole of protons from solution, while $H_2CO_3^*$ removes two, the acid equivalent demand due to the addition of bicarbonate alkalinity to the process water can be calculated according to Equation 86.

$$\text{Acid equivalent demand} = \text{Moles of total } CO^{3-} *(0.8337*1+0.1663*2) \qquad (86)$$

Considering each of the significant reduction reactions taking place in the prototype process, we can calculate the theoretical alkalinity generated from each reaction. As described in Section 7.2.1.6, iron reduction during steady-state operation was consistently observed at a seven percent conversion efficiency. During reduction, acid equivalents were generated, but the same stoichiometric consumption of acidity was consumed when the ferric EDTA was subsequently oxidized. As a result, there was a net production of alkalinity resulting from the generation of bicarbonate ion in the process water. Given a total iron EDTA concentration of 0.04 M, a flow rate of 0.186 liters per minute, and the stoichiometry described in Equation 65, the acid equivalents consumed per day from the reduction of ferric EDTA was calculated to be 0.1458. Similarly, the reduction of NO produces carbonate alkalinity. Reduction of 0.1937 moles of NO per day generates one third as much bicarbonate ion. According to Equation 86, this bicarbonate generation consumes 0.06456 equivalents of acid per day. Finally, sulfate reduction produced both bicarbonate ion and bisulfide ion (Equation 33). At a temperature of 35 ºC, the pK of H_2S dissociation is 6.82 (Table 5), and the ratio of HS^- to H_2S generated at neutral pH is 1.513:1. Based on the estimate that 0.01124 moles of HSO_4^-e were reduced to sulfide per day (Section ##), 4.472×10^{-3} acid equivalents are consumed per day from by sulfide formation. In addition, bicarbonate ion generated as a result of sulfate reduction (Equation 33) consumes 0.01748 moles of acidity per day at neutral pH. The sum of all reducing activity that proceeded in the upflow reactor resulted in a daily demand of 0.2201 acid equivalents.

During steady-state operation, a 10% sulfuric acid solution (1.8 M H_2SO_4 or 3.6 N) was used for process water neutralization. With 0.0917 liters of sulfuric acid solution added per day to maintain neutral pH, 0.3301 moles of acidity were added to the reactor per day. Based on the calculated daily acidity demand of 0.2201, only 73.3 percent of the added acidity was accounted for.
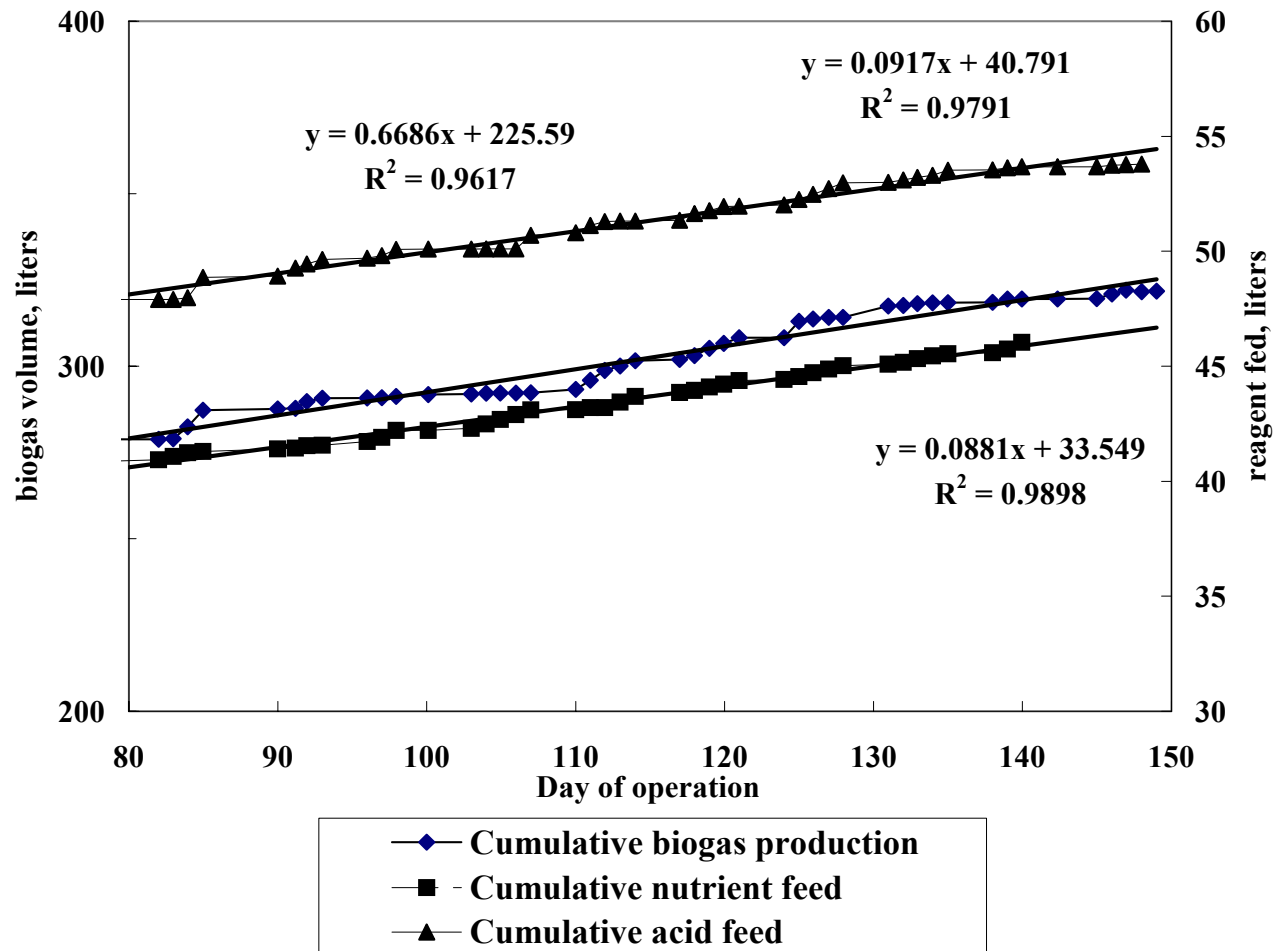
Figure 55. Ethanol/nutrient feed rate, 1.8 M sulfuric acid solution feed rate, and biogas generation rate.

7.1.1.5 Nitrogen Generation in Bioreactor. Theoretical nitrogen gas production from one liter of 0.045 M NO·Fe(II)EDTA^{2-} at 35ºC is 0.284 liters. The molar loading rate to the process water during the period of steady-state process operation was 0.1937 moles per day. During this same period, 0.6686 liters of gas were generated per day in the upflow bioreactor. Based on gas analysis, 95.41% of the biogas collected from the bioreactor during this period was nitrogen gas. Using the ideal gas law, we can determine the number of moles of nitrogen that was observed generated in the upflow bioreactor during the period of steady-state operation at a temperature of 35 ºC and a pressure of 1 atm. This calculation gives a molar yield of 0.0252 moles of N_2 generated per day. Because of the low solubility of nitrogen gas, it can be assumed that all of the generated N_2 is released to the bioreactor headspace at atmospheric conditions. Considering the stoichiometry of NO reduction, reduction of two moles of NO results in generation of one mole of N_2. The ratio of moles of N_2 generated in the upflow bioreactor to the moles of NO loaded to the system is 0.0252 to 0.1937, or 0.13. The theoretical ratio is 1 to 2, or 0.5. Therefore, approximately 74 percent of the nitrogen generated in the reduction of NO can not be accounted for in the upflow bioreactor flue gas.

This observation suggests that much of the NO reduction is occurring prior to the process water entering the upflow bioreactor, namely in the mix tank. Ethanol/nutrient solution was added to the process water after the mix tank in order to maximize the amount of reduction occurring in the upflow bioreactor. Because the reduction reactions require an electron donor to proceed, it was believed that by introducing ethanol after the mix tank and at the inlet to the upflow reaction, much of the biological activity would occur in the upflow reactor. It was initially believed that essentially all of the added ethanol would completely oxidize in the upflow reactor, and biological activity would occur primarily within the bounds of the bioreactor. The inability to close the mass balance of nitrogen using the biogas generated in the upflow bioreactor suggests that the majority of the NO reduction is occurring outside of the upflow reactor. Because significant iron reduction was observed to occur in the upflow bioreactor, and because the reduction of NO is thermodynamically preferred over the reduction of iron or other oxidized species such as sulfate, it is believed that NO reduction was occurring upstream of the upflow bioreactor, in the mix tank. Because no ethanol was observed in the mix tank or in the upflow bioreactor effluent, ethanol could not have been the electron donor used by those NO reducing bacteria that were active outside of the upflow reactor.

However, acetic acid was observed in the bioreactor effluent, as well as in the bioreactor influent which suggests that acetic acid served as the primary electron donor for NO reduction occurring in the mix tank. As described in Chapter 2, denitrification has been shown to proceed using acetic acid as the primary electron donor. In fact some reported sources suggest that acetic acid is the preferred substrate

for denitrifying bacteria and denitrification proceeds only after acetogenic bacteria oxidize ethanol to acetate in ethanol-fed denitrification systems. These factors all allow for the reduction of NO in the process mix tank. Unfortunately, biogas that was generated in the mix tank was not collected, and as a result the volume and composition of that biogas is unknown. Only 26% of the nitrogen gas expected to result from NO reduction could be accounted for in the upflow reactor biogas.
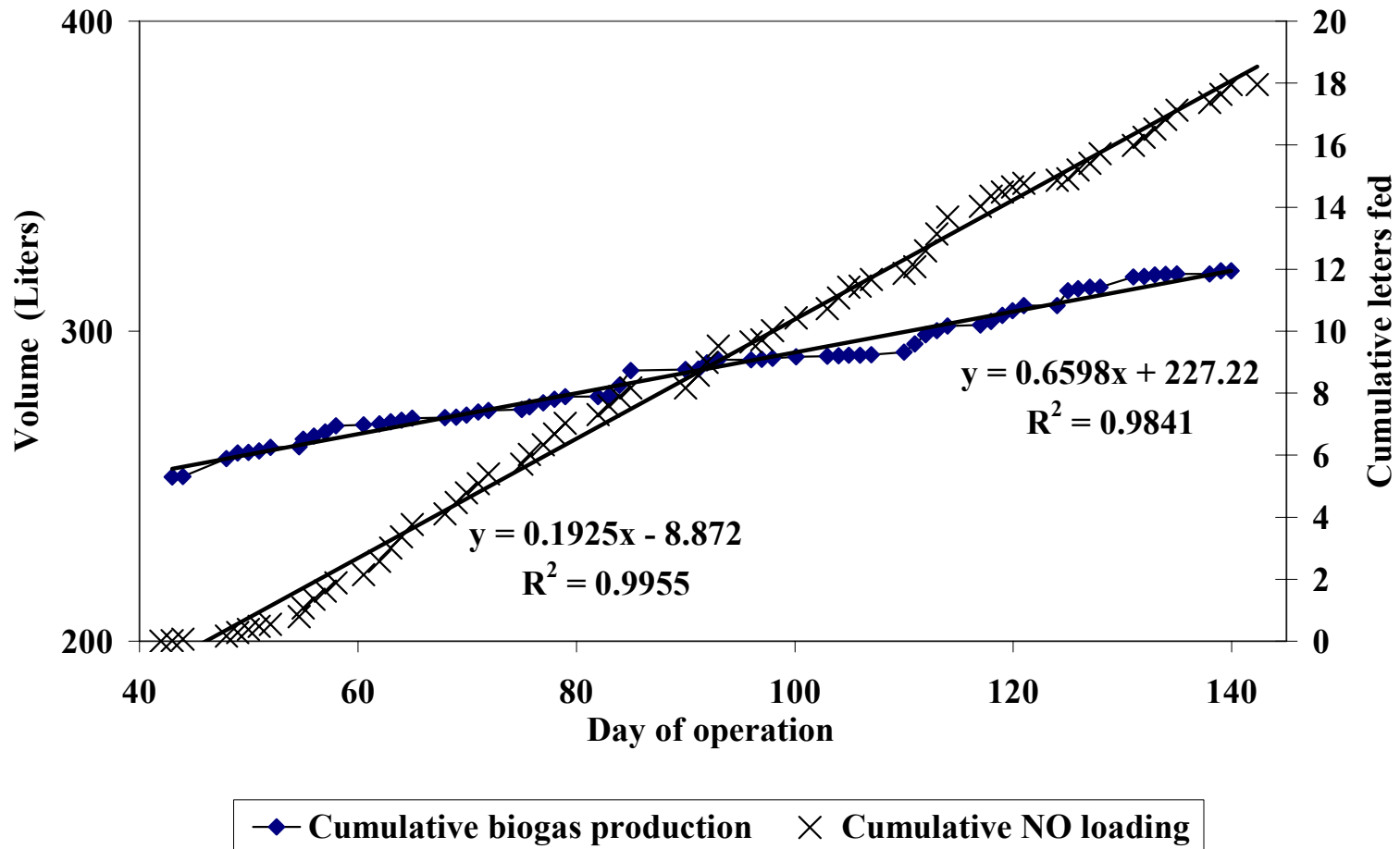
Figure 56. Volume of biogas production during Phase II of process operation.

7.2.1.6 Reduction of Ferric Iron in the Upflow Bioreactor. A significant amount of ferric EDTA reduction was observed in the upflow bioreactor, as shown in Chapter 5. Based on 10 samples analyzed for ferrous and total iron using an ion chromatographic method, the mean total iron concentration in the bioreactor influent was 0.05055 M, and in the effluent was 0.05161 M. This shows that at steady state conditions, iron was not lost to the system as it traveled through the upflow reactor. The mean influent ferrous iron concentration was 0.00712 M, and the effluent ferrous concentration was 0.01078 M. The mean reduction of ferric iron taking place in the 42.5 liter reactor at a flow rate of 0.186 liters per minute was 0.003662 M, or approximately 7.2 % of total iron EDTA in solution. The mean molar conversion of ferric EDTA to ferrous EDTA in the prototype reactor was therefore 0.9808 moles of iron EDTA per day. The steady-state molar reduction of ferric EDTA to ferrous EDTA was substantially greater than that of NO reduction in the upflow reactor, 0.0504 moles NO per day, and 0.1937 moles of NO per day in the entire prototype process. Because of this, we assume that the majority of the upflow reactor was dedicated to iron reduction for iron EDTA scrubber solution regeneration.

The prototype scale reactor was operated with ethanol/nutrient solution loading rate of approximately 300 ml per day. Over time, the build up of excess organic electron donor resulted in the formation of sulfide (sulfate reduction) and methane (methanogenesis) (see gas composition Days 63 and 70 in Figure 34) as well as accumulation of organics and formation of organic acids not originally present. By decreasing the ethanol-loading rate to near the amount needed for NO and ferric iron reduction, methanogenesis and sulfate reduction were minimized. Sulfide and methane production corresponds to a waste of ethanol reagent (and increased operating cost). Analysis of reactor effluent has shown an average sulfide concentration of 1.7 mg/l.

7.2.1.7 Sulfur Material Balance. Considering the fate of sulfur in the prototype process during steady-state operation, it was recognized that most sulfur in solution was present as fully oxidized sulfate. Sulfate was present as a result of addition of iron EDTA solution makeup. This solution was a 0.045 M solution made of ferrous sulfate and tetrasodium EDTA. So, for every liter of iron EDTA makeup solution added, 0.045 moles of sulfate was added to the system. Because the biomass wasting rate from the system was very low, little sulfate was added to the closed-loop process from this source. During steady-state operation, sulfuric acid was used to maintain process water pH at circum-neutral conditions. Essentially all of the sulfate introduced to the system during steady state of Phase II of prototype operation was added as a result of sulfuric acid addition. Because biological activity was consistent throughout steady state operation, pH increase and required acid addition was also consistent. From Figure 38, sulfate concentration in the upflow reactor effluent increased during steady state operation at a

rate of 123.1 mg/l per day. Considering a mean volume of total process water of 120 liters, this corresponds to a measured accumulation of sulfate of 14.77 grams per day.

This value is compared to the rate at which acid is loaded to the system. Figure 55 shows that the sulfuric acid solution was loaded at a rate of 0.917 liters per day. The acid solution was 10% sulfuric acid by volume (1.8 M). The loading rate of sulfate to the process water was therefore 15.85 grams of sulfate per day. In addition to this, a small mean concentration of approximately 1.7 grams per liter of total dissolved sulfide was measured in the process water, with no accumulation over the period of steady-state operation. Sulfide was observed to be present in the process as insoluble iron sulfide precipitate. At the time of steady-state operation, sulfide was not measured in the process water. However, after completion of data collection described herein, the zinc acetate method for measurement of acid volatile sulfide was employed to measure the total sulfide present in a sample of biomass wasted from the base of the upflow reactor. Using this method, the concentration of sulfide in the upflow reactor was measured to be 0.12 grams of sulfide per liter. Based on the mean biomass wasting rate of 0.4 liters per day, the amount of sulfur drawn from the system as sulfide precipitate was estimated to be 0.12 grams of sulfide per day, or 0.0144 grams of sulfur as sulfate per day. Finally, Figure 33 shows that no sulfate was measured in the upflow reactor biogas. Even during periods of substantial methanogenesis that preceded steady-state operation no hydrogen sulfide generation was observed. This suggests that sulfide formed in solution quickly reacted, either to form an insoluble metal sulfide or oxidized in the coupled reduction of other dissolved species. Based on these calculated values, 1.065 grams of sulfur as sulfate per day is unaccounted for in the system. Over the 80 days of steady-state operation, accumulation of 85.2 grams of sulfur as sulfate (0.8875 moles of S as sulfate) is unaccounted for in the system. 93.3 percent of the sulfur in the system was accounted for.

It is speculated that the sulfur that is unaccounted for collected in the apparatus slanted plate settler as insoluble metal sulfide. During steady-state operation, ORP of the process water was maintained at -75 to -140 mV, a range in which NO reduction and ferric EDTA reduction predominate. As a result, sulfate reduction in the prototype reactor was suppressed. Upflow reactor influent and effluent sulfate concentrations were nearly identical throughout steady-state operation of the process. In addition, the oxidation reduction potential of the mix tank during steady-state operation (around -110 mV vs. Ag/AgCl reference) was sufficiently high that sulfate reduction was suppressed. In contrast, the oxidation reduction potential of the slanted-plate settler was observed to be lower than that of the upflow reactor effluent, dropping below -200 mV vs. Ag/AgCl reference. It is assumed that loss of sulfate from the closed-loop process occurred in the quiescent base of the slanted plate settler.

Assuming that the unaccounted-for sulfur collected in the solid/liquid separator as a microbially-generated iron monosulfide, then 0.8875 moles of FeS, or 78.02 grams of FeS would have accumulated in

the settler over the 80 days of process steady-state performance. Following process operation, the unused solid/liquid separator was drained and a viscous black iron monosulfide precipitate was removed. The FeS concentration of this sludge was not measured quantitatively.

Therefore, sulfate reduction was observed to proceed in the process, even during the 80 day period of steady-state operation. It is estimated that approximately 6.7% of all sulfur introduced to the system during steady state operation was reduced to sulfide and precipitated as insoluble iron monosulfide precipitate. The observed sulfate reduction was not sufficient to reduce the overall concentration of ferrous iron in solution to a level where NO scrubbing efficiency was decreased. It is speculated that most of the sulfate reduction occurred in the process solid/liquid separator, which was unused for solids removal through the period of steady state operation. Finally, the presence of iron sulfide precipitate in the process did not prevent the development of populations of biomass with iron reducing and NO reducing activity.

In contrast to this period of steady-state operation, there was a period of approximately 20 days during Phase II, before the system stabilized, during which strict anaerobic conditions were established in much of the system. During this period, the rate of sulfur loading as sulfuric acid approximately the same as during steady-state operation (15.85 grams of sulfate per day), but the rate of sulfate accumulation observed in the system was far less, 8.00 grams of sulfate per day. This suggests that, under strictly anaerobic conditions, sulfate reduction proceeded to a much greater degree than was observed during steady-state operation, and that sulfur under these conditions, precipitated as FeS. This results in substantial loss of iron from the scrubber solution, and ultimately might result in loss of scrubber efficiency. At this point, iron monosulfide precipitate was observed in the process water at much greater concentrations.

7.2.2 Application of Kinetic Model for Process Evaluation

After having derived the kinetic expressions for the rate of microbially-mediated reduction of ferric EDTA and the nitrosyl adduct of ferrous EDTA, they can be used as the basis for preliminary design of larger scale treatment processes. As an example, the kinetic expressions were applied to the steady-state conditions of the prototype reactor and calculated results are compared with the observed performance of the prototype. There are several means of investigating the ability of the derived kinetic expressions to describe performance of the prototype. The following discussion descries the application of the Levenspiel method for kinetic data analysis, allowing estimation of reactor type and volume required to achieve a pre-selected conversion of reactants to products. Then, sludge age, substrate conversion, and

biomass washout was considered for both CSTR and plug-flow configurations. Finally, a tanks-in-series model was applied for comparison with prototype reactor results.

7.2.2.1 Levenspiel Plots. Based on the developed kinetic expressions for ferric EDTA reduction and NO reduction, we can determine what type of reactor should perform best given a specific set of process water conditions. By calculating and plotting Levenspiel plots - the conversion of Fe(III)EDTA vs. total flux devided by the rate of reduction (Figure 57), several trends become apparent. Looking at plots of varying ethanol concentration, it is observed that conversion efficiency increases with increasing ethanol concentration, and at higher ethanol concentration, less volume is required to achieve the same Fe(III)EDTA reduction efficiency. Figure 58 demonstrates the graphical estimation of the required prototype reactor volume, assuming the kinetic expression derived from batch experiments is applicable and applying conditions established during steady state operation of the prototype reactor ($X = 1.64$ g/l, $q = 0.186$ l/min, and initial ethanol concentration is 0.2 grams per liter). Based on the hydrodynamic analysis of the upflow reactor described in Appendix A, four rectangular segments were used to estimate the required volume of each tanks in order to achieve a conversion of 6.9%, as observed during steady-state operation. The Levenspiel analysis shows a required reactor volume of 69 liters, as compared to the actual prototype reactor volume of 42.5 liters. The estimated total volume of the four CSTR reactors was approximately 93 liters. This is more than twice the 42.5 liter volume of the upflow reactor that was used in the prototype process.
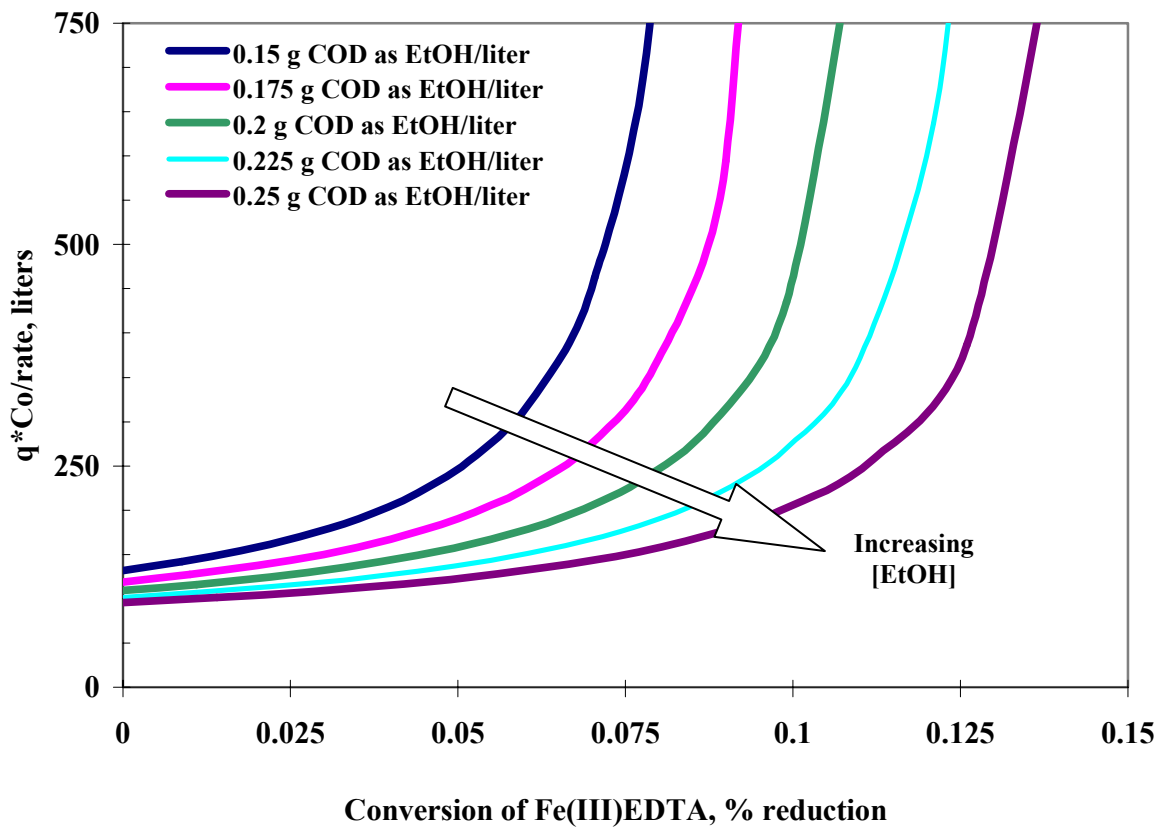
Figure 57. Levenspeil plot of ferric EDTA reduction over a series of initial ethanol concentrations, with a cell concentration of 1.64 grams per liter.
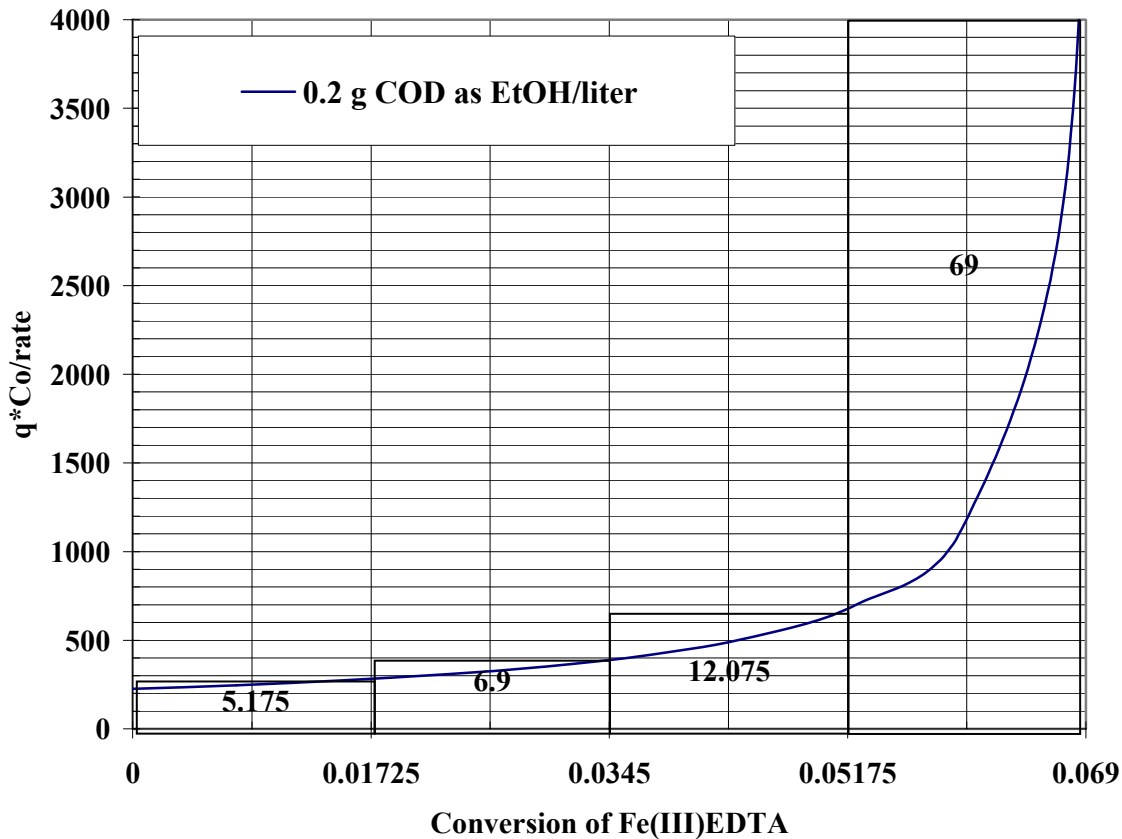
Figure 58. Estimation of the volume required for a Fe(III)EDTA reducing bioreactor to achieve 6.9% reduction of ferric EDTA, given an initial COD of 0.2 g COD as ethanol per liter, an initial cell concentration of 1.64 grams per liter, and a reactor that behaves as 4 tanks in series.

Also from the Levenspiel plot (Figure 58), a single CSTR used to achieve 6.9 percent conversion is represented by a rectangle filling the entire plot area with a volume of 276 liters. This illustrates the advantage of conducting Fe(III)EDTA reduction in a plug flow-type reactor configuration. There are several possible factors that contribute to the failure of the Levenspiel plot to properly describe prototype steady-state conditions. They include misestimation of the cell concentration in the reactor, potential syntropic relationshisp between different bacteria that were not observable in the batch reactor experiments, and oversimplification of substrate conditions in the prototype reactor.

7.2.2.2 Sludge Age and Bioreactor Stability. As described in Chapter 3, sludge age can be used in a continuously stirred suspended growth bioreactor to control the overall ability of an anoxic/anaerobic

bioreactor to remove COD and reduce oxidized species in solution, given a specified substrate utilization rate (U). Kinetic coefficients Y, k, Ks and k_d used to establish this relationship were determined under environmental conditions similar to those of the prototype upflow bioreactor. For the given values of the kinetic coefficients, listed in Table 9, the effluent COD (COD_{EFF}) from a reactor was calculated as a function of mean cell residence time (θ_C), and is shown in Figure 59.

Figure 59 illustrates the dependence of θ_C on effluent ethanol concentration for both the uninhibited reduction of ferric EDTA and the reduction of the nitrosyl adduct of ferrous EDTA. This plot has several implications for process performance and process design efforts. At increasing mean cell residence time, the process water and biomass are retained in the CSTR for longer periods of time, resulting in lower effluent ethanol concentrations. At low sludge ages below a minimum level, the biomass in the bioreactor will "wash-out." Washout occurs when the sludge age results in the wastage of biomass at a rate such that the biomass can not maintain its concentration by yielding new biomass. The critical sludge age at which washout occurs can be estimated using Equation 52. The calculated effluent concentration at sludge ages less than the wash-out threshold do not represent real conditions, but rather result from failure of the mathematical expression under conditions outside of normal operation. Ferric EDTA-reducing biota were observed to have a lower biomass yield than the NO-reducing population, and as a result iron reducers wash-out at a high sludge age. Specifically, the washout threshold for Fe(III)EDTA reducers was calculated to be 51.4 days, and the washout threshold for NO reducing bacteria was calculated to be approximately 11.7 days. Both calculated washout threshold values are plotted on Figure 59, as applied to an ideal CSTR.

As the concentration of ethanol is increased, the rate of iron reduction approaches the maximum velocity k (0.09091 M Fe(III)EDTA-/day *(g VSS/liter)$^{-1}$). Because the yield of new biomass is coupled to the rate of substrate utilization, the smaller increase in rate of substrate utilization at higher values of S (above the K_S of 0.3367 g COD/liter as ethanol) corresponds to a smaller increase in yield of new biomass. As the hydraulic loading rate increases, the hydraulic retention time in the CSTR and the sludge age of the biomass in the CSTR decreases. As a result, the amount of iron reduction completed in the reactor decreases. The increase in hydraulic loading rate coupled with the increase in organic loading rate (assumed in this exercise) increases to a. The threshold at which washout (residence time at which the rate of suspended biomass flux from the CSTR equals the rate of new biomass generation) is estimated to threaten CSTR failure is at a sludge age of approximately 51 days, as estimated by Equation 62.

By substituting the experimentally determined NO reduction kinetic expression into the CSTR mass balance, the effect of sludge age on effluent substrate concentration is illustrated. This plot indicates that at sludge ages greater than approximately 11.7 days, two values of S are possible for each sludge age. The meaning of this plot can be explained by considering two CSTRs of the same cell concentration,

same sludge age, and hydraulic loading rates, but with two different sludge ages. From Figure 59, we see that, at a sludge age of 76 days, two ethanol concentrations are possible: 0.024 g COD/liter and 1.41 g COD/liter. Figure 62 illustrates that above an ethanol concentration above 0.33 grams of COD per liter, ethanol inhibits the microbially-mediated reduction of the nitrosyl adduct of ferrous EDTA. So, at 1.41 grams per liter, ethanol will inhibit NO reduction substantially, while at a concentration of 0.024 grams of COD per liter as ethanol, NO reduction is in the first-order growth. In the reactor with the high ethanol concentration, inhibition would slow the rate of NO reduction, allowing further substrate accumulation and perpetuating inhibition. In this manner, the process performance would rapidly decline and the CSTR would fail. In contrast, the reactor with lower substrate concentration would not be inhibited; microbial reduction would proceed, resulting in a decrease in ethanol concentration and generation of new biomass which increases the overall activity of the reactor. Because the ethanol concentration will always decrease and new biomass will grow as a result of metabolic activity, instability resulting from high ethanol inhibition will not be possible.

7.2.2.3 Prototype Reactor Sludge Age. In the observed prototype bioreactor, biomass was retained in the system for longer than the hydraulic retention time. The steady-state mean cell detention time of the upflow bioreactor alone was 1446 minutes, approximately 1 day. The hydraulic retention time, based on the mean process water flow rate (0.194 liters per minute) and bioreactor volume (42.5 liters) was 219.1 minutes. Some detention of biomass was observed, with the observed sludge age 6.6 times greater than if the bioreactor were a true CSTR.   Detention of biomass resulted from the effect of gravitational settling that occurs as a result of the reactor's upflow configuration and the non-ideal hydraulic flow through the reactor. However, because the biomass was flocculent, the gravitational effect is limited and biomass readily washes from the upflow reactor. In contrast, the dense granules observed in upflow anaerobic sludge blanket reactors generally do not wash out and as a result very high sludge ages (100 days or greater) can be achieved in such reactors (Lettinga, 1987). The prototype reactor sludge age of one day is far less than that required for either NO reducing bacteria or Fe(III)EDTA reducing bacteria (11.7 days and 51.4 days, respectively). However, the process was operated in a closed loop with full process water recycle. Because the process was operated as a closed loop, much of the biomass that washed from the upflow reactor (1.01 grams per liter) returned later to the reactor in the influent (0.763 grams per liter). Based on this recycling of biomass, the observed sludge age of the entire process was calculated to be 75.9 days. In spite of washout from the reactor, biomass was maintained in the process and bioreactor destabilization and failure was avoided.

7.2.2.4 Separation of Hydraulic and Cell Detention Time. The long calculated washout threshold for Fe(III)EDTA reducers and NO reducers (51.4 days and 11.7 days, respectively) is prohibitively long to allow the feasible application of strictly suspended-growth reactors. The long required sludge age suggests that a system utilizing retained or attached biomass should perform better than a suspended growth system. Because bacteria in attached-growth systems are fixed in the reactor, their detention time is independent of hydraulic flow conditions and mean cell detention times on the order of 100 days can be obtained. Thus attached growth treatment is ideal for processes requiring large sludge ages, such as the process under consideration. Unfortunately, no attached growth was observed in the prototype reactor. Flocculent biomass was retaintained in the system by maintaining essentially 100% recycle through the system. So, while flocculent biomass readily washed out from the upflow reactor, the biomass stayed in the closed-loop process and high sluge ages were maintained.
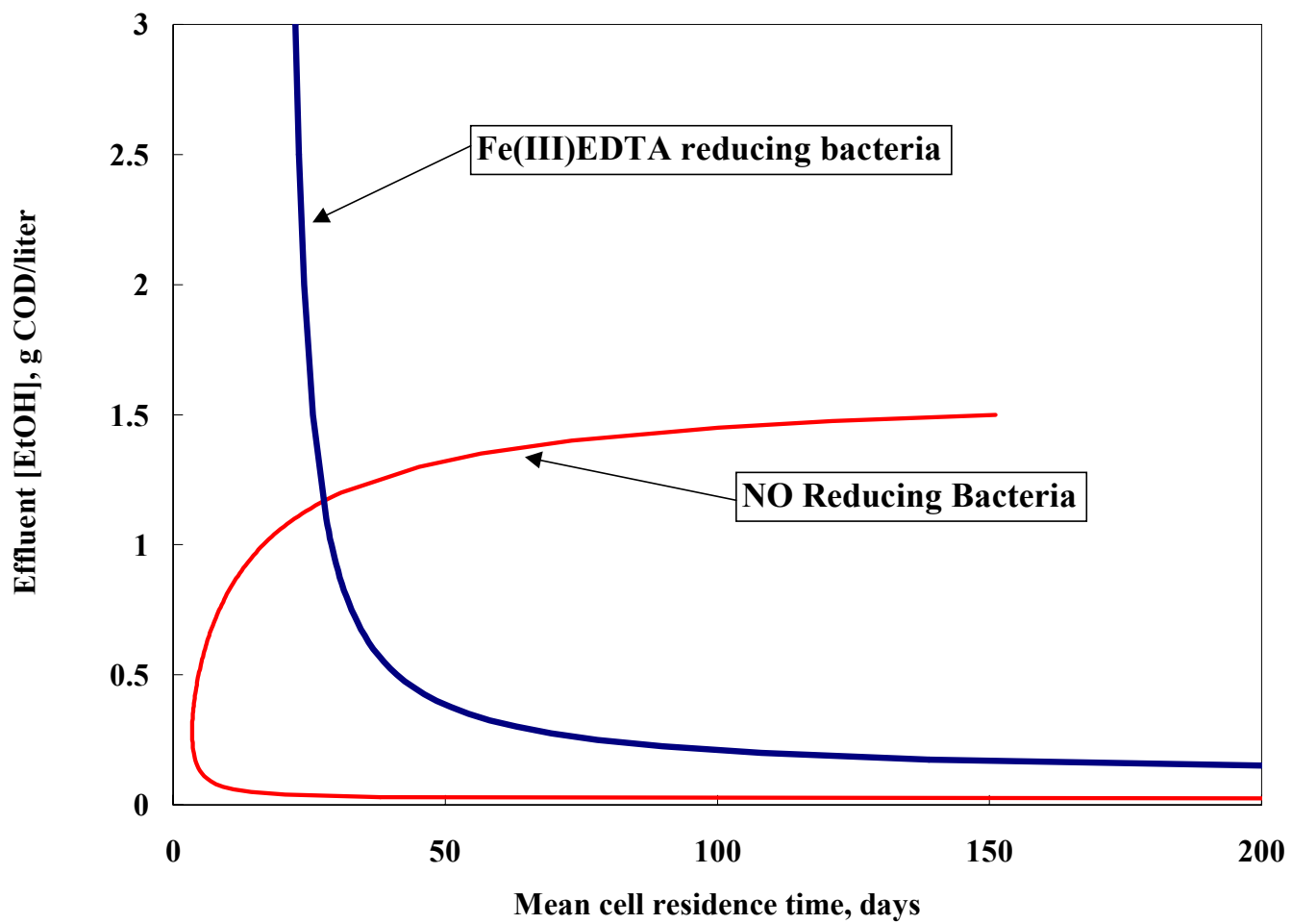
Figure 59. Calculated effluent ethanol concentration as a function of sludge age in a completely stirred tank reactor

7.2.2.5 Model of Iron Reduction in the Prototype Upflow Bioreactor. Based on the observed kinetics of ferric EDTA reduction and the observed hydrodynamics of the upflow bioreactor (Appendix A) a model of bioreactor performance was developed. The model was designed to predict the efficiency of iron reduction as a function of the concentration of COD as ethanol that is applied to the upflow bioreactor. This model assumes that the concentration of VSS in the bioreactor is the geometric mean of the biomass observed in the steady-state bioreactor (1.64 g VSS/l), as assumed in the previous mass balance consideration.   It also assumes an influent ferric EDTA concentration of 0.04 M, and that the 42.5 liter upflow reactor behaves as four tanks in series. The ethanol concentration in the upflow bioreactor is considered to decrease in each of the four conceptual CSTRs that describe the upflow reactor hydrodynamic performance. Based on the total COD consumption across the upflow bioreactor, the expected biomass yield was calculated. The modeled results are compared with conversion efficiency of a single CSTR.

Considering a single CSTR with an influent flowrate that is equal to the effluent flow rate, q, an influent concentration of C_0, and an effluent concentration of C_1, steady-state mass balance on the CSTR shows:

$$qC0 - qC1 - rV = 0 \tag{87}$$

, and given the definition of conversion

$$X = \frac{C_0 - C_1}{C_0} \tag{88}$$

$$X = \frac{rV}{C_0 q} \tag{89}$$

where r is the rate of iron reduction as a function of initial ethanol concentration, Equation 90. Considering one of the four tanks in series that make up the 42.5 liter upflow reactor, the first reactor has a volume of 10.625 liters, and the flow rate is 0.187 liters per minute. Assuming an initial ferric EDTA concentration of 0.4 M and an initial ethanol concentration of 0.18 M, it is possible to calculate the effluent concentration of Fe(III)EDTA (based on the observed batch kinetics). Based on the observed conversion of Fe(III)EDTA we can estimate the amount of ethanol consumed. Finally, based on the ethanol consumed, we can use the observed yield coefficient to estimate the mass of VSS generated in the CSTR the effluent concentrations of ethanol and ferric EDTA are then used as the influent concentration to determine the conversion across a second CSTR operated under otherwise identical conditions. This procedure was repeated for all four CSTRs in series. The total conversion of ferric EDTA was then

163

calculated from the influent of the first CSTR to the effluent of fourth CSTR, and the effluent ethanol and the mass of VSS generated was then estimated as described previously.

Model results show little difference between the CSTR and the upflow bioreactor in the efficiency with which they reduce ferric EDTA, as shown in Figures 60 and 61. These figures are an aggregate of the 4-tanks in series models run at varying initial ethanol concentrations. The primary difference between a 42.5 liter CSTR and the upflow reactor is the rate of generation of new biomass. The biomass yield of the upflow reactor is significantly lower than that of the single CSTR. This is explained by the fact that the biomass in the upflow reactor is introduced to ever decreasing concentrations of ethanol as bed height increases. The CSTR, in contrast has a constant high ethanol concentration throughout the reactor. Generation of excess biomass necessitates land filling and increases overall cost of process operation, which is undesirable.

One practical concern in operation of municipal wastewater treatment plants is shock loading of the bioreactor. As a result, municipal wastewater treatment anaerobic bioreactors are typically operated as CSTRs, as a CSTR has the ability to instantaneously dilute high organic concentrations that might otherwise inhibit microbial activity in the reactor. In the system under consideration, organic loading rate (rate at which ethanol is fed) is controlled by the operator. As a result, shock organic loading to the bioreactor in the process under consideration should not be problematic.
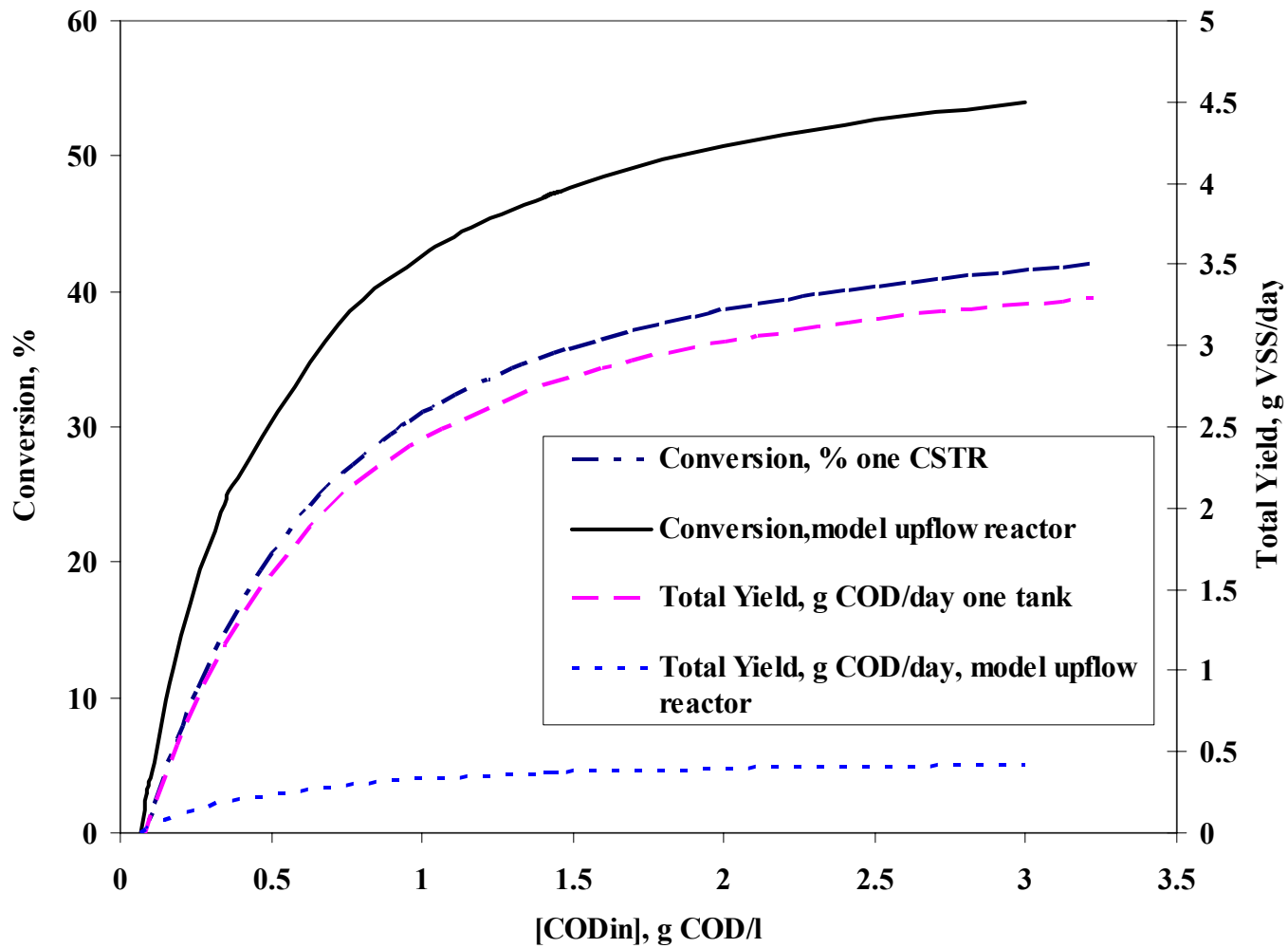
Figure 60. Conversion of ferric EDTA in a single CSTR as compared to the model upflow bioreactor, as well as the total observed yield for each as a function of influent ethanol COD.
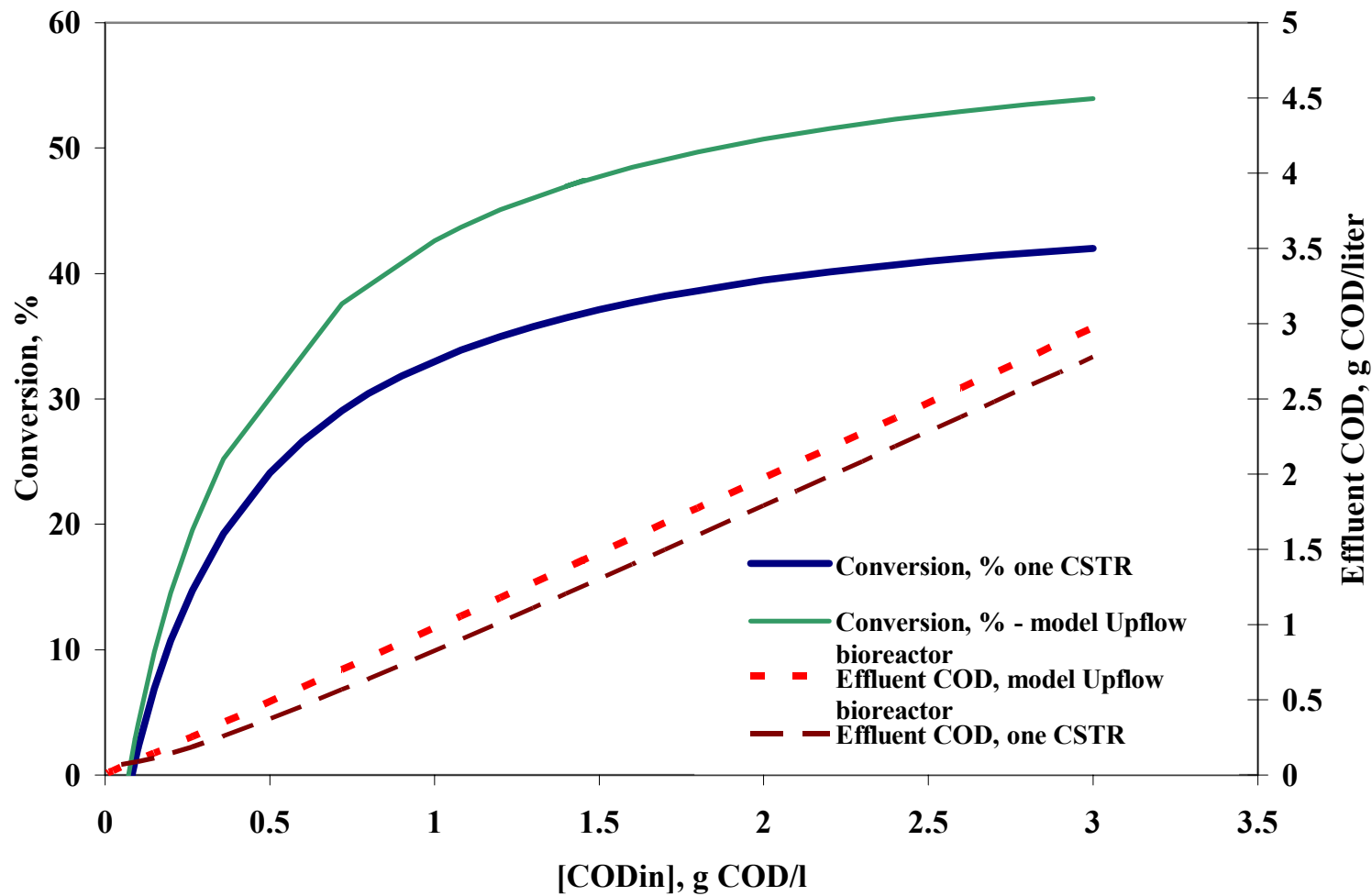
Figure 61. Conversion efficiency of the modeled upflow bioreactor and the effluent COD expected from the bioreactor versus influent ethanol COD concentrations.

7.2.3 Bioreactor/Process Configuration

Observed kinetic data, as well as observed and theoretically dictated thermodynamic limitations, have several implications for process configuration. Observed Monod kinetics of Fe(III)EDTA reduction show that reaction rate increases with increasing ethanol concentration, approaching a maximum rate, over the range of concentration considered. At the same time, it is also desirable to achieve a low COD concentration in the effluent of the bioreactor in order to prevent excessive build-up of ethanol and/or products of its oxidation and fermentation in the closed-loop process.

In contrast to Fe(III)EDTA reduction, the rate of NO reduction was found to decrease at higher concentration of ethanol. As shown in Figure 62, the concentration at which peak observed reduction of NO occurred was 138.9 mg/l ethanol (0.29 g/l COD as ethanol). At this ethanol concentration, iron reduction is only about 45 percent of the maximum utilization rate. In contrast, iron reducers achieve a reduction rate that is nearly 90% of the determined maximum rate at an ethanol concentration of 1.437 grams of ethanol per liter (3 grams per liter of COD). That these values differ from one another by more than an order of magnitude suggests that combining these two microbially-catalyzed reactions into one CSTR would be highly inefficient. Based on observed kinetics, separation of the two desired reduction reactions using two consecutive reactors with discrete substrate conditions, or a plug flow type reactor with staged substrate loading, as shown in Figure 63, should be preferable.

Even if it were desirable from a kinetic standpoint, it would not be optimal from an oxidation-reduction potential standpoint to use one CSTR in order to achieve reduction of Fe(III)EDTA and NO Fe(II)EDTA. Because a CSTR is completely mixed, contents will approach homogeneity and, in theory, constant ORP, pH, and ethanol conditions would be established throughout the bioreactor. Because the reduction of NO and the reduction of Fe(III)EDTA proceed, both theoretically and as observed qualitatively, under different ORP conditions, it is expected that a single CSTR would not allow either reduction reaction to proceed to its maximum efficiency. As a result, segregation of primary reduction reactions into two sequential steps (*i.e.*, a NO reducing reactor followed by a Fe(III)EDTA reducing reactor) is recommended.

By segregating these two reactions into two reactors in series (or a single PFR), issues related to the inhibition of NO reduction by ethanol can be avoided. The ethanol concentration in the first CSTR can be maintained at the observed ideal ethanol concentration for maximum NO reduction.

Effluent from the NO reduction reactor can be augmented with additional ethanol before being fed to the Fe(III)EDTA reducing reactor. This two-stage configuration also allows segregation of biomass streams into selected NO reducing and Fe(III)EDTA reducing streams. Recycle of biomass from

solid/liquid separation stage can then be segregated to overcome problems resulting from the differences in yield of biomass from the NO reducing stage to the Fe(III)EDTA reducing stage. Higher yield of NO reducers will require a higher wasting rate in order to maintain constant concentration of NO reducing bacteria. If both reactions were taking place in one CSTR, the concentration of Fe(III)EDTA reducing bacteria would not be sustained because wasting rate would exceed the rate of new Fe(III)EDTA reducer growth. By segregating the NO reduction from the Fe(III)EDTA reduction in two reactors, wasting rate, and therefore sludge age, can be maintained independently.

The prototype mix-tank effectively served as a CSTR bioreactor located just upstream of the upflow reactor that has been described at length. Because the process was operated as a closed loop, the mix-tank contained acetate that had accumulated in the process water as a result of partial oxidation of ethanol in the bioreactor. The acetate in the mix tank was utilized, to some extent by bacteria present in the mix-tank to achieve partial denitrification of the scrubber solution. The degree to which reduction took place in the mix-tank could not be determined with the collected process monitoring data. In particular, the mix-tank was not air tight, and the volume and composition of biogas that was generated in the mix-tank could not be quantified. However, by making some simplifying assumptions, it is estimated that 74% of biological NO reduction that took place outside of the upflow bioreactor, and suggests that cultivated NO reducers may prefer acetate to ethanol. By looking at the difference in acetate concentration measured in the bioreactor effluent as compared with the concentration of acetate just prior to the bioreactor, and assuming that all ethanol is at least partially oxidized in the upflow reactor, the approximate change in acetate concentration in the upflow reactor effluent to the mix-tank effluent was determined. This is described in the following consideration of prototype process mass balance for approximation of process biomass properties.

Figure 62 shows that substrate inhibition of NO reducing bacteria was observed to occur at ethanol concentrations greater than 0.33 grams of COD per liter. At ethanol concentrations in the stable region below the onset of inhibition, incremental increase in ethanol concentration leads to increased activity and cell growth. This activity in turn decreases the ethanol concentration, bringing the process back into balance. At ethanol concentrations in the unstable region, incremental increase in ethanol concentration results in a decrease in activity and a decrease in cell concentration, leading to process failure. Consequently, the ethanol concentration in a NO reducing bioreactor should be maintained below 0.33 grams of COD per liter in order to maintain process stability.

In the prototype reactor, ethanol was injected at one point, just upstream of the upflow bioreactor inlet. Based on the observed inhibition of NO reduction with ethanol and the observed establishment of acetoclastic NO reducers in the mix tank (after NO loading and ethanol addition) the configuration that is described in the following paragraph is proposed.

Ethanol is injected at the upflow reactor inlet, which is predominated by iron reducers. By the upflow reactor effluent, most of the injected ethanol is destroyed, but acetate generated as a result of ethanol oxidation (Equation 58) is released in the effluent. Following recycling of the process water to the scrubber for NO loading, the process water continues to a bioreactor where acetoclastic NO reducers consume acetate as their primary electron donor, uninhibited by ethanol concentrations greater than 0.33 grams of COD per liter as ethanol. Effluent from this reactor travels back to the upflow reactor, where additional ethanol is loaded and Fe(III)EDTA reduction proceeds. This proposed configuration is illustrated in Figure 63.

One method of addressing this matter is to load ethanol to the bioreactor at two points, based on the location of predominating populations. At the point where NO reducing bacteria predominate, ethanol would be injected at concentrations just below the inhibition threshold of 0.33 grams of COD per liter. Downstream of the NO reducing bacteria where Fe(III)EDTA reducing bacteria predominate, a higher concentration could be applied at a second injection point. This would allow ethanol to be loaded at concentrations that would maximize the rate of both reactions. The proposed configuration with two injection ports is shown in Figure 63. Phased ethanol loading addresses the limitations of differences in maximum reduction rate, but can not address the limitations imposed by the differences in bacterial populations sludge age for the process as operated in series.
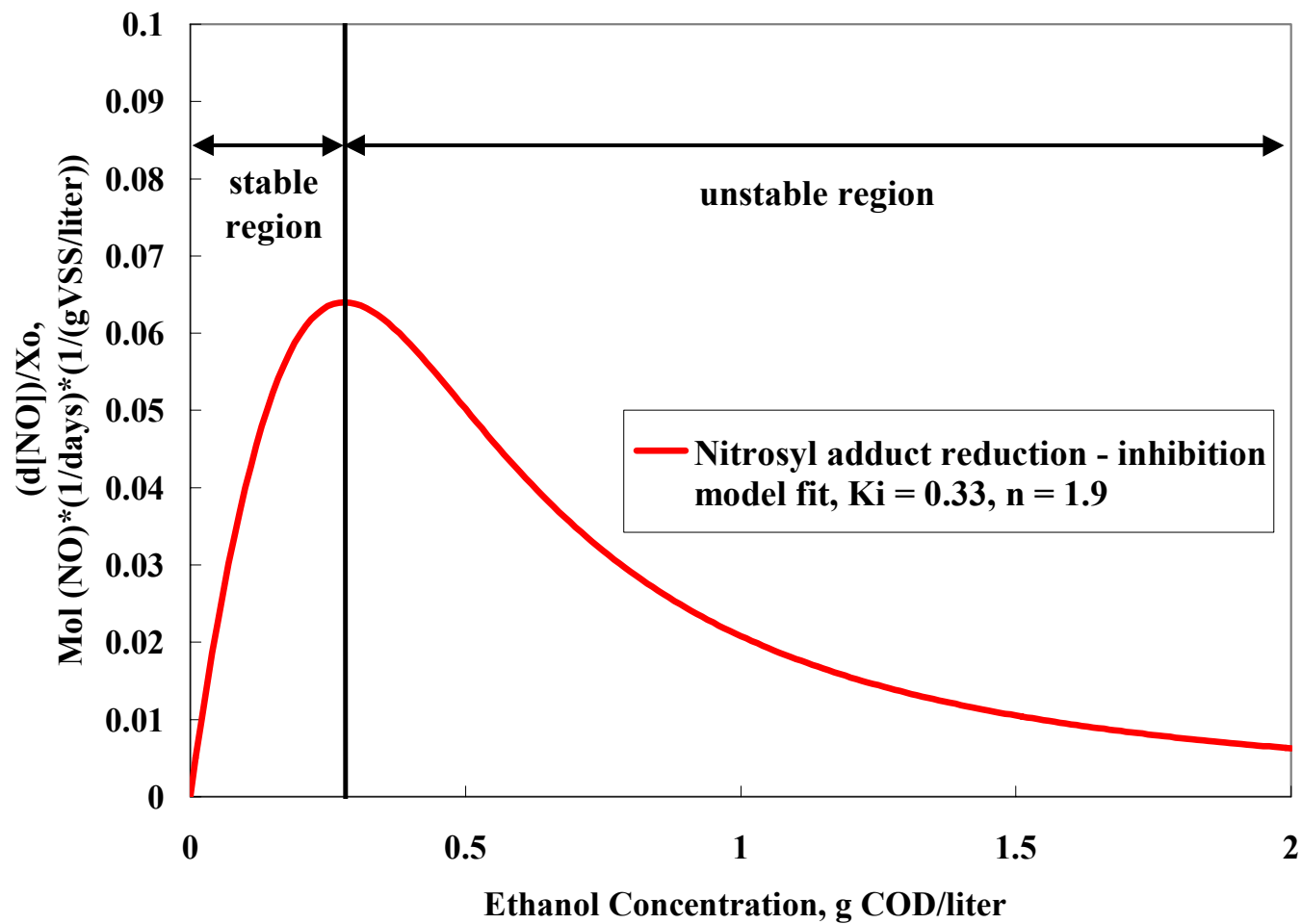
Figure 62. Substrate inhibition causes instability at ethanol concentrations greater than 0.33 g COD/liter
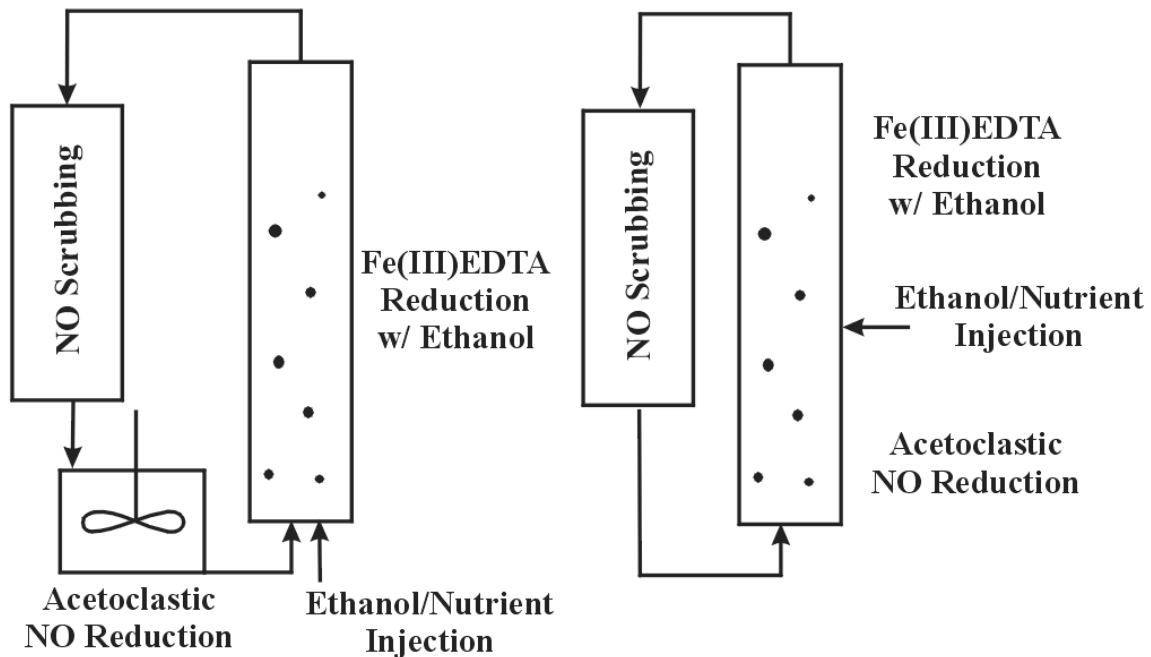
Figure 63. Two potential configurations that accommodate ethanol inhibition of NO reduction.

In summary, the region of operation that is acceptable for process operation is where ethanol concentration is below inhibition and sludge age is below washout for both bacterial populations. Figure 63 illustrates this region for both NO and Fe(III)EDTA reducers. The region of overlap is representative of the reactor conditions that are acceptable for both populations. In this region of overlap, neither population functions at the highest possible efficiency. By applying one or both of the proposed process modifications, increased process efficiency will be realized.
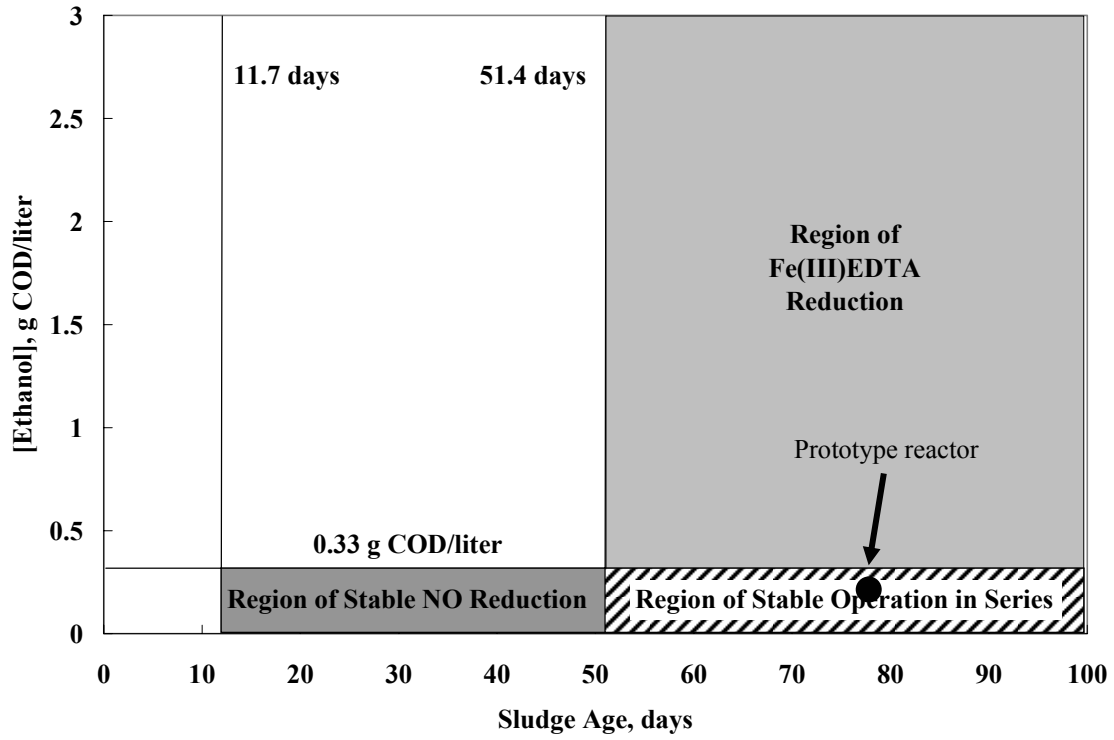
Figure 64. Sludge age and ethanol conditions under which biomass stability is maintained

8.0 SUMMARY, CONCLUSIONS, AND RECOMMENDATIONS

8.1 SUMMARY AND CONCLUSIONS

8.1.1 Summary of Findings

In the research described herein, a prototype apparatus was configured and operated in order to evaluate the efficacy of a process that integrates the absorption of nitric oxide in an aqueous solution of ferrous EDTA with microbially-mediated treatment and regeneration of spent scrubber solution. In addition to operation of the continuous-flow, closed-loop prototype process, a series of batch reactor experiments were conducted to evaluate the kinetics of microbially-catalyzed reduction of the nitrosyl adduct of ferrous EDTA and microbially-catalyzed reduction of oxidized ferric EDTA.

The prototype process was initially inoculated with anoxic denitrifying and strictly anaerobic biomass from two municipal wastewater treatment plants. After successful cultivation of biomass in the prototype bioreactor using nitrate and ferric EDTA as the primary electron acceptors and ethanol as the electron donoer, the prototype process was modified to allow the bioreactor to be loaded with nitric oxide present as the nitrosyl adduct of ferrous EDTA in place of nitrate. The process was operated in this manner for 107 days. After process modification, the process was upset for a period of 25 days during which excessive organic loading caused the process water ORP to drop to –220 mV versus a Ag/AgCl reference electrode. During this period, strictly anaerobic conditions predominated and sulfate reduction and methanogenesis were observed. Process balance was then re-established and a period of steady-state was observed for over seventy days. NO reduction was observed to proceed in the range of –75 to –120 mV (as measured Ag/AgCl reference electrode). Ferric EDTA reduction was observed to proceed in the range of –110 to –140 mV (as measured Ag/AgCl reference electrode). Sulfate reduction and methanogenesis began below –140 mV with a strong reducing environment observed in the range of –220 to –290 mV (as measured Ag/AgCl reference electrode).

The period of prototype bioreactor steady-state operation was identified by consistent performance of several key indicators of bioreactor loading and treatment performance. During this period, the molar loading rate of ethanol was maintained consistently near 0.1612 moles per day. The NO loading rate was held at 0.1937 moles per day. A mean scrubber water NO absorption efficiency of 97.9% was maintained over the period of steady state operation. The rate at which diatomic nitrogen was generated in the bioreactor was consistently at 0.02406 moles per day, as calculated from biogas production of 0.6686 liters per day with a consistent N_2 partial pressure of 0.91 atmospheres. The molar ratio of nitrogen gas generated in the bioreactor to the NO absorbed in the scrubber is far below the one to one ratio described by the stoichiometry of Equation 5, with 74 percent of the reduction of the nitrosyl adduct unaccounted for and likely carried out in the mix tank upstream of the bioreactor. Finally, the consumption of acid to counteract alkalinity generated as a result of microbially-catalyzed reduction during steady-state operation was 0.3301 moles of acid equivalents per day. Based on stoichiometry of observed reduction reactions, 73.3% of this acid equivalent could be accounted for.

Based on batch experimentation using biomass extracted from the prototype process, the microbially-catalyzed reduction of ferric EDTA proceeded according to the Monod kinetic expression over the range of initial ethanol concentration considered to be reasonable for practical application. Based on these batch tests, a half velocity constant of 0.3367 grams of COD as ethanol/liter, and a maximum specific utilization rate of 0.09091 mol/liter of Fe(III)EDTA*(g VSS/l)day^{-1} were determined. In addition, batch analyses of Fe(III)EDTA reducers showed an observed yield coefficient of 0.055 g VSS/g COD. Finally, batch tests conducted in the absence of ethanol showed an endogenous decay term of 0.0175 day^{-1}. Based on batch kinetic analyses, the rate of microbially-catalyzed Fe(III)EDTA reduction is described by Equation 88.

$$\frac{d(Fe(III)EDTA)}{dt} = \frac{0.09091\, moles\, Fe(III)EDTA/l * [EtOH] * X}{(0.3367\, g\, COD/l + [EtOH])} - 0.0175/day * X \tag{88}$$

Batch reactor kinetic tests showed strong inhibition of the microbially-catalyzed reduction of the nitrosyl adduct of ferrous EDTA at initial ethanol concentrations above a threshold concentration of 0.33 grams of COD as ethanol per liter. Based on batch analyses, a Monod half-velocity constant, K_S, of 0.39 g COD/l, a maximum specific utilization rate, k of 0.2 mol/liter [NO*Fe(II)EDTA^{2-}](g VSS/l)day^{-1}, and an inhibition constant, K_I of 0.33 g COD/l were determined. In addition to these values, batch experiments also showed a mean observed yield of 0.259 g VSS/g COD, and tests conducted in the absence of ethanol showed an endogenous decay coefficient of 0.0569 day^{-1}. Applying these data to Equation 82 gives the expression describing the observed performance of NO reducing bacteria as a function of ethanol concentration, shown in Equation 89.

$$\frac{d\left(NO \bullet Fe(II)EDTA\right)}{dt} = \frac{0.2\ moles\ NO \bullet Fe(II)EDTA/l * X}{1 + 0.39\ g\ COD/[ETOH] + \left([ETOH]/0.33\ g\ COD/l\right)^{1.9}} - 0.0569/day * X \qquad (89)$$

This expression describes the inhibition of NO reduction activity at ethanol concentration greater than 0.33 grams of COD/liter. Such conditions will result in instability and process failure in NO reducing systems.

8.1.2 Conclusions and Significance of Findings

The experiments described herein provide a theoretical and practical basis for establishing a full-scale bioreactor for the removal of NO from spent NO_X process water. The previously unreported observation that ethanol concentrations greater than 0.33 grams of COD/liter inhibit NO reduction rates will dramatically impact future process design. In addition, the novel observation that NO reducing and ferric EDTA reducing bacteria require long sludge ages suggests the use of attached growth in these bioreactors. Moreover, the differences in biomass detention time suggest a two independent loop process in which NO reduction and Fe(III)EDTA reduction are largely isolated from one another. The further development of process control and kinetic analysis in prototype and full-scale bioreactors is necessary to more accurately categorize process design (parameters, constraints, preferred environmental conditions)

As noted by Kumaraswamy and others (2004), the microbially-mediated reduction of ferric iron chelated to the EDTA ligand has not been described in literature. Doubt has been raised as to whether or not these reactions proceed, and no kinetic evalutation of that microbially-mediated reduction is reported in the available literature. In contrast, experiments described herein provide evidence that the microbially-mediated reduction of ferric EDTA chelate does proceed under anoxic and circum-neutral conditions, and that ethanol is consumed as the primary electron donor/carbon source in this microbially-mediated reduction. Finally, the kinetics of ferric EDTA reduction was shown to behave according to the Monod model with ethanol limited growth.

Reduction of the nitrosyl adduct of ferrous EDTA was also shown to proceed by microbially-catalyzed reaction under circum-neutral anoxic conditions using ethanol as the primary electron donor/carbon source. However, observation of NO reduction inhibition at ethanol concentrations greater than 0.33 grams of COD per liter has implications for process design and operation. This suggests that ethanol concentration should be maintained below 0.33 grams per liter in NO reducing zones of the process in order to prevent inhibition and system instability.

A prototype process for closed-loop scrubbing of NO_X, treatment, and regeneration of spent process water was successfully designed, configured and operated for 150 days. Biogas production and

composition provide a useful indication of bioreactor activity – indicating both the type of reduction reactions occurring in the bioreactor and the degree to which they proceed. Acid equivalent addition to maintain process water pH can be used to assess overall bioreactor microbial activity.

8.2 RECOMMENDATIONS FOR FUTURE INVESTIGATION

Through the course of the current investigation, interesting questions and potentially fruitful research avenues came to light. Because these issues were outside of the scope of the current investigation, they were not pursued. Following are recommended areas that were identified for further research related to this topic.

Use of alternate organic waste streams as primary electron donor/carbon source in the reduction of the nitrosyl adduct of Ferrous EDTA and reduction of ferric EDTA should be investigated. This would allow the concurrent treatment of an organic waste stream while mitigating the cost of ethanol for reduction of oxidized species in the process water described herein.

Performance of the prototype process suggested that acetate plays a significant role as an electron donor in the microbially-mediated reduction of the nitrosyl adduct of ferrous EDTA. It is believed that similar of the applicability acetate as primary electron donor/carbon source in the reduction of the nitrosyl adduct of Ferrous EDTA and reduction of ferric EDTA would be productive.

The fate of dissolved mercury in the biologically-active process water should be investigated. Specifically, there is interest in the potential to precipitation of dissolved mercury as a metal sulfide, and also concern about the potential for mercury methylation in the biologically active anaerobic process water.

Chelating agents other than EDTA should be evaluated for possible application in the described process. It is known that the number of ligand active sites and overall binding strength affect the rate, strength and reversibility of the binding of NO. By tuning these properties, more efficient scrubbing and biological treatment might be possible. A related investigation might consider the rate of oxidation of the chalete molecule in the biologically active process water.

In the absence of attached growth, technology such as membrane filtration could serve as a means of preventing wash-out of floccuent biomass. The high sludge ages required of NO and Fe (III) reducing systems obviates the need to maintain long cell retention times. In the case of the prototype process, this was achieved by maintaining a near 100% recycle rate to the upflow reactor. The flocculent nature of the

Fe(III)EDTA reducing and NO reducing bacteria prevent the establishment of attached or granular biomass populations that would allow separation of hydraulic and cell residence.

Future investigations should consider the role that sulfide in solution has on reduction of ferric EDTA and the nitrosyl adduct of ferrous EDTA. Unlike batch experiments, it was not possible to remove sulfide from the prototype process. During steady-state operation, an estimated 6.7% of sulfur introduced to the system as sulfate was reduced to sulfide and precipitated as iron monosulfide. It is possible that sulfide in process water contributes to regeneration of scrubber water by chemical reduction of ferric EDTA.

Finally, for many industrial waste-gas streams, it would be preferable to combine the scrubbing of NO_X with a traditional SO_X scrubbing process. However, absorption of SO_2 into solution adds a significant acid equivalent load to the process. The subsequent decrease in process water pH would require pH adjustment to near neutral levels before introduction to the biological treatment step. Laboratory-scale testing of a process that combines scrubbing of SO_X and NO_X would help to address technical hurdles related to such a combined process.

PROTOTYPE UASB TRACER STUDY

Hydrodynamic Considerations

In the absence of reactor wall friction and under ideal flow conditions, a UASB would be expected to operate under plug flow-type conditions, meaning that influent will travel axially as a "plug" of water through the reactor with no radial variation in concentration. However, in application, reactors never function under ideal hydrodynamic conditions, and an attempt should be made to determine the extent to which a particular reactor's flow pattern deviates from that of an ideal reactor.

Analysis of the hydrodynamic characteristics in the prototype reactor under consideration will be required in order to predict the degree to which this particular reactor will deviate from ideal plug flow conditions. Indications that the reactor will not exhibit strong plug flow characteristics may be beneficial for granule formation. A report by Liu and Tay (2002) reports the role of hydrodynamic shear force and stochastic particle movement (manipulated in a USB by upflow velocity) in enhancement of the microbial granulation process.

A preliminary analysis of the flow pattern characteristics was carried out on the prototype scale USB reactor in use for this investigation. Because of the difficulty of applying a clean pulse input to the reactor (an issue of reactor configuration) a positive step input study was conducted on the water filled reactor. Procedure/results of the step input tracer study on the water filled USB reactor, and further discussion are presented in the Hypotheses, Research Methods, and Experimental Design section.

Hydrodynamic characteristics of the prototype scale UASB reactor

The prototype UASB reactor has been demonstrated to exhibit hydrodynamic properties that can be described as performing as a non-ideal plug flow reactor. That is to say that a "slug" of water will travel through the reactor with some degree of axial dispersion and mixing. This dispersion can be

explained as resulting from such factors as temperature gradient diffusion, flow channeling and dead zones.

A preliminary analysis of the flow pattern characteristics was carried out on the prototype scale USB reactor in use for this investigation. Because of the difficulty of applying a clean pulse input to the reactor (an issue of reactor configuration) a positive step input study was conducted on the reactor when filled initially only with water. Procedure/results of the step input tracer study on the water filled UASB reactor, and further discussion are presented below.

Water flow rate through the reactor was recorded at several points during the tracer study, and was measured to be 0.3 liters per minute. At this flow rate, and given a reactor volume of 42.5 liters, the ideal hydraulic residence time is 141.67 minutes.

Results of the step input tracer study describe the reactor as behaving similarly to four continuously stirred reactors in series. Reasons for deviation from plug flow may include:

- Temperature gradient diffusion
- Channeling/dead zones
- Poor distribution of flow across cross sectional area
- Turbulence resulting from gas formation in the reactor

This analysis of reactor flow was conducted on an empty reactor. Presence of biomass will change both mean residence time of liquid in the reactor and flow characteristics. If possible, a second tracer study will be carried out when the bioreactor is loaded with biomass and operating at steady state. This data would provide more accurate assessment of reactor flow characteristics.

Tracer Study - Step Input

In a step input, a constant rate of tracer addition is initiated at time $t = 0$, with no tracer injected before $t = 0$, or:

$$C_0(t) = 0 \qquad\qquad t < 0$$
$$C_0(t) = \text{constant} \quad t \geq 0$$

The concentration of tracer in the influent is maintained at the same concentration until the concentration in the effluent is the same as the influent concentration. Because the inlet tracer concentration is constant with respect to time, we can consider it outside the integral, such that:

$$C_{out} = C_0 \int_0^t E(t')dt'$$

Dividing by C_0, gives

$$\left[\frac{C_{out}}{C_0}\right]_{step} = \int_0^t E(t')dt' = F(t)$$

This expression is differentiated to obtain the residence time distribution function E(t):

$$E(t) = \frac{d}{dt}\left[\frac{C(t)}{C_0}\right]_{step}$$

The response curve for a step input tracer study is defined as the concentration of tracer in the effluent as a function of time and for a positive step input will be of the same shape of the cumulative distribution function. The cumulative distribution function is a normalized response to the positive step input.

Plug flow response to step input:
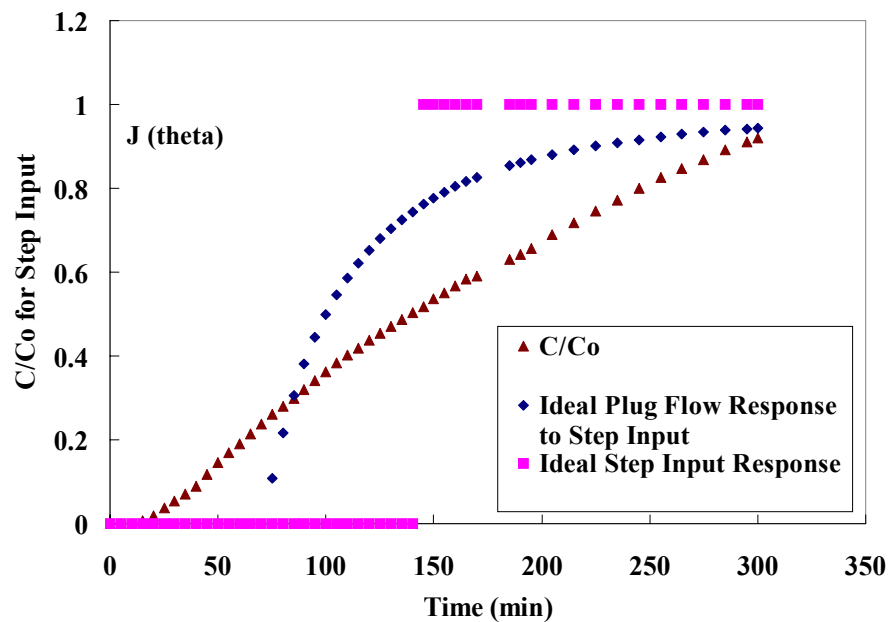
Figure A1. Prototype UASB reactor step input tracer response compared with ideal and ideal plug flow responses

N-Tanks in Series Equation:

$$\left(\frac{C_n}{C_0}\right)_{STEP} = J_n(\theta) = 1 - e^{-n\left(\theta/\theta_t\right)} \frac{1}{(i-1)!}\left(\frac{n\theta}{\overline{\theta_t}}\right)^{i-1}$$
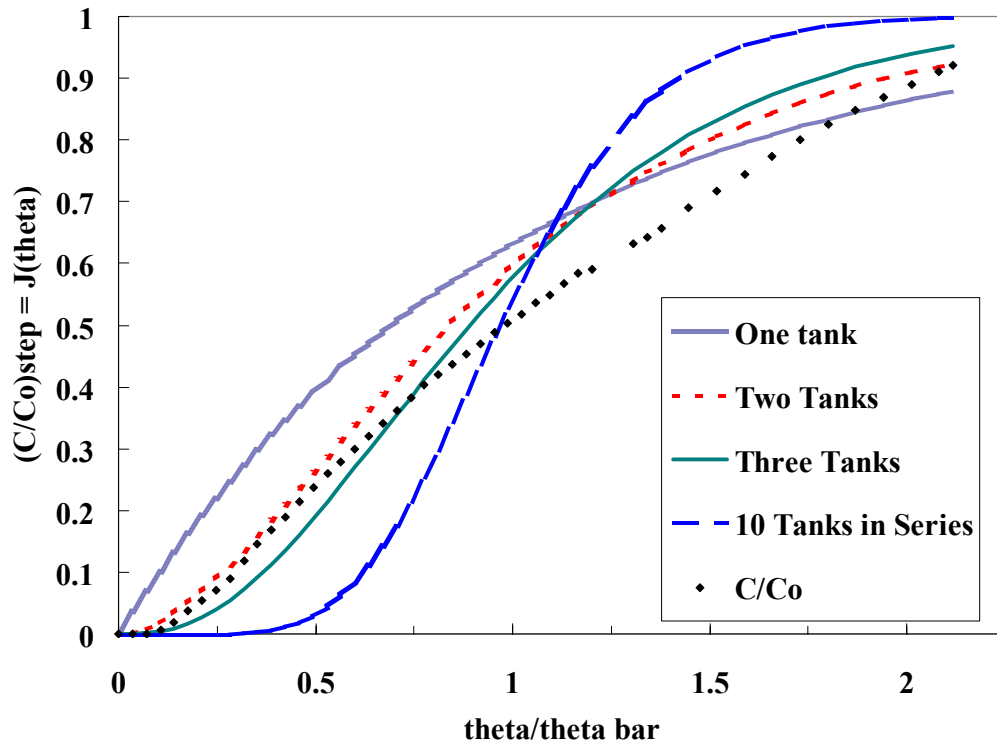
Figure A2. USB reactor step input response compared with various N-tanks in series responses

Mean Cell Residence Time can be calculated from the integral:

$$t_m = \int_0^\infty t\, E(t)\, dt$$

Graphical integration of the plot of t vs. (t*E(t)) using Simpson's three eighths rule gives a mean cell residence time of 189.8 minutes.

Variance (*i.e.* the square of the standard deviation) can then be calculated by the integral:

$$\sigma^2 = \int_0^\infty (t - t_m)^2 \times E(t)\, dt$$

Graphical integration of the plot of t vs. $(E(t)*(t-t_m)^2)$ using Simpson's three eighths rule gives a variance of 8867.7 minutes^2.

The number of tanks in series is calculated by:

$$n = \frac{t_m}{\sigma^2}$$

and was found to be 4.06. The 42.5 liter USB reactor will be considered to perform as four 10.625 liter continuously stirred tanks in series. This value only has meaning as an approximation of hydrodynamic dispersion. With appropriate kinetic data, reactor conversion efficiency can be calculated.

The indicator dye used to conduct the tracer study was methyl orange. The following figure shows the standard curve plot of methyl orange concentration versus absorbance response at a wavelength of 463 nm. Correlation in the region used for analysis was linear with a correlation coefficient of 0.9992.
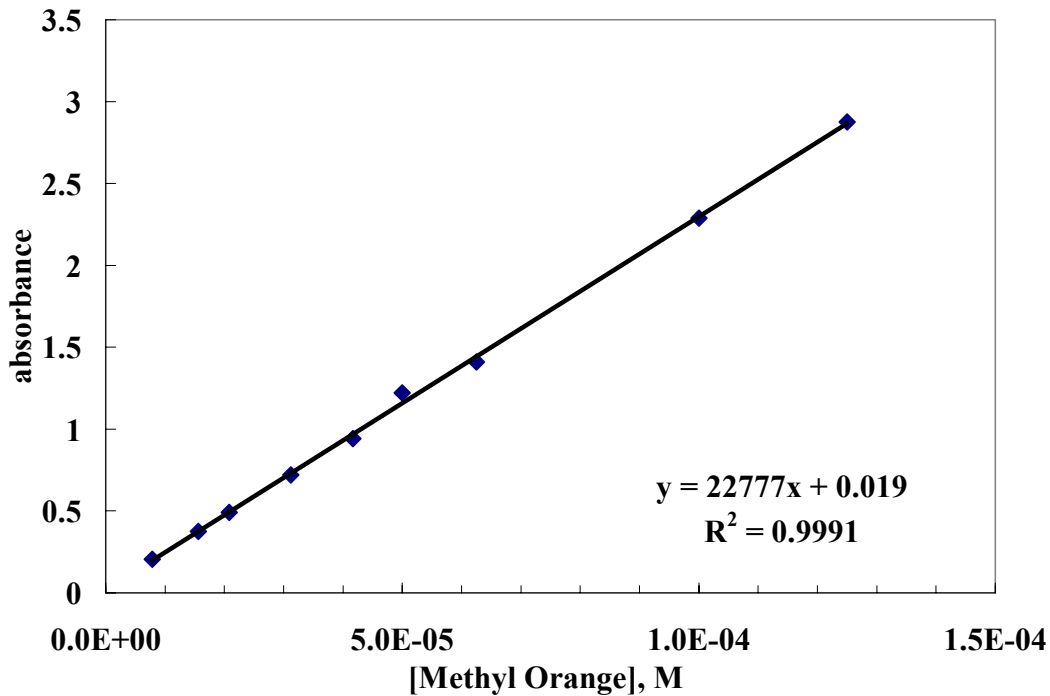
Figure A3. Methyl orange tracer standard curve comparison of absorbance and dye concentration

A Beckman DU 640 Spectrophotometer will be used to conduct spectrophotometric determinations. This instrument is a UV/V is scanning spectrometer, and performs a traditional wavelength scan by measuring with a single beam/single photodiode detector, taking readings at discrete points throughout the spectral range.

SATURATION OF A 0.45 MOLAR Fe(II)EDTA SOLUTION

A 100 ml solution of 0.45 M ferrous EDTA was sparged with 1019 ppm NO gas balanced with nitrogen gas at a gas flow rate of 0.63 liters per minute. The experiment was conducted at standard temperature and pressure. Effluent gas composition was logged at 10 second intervals. A polynomial was fit to the resulting curve and are beneath the curve calculated by numerical integration.
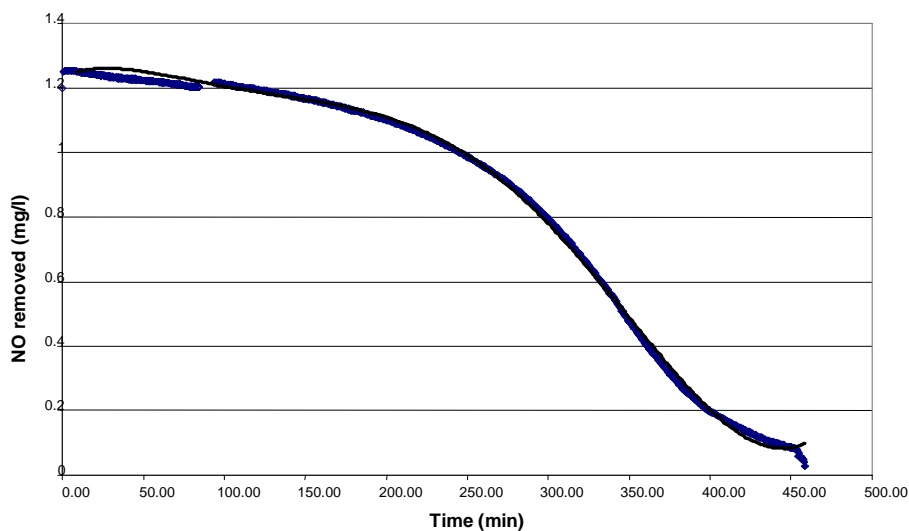
Figure B1. Saturation Curve - 0.045 M ferrous EDTA with 1019 PPM nitric oxide in nitrogen gas

A polynomial was fit to the NO_X absorption curve, and is defined by the expression shown below, with a correlation coefficient (R^2) of 0.9992.

$$y = -1E^{-15}x^6 + 2E^{-12}x^5 - 1E^{-09}x^4 + 4E^{-07}x^3 - 4E^{-05}x^2 + 0.0012x + 1.2356$$

The integral of that fit expression is shown below.

$$y = -1E^{-15}/7 \ x^7 + 2E^{-12}/6 \ x^6 - 1E^{-09}/5 \ x^5 + 4E^{-07}/4 \ x^4 - 4E^{-05}/3 \ x^3 + 0.0012/2 \ x^2 + 1.2356 \ x$$

which is evaluated over the period of data collection (from 0 to 448 min). This results in an area of 2071.53323326 (mg/l)×min.

This area is then multiplied by the gas flow rate (0.630 l/min) to get total NO absorbed, 1305.35 mg NO loaded to 0.1 liter of solution or 13.0535 grams of NO per liter of 0.45 molar Fe(II)EDTA solution. The molecular weight of NO is 30 grams per mole, so this corresponds to a molar loading of 0.435 moles of NO per liter.

APPENDIX C

[NO•Fe(II)EDTA^{2-}] SCRUBBER DESIGN EQUATION

As mentioned in Chapter 2, Dravo Lime Corporation (1992) developed a semi-empirical equation to determine the dependence of NO removal on absorber operating conditions in order to understand what is necessary to remove maximum NO_X at reasonable capitol and operation costs. A mathematical model was developed to determine the dependence of NO removal on flue gas velocity, absorber liquid rate, ferrous EDTA concentration, absorber length, and gas-liquid contact time. The equation developed by Dravo researchers (Li et al., 1996) is as follows:

$$NTU = -\ln(1- (\% \text{ removal}/100)) = (k_2 [Fe^{++}] D_{NO})^{1/2} / (H/p_T) *(a*Z)/(p_M*v),$$

where:
NTU = NO removal as number of transfer units (dimensionless)
K_2 = reaction rate constant for second=order reaction between dissolved (but not
    yet reacted) NO and ferrous EDTA = 2.2445 x 10^{12} ft^3/lb mole-sec @ 122°F
$[Fe^{++}]$ = ferrous EDTA concentration in absorber liquid, mM 6.2362 *10^{-5} = lb
    mole/ft^3
D_{NO} = diffusivity of dissolved NO in absorber liquid = 4.4 x 10^{-8} ft^2/sec @ 122°F
A = gas-liquid interfacial area per volume of contact zone, ft^2/ft^3
Z = length of gas-liquid contact zone, ft
p_M = molar density of flue gas = 0.00235 lb-moles/ft^3 @ 122 °F
v = flue gas velocity in absorber, ft/sec
p_T = total pressure, 1 atm
H = Henry's Law constant for NO in water = 11383.25 ft3-atm/(lb-mole) @ 122°F
    (if flue gas is saturated with water vapor, the effective solubility of NO in
    water is 12813.56 ft^3/lb-mole)

At low ferrous EDTA concentrations with moderate to high absorber gas velocities (*eg.*, > 4 feet/sec), NO absorption has been found to be liquid film resistance-limited.

As described above, dimensionless number of transfer units can easily be converted to percent removal by the conversion

NTU = -ln(1- (% removal /100))

Illustrated below are plots of percent removal vs. number of transfer units. The second focuses on the near-linear portion between 0 and 40 % removal.

Conversion of NTU to Percent Removal
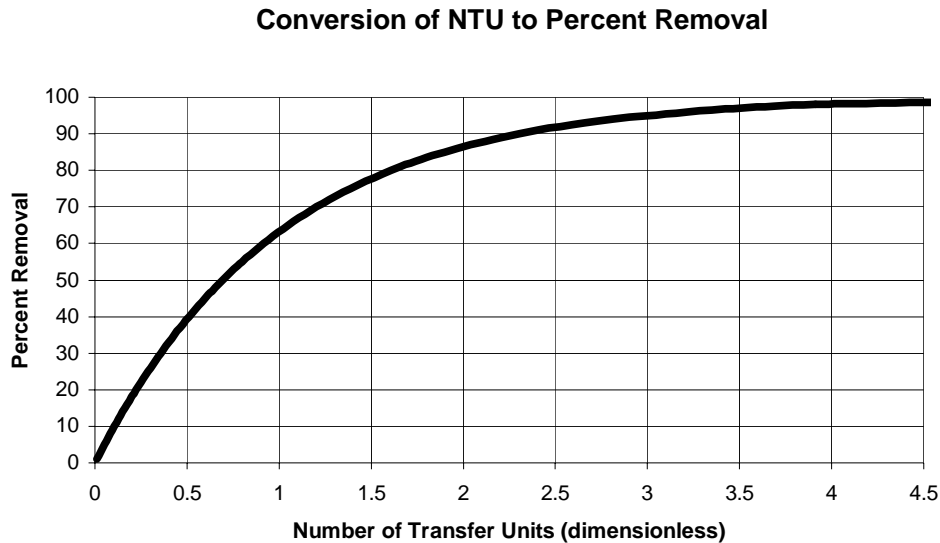
Figure C1. Plot showing the correlation between number of transfer units and percent removal

Derivation of Model Equation for NOX removal

Similar to the Dravo equation described above, researchers at Argonne National Laboratory (Li et al., 1996) derived a mathematical model describing dependence of NO_X removal on absorber flue-gas flow rate and liquor flow rate, Fe(II) EDTA concentration, absorber length, and gas-liquid interfacial area. They began their derivation by listing the four types of reactions involved:

- Complexation
- Regeneration
- Oxidation
- Reduction

Complexation

Fe(II)*EDTA + NO $\leftrightarrow$ Fe(II)EDTA* NO
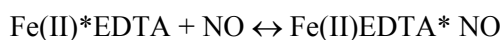
Regeneration

Removal of nitrosyl oxide from Fe(II)*EDTA complex so that it can be reused for NO removal from gas

Fe(II)*EDTA*NO + reactant ↔ Fe(II)*EDTA

Oxidation

In the presence of an oxidizer (like flue gas oxygen) Fe(II) in the chelate is oxidized to Fe(III). Fe(III)EDTA is not effective at removing NO from gas. The general oxidation reaction can be expressed as:

Fe(II)EDTA + oxidizer → Fe(III)EDTA
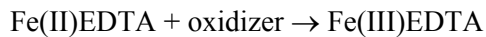
Using some reducing agent, Fe(III) in Fe(III)*EDTA + oxidized reducer

Assumption:

When considering important factors involved in mass transfer of NO from gas to liquid phase, it is generally considered that the reaction of NO in solution with Fe(II)*EDTA is the slowest step in the process. For that reason, the reaction

Fe(II)*EDTA + NO → Fe(II)*EDTA*NO
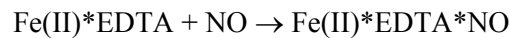
Is the only one considered in mass transfer modeling. It is also assumed that most of the NO in flue gas is present as NO, and concentrations of other nitrogen oxides are negligible. Typically, NO makes up about 90-95% of total NO_X concentration in the flue gas, so this assumption is acceptable.

Several studies have found the rate of the previous reaction to be first-order with respect to [NO] and first order with respect to Fe(II)*EDTA.

$$r_{NO} \; k C_{Fe(II)EDTA} C_{NO_L}$$

where:

K = reaction rate constant (L/mole*hr)

$r_{NO} =$ rate of NO removal (mole/l*hr)

$C_{Fe(II)EDTA}$ = concentration of ferrous EDTA (mole/L)

C_{NO} = concentration of NO in solution (mole/L)

Mass Transfer

In the next step, this reaction rate is combined with the mass transfer in the boundary between gas and liquid phases in the scrubbing tower.

Assumption:

Because gas velocity is considerably higher than liquid velocity, it is assumed that the thickness of the model gas film and therefore the gas film NO concentration gradient will be negligible when compared with liquid phase film thickness and concentration gradient. It is also assumed that the concentration of free $NO_{aqueous}$ in the bulk liquid is negligible compared to that at the gas liquid interface, and that the reaction in question occurs almost entirely within the liquid film. The other previously described reactions do not involve NO and therefore can occur anywhere in the liquid phase (bulk or film).

Mass balance for NO and Fe(II)*EDTA in the liquid film (δ_L):

$$D_{NO} \frac{d^2 C_{NO}}{dX^2} - r_{NO} = 0 , \quad 0 < X < \delta_L$$

and

$$D_{Fe^{2+}} \frac{d^2 C_{Fe(II)EDTA}}{dX^2} - r_{NO} = 0 , \quad 0 < X < \delta_L$$

Because of the low solubility of NO in water, $C_{Fe(II)EDTA} \gg C_{NO}$ and Fe(II) EDTA depletion resulting from reaction with NO will be low.

$$\frac{d^2 C_{Fe(II)EDTA}}{dX^2} = 0 , \quad 0 < X < \delta_L$$

$$\iint \frac{d^2 C_{Fe(II)EDTA}}{dX^2} = 0$$

$$C_{Fe(II)EDTA} = a\,X + b$$

Fe(II)EDTA is non-volatile, so at the gas/liquid interface the change in $C_{Fe(II)EDTA}$ with respect to X is 0, or

$$dC_{Fe(II)EDTA}\big/dX = 0, \quad at\ X = 0$$

which implies that:

$$C_{Fe(II)EDTA} = 0\,X + b$$

$$C_{Fe(II)EDTA} = b$$

so,

$$C_{Fe(II)EDTA} = C_{Fe(II)EDTA_{bulk}}$$

Because the change in $C_{Fe(II)EDTA}$ is considered to be negligible perpendicular to the gas/liquid interface, the mass balance for NO in liquid becomes:

$$D_{NO}\frac{d^2 C_{NO}}{d\,X^2} - KC_{Fe(II)EDTA}C_{NO} = 0, \quad 0 < X < \delta_L$$

$$C_{NO}\left(X=0\right) = C_{NO}^{int\,erface} = \frac{P_{NO}}{H}, \quad C_{NO}\left(X = \delta_L\right) \rightarrow 0$$

where:

P_{NO} = partial pressure of NO in bulk gas phase

H = Henry's Law Constant for NO

The reaction between $C_{Fe(II)EDTA}$ and NO is considered to be sufficiently fast that it is completed by the end of the liquid film.

Substituting:

$$Y = \frac{X}{\delta_L}$$

$$\frac{D_{NO}}{\delta_L} \frac{d^2 C_{NO}}{dY^2} - K C_{Fe(II)EDTA} C_{NO} = 0, \quad 0 < Y < 1$$

$$\frac{d^2 C_{NO}}{dY^2} - \frac{K \delta_L C_{Fe(II)EDTA} C_{NO}}{D_{NO}} = 0, \quad 0 < Y < 1$$

$$\gamma^2 = \frac{K \delta_L^2 C_{Fe(II)EDTA}}{D_{NO}}$$

$$\frac{d^2 C_{NO}}{dY^2} - \gamma^2 C_{NO} = 0$$

$$C_{NO} = A \cosh(\gamma Y) + B \sinh(\gamma Y)$$

at gas liquid interface, y = 0, (x=0)

$$C_{NO} = C_{NO}^{int\,erface} = \frac{P_{NO}}{H} = A$$

and at the end of the liquid film y = 1, (x = δ_L)

$$C_{NO} \to 0$$

The C_{NO} in the bulk liquid is negligible in comparison with C_{NO} at the interface.

$$0 = \frac{P_{NO}}{H} \cosh(\gamma) + B \sinh(\gamma)$$

$$B = \frac{-P_{NO}}{H \tanh(\gamma)}$$

so,

$$C_{NO} = \frac{P_{NO}}{H} (\cosh(\gamma Y) - \frac{\sinh(\gamma Y)}{\tanh(\gamma Y)})$$

Flux of absorption of NO at the gas liquid interface is:

$$N_{NO} = -D_{NO} \frac{dC_{NO}}{dX}\bigg|_{X=0} = \frac{-D_{NO}}{\delta_L} \frac{dC_{NO}}{dY}\bigg|_{Y=0}$$

$$dC_{NO} = \frac{P_{NO}}{H} (\gamma \sinh(\gamma Y) - \frac{\gamma \cosh(\gamma Y)}{\tanh(\gamma Y)})$$

Thus,

$$N_{NO} = \frac{-D_{NO}}{\delta_L} \frac{P_{NO}}{H} (-\frac{\gamma}{\tanh(\gamma)})$$

$$N_{NO} = \frac{D_{NO}}{\delta_L} \frac{P_{NO}}{H} (\frac{\gamma}{\tanh(\gamma)})$$

Writing a mass balance for NO in the gas phase:

$$Q_g C_{NO}^g\big|_Z - Q_g C_{NO}^g\big|_{Z+\Delta Z} - N_{NO} \, a \, \varepsilon_L A \, dZ = \frac{\partial}{\partial t}(C_{NO}^g A \, dZ \, \varepsilon_g)$$

where:

191

ε_L, ε_g = volume fractions occupied by liquid and gas, respectively

A = cross sectional area of empty reactor

a = gas/liquid interfacial area per unit liquid volume (function of bubble size, sprayer type or trickling media)

$C_{NO}{}^g$ = P_{NO}/RT (related to the partial pressure in the gas phase)

Because the time spent by the gas in the reactor is small as compared to liquid phase, it can be assumed that the mass balance in the gas phase is pseudo-steady-state, making the mass balance for NO in the bulk gas:

$$\frac{\left[Q_g\,P_{NO}\big|_{Z+dZ} - Q_g\,P_{NO}\big|_Z\right]}{dZ} - N_{NO}\,a\,\varepsilon_L\,A\,RT = 0$$

$$\frac{d}{dZ}\left(Q_g\,P_{NO}\right) = -N_{NO}\,a\varepsilon_L\,A\,RT = 0$$

NO is dilute in the flue gas, so axial variations of Q_g can be neglected.

$$\frac{dP_{NO}}{dZ} = \frac{N_{NO}a\varepsilon_L\,ART}{Q_G} = \frac{D_{NO}}{\delta_L\,H}P_{NO}\frac{\gamma}{\tanh(\gamma)}\frac{a\varepsilon_L\,ART}{Q_G}$$

$$\frac{dP_{NO}}{P_{NO}} = \frac{D_{NO}}{\delta_L\,H}\frac{\gamma}{\tanh(\gamma)}\frac{a\varepsilon_L\,ART}{Q_G}dZ$$

Integrating this over the length of the reactor (Z) gives

$$\left[\ln P_{NO}\right]_{P_{NOfeed}}^{P_{NOeffluent}} = -\frac{D_{NO}}{\delta_L\,H}\frac{\gamma}{\tanh(\gamma)}\frac{a\varepsilon_L\,RTV}{Q_G}$$

Because the reaction under consideration is fast, the tanh (γ) $\rightarrow$ 1.

Percent removal is defined by:

$$\% \ removal = 100\left(1 - \frac{P_{NO_{effluent}}}{P_{NO_{feed}}}\right)$$

$$\frac{P_{NO_{effluent}}}{P_{NO_{feed}}} = 1 - \frac{\% \, removal}{100}$$

$$\ln\left(\frac{P_{NO_{effluent}}}{P_{NO_{feed}}}\right) = \ln\left(1 - \frac{\% \, removal}{100}\right) = -\frac{D_{NO}}{\delta_L H}\frac{a\varepsilon_L RTV}{Q_G}\gamma$$

$$1 - \frac{\% \, removal}{100} = \exp\left(-\frac{D_{NO}}{\delta_L H}\frac{a\varepsilon_L RTV}{Q_G}\gamma\right)$$

$$\% \, removal = 100\left(1 - \exp\left(-\frac{D_{NO}}{\delta_L H}\frac{a\varepsilon_L RTV}{Q_G}\gamma\right)\right)$$

$$-\ln\left(1 - \frac{\% \, removal}{100}\right) = \frac{D_{NO}\, a}{\delta_L}\frac{RT}{H}\frac{V}{Q_G}\varepsilon_L \gamma$$

Recalling that:

$$\gamma^2 = \frac{K\delta_L^2\, C_{Fe(II)EDTA}}{D_{NO}}$$

$$\gamma = \sqrt{\frac{K\delta_L^2\, C_{Fe(II)EDTA}}{D_{NO}}}$$

which is proportional to $C_{Fe(II)EDTA}^{1/2}$, plotting [-ln(1-(% removal/100)] vs. $C_{Fe(II)EDTA}^{1/2}$ will yield a straight line if the developed model is valid.

$$NTU = -\ln\left[1 - \frac{\% \, removal}{100}\right] = \frac{D_{NO} \, a \varepsilon_L}{\delta_L} \frac{L}{u_G} \frac{RT}{H} \frac{\sqrt{K} \delta_L}{\sqrt{D_{NO}}} \sqrt{C_{Fe(II)EDTA}}$$

$$NTU = -\ln\left[1 - \frac{\% \, removal}{100}\right] = \sqrt{D_{NO} K} \, a \varepsilon_L \frac{L}{u_G} \frac{RT}{H} \sqrt{\frac{C_{Fe(II)EDTA}}{C_{Fe(II)_{TOTAL}}}} \sqrt{C_{Fe(II)_{TOTAL}}}$$

APPENDIX D

DEVELOPMENT OF MASS BALANCE BASED MODEL

Assuming a constant cell concentration X with a decrease in substrate concentration that is proportional to the reduction of oxidized species by a stoichiometrically derived value ρ, such that:

$$[S] = [S_0] - \rho * ([NO_{3\,0}^-] - [NO_{3\,t}^-])$$

Also assume that kinetics of reduction reaction is a function both of electron donor and electron acceptor concentration and reaction rates.

$$d[NO_3^-] * \frac{(K_{S-ea} + [NO_3^-])(K_{s-ed} + [S])}{[S][NO_3^-]} = -kXdt$$

Considering only the left hand side of the reaction for now:

$$\left(\frac{K_{s-ea}K_{s-ed} + K_{s-ed} * [NO_3^-] + K_{S-ea} * [S] + [S] * [NO_3^-]}{[NO_3^-][S]} \right) * d[NO_3^-]$$

$$\left(\frac{K_{s-ea}K_{s-ed}}{[NO_3^-] * [S]} + \frac{K_{s-ed}[NO_3^-]}{[NO_3^-] * [S]} + \frac{K_{s-ea} * [S]}{[NO_3^-] * [S]} + \frac{[NO_3^-] * [S]}{[NO_3^-] * [S]} \right) * d[NO_3^-]$$

$$\left(\frac{K_{s-ea}K_{s-ed}}{[NO_3^-] * [S]} + \frac{K_{s-ed}}{[S]} + \frac{K_{s-ea}}{[NO_3^-]} + 1 \right) * d[NO_3^-]$$

Plugging in for [S] yields:

$$\left(\frac{K_{s-ea}K_{s-ed}}{[NO_3^-] * [S_0] - \rho * ([NO_{3\,0}^-] - [NO_{3\,t}^-])} + \frac{K_{s-ed}}{[S_0] - \rho * ([NO_{3\,0}^-] - [NO_{3\,t}^-])} + \frac{K_{s-ea}}{[NO_3^-]} + 1 \right) * d[NO_3^-]$$

Integrating with respect to nitrate concentration gives:

$$K_{s-ea} K_{s-ed} * \int \frac{d[NO_3^-]}{[NO_3^-] * ([S_0] - \rho * ([NO_3^-]_0 - [NO_3^-]_t))} + K_{s-ed} *$$

$$\int \frac{d[NO_3^-]}{[S_0] - \rho * ([NO_3^-]_0 - [NO_3^-]_t)} + K_{s-ea} * \int \frac{d[NO_3^-]}{[NO_3^-]} + \int d[NO_3^-]$$

Through the following substitution:

$$x = [NO_3^-]$$
$$dx = d[NO_3^-]$$
$$a = [So] - \rho * ([NO_3^-]_0$$
$$b = \rho$$

$$K_{s-ea} K_{s-ed} * \int \frac{dx}{x * (a + bx)} + K_{s-ed} * \int \frac{dx}{(a + bx)} + K_{s-ea} * \int \frac{dx}{x} + \int dx$$

Recognizing that:

$$\int \frac{dx}{x*(a+bx)} = -\frac{1}{a}\ln\left(\frac{a+bx}{x}\right) + C$$

$$\int \frac{dx}{(a+bx)} = \frac{1}{b}\ln(a+bx) + C \text{, and}$$

$$\int \frac{dx}{x} = \ln(x) + C$$

we can solve the previous integral to get:

$$K_{s-ea} K_{s-ed} * \frac{1}{a}\ln\left(\frac{a + bx}{x}\right) + K_{s-ed} * \frac{1}{b}\ln(a + bx) + K_{s-ea} * \ln(x) + x + C$$

Substituting back in for x, a, and b gives:

$$K_{s-ea} K_{s-ed} * \frac{1}{([S_0] - \rho * [NO_3^-]_0)}\ln\left(\frac{([S_0] - \rho * [NO_3^-]_0) + \rho * [NO_3^-]}{[NO_3^-]}\right) +$$

$$K_{s-ed} * \frac{1}{\rho}\ln\left(([S_0] - \rho * [NO_3^-]_0) + \rho * [NO_3^-]\right) + K_{s-ea} * \ln[NO_3^-] + [NO_3^-] + C$$

Considering then the right hand side of the equation:

$$-kXdt$$

This can also be put in terms of bed height. For constant flow rate:

$$-kX dt = -kX dt \frac{A}{Q} \frac{dl}{dt} = -kX \frac{A}{Q} dl$$

Integrating yields:

$$-\int kX \frac{A}{Q} dl = -kX \frac{A}{Q} l + C$$

Combining left and right hand sides of the equation yields:

$$K_{s-ea} K_{s-ed} * \frac{1}{\left([S_0] - \rho * [NO_3^-]_0\right)} \ln\left(\frac{([S_0] - \rho * [NO_3^-]_0) + \rho * [NO_3^-]}{[NO_3^-]} \right) +$$

$$K_{s-ed} * \frac{1}{\rho} \ln\left(([S_0] - \rho * [NO_3^-]_0) + \rho * [NO_3^-]\right) + K_{s-ea} * \ln[NO_3^-] + [NO_3^-] + C$$

$$= -kX \frac{A}{Q} l$$

Evaluating this equation at the bottom of the reactor where:

$$L = \text{bed height} = 0$$
$$[NO_3^-] = [NO_3^-]_0$$

$$K_{s-ea} K_{s-ed} * \frac{1}{\left([S_0] - \rho * [NO_3^-]_0\right)} \ln\left(\frac{([S_0] - \rho * [NO_3^-]_0) + \rho * [NO_3^-]_0}{[NO_3^-]_0} \right) +$$

$$K_{s-ed} * \frac{1}{\rho} \ln\left(([S_0] - \rho * [NO_3^-]_0) + \rho * [NO_3^-]_0\right) + K_{s-ea} * \ln[NO_3^-]_0 + [NO_3^-]_0 + C$$

$$= 0$$

$$C = -\left(\frac{K_{s-ea} K_{s-ed}}{\left([S_0] - \rho * [NO_3^-]_0\right)} \ln\left(\frac{[S_0]}{[NO_3^-]_0} \right) + \frac{K_{s-ed}}{\rho} \ln[S_0] + K_{s-ea} * \ln[NO_3^-]_0 + [NO_3^-]_0 \right)$$

Giving a final equation of:

$$\frac{K_{s-ea}K_{s-ed}}{\left([S_0]-\rho*[NO_3^-]_0\right)}\ln\left(\frac{\left([S_0]-\rho*[NO_3^-]_0\right)+\rho*[NO_3^-]}{[NO_3^-]}\right)+$$

$$\frac{K_{s-ed}}{\rho}\ln\left(\left([S_0]-\rho*[NO_3^-]_0\right)+\rho*[NO_3^-]\right)+K_{s-ea}*\ln[NO_3^-]+[NO_3^-]$$

$$-\frac{K_{s-ea}K_{s-ed}}{\left([S_0]-\rho*[NO_3^-]_0\right)}\ln\left(\frac{[S_0]}{[NO_3^-]_0}\right)-\frac{K_{s-ed}}{\rho}\ln[S_0]-K_{s-ea}*\ln[NO_3^-]_0-[NO_3^-]_0$$

$$=-kX\frac{A}{Q}l$$

This expression can be evaluated under a given set of conditions to determine the reactor bed height by which a given conversion of nitrate will be reached.

APPENDIX E

PHENANTHROLINE METHOD – SUMMARY

A variation on Standard Method 3500-D (1995) - the Phenanthroline Method for ferrous iron/total iron analysis is proposed for analysis of ferrous iron present in solution as ferrous EDTA.

Method Principle:

The sample is acidified at the time of collection (2 ml of concentrated hydrochloric acid per 100 ml of sample). This serves to slow the oxidation of ferrous iron dramatically as well as to dissociate the Fe(II)EDTA complex. The sample bottle should be filled directly from the source and stopped immediately to prevent sample oxidation. 20 ml of phenanthroline solution and 10 ml of $NH_4C_2H_3O_2$ buffer solution should then be added to 50 ml of acidified sample. This solution should be stirred thoroughly, diluted to 100 ml (20 ml of distilled water) and analyzed within 5 to 10 minutes. Sample exposure to sunlight should be minimized so that full phenanthroline color development is achieved. Because of the slow kinetics of complexation, excess phenanthroline is required. Therefore, for samples with ferrous iron concentrations greater than 50 μg, a larger volume of phenanthroline solution or a more concentrated phenanthroline solution should be used.

The procedure for total iron in complex with EDTA analysis (ferrous + ferric) is similar to that for ferrous iron, but requires reduction of all iron present to ferrous iron before a spectrophotometric method can be used to detect total iron. If the total iron concentration is expected to be greater than 200 micrograms per liter, samples should be diluted in oxygen free distilled water. Again, the sample should be acidified with 2 ml of concentrated hydrochloric acid and 1 ml of $NH_2OH \bullet HCl$ solution. The sample is then heater to a boil (with glass beads in solution), and boiled until the volume is reduced to 15-20 ml. The sample is cooled to room temperature, and transferred to a 50-100 ml volumetric flask or nessler tube. 10 ml of $NH_4C_2H_3O_2$ buffer solution, 4 ml of phenanthroline solution, and DI water to fill should be added. The sample should be mixed for 10-15 minutes to allow maximum color development, and then analyzed spectrophotometricly.

PRELIMINARY COST ANALYSIS

Preliminary Cost Analysis of a Combined Limestone Flue Gas Desulfurization Scrubbing / Forced Air Oxidation Process and NO$_X$ Absorption with Biological Treatment and Regeneration of Spent Scrubber Solution

Summary

The following preliminary cost analysis was conducted to provide some insight into the costs associated with the absorption of NO$_X$ from scrubber solution and subsequent biological treatment and regeneration of spent scrubber solution. The general conclusion, given the results of Table F1, is that scrubbing of NO$_X$ with biological treatment and regeneration of spent scrubbing solution is a potentially economically feasible alternative to selective catalytic reduction.

Table F1. Summary of cost analysis of FGD with forced air oxidation and NO$_X$ absorption/biological process water treatment

Cost Component	M$/yr	$/MWh	$/ton NO removed	Percent Total
Annual Fixed Cost	$2.20	$0.84	$223.36	18.26%
Annual Variable Cost	$7.48	$2.85	$760.42	62.16%
Total Annual O&M Cost	$9.68	$3.68	$983.78	80.42%
Annualized Capital Cost	$2.36	$0.90	$239.52	19.58%
Total Levelized Annual Cost	12.03	4.58	$1,223.31	100.00%

Table F2. Summary of costs of air pollution control equipment for a 300 MW (net) utility boiler

Summary of Costs ($US, 2003) for APC Equipment for a 300 MW (net) Utility Boiler	
Total Plant Cost (LSFO-FGD/NO_X Scrub)	$149,456,174
Total Plant Cost (LSFO-FGD only)	$119,309,739
Cost of Adding NO_X absorption to existing LSFO-FGD	$ 30,146,435
Total Plant Cost of Biological treatment and regeneration of spent scrubber solution	$2,601,265
Total Plant Cost for (LSFO-FGD/NO_X Scrub w/ Biological treatment and regeneration of spent scrubber solution)	$32,747,700
amortized cost over 30 years, assuming 6%apr/12 mo/yr	$196,339
annualized capital cost	$2,356,068
tons of NO removed per year	9836.476
MWh/yr	2,628,000

Disclaimer

The cost estimate described herein is not exhaustive. It is designed to give some insight into the order of magnitude of capital and operation and maintenance costs associated with the addition of NO_X scrubbing and scrubber solution treatment and regeneration to A Limestone Scrubber system with forced air oxidation. Known omissions to this model include the cost of excess biomass landfilling, the credit for production of a salable gypsum product, and bioreactor piping requirements. Some contingency was factored into the cost analysis in an attempt to address these omissions. Also, it should be noted that the cost analysis was not conducted by an experienced costing engineer.

Overview of Limestone FGD Process with Forced Air Oxidation

Limestone with forced air oxidation (LSFO) FGD is a modification of a traditional wet limestone FGD process. LSFO uses a limestone slurry to increase absorption capacity in a spray or packed tower, with subsequent oxidation of calcium sulfite to form calcium sulfate (gypsum) slurry. This process is capable of removing in excess of 90% of SO_2 present in flue gas, and the generated gypsum slurry can be thickened and dewatered to produce a relatively pure gypsum product with low water content that can either be landfilled or sold for use in gypsum wallboard production.

Process Description

The process under consideration adds nitric oxide (NO) scrubbing to traditional SO_2 scrubbing by amending the limestone slurry with iron EDTA. Ferrous EDTA in solution increases the solubility of nitric oxide by removing the dissolved NO from bulk solution through formation of a reversible nitrosyl adduct. By reducing the concentration of free NO in bulk solution to below saturation, more gas phase NO can dissolve. The capacity of the scrubbing solution to absorb NO is a function of free ferrous iron concentration present in the chelated form. It is therefore necessary to remove the NO from the ferrous chelate and maintain a significant amount of the iron EDTA in the reduced ferrous form. The process under consideration achieves both of these goals by promoting the microbially catalyzed reduction of the nitrosyl adduct of ferrous EDTA as well as the oxidized ferric EDTA that is not functional for NO absorption. For purposes of this preliminary cost analysis, ethanol is used as the primary electron donor/carbon source required by the prevailing bacteria to complete the desired redox reactions and generate new biomass. For purposes of this cost analysis, it is assumed that chemical reduction has a minimal impact on total spent scrubber solution reduction as compared to microbially catalyzed reduction.

Process Design

The equipment areas incorporated into the combined LSFO/NO$_X$ scrubbing system are divided into the following areas:

- Reagent Feed System
- SO$_2$ Removal System
- Flue Gas System
- Solid Handling System
- Biological Treatment and Regeneration System
- General Support Equipment
- Additional Equipment

The following table summarizes major criteria in each of these systems.

Table F3 Combined Ferrous EDTA/Limestone System with Forced Oxidation Process Design Criteria For one 300 MW (net) unit

Flue Gas Handling Area Criteria

Flue gas flow rate	1,020,000 acfm @ 277ºF
Absorber pressure drop	12 in. H_2O
Total system pressure drop	14 in. H_2O
Packed tower outlet gas temperature	127 ºF

SO_2/NO_X Removal Area Criteria

SO_2 removal (2.6% S Coal)	99%
NO_X removal	70%
Scrubber modules	5@30' diameter
Scrubber design	Packed tower
L/G ratio	96 gpm/1000 saturated acfm
Scrubber slurry solids concentration	2%
$CaCO_3$ reagent feed ratio	1.10 lb mole $CaCO_3$
	lb mole SO_2 removed
Packing material	Pall rings, 3"
Bed porosity	0.80
Absorber tower superficial velocity	6 fps
Reaction mix tank retention time	6 min
Oxidation feed rate (in subsequent oxidation tank)	2lb mole O_2
	Lb mole SO_2 removed
Percent oxidation	100%
Scrubber slurry pH	5.3

Reagent Feed Area Criteria

Total limestone storage	60 days
Limestone day bin storage	30 hrs
Limestone slurry tank storage	8 hrs

Solids Handling Area Criteria

Thickener underflow % solids	45%
Thickener overflow tank capacity	30 min
Thickener size	$2ft^2$/tpd dry solids
Vacuum filter product % solids	85%
Vacuum filter size	150 lb/hr/ft^2

Biological Treatment and Regeneration Area Criteria

NO·Fe(II)EDTA reducing vessel residence time	227 minutes
Fe(III)EDTA reducing vessel residence time	65.8 min
Liquid Flow Rate	6,075 gpm
Ethanol Feed Ratio	1.2 x stoichiometric reqmt
ferrous EDTA makeup	1% of daily flow

General Support Area Criteria

Makeup water tank capacity	
Seal water tank capacity	

Material Balance

The following material balance was generated using a spreadsheet entitled: Economics of Limestone Forced Oxidation FGD Systems, Model Version 8/8/1991. The spreadsheet was developed for EPRI and its members by United Engineers & Constructors, Inc. (Radcliffe, 1991). A copy of the spreadsheet will be provided upon request.

Table F4. FGD material balance for streams downstream of I.D. fan, flue gas to absorber, flue gas in absorber, flue gas from absorber, total flue gas from all absorbers, and reheated flue gas to chimney

	FGD MATERIAL BALANCE					
-	-	-	-	-	-	-
Stream Number	1	2	3	4	5	6
Stream Name	Flue Gas Downstream of I. D. Fans	Flue Gas to Absorber	Flue Gas in Absorber	Flue Gas from Absorber	Total Flue Gas from Absorbers	Reheated Flue Gas to Chimney
------------------	---------	---------	---------	---------	---------	----------
Temperature, °F	282	282	127	127	127	127
Pressure, " H2O	13	13	12	1	1	1
K SCFM	685	137	149	149	746	746
K ACFM	964	193	166	171	854	854
CO2, K Lb/Hr	578.7	115.7	115.7	117.3	586.7	586.7
N2, K Lb/Hr	2,267.6	453.5	461.0	461.0	2,305.2	2,305.2
SO2, K Lb/Hr	11.5	2.3	2.3	0.0	0.1	0.1
O2, K Lb/Hr	186.1	37.2	39.5	39.4	197.2	197.2
HCl, K Lb/Hr	0.3	0.1	0.1	0.0	0.0	0.0
Other Gases, K Lb/Hr	1.4	0.3	0.3	0.3	1.4	1.4
H2O, K Lb/Hr	147.2	29.4	57.7	57.7	288.5	288.5
Fly Ash, Lb/Hr	87.5	17.5	17.5	17.5	87.5	87.5
Total, K Lb/Hr (gas only)	3,192.8	638.6	676.6	675.8	3,379.1	3,379.1

Table F5. FGD material balance for inlet reheat air, hot reheat air, oxidation air to each tank, total oxidation air, hot bypass flue gas, and total flue gas to chimney

Stream Number	7	8	16	17	28	29
Stream Name	Inlet Reheat Air	Hot Reheat Air	Oxidation Air to Each Tank	Total Oxidation Air	Hot Bypassed Flue Gas	Total Flue Gas to Chimney
-------------------	---------	---------	---------	---------	---------	---------
Temperature, °F	60	440	60	60	282	127
Pressure, " H_2O	0	1	275	0	1	1
K SCFM	0.0	0.0	2.2	11.0	0	746
K ACFM	0.0	0.0	1.3	11.2	0	854
CO_2, K Lb/Hr	--	--	--	--	0.0	586.7
N_2, K Lb/Hr	0.0	0.0	7.5	37.6	0.0	2,305.2
SO_2, K Lb/Hr	--	--	--	--	0.0	0.1
O_2, K Lb/Hr	0.0	0.0	2.3	11.3	0.0	197.2
HCl, K Lb/Hr	--	--	--	--	0.0	0.0
Other Gases, K Lb/Hr	--	--	--	--	0.0	1.4
H_2O, K Lb/Hr	0.0	0.0	0.1	0.6	0.0	288.5
Fly Ash, Lb/Hr	--	--	--	--	0.0	87.5
Total, K Lb/Hr (gas only)	0.0	0.0	9.9	49.6	0.0	3379.1
-	-	-	-	-	-	-
NOTES: 1. K = Thousands						

Table F6. FGD material balance for streams to preheater, demister water, limestone slurry to reaction tank, process water to reaction tank, slurry to absorber, slurry to thickener, process water to reaction tanks, and limestone to ball mill

	FGD MATERIAL BALANCE (Continued)							
Stream Number	9	10	11	12	13	14	15	18
Stream Name	Steam to preheater	Demister H$_2$O	Limestone Slurry to Rxn Tank	Process Water to Rxn Tank	Slurry to Absorber	Slurry to Thickener	Process Water to Rxn Tanks	Limestone to Ball Mill
------------------	--------	--------	---------	---------	---------	---------	---------	---------
Temperature, °F	572	60	68	68	126	126	68	60
Flow, GPM	--	127	35	346	16633	348	1729	--
Wt % Solids	--	0%	20%	0%	3%	3%	0%	100%
CaSO$_3$*1/2H$_2$O, K Lb/Hr	--	--	--	--	197.0	4.1	--	--
CaSO$_4$*2H$_2$O, K Lb/Hr	--	--	--	--	29.2	0.6	--	--
Inerts, K Lb/Hr	--	--	0.3	--	13.6	0.3	--	1.4
CaCl$_2$, K Lb/Hr	--	--	--	--	4.0	0.1	--	--
CaCO$_3$, K Lb/Hr	--	--	3.9	--	13.4	0.3	--	19.5
H$_2$O, K Lb/Hr (steam)	0.0	63.5	16.8	173.1	8,315.5	174.0	865.3	--
	----	----	----	----	----	----	----	----
Total, K Lb/Hr	0.0	63.5	20.9	173.1	8,572.6	179.4	865.3	20.9

Table F7. FGD material balance for water to ballmill, limestone slurry to LS slurry tank, water to LS slurry tank, LS slurry to reaction tank, slurry from reaction tanks to thickener, thickener overflow, thickener underflow vacuum filter, filtrate to process water tank, and filter cake.

Stream Number	19	20	21	22	23	24	25	26	27
Stream Name	Water To Ball Mill	LS Slurry to LS Slurry Tank	Water to LS Slurry Tank	Limestone Slurry to Rxn Tank	Slurry from Rxn Tanks to Thickenr	Thickener Overflow	Thickener Undrflow to Vacuum Filtr	Filtrate to process Water Tank	Filter Cake
Temperature, °F	60	90	60	68	126	80	80	60	60
Flow, GPM	63	75	105	174	1740	1674	82	55	--
Wt % Solids	0%	40%	0%	20%	3%	0%	45%	0%	85%
$CaSO_3 \cdot 1/2\ H_2O$, K Lb/Hr	--	--	--	--	20.6	--	20.6	--	20.6
$CaSO_4 * 2H_2O$, K Lb/Hr	--	--	--	--	3.1	---	3.1	--	3.1
Inerts, K Lb/Hr	--	1.4	--	1.4	1.4	--	1.4	--	1.4
$CaCl_2$, K Lb/Hr	--	--	--	--	0.4	--	0.4	--	0.4
$CaCO_3$, K Lb/Hr	--	19.5	--	19.5	1.4	--	1.4	--	1.4
H_2O, K Lb/Hr	31.4	31.4	52.4	83.8	869.9	837.6	32.4	27.7	4.7
Total, K Lb/Hr	31.4	52.4	52.4	104.7	896.9	837.6	59.3	27.7	31.6

<u>**Cost Summary**</u>

A preliminary cost estimate for a combined SO_X/NO_X scrubbing process was arrived at by scaling up data reported in a 1992 report from the Dravo Lime Company to the DOE Federal Energy Technology Center entitled "Enhanced NO_X Removal in Wet Scrubbers Using Metal Chelates."

Table F8. Dimensions and operating parameters of Dravo pilot scale apparatus

	units	Dravo pilot scale operation conditions
Diameter	**Feet**	3
CS area	**Feet^2**	7.07
Effective volume (empty bed)	**Feet^3**	84.8
Effective bed height	**Feet**	12
Gas flow rate	**Fps**	6
Gas flow rate (empty bed)	**acfm**	42.4
Liquid flow rate	**gpm**	9.12E+06

From a figure located in the Dravo Report, it was determined that a gas flow rate of 6 fee per second and a L/G ratio of 96gpm/1000 acfm would allow the removal of 70% of total NO_X in the flue gas. Using this information, a preliminary cost estimate was made for a scrubber system that would meet treatment requirements for a 300 net MW unit. Using the Electric Power Research Institute's (EPRI's) TAG Methodology as a guide, a combined NO_X/SO_X scrubbing process with biological treatment and regeneration was modeled with the following parameters:

Table F9. Technical inputs to model for plant and boiler

PLANT TECHNICAL INPUT	
-	-
Total Gross Rating (MW), (50-1300 MW)=	313.00
Gross Plant Heat Rate (GPHR) =	9,318
Total Net Rating (Less Auxiliary Power, MW) =	300.00
Net Plant Heat Rate (NPHR, Without FGD) =	9,722
Total FGD Utility Use (MW) =	5.46
Plant Capacity Factor, % =	100%
TECHNICAL INPUTS FOR BOILER	Applach.
-	----------
Boiler Heat Input (MMBtu/Hr)	2,916
Total Air Downstream of Economizer (%)	120.0%
Air Heater Leakage, % of Econ. Flue Gas	13.7%
Air Heater Outlet Gas Temp (°F)	277
Inlet Air Temp (°F)	60
Ambient Absolute Pressure (in. Hg)	29.4
Pressure After Air Heater (in. H2O)	-12
Moisture in Air, Lb/Lb Dry Air	0.013
Carbon Loss (%)	0.5%
ASH SPLIT, %	
Fly Ash or Ash Overhead	80%
Bottom Ash	20%
Partic. in Gas Downstream of ESP, Lb/MMBtu	0.03
Days of Power Outage Required for FGD Installation	0

Table F10. Technical inputs for FGD system

TECHNICAL INPUTS FOR FGD SYSTEM	Applach.
-	---------
Number of Operators (40 Hr Shifts/Week)	20
Overall Percent SO2 Removal	99%
Absorber Percent SO2 Removal	99%
Adiabatic Saturation Temp, °F	127
Flue Gas Reheat, °F	0
Reheated Flue Gas Temp , °F	127
Makeup Water Temp , °F	60
Delta H of Reheat Steam, Btu/Lb	855.14
L/G Ratio, gpm/1000 saturated ACFM	100
Reagent Ratio, LbMol $CaCO_3$/LbMol SO_2 Removed	1.10
Mole % of CaSulfate Produced in Absorber	10%
Mole % of CaSulfite Produced in Absorber	90%
Scrubber Slurry Solids Concentration, wt%	3%
Reaction Tank Retention Time, min	6
Oxidation Air, LbMol O_2/Lb/Mol SO_2 Removed	2
Solids Handling and Equipment Selection	
Landfill Disposal or Stacking	1
(1 = Landfill, 2 = Stacking)	
Landfill Disposal of Solids	
-Percent Solids to Landfill	85%
Stacking of Solids	
-Stack Leachate Return (% of Free H2O)	0%
Number of Operating Absorbers	5
Number of Spare Absorbers	0
Absorber Capacity (% each, Max Capacity = 650 MW ea)	20%
Absorber Material (1 = RLCS, 2 = Poly-lined CS	3
3 = 904 SS, 4 = 317 SS)	
Absorber Area Enclosed with Building? (Yes/No)	Yes
Distance from Reagent Handling Area to Absorbers, ft	50
Distance from Absorbers to Waste\Handling Area, ft	50
For Additional Equipment Sparing\Capacity	
Inputs GO TO AH129	
Absorber Pressure Drop, "$H_2$0	12
Reheat Pressure Drop, "$H_2$0	3
Chimney Pressure Drop, "$H_2$0	1
Total I.D. Fan Pressure Drop, "$H_2$0	13

Table F11. Scrubber economic inputs

SCRUBBER ECONOMIC INPUTS		
Discount Rate (MAR) =		11.5%
AFUDC Rate =		11.5%
Construction Period (years) =		2
First Year Fixed Charge Rate =		21.2%
Levelized Fixed Charge Rate (FCR) =		16.5%
Service Life (years) =		30
Start-Up Date (Year) =		2003
(Costs Escalated from January, 1989 Basis)		
Inflation Rate =		5.0%
Royalties Adjustment (% of Total Process Capital) =		0.5%
Land Cost (Start-up Date $)		$0
Constant Dollar Analysis:		
Discount Rate (MAR, Constant $) =		6.2%
Levelized Fixed Charge Rate (FCR, Constant $) =		10.6%
Escalation Rates:	Total Current$	Real/ Constant$
Consumables (O & M) =	5.00%	0.00%
Capital Costs (prior to startup) =	5.00%	0.00%
Additional Power and Steam Cost =	5.32%	0.30%
Market Demand =	0.00%	

Total Plant Cost

       Process facilities capital – total construction costs

       General facilities capital – roads, office buildings, shops, labs (5-20% of process)

       Engineering and home office overhead including fee – (7 – 15% of process cap.)

       Contingencies – project and process

              Project – uncertainty in project cost (30% from table 3.2 (Radcliffe, 1991))

              Process – uncertainty in process performance (30% from Table 3-3 (Radcliffe, 1991))

Total plant investment (TPI) at in-service date includes AFUDC and escalation of construction costs over the period of construction. Because much of the construction associated with the process modification under consideration is assembly of pre-fabricated units, it is assumed that construction time will not exceed one year. In this case, TPI = TPC, and AFUDC is therefore equal to $0. Considering the adjustment factor (Table 3-4)

Total Capital Requirement

Total plant investment at the in-service date, including allowance for funds used

during construction (AFUDC) or interest during construction

Prepaid royalties (assume 0.5% of process capital)

Preproduction (startup) costs

Inventory Capital (fuel storage, consumables, etc.)

Initial cost for catalyst/reagent

Land – (assume 0%)

Table F12. Bioreactor total plant cost

Bioreactor Total Plant Cost		
Reagent Startup Cost		
ferrous sulfate	$34,390.93	$US, Jan 2003
EDTA	$235,765.83	$US, Jan 2003
Tank & impeller (1)	$500,000.00	$US, Jan 1990
Tank & impeller (2)	$250,000.00	$US, Jan 1990
installation cost (described above)	$3,586.70	$US, Jan 2003
Convey 9000 lb of Ferrous sulfate per day	$10,000	$US, Jan 1990
Pump 2300 gal ETOH per day (1.6 gpm) ss pump	$1000	$US, Jan 1990
Pump 2300 gal EDTA soln. per day, ss pump	$1000	$US, Jan 1990
Total reagent equipment conveyance cost	$12,000.00	$US, Jan 1990
Concrete/mounting for pumps (100% equip cost)	$12,000.00	$US, Jan 1990
instalation cost (65% equip cost)	$7,800.00	$US, Jan 1990
Total Reagent conveyeynce cap. Cost	$31,800.00	$US, Jan 1990
total (Jan, 1990)	$781,800.00	$US, Jan 1990
total (Jan, 2003)	$1,373,107.95	$US, Jan 2003
General facilities capital (10% of process cap)	$137,310.79	$US, Jan 2003
Engineering / home office overhead (7% of cap.)	$96,117.56	$US, Jan 2003
Prepaid royalties (0.5% of process capital)	$6,865.54	$US, Jan 2003
Preproduction costs		
one month fixed operating cost	$60,422.10	$US, Jan 2003
one month variable operating cost	$32,089.29	$US, Jan 2003
10% of monthly reagent	$44,024.87	$US, Jan 2003
Changes and modifications (2% TPI)	$27,462.16	$US, Jan 2003
Preproduction costs (total)	$163,998.42	$US, Jan 2003
Contingencies		
Project (30%)	$411,932.38	$US, Jan 2003
Process (30%)	$411,932.38	$US, Jan 2003
Total initial cost	$2,601,265.03	$US, Jan 2003
Amortized cost (30 years, 6% monthly)	$15,595.90	$US, Jan 2003

Table F13. Bioreactor annual operation and maintenance costs

Bioreactor O&M		
		units
Operator jobs (additional)	3	Full time jobs
Average Labor Rate (ENR, Sept. 1, 2003)	$27.59	(US$, 2003/hr)
shift hours per year	8760	Hours/year
net capacity of plant	300,000	kW
OLC (Operating labor cost)	$2.42	$/kW-yr
OLC (Operating labor cost)	$725,065.20	(US$, 2003/year)
Variable O&M	0.1486	mills/kWh
Total Maintenance Costs, 5% of total plant capital cost/yr	$68,655.40	(US$, 2003/year)
Maitainance Labor, 40% of total maintenance	$27,462.16	(US$, 2003/year)
Maintainance Materials, 60% of total maintenance	$41,193.24	(US$, 2003/year)
Overhead charges, 30% of O&M Labor	$225,758.21	(US$, 2003/year)

Fixed O&M is taken as 65% of baseload. Fixed O&M = 0.65*total O&M cost ($/kW-yr)

Variable O&M is 35% of baseload.

Variable O&M = (1-0.65)* total O&M cost ($/kW-yr) * (1000 mills/$)/ (0.65*8760 hrs/yr)

Variable O&M is in units of mills/kWh.

Operating Labor Cost (OLC)

From Table 3-10 (Radcliffe, 1991), total maintenance costs are assumed to be 5% of total plant capital cost/yr. Assuming a maintenance labor/materials ratio of 40/60, we can break this maintenance cost into maintenance labor and maintenance materials subsets.

Table F14. Estimate of bioreactor consumables costs

Reagent	Value	Cost (2003)
95% Ethanol (5000 - 6000 gallon tanker)	2	$/gal, delivered
$ per pound of Vercene 100 liq., 39% tetrasodium EDTA by weight	0.33	$/lb, delivered
Technical grade ferrous sulfate	0.135	$/lb, delivered

Table F15. NO$_X$ Scrubbing and scrubber treatment reagent costs.

NO$_X$ Scrubbing and and Regeneration Related Reagents Annual Reagent Costs (US$,2003/year)	
Ethanol	$1,747,673.23 *
ferrous sulfate	$450,044.78
Tetra-sodium EDTA	$3,085,266.43
total	$5,282,984.44
Total Annual Cost	$6,302,463.25
* cost could be partially mitigated by replacing ethanol with an appropriate waste stream (carbon source/electron donor)	

By-product credits

Gypsum credits were not factored into the cost estimate. Biomass landfill disposal costs were also not considered.

Levelized Costs

Using a 15 year payment period and a 6% interest rate per period with monthly periods (12 per year) to give a monthly rate of 6%/12 or 0.005, with a total number of payments of 15*12 or ** payments.

The Engineering News Record Construction Cost index was used as a simple method to factor inflation and adjust all costs to US$, January 2003.

For example, given the following indices:

Construction Cost Index, January 1990, 4680
Construction Cost Index, January 2003, 6581

the cost of a $100 item in US$, Jan, 1990 would be adjusted to $, January,2003 by the following calculation:

$$\$100 \times \frac{6581}{4680} = \$140.62$$

The index factors in the cost of 200 hours of common labor at the 20-city average of common labor rates, 25 cwt of standard structural steel shapes at the mill price prior to 1996 and the fabricated 20-city price from 1996, 1.128 tons of portland cement at the 20-city price, and 1,088 board-ft of 2 x 4 lumber at the 20-city price. A more detailed description of this cost index can be found at the Engineering News Record website:

http://enr.construction.com/features/conEco/costIndexes/default.asp

Table F16. Cost summary of limestone forced oxidation FGD with NO$_X$ absorption

SUMMARY – LSFO FGD with NO$_X$ Absorption					
INPUTS					
Fuel Type	Appalachian		Reagent Type	OH - Ls	
% S Coal	2.60		Reagent Cost ($/ton)	6.00	
Plant's Net Rating (MW)	300.00		SO2 Removal	99%	
Plant Capacity Factor	100%		Ca/S Removed Molar Ratio	1.10	
Plant Location	Ohio				
OUTPUTS					
Reagent Required (tons/hr)	10.47		Boiler Efficiency (%)	88.00	
Fly Ash from Coal (tons/hr)	8.42		FGD Power Consumption (MW)	5.46	
FGD Sludge, dry (tons/hr)	13.45				
CAPITAL COSTS (+/- 20%)	(US$, 2003)	$/KW	OVERALL MATERIAL COST ADJUSTMENTS		
10 Reagent Feed System	19,451,390	64.8	Retrofit Factor	1.305	
20 SO2 Removal System	60,762,552	202.5	Installation Factor	1.902	
30 Flue Gas System	12,829,536	42.8			
40 Regeneration	0	0.0			
50 Byproduct Handling	0	0.0			
60 Solids Handling	4,125,602	13.8			
70 General Support Equipment	1,030,573	3.4			
80 Miscellaneous Equipment	2,316,924	7.7			
TOTAL PROCESS CAPITAL	100,516,577	335.1			
General Facilities	10,051,658	33.5			
Engineering & Home Off. Fees	10,051,658	33.5			
Process Contingency	2,412,398	8.0			
Project Contingency	17,669,676	58.9			
TOTAL PLANT COST (TPC)	140,701,967	469.0			

Table F17. Cost summary of limestone forced oxidation FGD with NO$_X$ absorption (continued)

TOTAL CASH EXPENDED (TCE)	137,351,920	457.8
Allowance for Funds (AFDC)	7,705,108	25.7
TOTAL PLANT INVESTMENT (TPI)	145,057,028	483.5
Preproduction Costs	3,806,067	12.7
Inventory Capital	90,496	0.3
Initial Catalyst and Chemicals	0	0.0
Royalties	502,583	1.7
TOTAL CAPITAL REQUIREMENT (TCR)	149,456,174	498.2
Market Demand Escalation	0	0.0
Power Outage Penalty	0	0.0
Land Cost	0	0.0
TOTAL CAPITAL REQUIREMENT (TCR)	149,456,174	498.2
(Including Market Demand Escalation, Power Outage Penalty and Land Cost)		

Table F18. Cost summary of limestone forced oxidation FGD without NO$_X$ absorption

SUMMARY – LSFO FGD without NO$_X$ Absorption					
INPUTS					
					OH - Ls
Fuel Type =	Applach.		Reagent Type		
% S Coal =	2.60		Reagent Cost ($/ton)		6.00
Plant's Net Rating (MW) =	300.00		SO2 Removal =		99%
Plant Capacity Factor =	100%		Ca/S Removed Molar Ratio		1.10
Plant Location =	Ohio				
OUTPUTS					
Reagent Required (tons/hr) =	10.47		Boiler Efficiency (%)		88.00
Fly Ash from Coal (tons/hr) =	8.42		FGD Power Consumption (MW)		4.54
FGD Sludge, dry (tons/hr) =	13.45				
CAPITAL COSTS (+/- 20%)	US$, 2003	$/KW	OVERALL MATERIAL COST ADJUSTMENTS		
10 Reagent Feed System	19,451,390	64.8	Retrofit Factor		1.299
20 SO2 Removal System	42,456,019	141.5	Installation Factor		1.900
30 Flue Gas System	10,842,688	36.1			
40 Regeneration	0	0.0			
50 Byproduct Handling	0	0.0			
60 Solids Handling	4,125,602	13.8			
70 General Support Equipment	1,037,975	3.5			
80 Miscellaneous Equipment	2,316,924	7.7			
TOTAL PROCESS CAPITAL	80,230,599	267.4			
General Facilities	8,023,060	26.7			
Engineering and Home Office Fees	8,023,060	26.7			
Process Contingency	1,925,534	6.4			
Project Contingency	14,066,765	46.9			
TOTAL PLANT COST (TPC)	112,269,019	374.2			

Table F19. Cost summary of limestone forced oxidation FGD without NO$_X$ absorption (continued)

TOTAL CASH EXPENDED (TCE)	109,595,947	365.3
Allowance for Funds (AFDC)	6,148,065	20.5
TOTAL PLANT INVESTMENT (TPI)	115,744,012	385.8
Preproduction Costs	3,074,078	10.2
Inventory Capital	90,496	0.3
Initial Catalyst and Chemicals	0	0.0
Royalties	401,153	1.3
TOTAL CAPITAL REQUIREMENT (TCR)	119,309,739	397.7
Market Demand Escalation	0	0.0
Power Outage Penalty	0	0.0
Land Cost	0	0.0
TOTAL CAPITAL REQUIREMENT (TCR)	119,309,739	397.7
(Including Market Demand Escalation, Power Outage Penalty and Land Cost)		
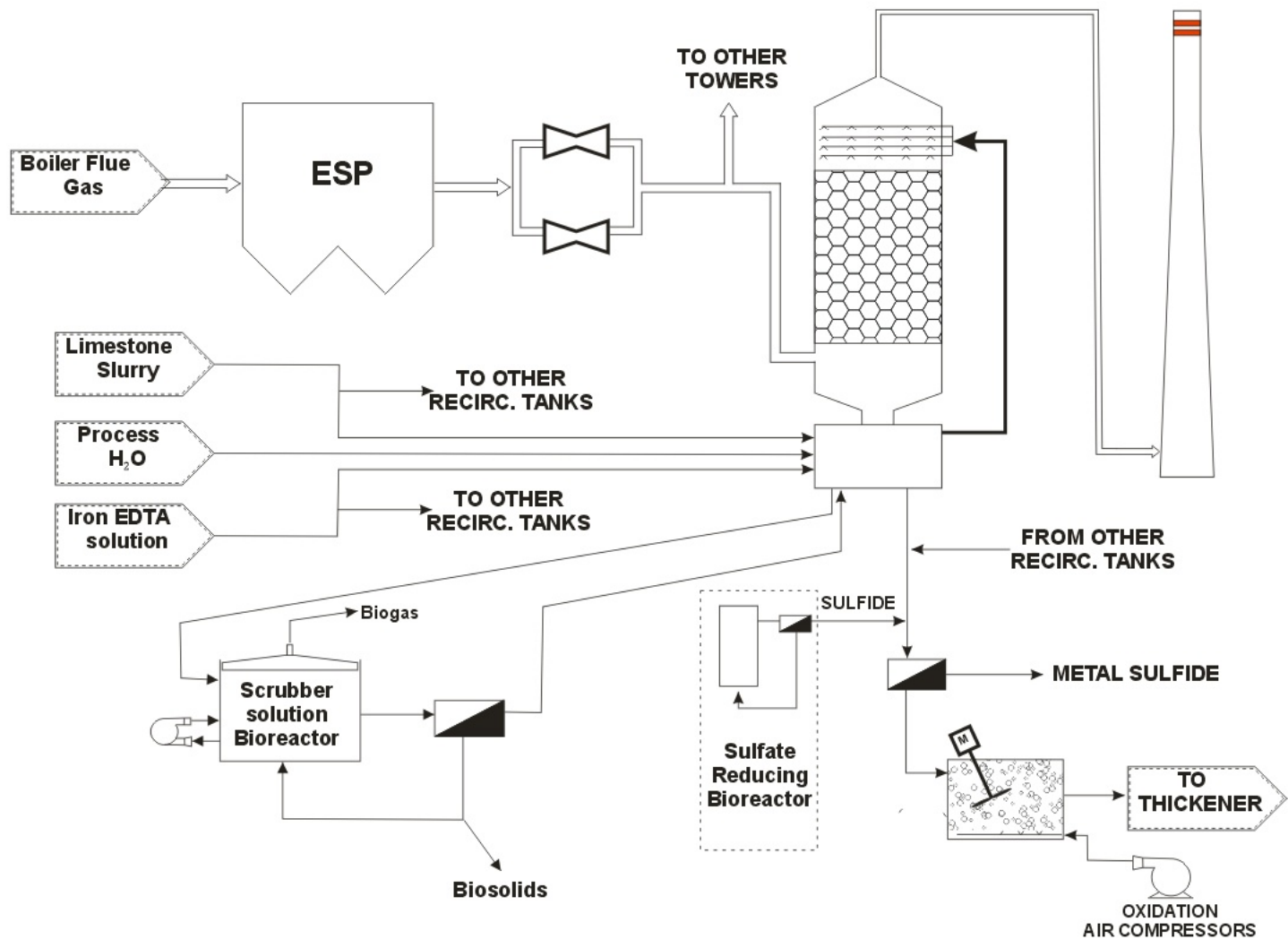
Figure F1. LSFO FGD with NO$_X$ Absorption and Biological Scrubber Solution Treatment and Regeneration Process Schematic

BIBLIOGRAPHY

Æsøy A., Ødegaard H. (1994) Nitrogen removal efficiency and capacity in biofilms with biologically hydrolyzed sludge as carbon source. *Water Science and Technology* **30,** 63-71.

Agency U. S. E. P. (1998) *NOx - How Nitrogen Oxides Affect the Way We Live and Breathe* EPA 456/F-98-005.

Amrhein G. P. (2001) Mercury Removal in Utility Wet Scrubber Using a Chelating Agent.

Anderson R. R., White C. M. (1994) Analysis of Fischer-Tropsch By-Product Waters by Gas Chromatography. *Journal of High Resolution Chromatography* **17,** 245-249.

APHA/AWWA/WEF (1995) *APHA/AWWA/WEF Standard Methods for the Examination of Water and Wastewater*.

Bailey J. E., Ollis D. F. (1986) *Biochemical Engineering Fundamentals*. McGraw-Hill Book Company. New York, New York.

Barber W. P., Stuckey D. C. (2000) Nitrogen removal in a modified anaerobic baffled reactor (ABR): 2, Nitrification. *Water Research* **34,** 2423-2432.

Batstone D. J., Keller J., Angelidaki I., Kalyuzhnyi S. V., Pavlostathis S. G., Rozzi A., Sanders W. T. M., Siegrist H., Vavilin V. A. (2002) The IWA Anaerobic Digestion Model No 1 (ADM1). *Water Science and Technology* **45,** 65-73.

Bayoumy M. E., Bewtra J. K., Ali H. I., Biswas N. (1999) Removal of heavy metals and COD by SRB in UAFF reactor. *Journal of Environmental Engineering*, 532-539.

Beaubien A., Hu Y., Bellahcen D., Urbain V., Chang J. (1995) Monitoring metabolic activity of denitrification processes using gas production measurements. *Water Research* **29,** 2269-2274.

Bellouti M., Alves M. M., Novais J. M., Mota M. (1997) Flocs vs granules: differentiation by fractal dimension. *Water Research* **31,** 1227-1231.

Benoit J. M., Gilmour C. C., Mason R. P. (2001a) Aspects of bioavailability of mercury for methylation in pure cultures of *Desulfobulbus propionicus* (1pr3). *Applied Environmental Microbiology* **67,** 51-58.

Benoit J. M., Gilmour C. C., Mason R. P. (2001b) The influence of sulfide on solid-phase mercury bioavailability mor methylation by pure cultures of *Desulfobulbus propionicus* (1pr3). *Environmental Science & Technology* **35,** 127-132.

Bhattacharya S. K., Uberoi V., Dronamraju M. M. (1996) Interaction between Acetate Fed Sulfate Reducers and Methanogens. *Water Research* **30,** 2239-2246.

Bhatti Z. I., Furukawa K., Fujita M. (1996) Feasibility of methanolic waste treatment in UASB reactors. *Water Research* **30,** 2559-2568.

Blaedel W. J., and Meloche V.W. (1963) Elementary Quantatative Analysis: Theory and Practice. Harper and Row Publishers. New York.

Borzacconi L., Ottonello G., Castelló E., Pelaez H., Gazzola A., Viñas M. (1999) Denitrification ina carbon and nitrogen removal system for leachate treatment: performance of a upflow sludbge blanket (UASB) reactor. *Water Science and Technology* **40,** 145-151.

Breckenridge L. (2000) Moving Bed Biofilter and Condenser for Flue Gas Pollutant Removal and Collection. USA.

Brito A. G., Melo L. F. (1999) Mass transfer coefficients within anaerobic biofilms: effects of external liquid velocity. *Water Research* **33,** 3673-3678.

Broholm M. M., Crouzet C., Arvin E., Mouvet C. (2000) Concurrent nitrate and Fe(III) reduction during anaerobic biodegradation of phenols in a sandstone aquifer. *Journal of Contaminant Hydrology* **44,** 275-300.

Brooks S. C., Carroll S. L., Jardine P. M. (1999) Sustained Bacterial Reduction of CoIIIEDTA- in the Presence of Competing Geochemical Oxidation during Dynamic Flow. *Environ. Sci. Technol.* **33,** 3002-3011.

Brown, L. et al. (1997) State of the World. Worldwatch Institute, Washington, DC.

Buisman C. J. (1995) Process for the treatment of water containing sulphur compounds. U.S.A.: Paques B.V.

Buisman C. J. N. (1993) Process for the removal of sulfur dioxide from waste gas. U.S.A.: Paques, B.V.

Buisman C. J. N., Dijkman H., Verbraak P. L., Den-Hartog A. J. (1999) Process for purifying flue gas containing nitrogen oxides: Biostar Development C.V. U.S. Patent # 5,891,408

Buisman C. J. N., Dijkman H., Verbraak P. L., Den-Hartog A. J. (2001) Apparatus for purifying flue gas containing nitrogen oxides. U.S.A.: Biostar Development C.V. U.S. Patent # 6,235,248

Caixeta C. E. T., Cummarota M. C., Xavier A. M. F. (2002) Slaughterhouse wastewater treatment: evaluation of a new three-phase separation system in a UASB reactor. *Bioresource Technology* **81,** 61-69.

Cao G.-m., Zhao Q.-x., Sun X.-b., Zhang T. (2002) Characterization of nitrifying and denitrifying bacteria coimmobilized in PVA and kinetics model of biological nitrogen removal by coimmobilized cells. *Enzyme and Microbial Technology* **30,** 49-55.

Cervantes F. J., De la Rosa D. A., Gomez J. (2001) Nitrog1en removal from wastewaters at low C/N ratios with ammonium and acetate as electron donors. *Bioresource Technology* **79,** 165-170.

Chang S.-G., Littlejohn D., Shi Y. (1997) Metal Regeneration of Iron Chelates in Nitric Oxide Scrubbing. USA: The Regents of California.

Christensen T. H., Bjerg P. L., Banwart S. A., Jakobsen R., Heron G. (2000) Characterization of redox conditions in groundwater contamination plumes. *Journal of Contaminant Hydrology* **45,** 165-241.

Christensson M., Lie E., Welander T. (1994) A Comparison between ethanol and methanol as carbon sources for denitrification. *Water Science and Technology* **30,** 83-90.

Dravo Lime Company. (1992) *Enhanced NO$_X$ Removal in Wet Scrubbers Using Metal Chelates, Final Report Volume 1 of 2*. Prepared for the U.S. Department of Energy Pittsburgh Energy Technology Center,Submitted by Dravo Lime Company DOE Contract DE-AC22-90PC90362.

Compeau G., Bartha R. (1984) Methylation and demethylation of mercury under controlled redox, pH, and salinity conditions. *Applied and Environmental Microbiology* **48,** 1203-1207.

Constantin H., Fick M. (1997) Influence of C-sources on the denitrification rate of a high-nitrate concentrated industrial wastewater. *Water Research* **31,** 583-589.

Cooper C. D., Alley F. C. (1994) *Air Pollution Control: A Design Approach*. Waveland Press, Inc. Prospect Heights, Illinios.

Copp J. B., Dold P. L. (1998) Confirming the nitrate-to-oxygen conversion factor for denitrification. *Water Research* **32,** 1296-1304.

Cornish-Bowden A. (1995) *Fundamentals of Enzyme Kinetics*. Portland Press, Ltd. London, U.K.

Cuervo-Lopez F. M., Martinez F., Gutierrez-Rojas M., Noyola R. A., Gomez J. (1999) Effect of nitrogen loading rate and carbon source on denitrification and sludge settleability in upflow anaerobic sludge blanket (UASB) reactors. *Water Science and Technology* **40,** 123-130.

De Smul A., Dries J., Goethals L., Grootaerd H., Verstraete W. (1997) High rates of microbial sulphate reduction in a mesophilic ethanol-fed expanded-granular-sludge-blanket reactor. *Applied Microbiology and Biotechnology* **48,** 297-303.

De Vegt A. L., Buisman C. J. N. (1996) Sulfur compounds and heavy metal removal using bioprocess technology. In: *The 1996 TMS Annual Meeting and Exhibition*. Edited by Warren G. W.

Dow (2004) *Selecting the Correct Dow Chelating Agent*. The Dow Chemical Company, Midland, Michigan.

Downs W., Bailey R. T. (2001a) Apparatus for Control of Mercury. U.S.A.: McDermott Technology, Inc.

Downs W., Bailey R. T. (2001b) Method for Control of Mercury. U.S.A.

Dravo Lime C. (1992) *Enhanced NO_X Removal in Wet Scrubbers Using Metal Chelates, Final Report Volume 2 of 2*. Prepared for the U.S. Department of Energy Pittsburgh Energy Technology Center,Submitted by Dravo Lime Company DOE Contract DE-AC22-90PC90362.

Dries J., De Smul A., Goethals L., Grootaerd H., Verstraete W. (1998) High rate biological treatment of sulfate-rich wastewater in an acetate-fed EGSB reactor. *Biodegredation* **9,** 103-111.

du Plessis C. A., Kinney K. A., Schroeder E. D., Chang D. P. Y., Scow K. M. (1988) Denitrification and Nitric Oxide Reduction in an Aerobic Toluene-Treating Biofilter. *Biotechnology and Bioengineering* **58,** 408-415.

Engelmann M. D., Bobier R. T., Hiatt T., Cheng I. F. (2003) Variability of the Fenton reaction characteristics of the EDTA, DTPA, and citrate complexes of iron. *BioMetals* **16,** 519-527.

Engineering News Record, McGraw-Hill Construction, © 2003 The McGraw-Hill Companies, Inc. http://enr.construction.com/features/conEco/costIndexes/default.asp, accessed: 9/24/2003

Etchebehere C., Errazquin I., Barrandeguy E., Dabert P., Molleta R., Muxi L. (2001) Evaluation of the denitrifying microbiota of anoxic reactors. *FEMS Microbiology Letters* **35,** 259-265.

Fang H. H. P., Lau I. W. C. (1996) Startup of thermophilic (55ºC) UASB reactors using differetn mesophilic seed sludges. *Water Science and Technology* **34,** 445-452.

Flanagan W. P., Apel W. A., Barnes J. M., Lee B. D. (2002) Development of gas phase bioreactors for the removal of nitrogen oxides from synthetic flue gas streams. *Fuel* **81,** 1953-1961.

Ford P. C., Lorkovic I. M. (2002) Mechanistic Aspects of the Reactions of Nitric Oxide with Transition-Metal Complexes. *Chem. Rev.* **102,** 993-1017.

Frette L., Gejlsbjerg B., Westermann P. (1997) Aerobic denitrifiers isolated from an alternating activated sludge system. *FEMS Microbiology Ecology* **24,** 363-370.

Fuerhacker M., Bauer H., Ellinger R., Sree U., Schmid H., Zibuschka F., Puxbaum H. (2001) Relationship between release of nitric oxide and CO2 and their dependence on oxidation reduction potential in wastewater treatment. *Chemosphere* **44,** 1213-1221.

Ghangrekar M. M., Asolekar S. R., Ranganathan K. R., Joshi S. G. (1996) Experience with UASB reactor start-up under different operating conditions. *Water Science and Technology* **34,** 421-428.

Gimenez J. R., Nassr S. C., Maestri R. D., Monteggia L. O. (2002) Physical modeling of an upflow anaerobic sludge blanket reactor: near-field study. *Water Science and Technology* **45,** 157-162.

Glass C., Silverstein J. (1998) Denitrification kinetics of high nitrate concentration water: pH effect on inhibition and nitrite accumulation. *Water Research* **32,** 831-839.

Gorby V. (2001) Ion Transfer of Acids and Bases. In: *Laboratory of Electrochemistry*. Lausanne, Switzerland: L'Ecole Polytechnique Fédérale de Lausanne, pp. 140.

Gorby Y., A., Caccavo F., Jr., Bolton H., Jr. (1998) Microbial Reduction of Cobalt III EDTA - in the Presence and Absence of Manganese(IV) Oxide. *Environ. Sci. Technol.* **32,** 244-250.

Grady C. P. L. J., Daigger G. T., Lim H. C. (1999) *Biological Wastewater Treatment, 2nd Edition*. Marcel Dekker, Inc. New York, NY.

Guiot S. R., Tartakovsky B., Lanthier M., Levesque M.-J., Manuel M. F., Beaudet R., Greer C. W., Villemur R. (2002) Strategies for augmenting the pentachlorophenol degradation potentials of UASB anaerobic granules. *Water Science and Technology* **45,** 35-41.

Gupta A., Flora J. R. V., Gupta M., Sayles G. D., Suidan M. T. (1994a) Methanogenesis and sulfate reduction in chemostats-I. kinetic studies and experiments. *Water Research* **28,** 781-793.

Gupta M., Gupta A., Suidan M. T., Sayles G. D., Flora J. R. V. (1994b) ORP measurement in anaerobic systems using flow-through cell. *Journal of Environmental Engineering* **20,** 1639-1645.

Haendriksen H. V., Ahring B. K. (1996) Integrated removal of nitrate and carbon in an upflow anaerobic sludge blanket (UASB) reactor: operating performance. *Water Research* **30,** 1451-1458.

Hansen T. A. (1993) *The Sulfate Reducing Bacteria: Contemporary Perspectives*, Edited by Odom J. M. and Singleton Jr. R. Springer-Verlag. New York, NY.

Harper S., Pohland F. G. (1986) Recent Developments in Hydrogen Management During Anaerobic Biological Wastewater Treatment. *Biotechnology and Bioengineering* **XXVIII,** 585-602.

Hauck S., Benz M., Brune A., Schink B. (2001) Ferrous iron oxidation by denitrifying bacteria in profundal sediments of a deep lake (Lake Constance). *FEMS Microbiology Ecology* **37,** 127-134.

Hayton T. W., Legzdins P., Sharp W. B. (2002) Coordination and Organometallic Chemistry of Metal-NO Complexes. *Chem. Rev.* **102,** 935-991.

Hellinga C., Schellen A. A. J. C., Mulder J. W., van Loosdrecht M. C. M., Heijnen J. J. (1998) The Sharon Process: an innovative method for nitrogen removal from ammonium-rich waste water. *Water Science and Technology*, 135-142.

Jalali K., Baldwin A. (2000) The Role of Sulfate Reducing Bacteria in Copper Removal from Aqueous Sulfate Solutions. *Water Research* **34,** 797-806.

Jayantha K. S., Ramanujam T. K. (1995) Start-up criteria for a upflow anaerobic sludge blanket (UASB) reactor. *Bioprocess Engineering* **13,** 307-310.

Jeison D., Chamy R. (1999) Comparison of the behaviour of expanded granular sluge bed (EGSB) and upflow anaerobic sludge blanket (UASB) reactors in dilute and concentrated wastewater treatment. *Water Science and Technology* **40,** 91-97.

Jetten M. S. M., Horn S. J., van Loosdrecht M. C. M. (1997) Towards a more sustainable municipal wastewater treatment system. *Water Science and Technology* **35,** 171-180.

Joshi J. B., Mahajani V. V., Juvekar V. A. (1985) Invited Review: Absorption of NO_X Gases. *Chem. Engineering Communication* **33,** 1-92.

Juzeliunas E., Juttner K. (1998) EQCM study of iron deposition form Fe^{II}/Fe^{III} (EDTA) solutions. *Electrochemica Acta* **43,** 1691-2696.

Ka J.-O., Urbance J., Ye R. W., Ahn T.-Y., Tiedje J. M. (1997) Diversity of oxygen and N-oxide regulation of nitrite reductases in denitrifying bacteria. *FEMS Microbiology Letters* **156,** 55-60.

Kaluza, U., Klingelhöfer, P., and Taeger, K. (1998) Microbial degradation of EDTA in an Industrial Wastewater Treatment Plant. Water Research **32**, No. 9, 2843-2845.

Kalyuzhnyi S., Fedorovich V. (1997) Integrated Mathematical Model of UASB Reactor for Competition Between Sulphate Reduction and Methanogenesis. *Water Science and Technology* **36,** 201-208.

Kari F. G., Hilger S., Canonica S. (1995) Determination of the Reaction Quantum Yield for the Photochemical Degradation of Fe(III)-EDTA: Implications for the Environmental Fate of EDTA. *Environ. Sci. Technol.* **29,** 1008-1017.

Kavanaugh M. C., Trussell R. R. (1980) Design of aeration towers to strip volatile contaminants from drinking water. *J. Am. Water Works Assoc.* **72,** 684–692.

King J. K., Harmon S. M., Fu T. T., Gladden J. B. (2002) Mercury removal, methylmercury formation, and sulfate-reducing bacteria profiles in wetland mesocosms. *Chemosphere* **46,** 859-870.

King J. K., Kostka J. E., Frischer M. E., Saunders F. M. (2000) Sulfate-reducing bacteria methylate mercury at variable rates in pure cultures and in marine sediments. *Applied Environmental Microbiology* **66,** 2430-2437.

King J. K., Kostka J. E., Frischer M. E., Saunders F. M., Jahnke R. A. (2001) A quantitative relationship that demonstrates mercury methylation rates in marine sediments are based

on community composition and activity of sulfate-reducing bacteria. *Environmental Science & Technology* **35,** 2491-2496.

Kleerebezem R., Hulshoff Pol L. W., Lettinga G. (1999) Energetics of product formation during anaerobic degradation of phthalate isomers and benzoate. *FEMS Microbiology Ecology* **29,** 273-282.

Kleifges K. H., Juzeliunas, E., and Juttner, K (1997) Electrochemical study of direct and indirect NO reduction with complexing agents and redox mediator. *Electrochemica Acta* **32,** 2947-2953.

Knobel A. N., Lewis A., E. (2002) A mathematical model of a high sulphate wastewater anaerobic treatment system. *Water Research* **36,** 257-265.

Koenig A., Liu L. H. (2001) Kinetic Model of Autotrophic Denitrification in Sulphur Packed-bed Reactors. *Water Research* **35,** 1969-1978.

Krauskopf K. B. (1967) *Introduction to Geochemistry*. McGraw-Hill Publishers. Ney York, New York.

Kumaraswamy, R., Muyzer, G., Kuenen, J.G., and Loosdrecht, M.C.M., (2004) Biological removal of NOx from flue gas. Water Science and Technology **50**, no. 6, 9-15.

Laguna A., Ouattara, A., Gonzalez, R.O., Baron, O., Fama, G., El Mamouni, R., Guiot, S., Monroy, O., Macarie, H. (1999) A simple and low cost technique for determining the granulometry of upflow anaerobic sludge blanket reactor sludge. *Water Science and Technology* **40,** 108.

Lee B. D., Apel W. A., Smith W. A. (2001) Oxygen Effects on Thermophilic Microbial Populations in Biofilters Treating Nitric Oxide Containing Off-Gas Streams. *Environmental Progress* **20,** 157-166.

Lemmer H., Zaglauer A., Neef A., Meier H., Amann R. (1997) Denitrification in a methanol-fed rixed-bed reactor. Part 2: Composition and ecology of the bacterial community in the biofilms. *Water Research* **31,** 1903-1908.

Lensing H. J., Vogt M., Herrling B. (1994) Modeling of biologically mediated redox processes in the subsurface. *Journal of Hydrology* **159,** 125-143.

Lettinga G., Zehnder, A.J.B, Grotenhuis, J.T.C., Hulshoff Pol, L.W. (1987) *Granular anaerobic sludge; microbiology and technology. Proceedings of the Gasmat-Workshop Lunteren Netherlands, October 25-27,*.

Levenspiel O. (1980) The Monod Equation: A revisitand a Generalization to Product Inhibition Situations. *Biotechnology and Bioengineering* **22,** 1671-1687.

Li W., Keener, T.C. (1996). *Studies of Chemical Reduction of Fe(III)*EDTA in an SO_X/NO_X Aqueous Scrubber System*. Argonne National Laboratory/University of Cincinatti U.S. Government Contract No. W-31-109-ENG-38.

Li W., Mendelsohn, M., Harkness, J.B.L., Livengood, C.D., Parulekar, S. (1996). *Modeling and Simulation of NO_X/SO_X Removal in an Aqueous Scrubber System Using the Additive Fe(II)*EDTA*. Argonne National Laboratory/Illinois Institute of Technology.

Lide D. R., Frederikse H. P. R. (1995) *CRC Handbook of Chemistry and Physics*, Edited by Lide D. R. and Frederikse H. P. R. CRC Press, Inc. Boca Raton, FL.

Lie E., Welander T. (1994) Influence of dissolved oxygen and oxidation-reduction potential on the denitrification rate of activated sludge. *Water Science and Technology* **30,** 91-100.

Lin Y., H., Lee, Kwang, K. (2001) Verification of Anaerobic Biofilm Model for Phenol Degradation with Sulfate Reduction. *Journal of Environmental Engineering*, 119 - 125.

Littlejohn D. a. C. S. G. (1990) *Ind. Eng. Chem. Res.* **29**.

Liu D. K., Chang S.-G. (1988) Removal of Nitric Oxide from Flue Gas Using Water-Soluble Iron(I1) Dithiocarbamates. *Environ. Sci. Technol.* **22,** 1196-1200.

Liu T., Sung S. (2002) Ammonia inhibition on thermophilic aceticlastic methanogens. *Water Science and Technology* **45,** 113-120.

Liu Y., Tay, Joo-Hwa (2002) The Essential Role of Hydrodynamic shear force in the formation of biofilm and granular sludge. *Water Research* **36,** 1653-1665.

Livengood C. D., Mendelsohn M. H. (1998) Investigation of modified speciation for enhanced control of merury. In: *Advanced Coal-Based Power and Environmental Systems '98 Conference*. Morgantown, West Virginia, pp. 10.

Lovely D. R., Woodward J. C. (1996) Mechanisms for chelator stimulation of microbial Fe(III)-oxide reduction. *Chemical Geology*, 19-24.

Ma Z., Zhao B., Yuan Z. (1999) Application of electrochemical and spin trapping techniques in the investigation of hydroxyl radicals. *Analytica Chimica Acta* **389,** 213-218.

Mack J. D. (1977) Inhibition and chemical kinetics associated with the anaerobic decomposition of phenol by non-methanogenic bacteria. In: *Department of Civil and Environmental Engineering*. Pittsburgh, PA: University of Pittsburgh.

Martell A. E., Calvin M. (1953) *Chemistry of the Metal Chelate Compounds*. Prentice-Hall, Inc. New York, New York.

Massey, W. L. and F. G. Pohland (1978). "Phase separation of anaerobic stabilization by kinetic controls." J. Water Pollut. Control Fed. **50**: 2204-2222.

McCarty P. L., Smith D. P. (1986) Anaerobic wastewater treatment. *Environ. Sci. Technol.* **20,** 1200 - 1206.

Mendelsohn M. H., Harkness J. B. L. (1991) Enhanced Flue-Gas Denitrification Using Ferrous-EDTA and a Polypholic Compound in an Aqueous Scrubber System. *Energy & Fuels* **5,** 244-248.

Mengis M., Gachter R., Wehrli B. (1996) **Nitrous Oxide Emissions to the Atmosphere from an Artificially Oxygenated Lake**. *Limnology and Oceanography* **41,** 548-553.

MENGIS M., GACHTER R., WEHRLI B. (1997) Sources and sinks of nitrous oxide (N_2O) in deep lakes. *Biogeochemistry* **38,** 281–301.

Metcalf and Eddy I. (1991) *Wastewater Engineering - Treatment, Disposal, and Reuse*. McGraw-Hill, Inc.

Milobowski M. G., Amrhein G. T., Kudlac G. A., Yurchison D. M. (2001) Wet FGD Enhanced Mercury Control for Coal-Fired Utility Boilers. In: *The U.S. EPA/DOE/EPRI Combined Power Plant Air Pollutant Control Symposium: "The Mega Symposium"*. Chicago, Illinois, U.S.A.

Mizuno O., Takagi H., Noike T. (1998) Biological Sulfate Removal in an Acidogenic Bioreactor with an Ultrafiltration Membrane System. *Water Science and Technology* **38,** 513-520.

Mizuta T., J. W., Miyushi K. (1993) *Bulletin of the Chemical Society of Japan* **66**.

Mizuta T., Wang J., Miyushi K. *Inorganic Chem. Acta.* **230**.

Moir J. W. B. (1999) Cytochrome c' from Paracoccus denitrificans: spectroscopic studies consistent with a role for the protein in nitric oxide metabolism. *Biochemica et Biophysica Acta* **1430,** 65-72.

Monod J. (1949) The growth of bacterial cultures. *Ann. Rev. of Microbiol.* **3,** 371-394.

Mulder A. (1992) United States Patent Number 5,078,884: Anoxic Ammonia Oxidation. Delft, Netherlands: Assignee: Gist-Brocades N.V.

Nielsen P. H. (1996) The significance of microbial Fe(III) reduction in the activated sludge Process. *Water Science Technology* **34,** 129-136.

Nowack B. (2002) Environmental Chemistry of Aminopolycarboxylate Chelating Agents. *Environ. Sci. Technol.* **36,** 4009-4016.

Nowack B., Xue H., Sigg L. (1997) Influence of Natural and Anthropogenic Ligands on Metal Transport during Infiltration of River Water to Groundwater. *Environ. Sci. Technol.* **31,** 866-872.

Nymoen H., Valzen D. v., Langenkamp H. (1993) Absorption of NO in aqueous solutions of Fe(II)EDTA: determination of the equilibrium constant. *Chemical Engineering and Processing* **32,** 9-12.

Ogura K., Ishikawa H. (1983) NITROSYLMETALLOCHELATES-III. ROTATING RINGDISK ELECTRODE STUDY OF REDOX REACTION OF Fe(II)EDTA WITH NO *Electrochemica Acta* **28,** 167-170.

Ogura K., Ozeki T. (1981) NITROSYLMETALLOCHELATES-I. MECHANISM OF FeNO-EDTA COMPLEX FORMATION AND ITS OXIDATION. *Electrochemica Acta* **26,** 877-882.

Ogura K., Watanabe M. (1982) NITROSYLMETALLOCHELATES-II. COMPOSITION OF Fe-NO-AMINOCARBOXYLIC ACID COMPLEXES IN SOLUTION. *Electrochemica Acta* **27,** 110-114.

Onay T. T., Pohland F. G. (1998) In situ nitrogen management in controlled bioreactor landfills. *Water Research* **32,** 1383-1392.

Oremland R. S., Silverman M. P. (1979) Microbal Sulfate Reduction MEasured by an Automated Electrical Impedance Technique. *Geomicrobiology Journal* **1,** 355-372.

Paquette K. E., Helz G. R. (1997) Inorganic speciation of mercury in sulfidic waters: the importance of zero-valent sulfur. *Environmental Science & Technology* **31,** 2148-2153.

Parkin G. F., Lynch N. A., Kuo W. C., Van Keuren E. L., Bhattacharya S. K. (1990) Interaction Between Sulfate Reducers and Methanogens Fed Acetate and Propionate. *Research Journal Water Pollution Control Federation* **62,** 780-788.

Patureau D., Bernet N., Dabert P., Godon J. J., Steyer J. P., Delgenes J. P., Moletta R. (1998) Physiological, molecular and modeling studies of an aerobic denitrifier: *Microvirgula aerodenitrificans*. Use of its properties in an integrated nitrogen removal plant. *Water Science and Technology* **38,** 167-175.

Paulo P. L., Jiang B., Roest K., van Lier J. B., Lettinga G. (2002) Start-up of a thermophilic methanol-fed UASB reactor: change in sludge characteristics. *Water Science and Technology* **45,** 145-150.

Payne W. J. (1981) *Denitrification*. Wiley-Interscience. New York, New York.

Percheron G., Michaud S., Bernet N., Moletta R. (1998) Nitrate and Nitrite Reduction of a Sulphide-Rich Environment. *Journal of Chemical Technology and Biotechnology* **72,** 213-220.

Pereira M. A., Pires M. M., Alves M. M. (2002) Anaerobic degradation of oleic acid by suspended and granular sludge: identification of palmitic aicd as a key intermediate. *Water Science and Technology* **45,** 139-144.

Perry, Robert H., Green, Don W., Maloney, James O. Perry's Chemical Engineers' Handbook, Sixth Edition. McGraw-Hill, New York, New York. ©1984

Peters, Max S., and Timmerhaus, Klaus D. Plant Design and Economics for Chemical Engineers: Fourth Edition. McGraw-Hill, Inc. New York, ©1991

Plumb R. C., Martell A. E. and Bersworth F. C. (1950) Spectrophotometric determination of displacement series of metal complexes of the sodium salts of ethylenediaminetetraacetic acid. *Journal of Physical and Colloid Chemistry* 54, 1208±1215.

Pohland F. G., Kim J. C. (2000) Microbially mediated attenuation potential of landfill bioreactor systems. *Water Science and Technology* **4,** 247–254.

Puñal A., Lema J. M. (1999) Anaerobic treatment of wastewater from a fish-canning factory in a full-scale upflow anaerobic sludge blanket (UASB) reactor. *Water Science and Technology* **40,** 57-62.

Puñal A., Trevisan M., Rozzi A., Lema J. M. (2000) Influence of C:N ratio on the start-up of upflow anaerobic filter reactors. *Water Research* **34,** 2614-2619.

Quarmby J., Forster C. F. (1995) An examination of the structure of UASB granules. *Water Research* **29,** 2449-2454.

Ra C. S., Lo K. V., Shin J. S., Oh J. S., Hong B. J. (2000) Biological nutrient removal with an internal organic carbon source in piggery wastewater treatment. *Water Research* **34,** 63-71.

Radcliffe, P. T., Electric Power Research Institute, Economic Evaluation of Flue Gas Desulfurization Systems, Vol. 1, Prepared by United Engineers and Constructors, Inc., Englewood, Colorado. EPRI GS-7193, Project 1610-6, Final Report, February, 1991.

Rittmann B. E., McCarty P. L. (2001) *Environmental Biotechnology: Principles and Applications*. McGraw-Hill Inc. New York, New York.

Sada E., Kumazawa H., Takada Y. (1984) Chemical reactions accompanying absorption of NO into aqueous mixed solutions of Fe^{II}-edta and Na_2SO_3. *Ind. Eng. Chem. Fundam.* **23,** 60-64.

Sada E., Kumazawa T. (1980) Individual and Simultaneous Absorption of Dilute NO and SO_2 in Aqueous Slurries of $MgSO_3$ with Fe(II)-EDTA. *Industrial Engineering Chem. Process Des. Dev.* **19,** 377-382.

Saito T., Sekiya T., Takagi H., Washio K. (1976) Method of removing nitrogen monoxide from a nitrogen monoxide-containing gas. U.S.A.: Asahi Kasei Kogyo Kabushiki Kaisha.

Sam-Soon P., Loewenthal R. E., Dold P. L., Marais G. (1987) Hypothesis for pellitisation in the Upflow Anaerobic Sludge Bed reactor. *Water South Africa* **13,** 69-80.

Sam-Soon P., Loewenthal R. E., Wentzel M. C., Marais G. (1990) Growth of biopellets on glucose in upflow anaerobic sludge bed (UASB) systems. *Water South Africa* **16,** 151-164.

Sam-Soon P., Loewenthal R. E., Wentzel M. C., Marais G. (1991a) Effect of sulphate on pellitisation in the UASB system with glucose as substrate. *Water South Africa* **17,** 47-56.

Sam-Soon P., Loewenthal R. E., Wentzel M. C., Moosbrugger R. E., Marais G. (1991b) Effects of a recycle in upflow anaerobic sludge bed (UASB) systems. *Water South Africa* **17,** 37-46.

Sam-Soon P. A. L. N. S., Loewenthal R. E., Wentzel M. C., Marais G. (1990) Effect of nitrogen limitation on pellitisation in upflow anaerobic sludge bed (UASB) systems. *Water South Africa* **16,** 165-170.

Sander R. (1999) *Compilation of Henry's Law Constants for Inorganic and Organic Species of Potential Importance in Environmental Chemistry; Version 3*. Max-Planck Institute of Chemistry, Mainz.

Sanders W. T. M., Zeeman G., Lettinga G. (2002) Hydrolosys kinetics of dissolved polymer substrates. *Water Science and Technology* **45,** 99-104.

Santana-Casiano J. M., Gonzalez-Davila M., Rodriguez M. J., Millero F. J. (2000) The effect of organic compounds in the oxidation kinetics of Fe(II). *Marine Chemistry* **70,** 211-222.

Schneppensieper T., Finkler, Stefan, Gap, Almut, Van Eldik, Rudi, Hues, Martin, Nieuwenhuizen, Peter, Wreesmann, Carel, Abma, Wiebe (2000) Tuning the reversible binding of NO to Iron(II) Aminocarboxylate and Related Complexes in Aqueous Solution. *European Journal of Inorganic Chemistry*, . 491 - 501.

Schneppensieper T., Wanat A., Stochel G., van Eldik R. (2002) Mechanistic Information on the Reversible Binding of NO to Selected Iron(II) Chelates from Activation Parameters. *Inorganic Chemistry* **41,** 2565-3573.

Schoharting B., Rehner R., Metzger J. W., Krauth K., Rizzi M. (1998) Release of nitrous oxide (N_2O) from denitrifying activated sludge caused by H2S-containing wastewater: quantification and application of a new mathematical model. *Water Science and Technology* **39,** 237-246.

Schulthess R. v., Kuhni M., Gujer W. (1995) Release of Nitric and Nitrous Oxide from Denitrifying Activated Sludge. *Water Research* **29,** 215-226.

Seghezzo L., Zeeman G., van Lier J. B., Hamelers H. V. M., Lettinga G. (1998) A Review: the anaerobic treatment of sewate in UASB and EGSB reactors. *Bioresource Technology* **65,** 175-190.

Sekiguchi Y., Kamagata Y., Ohashi A., Harada H. (2002) Molecular and conventional analyses of microbial diversity in mesophilic and thermophilic upflow anaerobic sludge blanket granular sludges. *Water Science and Technology* **45,** 19-25.

Sharma N. R. (1995) Fabrication and Testing of an Integrated Microelectrode Chemical Sensor Array on Silicon. In: *School of Electrical Engineering*. Seattle, Washington: University of Washington.

Shen C. H., Rochelle G. T. (1998) Nitrogen Dioxide Absorption and Sulfite Oxidation in Aqueous Sulfite. *Environ. Sci. Technol.* **32,** 1994-2003.

Shepherd R. E., Sweetland M. A., Junker D. E. (1996) Ligand Field Factors in Promoting S = 3/2 {FeNO) 7 Nitrosyls. *Journal of Inorganic Biochemistry*, 1-14.

Shi Y., Littlejohn D., Chang S.-G. (1996) Integrated Tests for Removal of Nitric Oxide with Iron Thiochelate in Wet Flue Gas Desulfurization Systems. *Environ. Sci. Technol.* **30,** 3371-3376.

Siegrist H., Gujer W. (1994) Nitrogen removal in activated sludge systems including denitrification in scondary clarifiers. *Water Science and Technology* **30,** 101-111.

Sillanpaa M., Pirkanniemi K. (2001) Recent Developments in Chelate Degradation. *Environmental Technology* **22,** 791-801.

Skiadas I. V., Ahring B. K. (2002) A new model for anaerobic processes of up-flow anaerobic sludge blanket reactors based on cellular automata. *Water Science and Technology* **45,** 87-92.

Skoog D. A., Holler F. J., Nieman T. A. (1997) *Principles of Instrumental Analysis*. Saunders College Publishing. Philadelphia, PA.

Slickers A. O., Third K. A., Abma W., Kuenen J. G., Jetten M. S. M. (2003) CANON and Anammox in a gas-lift reactor. *FEMS Microbiology Letters* **218,** 339-344.

Sloss L. L. (1992) *Nitrogen Oxides Control Technology Fact Book*.

Snoeyink V. L., Jenkins D. (1980) *Water Chemistry*. John Wiley & Sons. New York, New York.

Spanjers H., Weijma J., Abusam A. (2002) Modeling the competition between sulphate reducers and methanogens in a thermophilic methanol-fed bioreactor. *Water Science and Technology* **45,** 93-98.

Speece R. E. (1996) *Anaerobic Biotechnology for Industrial Wastewaters*. Archae Press.

Speece R. E., Duran M., Demirer G., Zhang H., DiStefano T. (1997) The role of process configuration in the performance of anaerobic systems. *Water Science and Technology* **36,** 539-547.

Straub K. L., Benz M., Schink B. (2001) Iron metabolism in anoxic environments at near neutral pH. *FEMS Microbiology Ecology* **34,** 181-186.

Stumm W., Morgan J. J. (1996) *Aquatic Chemistry - Chemical Equilibria and Rates in Natural Waters*. John Wiley & Sons.

Sublette K. L. (1991) Microbial removal of no.sub.x from gases. U.S.A.: ABB Environmental Services Inc.

Suchak N. J., Jethani K. R., Joshi J. B. (1991) Modeling and simulation of NOX absorption in pilot-scale packed columns. *AIChE Journal* **37,** 323-339.

Syutsubo K., Harada H., Ohashi A., Suzuki H. (1997) An effective start-up of thermophilic UASB reactor by seeding mesophilically-grown granular sludge. *Water Science and Technology* **36,** 391-398.

Szydiowski F. J., Dunmire D. L., Peck E. E., Eggers R. L., Matson W. R. (1981) Simultaneous Determination of Iron(II), Iron(III), and Total Iron in Sphagnum Moss Peat by Programmable Voltammetry on a Graphite Tubular Electrode. *Analytical Chemistry* **53,** 193-196.

Tarre S., Green M. (2000) Precipitation potential as a major factor in formation of granular sludge in an upflow sludge blanket reactor for denitrification of drinking water. *Applied Microbiology and Technology* **42,** 482-486.

Tarre S., Moshe A., Green M. (2000) Denitrification of greenhouse leachates in an upflow sludge blanket reactor. *Water Science and Technology* **41,** 95-101.

Tchobanoglous, George, and Burton, Franklin L. <u>Wastewater Engineering: Treatment, Disposal, and Reuse</u> /Metcalf & Eddy, Inc. -3rd ed. McGraw-Hill, Inc. ©1991

Thaveesri J., Gernaey K., Kaonga B., Boucneau G., Verstraete W. (1994) Organic and Ammonium Nitrogen and Oxygen in Relation to Granular Sludge Growth in Lab-Scale UASB Reactors. In: *Water Science and Technology*, Volume 30, pp. 43-53.

United States Environmental Protection Agency (2004) Clean Air Act of 1970/1977, http://www.epa.gov/history/topics/caa70/index.htm, Accessed: April 24, 2004, Last updated: November 15, 2002

United States Environmental Protection Agency (2004) Clean Air Act Amendments of 1990, http://www.epa.gov/history/topics/caa90/index.htm, Accessed: April 24 2004, Last updated: November 15, 2002

U.S Environmental Protection Agency, Office of Air and Radiation, (2003) Ozone: Good Up High Bad Nearby. Report # MC6101A

United States Environmental Protection Agency, Office of Air and Radiation. (2003) The Plain English Guide to the Clean Air Act. Report # EPA-400-K-93-001, April, 2003. http://www.epa.gov/oar/oaqps/peg_caa/pegcaain.html

United States Environmental Protection Agency, Office of Air and Radiation, Clean Air Market Programs, (2002) Nitrogen: Multiple and Regional Impacts. Report # EPA-430-R-01-006, February 2002, 38 pages

van der Maas P., van de Sandt T., Klapwijk B., Lens P. (2003) Biological Reduction of Nitric Oxide in Aqueous Fe(II)EDTA Solutions. *Biotechnol. Prog.* **19,** 1323-1328.

van der Maas P., Weelink S., Hulshoff Pol L., Klapwijk B., Lens P. (2002) BioDeNOx: Fe-EDTA as electron mediator between denitrification and iron reduction. In: *Annual Conference of the Air & Waste Management Association*. Baltimore, Maryland, pp. 7.

van Dongen U., Jetten M. S. M., van Loosdrecht M. C. M. (2001) The SHARON®-Anammox® process for treatment of ammonium rich wastewater. *Water Science and Technology* **44,** 153-160.

Verma P. S., Saxena R. C., Jayaraman A. (1997) Cyclic voltammetric studies of certain industrially potential iron chelate catalysts. *Fresenius J Anal Chem* **357,** 56-60.

Voet D., Voet J. G., Pratt C. W. (2002) *Fundamentals of Biochemistry*. John Wiley & Sons, Inc. New York, New York.

von Canstein H., Li Y., Leonhaüser J., Haase E., Felske A., Deckwer W.-D., Wagner-Döbler I. (2002) Spatially oscillating activity and microbial succession of mercury-reducing biofilms in a technical-scale bioremediation system. *Applied and Environmental Microbiology* **68,** 1938-1946.

von Canstein H., Li Y., Timmis K. N., Deckwer W.-D., Wagner-Döbler I. (1999) Removal of mercury from chloralkali elecrolysis wastewater by a mercury-resistant *Pseudomonas putida* strain. *Applied and Environmental Microbiology* **65,** 5279-5284.

Wagner-Döbler I., Lünsdorf H., Lübbehüsen T., von Canstein H. F., Li Y. (2000a) Structure and species composition of mercury-reducing biofilms. *Applied and Environmental Microbiology* **66,** 4559-4563.

Wagner-Döbler I., von Canstein H., Li Y., Timmis K. N., Deckwer W.-D. (2000b) Removal o f mercury from chemical wastewater by microorganisms in technical scale. *Environ. Sci. Technol.* **34,** 4628-4634.

Wanat A., Schneppensieper T., Stochel G., van Eldik R., Bill E., Wieghardt K. (2002) Kinetics, Mechanism, and Spectroscopy of the Reversible Binding of Nitric Oxide to Aquated Iron(II). An Undergraduate Text Book Reaction Revisited. *Inorganic Chemistry* **41,** 4-10.

Watmough N. J., Butland G., Cheesman M. R., Moir J. W. B., Richardson D. J., Spiro S. (1999) Nitric oxide in bacteria: synthesis and consumption. *Biochemica et Biophysica Acta* **1411,** 456-474.

Weijma J., Gubbels F., Hulshoff Pol L. W., Stams A. J. M., Lens P., Lettinga G. (2002) Competition for H_2 between sulfate reducers, methanogens and homoacetogens in a gas-lift reactor. *Water Science and Technology* **45,** 75-80.

Weisweiler W., Blumhofer R., Westermann T. (1986) Absorption of Nitrogen Monoxide in Aqueous Solutions Containing Sulfite and Transition-Metal Chelates such as Fe (II)-EDTA, Fe (II)-NTA, Co (II)-Trien and Co (II)-Treten. *Chem Eng. Process.* **20,** 155-166.

Wentzel M. C., Moosbrugger R. E., Sam-Soon P. A. L. N. S., Ekama G. A., Marais G. v. R. (1994) Tentative guidelines for waste selection, process design, operation and control of upflow anaerobic sludge bed reactors. *Water Science and Technology* **30,** 31-42.

Xue H., Sigg L., Kari F. G. (1995) Speciation of EDTA in Natural Waters: Exchange Kinetics of Fe-EDTA in River Water. *Environ. Sci. Technol.* **29,** 59-68.

Yamaguchi T., Harada H., Hisano T., Yamazaki S., Tseng J.-C. (1999) Process behavior of UASB reactor treating a wastewater containing high strength sulfate. *Water Research* **33,** 3182-3190.

Yang H., Minuth B., Allen D. G. (2002) Effects of Nitrogen and Oxygen on Biofilter Performance. *Journal of the Air and Waste Management Association* **52,** 279-286.

Yu H. Q., Fang H. H. P., Tay J. H. (2000) Effects of Fe^{2+} on sludge granulation in upflow anaerobic sludge blanket reactors. *Water Science and Technology* **41,** 199-205.

Zang V., van Eldik R. (1990) Kinetics and Mechanism of the Autoxidation of Iron(II) Induced through Chelation by Ethylenediaminetetraacetate and Related Ligands. *Inorganic Chemistry* **29,** 1705-1711.